Synthesis and properties of graphene quantum dots and nanomeshes

Julien Lavie

▶ **To cite this version:**

Julien Lavie. Synthesis and properties of graphene quantum dots and nanomeshes. Organic chemistry. Université Paris Saclay (COmUE), 2018. English. NNT : 2018SACLS370 . tel-02356790v2

HAL Id: tel-02356790

https://theses.hal.science/tel-02356790v2

Submitted on 29 Nov 2019

HAL is a multi-disciplinary open access archive for the deposit and dissemination of scientific research documents, whether they are published or not. The documents may come from teaching and research institutions in France or abroad, or from public or private research centers.

L'archive ouverte pluridisciplinaire **HAL**, est destinée au dépôt et à la diffusion de documents scientifiques de niveau recherche, publiés ou non, émanant des établissements d'enseignement et de recherche français ou étrangers, des laboratoires publics ou privés.

université PARIS-SACLAY

NNT : 2018SACLS370

Thèse de doctorat

Synthesis and properties of graphene quantum dots and nanomeshes

Thèse de doctorat de l'Université Paris-Saclay
préparée à l'Université Paris-Sud

École doctorale n°571 Sciences chimiques : molécules, matériaux, instrumentation et biosystèmes (2MIB)
Spécialité de doctorat: Chimie

Thèse présentée et soutenue à Saint-Aubin, le 08 octobre 2018, par

M. Julien Lavie

Composition du Jury :

M. Alain Pénicaud Directeur de Recherche, CNRS (– CRPP)	Président du jury
Mme Stéphanie Legoupy Directeur de Recherche, CNRS (– MOLTECH ANJOU)	Rapporteur
M. Jean Weiss Directeur de Recherche, CNRS (– Institut de Chimie de Strasbourg)	Rapporteur
M. Vincent Huc Chargé de Recherche, CNRS (– ICMMO)	Examinateur
M. Jean-Sébastien Lauret Professeur, Université Paris-Sud (– LAC)	Examinateur
M. Stéphane Campidelli Chercheur, CEA (– NIMBE)	Directeur de thèse

Index of abbreviations

2D	Two-dimensional
2-TBQP	2,7,13,18-Tetrabromodibenzo[a,c]dibenzo[5,6:7,8]quinoxalino-[2,3-i]phenazine
AC	Armchair
AFM	Atomic force microscopy
C78	$C_{78}H_{26}$
C78C12	$C_{126}H_{122}$
C78Cl	$C_{78}Cl_{26}$
C96	$C_{96}H_{30}$
C96C12	$C_{168}H_{174}$
C96Cl	$C_{96}Cl_{27}H_3$
C96L	Linear $C_{96}H_{30}$
C96LC12	Linear $C_{144}H_{126}$
C96LCl	Linear $C_{96}Cl_{30}$
C132	$C_{132}H_{34}$
C132C12	$C_{240}H_{250}$
C132Cl	$C_{132}H_2Cl_{32}$
C162	$C_{162}H_{38}$
C162C12	$C_{258}H_{230}$
C162Cl	$C_{162}H_2Cl_{36}$
CDHC	Photochemical cyclodehydrochlorination
C-dots	Carbon dots
CHmP	Cyclohexa-m-phenylene
CHP	Cyclohexyl pyrrolidone
CNT	Carbon nanotube
CQD	Carbon quantum dots
CVD	Chemical vapor deposition
DCE	1,2-Dichloroethane
DCM	Dichloromethane
DCTB	*Trans*-2-[3-(4-*tert*-Butylphenyl)-2-methyl-2-propenylidene]malononitrile
DDQ	2,3-Dichloro-5,6-dicyano-1,4-benzoquinone
DFT	Density functional theory
DMF	*N*,*N*-Dimethylformamide
ESI-MS	Electro-spray ionization mass spectrometry
FET	Field effect transistor
GAL	Graphene anti-dot lattice

GNM	Graphene nanomesh
GNR	Graphene nanoribbons
GNRod	Graphene nanorods
GO	Graphene oxide
GQD	Graphene quantum dots
HBC	Hexa-peri-hexabenzocoronene
HOPG	Highly oriented pyrolytic graphite
HPLC	High-performance liquid chromatography
HRTEM	High-resolution transmission electron microscopy
IEF	Insitut d'electronique fondamentale
i-PrOBpin	iso-(propoxy)boronpinacol
LAC	Laboratoire Aimé Cotton
LBNL	Lawrence Berkley national laboratory
LDA	Lithium diisopropylamide
LDI-MS	Laser desorption ionization mass spectroscopy
LED	Light emitting diode
LICSEN	Laboratoire d'innovation en chimie des surfaces et nanosciences
MALDI-TOF MS	Matrix assisted laser desorption ionization-time of flight mass spectroscopy
MW	Molecular weight
MWCNT	Multi-wall carbon nanotubes
NBS	*N*-bromosuccinimide
NMR	Nuclear magnetic resonance
PAH	Polycyclic Aromatic Hydrocarbon
PL	Photoluminescence
PLE	Photoluminescence excitation
PMMA	Poly(methyl methacrylate)
PmPV	Poly(m-phenylenevinylene-co-2,5-dioctoxy-p-phenylenevinylene)
PS	Polystyrene
PTCDI	Perylene- 3,4,9,10-tetracarboxylic-3,4,9,10-diimide
QD	Quantum dots
RIE	Reactive Ion Etching
SC	Sodium cholate
SDBS	Sodium dodecylbenzenesulfonate
SDC	Sodium deoxycholate
SDS	Sodium deoxysulfate
SPEC	Service de Physique de l'Etat Condensé
SPhos	2-Dicyclohexylphosphino-2',6'-dimethoxybiphenyl

STM	Scanning tunneling microscopy
TBAF	Tetra-n-butylammonium fluoride
TBB	1,3,5- Tris-(4-bromophenyl)benzene
TBTTA	Tetrabromotetrathienoanthracene
TCB	1,2,4-Trichlorobenzene
TCNQ	Tetracyanoquinodimethane
TEB	1,3,5- Tris-(4-ethynylphenyl)benzene
TEM	Transmission electron microscopy
THF	Tetrahydrofurane
TMS	Trimethylsilyl
TOF	Time of flight
UHV	Ultra-high vacuum
UV	Ultraviolet
UW	University of Wisconsin-Madison
UCLA	University of California Los Angeles
V_{GS}	Electric field between the source and gate
ZZ	Zig-zag

Thesis outline

Remerciements

Je souhaite remercier le Dr. Stéphanie Legoupy et le Dr. Jean Weiss pour avoir accepté d'être rapporteurs, d'avoir lu ma thèse en détail et fait un rapport complet sur mes travaux. Je remercie le Dr. Alain Penicaud pour avoir participé au jury et pour avoir aussi présidé ma soutenance de thèse, ainsi que le Dr. Vincent Huc pour avoir participé à mon jury de thèse en tant qu'examinateur. Enfin, je remercie le Prof. Jean-Sébastien Lauret pour avoir participé à mon jury de thèse mais aussi pour son aide et ses explications sur toute la partie optique de ce projet. J'ai eu beaucoup de plaisir à apprendre les rudiments de l'optique avancée grâce à lui et je suis content d'avoir découvert beaucoup de choses. Je voudrais aussi tous les remercier pour leurs retours constructifs sur cette thèse et leurs remarques pertinentes sur l'ensemble de ce projet.

Je remercie vivement mon directeur de thèse, le Dr. Stéphane Campidelli, pour le temps et l'énergie qu'il m'a consacrés. Il a été d'un grand soutien tout au long de ce projet et il m'a permis de me dépasser à chaque étape. Il m'a appris beaucoup de chose sur la science, le monde de la recherche et sur moi-même et vivre cette belle aventure avec lui a été très formateur. J'espère qu'il pourra porter ce projet le plus loin possible et qu'il aura tout le succès qu'il mérite avec ses autres projets et ses autres thésards.

Merci à Shen Zhao qui a effectué les caractérisations optiques avancées sur mes boîtes quantiques et qui a permis d'avoir autant de résultats. Ça a été un plaisir de travailler et d'échanger avec lui tout au long de cette thèse. Merci aussi aux Dr. Loïc Rondin et Gaëlle Allard pour leur aide et leurs conseils durant cette thèse.

Merci aux Dr. Sylvain Latil et Yannick Dappe pour leur aide sur la partie théorique et notamment pour les explications détaillées sur la physique théorique de ces matériaux. Merci à Diane Lebeau, Solène Legand, Vincent Guérineau et Nicolas Ellie pour leur sympathie et leur disponibilité pour les caractérisations en MALDI-TOF. Merci au Dr. Hanako Okuno pour ses travaux en HR-TEM qui ont permis d'avoir des images impressionnantes pour illustrer ces travaux.

Je remercie tous les permanents du LICSEN : les Dr. Bruno Jousselme, Renaud Cornut, Fanny Hauquier, Arianna Filoramo, Guy Deniau, Geraldine Carrot, Ludovic Tortech, Bernard Geffroy, Jocelyne Leroy, Pascal Viel, Cédric Zobrist ainsi que Maud Gallois, Nabila Debou et Philippe Surugue pour leurs conseils et leur aide autant pour les manipulations que pour les présentations. Je voudrais particulièrement remercier le Dr. Vincent Derycke qui m'a suivi et aidé tout au long de cette thèse, j'ai beaucoup aimé discuter avec lui de physique et de la recherche en général.

Merci au Dr. Serge Palacin, Bruno Lectard et au Dr. Lucie Krzaczkowski pour leur disponibilité, leurs conseils et l'aide précieuse qu'ils m'ont apportés tout au long de cette thèse. Ils ont beaucoup facilité sont déroulement et ont permis qu'elle s'effectue dans de bonnes conditions.

Je remercie les personnes avec qui j'ai travaillé sur ce projet, d'abord Manel Hanana et Khaoula Khedhiri que j'ai encadrées et avec qui ça a été un plaisir de travailler. Ensuite, Joffrey Pijeat avec qui nous avons mené des projets parallèles et avec qui ça a été un plaisir de collaborer soit pour trouver des solutions, de nouvelles idées ou tout simplement pour se soutenir. J'espère qu'ils auront beaucoup de succès dans leurs projets futurs et j'espère pouvoir les appeler « docteurs » dans quelques années !

Je voudrais aussi remercier Lucile Orcin-Chaix avec qui j'ai commencé ce projet en stage et qui l'a suivi durant ma thèse notamment sur l'optique. J'ai réussi à comprendre la partie compliquée de l'optique grâce à elle et je suis content d'avoir en plus construit une amitié hors travail qui par Jupiter perdurera bien après cette thèse ! Merci aussi à mon « co-thésard » Olivier Henrotte, mon belge préféré avec qui j'ai passé ces trois années avec leurs bons et leurs mauvais moments. Je lui souhaite bon courage pour sa soutenance mais avant ça j'ai besoin de lui pour le gold !

Je remercie tous les stagiaires, thésards et autres CDD qui ont participé à la bonne ambiance de ce labo et qui ont permis de travailler dans d'excellentes conditions tout au long de cette thèse, Gaëlle Charrier, Aurélien Doublet, Kevin Jaouen, Hanine Kamaleddine, Marine Le Goas, Florian Lebon, Julie Machado, Thomas Petenzi, Marta Reig, Sarah Bernardi, Halima Noubli,

Fatima El Orf, Andrea Falconi, Aurélie Rachet, Guillaume Penvern, Marianne Kjellberg, Matteo Balestrieri, Alex Boschi, Al-Saleh Keita, Gabriel Gelin, Geoffrey Barral, Nathalie Fresneau, Romain Brisse, Tiphaine Bourgeteau, Antoine Desrues et Hugo Casadesmond.

Merci à tous mes amis en thèse ou non qui sont venus à la soutenance ou qui m'ont encouragé pour cette épreuve et tout au long de la thèse, notamment Romain, Sophie, Fabien, Maxime, Clémentine, Rémi.

Enfin je voudrais remercier mes parents qui m'ont soutenu et encouragé depuis les débuts où je voulais être « un chercheur ». Et un grand merci à celle qui sera bientôt ma femme, Caroline, elle qui m'a soutenu et aidé, notamment pour affronter les périodes de rédaction et de soutenance. Merci à tous mes amis en thèse ou non qui sont venus à la soutenance ou qui m'ont encouragé pour cette épreuve et tout au long de la thèse, notamment Romain, Sophie, Fabien, Maxime, Clémentine, Rémi.

Enfin je voudrais remercier mes parents qui m'ont soutenu et encouragé depuis les débuts où je voulais être « un chercheur ». Et un grand merci à celle qui sera bientôt ma femme, Caroline, elle qui m'a soutenu et aidé, notamment pour affronter les périodes de rédaction et de soutenance.

Chapter 1: Introduction

Chapitre 1 : Introduction

Chapter 1: Introduction

1.1. Context

In a world more and more connected, the security of data transfer is a major concern for the development of new technologies. Currently, data is secured using cryptography. This method is based on the use of a logic key by the sender to encrypt a message. This key is transmitted to the recipient through a parallel channel so he could decrypt the message. However, the interception of the key directly allows the decryption of the message without any way for the sender or the recipient to know that the key was intercepted. A new method of encryption based on the use of quantum object was developed to tackle this issue, it is called quantum cryptography. In fact, the measure of the properties of a quantum object changes these properties and therefore the interception of a key would be detected by the recipient. There are various quantum objects that can be used for such applications but the one with the most promising experimental results to date is a photon from a single photon source. Many materials can be used as a single photon source like defects in crystals, quantum dots or molecules. Molecules have advantage to be tunable and one can think about controlling the optical properties of the single photon source controlling the structure of the molecule. Several examples of single photon emitters based on polycyclic aromatic hydocarbons (PAHs) such as terrylene or dibenzanthathrene have been described in the literature. Actually PAH molecules can be considered as small pieces of graphene and therefore, as graphene is a zero bandgap semiconductor, the bandgap and consequently the wavelength of the emitted photons can be tuned from an energy of 4.77 eV (emission of a benzene molecule) to 0 eV (2D graphene).

Chapter 1: Introduction

1.2. Graphene

1.2.1. Generalities

Graphene is a monolayer of sp^2 carbon atoms organized into a two-dimensional (2D) honeycomb lattice (Figure 1.1). It is the building block of graphite which is the stacking of multiple layers of graphene. The existence of graphene was postulated in 1947[1–3] but such monoatomic layer was supposed to be unstable[4,5] until A. Geim and K. Novoselov were able to isolate it in 2004 from graphite using scotch tape.[6] The first studies of graphene focused on its electronic properties and it was found that graphene is a semi-metal (or a zero bandgap semiconductor). It means that graphene does not exhibit bandgap between the conduction and valence bands as it was predicted by theoretical calculation.[7] The mobility was found to be on the order of 10 000 $cm^2.V^{-1}.s^{-1}$ for graphene deposited on SiO_2[6] and up to 200 000 $cm^2.V^{-1}.s^{-1}$ for suspended graphene[8]

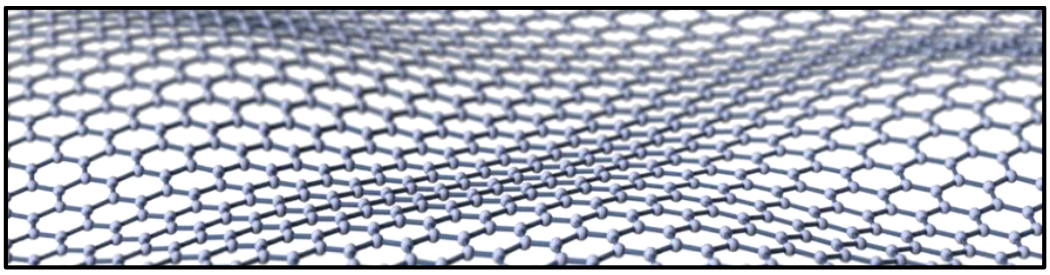

Figure 1.1: Artistic representation of graphene.

The valence and conduction bands of graphene are cone-shaped, they meet at the Dirac point and the density of state at this point is zero (Figure 1.2). Very early, theoretical calculations predicted outstanding properties for graphene, including the best known mechanical properties,[9] high thermal conductivity[10–12] and intriguing quantum Hall effect[13–15] and these properties were soon confirmed experimentaly.[16–18] This turned graphene into a hot topic in modern science and only six years after their discovery A. Geim and K. Novoselov received the Nobel Prize.

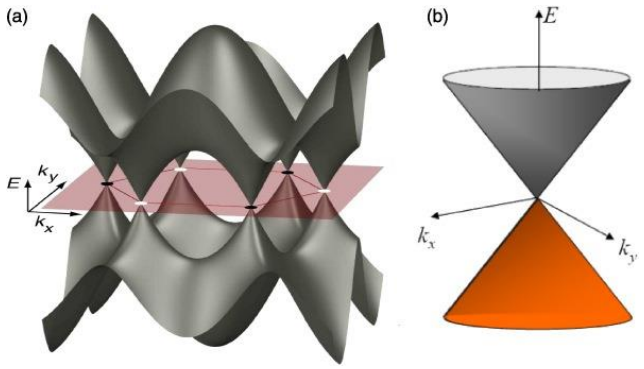

Figure 1.2: a) Band structure of graphene; b) close-up of the low energy region showing the so-called "Dirac cone".

With such properties, graphene was considered as a promising material for a wide range of applications from electronics,[19] energy conversion and storage,[20] catalysis,[21] electrochemistry[22] or photonics.[23] In fact, the first domain of applications that was studied was electronics with the realization of Field Effect Transistors (FET) in which graphene plays the role of channel (the active part of the device) between the source and the drain electrodes (Figure 1.3a). In FET, the current flowing through the channel (from source to drain) can be controlled applying an electric field between the source and gate (V_{GS}). There are two types of FETs: radiofrequency devices and digital logic devices. Considering its high carrier mobility and its two dimensional structure, graphene is well suited for radiofrequency FETs in which the channel should respond quickly to variations of voltage[24] and should exhibit a high current for the ON-state. In 2010, IBM fabricated wafer-scale epitaxial graphene FETs that achieved a frequency of 100 GHz.[25] On the contrary, for digital logic devices, the information is stored by the switching between the ON-state (1) and the OFF-state (0); the low I_{ON}/I_{OFF} ratio observed in graphene FETs constitutes a severe limitation to the use of graphene in such electronic devices. Actually, silicon based FET have ON/OFF ratios between 10^4 and 10^7 while graphene FETs exhibit ON/OFF ratios between 2 and 100 (Figure 1.3b). This relatively low ratio leads to high power dissipation during the OFF-state.[26]

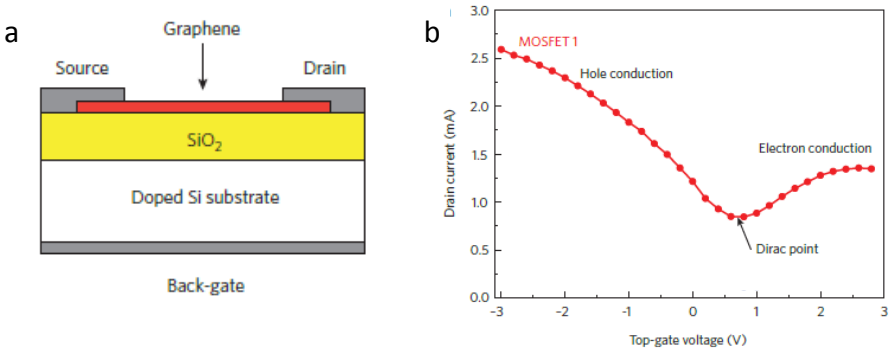

Figure 1.3: a) Schematic representation of the basic design of a graphene FET and b) Current-Voltage curve of a graphene FET with a channel length of 5µm and width of 10 µm[27] *(inspired from refs* 24 and 27*)*

This limitation makes F. Schwierz write at the end of his review in 2010: "The primary challenges facing the community at present, therefore, are to create in a controlled and practical fashion a bandgap in graphene, which would allow logic transistors to switch off and radiofrequency transistors to avoid the second linear regime (...)."[24] Therefore, the gap engineering of graphene and the preservation of its outstanding properties is a major challenge for future application.

1.2.2. Bandgap opening

To open a bandgap in graphene, various methods based either on physical or chemical approaches have been proposed. As graphene is a single layer of carbon atoms with a well-defined structure, any modification to its environment can affect its electronic properties. Theoretical calculations showed that the simple presence of water molecules in air have an impact on the electronic properties of graphene.[28] Yavari *et al.* showed that a bandgap of *ca.* 0.2 eV could be obtained by exposing graphene to an absolute humidity level of 0.31 kg of water per kg of dry air in an environmental chamber.[29] The effect is reversible and in vacuum the observed bandgap returns to almost zero as expected for graphene. The adsorption of polycyclic aromatic molecules such as pyrene or perylene derivatives on graphene is an easy and versatile way of functionalizing graphene.[30,31] Whereas theoretical studies on perylene-3,4,9,10-tetracarboxylic-3,4,9,10-diimide (PTCDI) showed that the adsorption of aromatic

molecule should open a bandgap,[32,33] experimentally only a shift of the Dirac point was observed.[34] Despite the large amount of literature on the bandgap engineering on graphene made by adsorption of gas or molecules,[35] these methods are not suitable, so far, to produce materials that can be manipulated and used in devices in an easy and reproducible way.

The covalent functionalization of graphene with hydrogen, fluorine atoms or organic molecules has a strong impact on its electronic properties. The hydrogenation of graphene gave rise to a new 2D material called graphane which is made of a single layer of sp^3 carbons (Figure 1.4a).[36,37] Graphane is an insulator but both theoretical[38,39] and experimental[40] work showed that a partial hydrogenation can permit to open a bandgap up to 4 eV. However, the control of the level of hydrogenation is experimentally complicated and the loss of aromaticity induces a decrease of carrier mobility (down to about 9 $cm^2V^{-1}s^{-1}$). The reaction of graphene with fluorine gives rise to fluorographene which have the same structure as graphane but with fluorine atoms instead of hydrogens (Figure 1.4b).[41] It was found to be a wide gap semiconductor[42] (3.8 eV) but once again the carrier mobility is not comparable to the one of graphene. In the case of organic molecule, whereas many studies are done on the organic functionalization of graphene,[43–45] very few are able to open a bandgap. Some examples are the covalent functionalization with *p*-nitrobenzenediazonium[46] or azidotrimethylsilane[47] which are able to open gaps of 0.36 and 0.66 eV respectively.

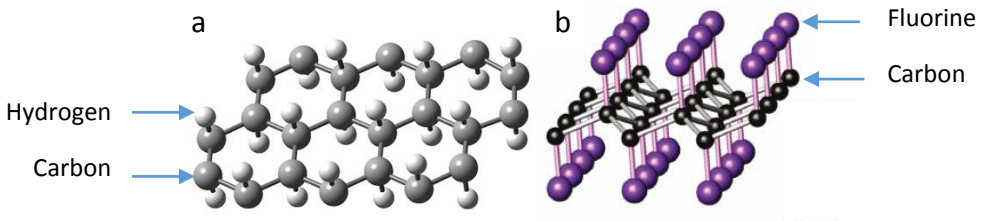

Figure 1.4: a) Graphane and b) Fluorographene structures.[36]

The inclusion of heteroatoms in the graphene structure is called doping; the presence of heteroatoms impacts the electronic properties. For example, atoms like boron or oxygen create a p-type[48–50] doping whereas atoms like nitrogen and phosphorous create a n-type[51–53] doping. Theoretical calculations[49,54,55] showed that the doping of graphene could open a

bandgap and it was possible to obtain experimentally a bandgap of *ca.* 0.2 eV with nitrogen doped graphene (Figure 1.5a).[56] However, once again, the precise control on the bandgap is not straightforward due to the wide variety of nitrogen configuration in the materials (Figure 1.5b).

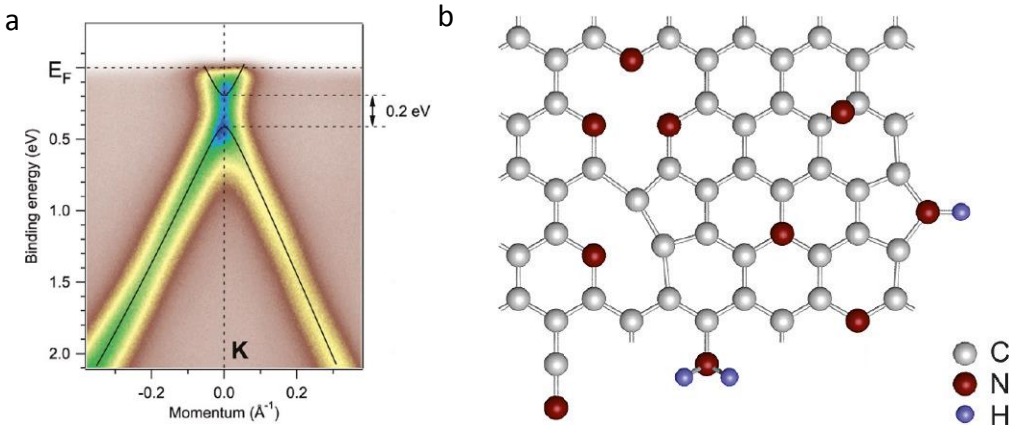

Figure 1.5: a) Angle-resolved photoemission spectroscopy (ARPES) showing a bandgap of 0.2 eV in nitrogen doped graphene made by Chemical vapor deposition (CVD) using 1,3,5-triazine[56] and b) representation of the multiple configurations of nitrogen impurities in nitrogen-doped graphene.

It is well known that when a material is reduced to nanoscale dimensions, the electronic confinement induces unique size-dependent properties. One famous example is the semiconductor quantum dots (QD) in which the confinement of the electrons leads to strongly luminescent materials with adjustable bandgap.[57–59] The reduction of one dimension of graphene down to the nanoscale leads to graphene nanoribbons (GNRs) whereas the reduction of the two dimensions leads to graphene quantum dots (GQDs) (Figure 1.6).

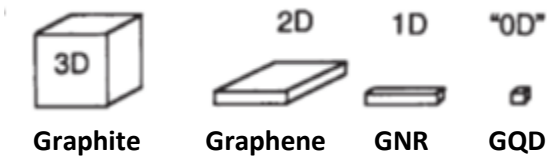

Figure 1.6: Evolution of the shape of the material with the size reduction.

A very appealing alternative to reduce the dimensionality of graphene consists in forming an ordered array of holes in a graphene sheet. This 2D-material theoretically proposed in 2008[60] is called a Graphene Nanomesh (GNM) or a Graphene Anti-dot Lattice (GAL).

For the production of these graphene derivatives two different strategies can be adopted, the top-down strategy and the bottom-up strategy. In the following section, I will give an overview of the fabrication of GQDs, GNRs and GNMs using these two approaches.

1.3. Top-Down approach

The top-down approach is widely known as the strategy that starts from a macroscopic scale system and breaks it down to the nanoscale. This approach constitutes a fast and easy process that allows mass production of graphene materials for a large range of applications.

1.3.1. Graphene quantum dots

The fabrication of GQDs *via* the top-down approach requires bulk carbon material which will be sized down to the nanometer scale. The top down approach is used with a wide range of starting material like graphite, coal, carbon black, carbon fibers, carbon nanotubes, graphene oxide or graphene.[61,62] The majority of top-down routes are based on chemical techniques that can be described as defect-mediated fragmentation process where an oxidation step acts as the defect generation and the reduction as the cleaving step (Figure 1.7).

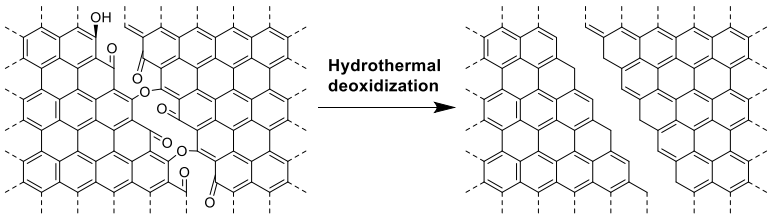

Figure 1.7: Principle of the GO cutting by oxidation and reduction (inspired from ref 44)

The first preparation of graphene quantum dots was reported in 2010 by the group of H.Dai who used graphite as starting material (Figure 1.8).[63] Graphite was oxidized into Graphene Oxide (GO) with Hummers' method[64] to favor the separation of graphene sheets. The GO was then oxidized a second time under mild sonication to break it down to the nanometer scale.

This step was followed by a reduction step to transform the GO-QDs into GQDs. The nanoparticles that they obtained exhibited a diameter distribution between 5 and 13 nm and thicknesses between 1 and 3 layers of graphene (1-2 nm). It is worth mentioning that Dai and co-workers demonstrated that their GQDs could emit light in the visible and NIR region and this property has excited the interest of the entire community because of the potential interest of these GQDs biology.

Other solvothermal methods were used to produce GQDs, they differed from the previous one by the use of microwave to speed up the exfoliation and reduction steps.[65] With this method, single layer GQDs were prepared with an average diameter of 3 nm with a 5 min process.[66]

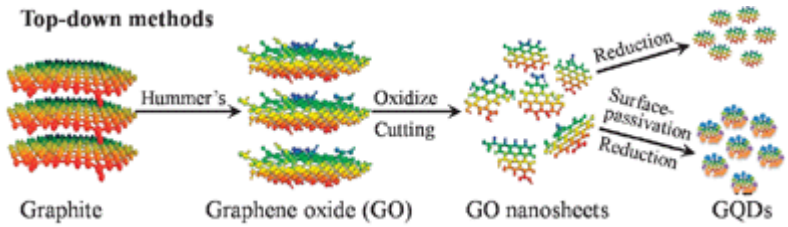

Figure 1.8: Usual method for the preparation of GQDs by chemical ablation.[67]

The electrochemistry at high redox potential (ranging from ±1.5 V to ±3 V) is another method for the preparation of GQDs. A potential applied between the graphite electrodes was used to directly oxidize the C-C bonds or oxidize water to generate hydroxyl and oxygen radicals to cleave the C-C bonds. This method can achieve the synthesis in one-pot of GQDs with diameters between 3 and 5 nm and thicknesses between 1 and 3 layers of graphene (1-2 nm).[68] It can also be done with a platinum foil used as counter electrode in alkaline conditions[69] to form GQDs exhibiting diameters between 5 and 10 nm and constituted only of monolayers.

The cage opening of fullerene C_{60} is another interesting approach that uses surface chemistry to form GQDs. In this method, C_{60} was evaporated in the chamber of a scanning tunneling microscope (STM) on a Ru(0001) surface and annealed.[70] Depending on the temperature (between 725 and 825 K) and the annealing time, the GQDs can take different shapes like

triangles, parallelograms or hexagons. These structures have lateral dimensions between 5 and 10 nm and the resulting bandgap are between 0.25 and 0.8 eV.

Up to now, the optical studies on GQDs are mainly limited to optical absorption and photoluminescence (PL) measurements on samples produced by these top-down techniques and therefore containing a lot of defects and uncontrolled edges.[71] The only experimental report available at the single nanoparticle level was done with GQDs prepared with a hydrothermal cutting method which presented disparities in size (width from 10 to 35 nm) and thicknesses. This work showed that the PL from these objects is caused by the emission of defects which means that the PL is not intrinsic to the GQD.[72] This study demonstrates that the uncontrolled edges blur out the intrinsic properties and that the bottom-up synthesis approach is mandatory to study the electronic and optical properties of such graphene nano-objects.

1.3.2. Graphene nanoribbons

The study of size reduction of graphene attracted huge attention and both theoretical[73–76] and experimental[77–80] works have shown that quantum confinement and edge effects permits to open a bandgap in narrow graphene ribbons. The first GNRs were prepared by the group of Dai from expanded graphite *via* rapid thermal annealing followed by dispersion using poly(*m*-phenylenevinylene-co-2,5-dioctoxy-*p*-phenylenevinylene) (PmPV) in 1,2-dichloroethane (DCE).[77] However, the GNR were obtained with a poor yield and a broad width distribution (from less than 10 nm to 100 nm) which led to the development of a new method based on the etching of carbon nanotubes (CNTs). This method was also developed by the group of H. Dai in 2009 and starts from multi-wall carbon nanotubes (MWCNTs) deposited on a silicon substrate and embedded in poly(methyl methacrylate) (PMMA) (Figure 1.9a).[81] The PMMA-MWCNT film was exposed to an argon plasma to selectively etch the upper part of the tubes and depending on the etching time, single layer GNRs can be isolated with width from 10 to 20 nm. The same year, the group of J. M. Tour used chemical unzipping of carbon nanotubes to produce well-defined GNRs (Figure 1.9b).[82] This method was based on the creation of defects *via* oxidation to open the CNT in one direction. The MWCNTs were oxidized with

potassium permanganate in concentrated sulfuric acid. The GNRs were then isolated and they exhibited width from 20 to 100 nm with a yield up to 100% depending on the oxidation conditions.

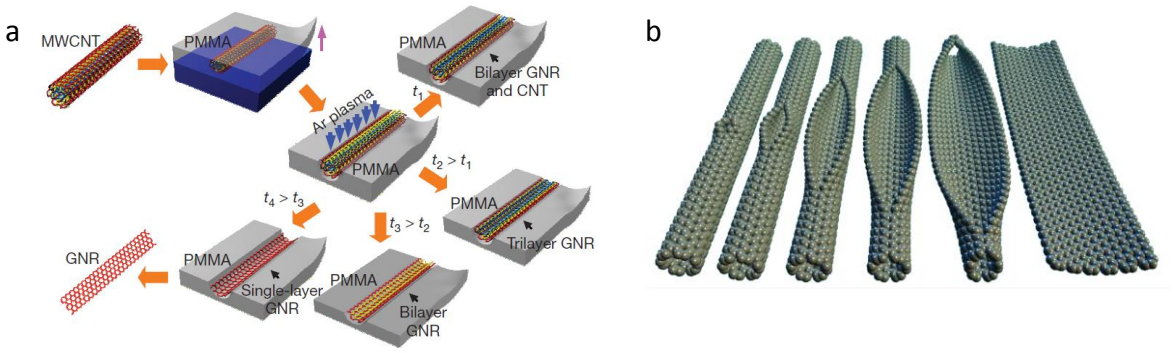

Figure 1.9: The methods for the preparation of top-down GNRs. a) The group of H. Dai reported the use of argon plasma to etch the upper part of a MWCNT and depending on the etching time, they could selectively produce single or multi-layer GNR. b) The group of J.M. Tour developed an unzipping method based on chemical oxidation to open CNTs.[82]

These techniques based on CNTs can take advantage of the specific chirality of CNTs to try to control the type of GNRs formed. In the ideal case, GNRs edges can have two basic shapes, the armchairs and zig-zags and both have different effects on the band structure of graphene (Figure 1.10a).[76] For instance, the zigzag edges in GNRs can induce spin polarized states.[74] The bandgap of both zig-zag and armchair nanoribbons is inversely proportional to their width.[24] Considering the calculated gaps for ideal GNRs (Figure 1.10b), to produce GNRs exhibiting a bandgap similar to the one of silicon around 1 eV, the width should be below 10 nm.

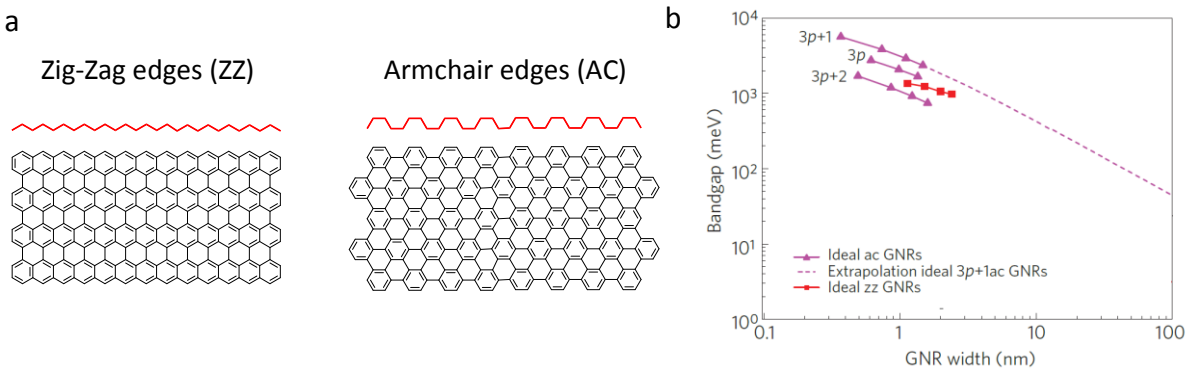

Figure 1.10: a) GNR edge shapes and b) evolution of the bandgap with the width of the GNR (adapted from ref 24)

The methods developed by J. M. Tour and H. Dai can achieve GNRs with width of less than 10 nm with FETs exhibiting I_{ON}/I_{OFF} > 100. However, such top-down approaches do not permit to control efficiently and in a reproducible way the width of the GNRs which can range from 10 to 100 nm. In addition, the edges can be either zigzag, armchair or a disordered mix of zigzag/armchair edges and their oxidation/defect states are not controlled. Finally, as the low control of the structure of GQDs heavily impacts their optical properties, the electronic properties of top-down GNR are heavily impacted by the variations of edge type (AC, ZZ or disordered) and their oxidation state.

1.3.3. Graphene nanomeshes

The first theoretical exploration of the GNMs[60] in 2008 showed that it should be possible to open a bandgap in graphene by introducing a regular pattern of holes in the graphene lattice. It was also shown that the bandgap is controlled by the ratio between removed atoms (holes) and atoms left in between these holes (necks) (Figure 1.11).

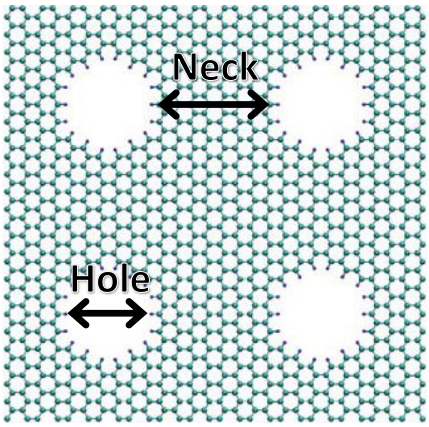

Figure 1.11: GNM with necks and holes definitions (inspired from ref 83)

Several attempts to prepare GNM came from the straightforward approach of drilling holes in graphene using electron and ion-beam lithography.[66, 67] The pores position, shape and size were controlled by the positioning and movement of the beam. With about 1 second for each hole these techniques were time consuming for large surfaces and unpractical for a regular pattern preparation.

In 2010 several groups in University of California Los Angeles (UCLA), University of Wisconsin-Madison (UW), Lawrence Berkley National Laboratory (LBNL) and Rice University have used a general approach based on nanolithography for the realization of GNMs. To fabricate the GNMs, graphene sheets deposited or synthesized on substrates were covered with porous templates made with a block copolymer,[86,87] by imprinting,[88] using colloidal mask[89] or aluminum oxide membranes.[90] The holes in graphene were created by etching process and finally the porous mask were removed giving rise to the nanomesh structures (Figure 1.12).

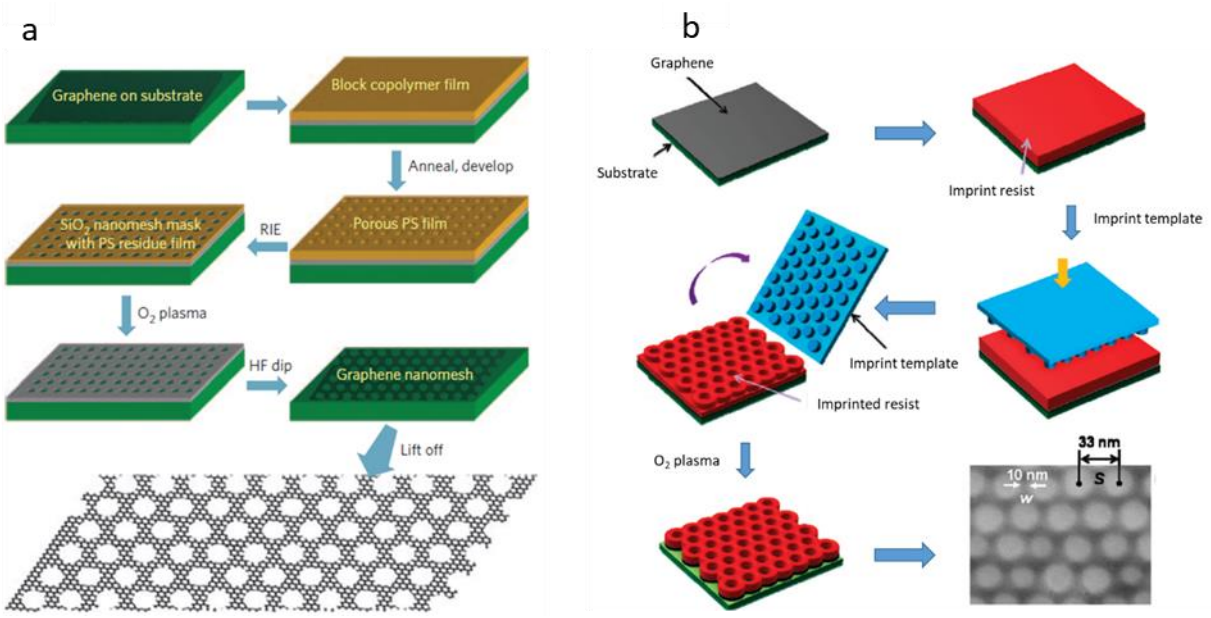

Figure 1.12: Two methods for the preparation of GNMs reported by the groups of UCLA (a) and of LBNL (b). a) graphene is covered with a thin layer of SiO_2 and with a polystyrene/polymethylmethacryalte (PS/PMMA) block copolymer. The PMMA is removed with UV exposure and glacial acid development and the resulting structure is subjected to etching and O_2 plasma. Finally, SiO_2 is removed leading to the graphene nanomesh. b) graphene is covered by PS. Then an imprint template made of SiO_2 is used to imprint the PS layer. Finally, O_2 plasma is used to etch both the PS and the graphene to obtain the GNM structure. (Adapted from ref 86 and 88)

Several other methods were then developed like local catalytic hydrogenation[91] or UV-assisted photodegradation[92] but they showed less control on the final structure compared to the previous methods presented.

The GNMs have been theoretically and experimentally studied for a wide range of application like FET,[93] biosensors[94] or gas sensing.[95] However, for each sample, the variability over the necks and holes width, the defects, contaminants and partial oxidations have a huge impact on the final electronic properties of the GNM. In fact, several theoretical studies showed that irregularities in the nanomesh structure can degrade the carrier mobility.[96–98] All these results show, once again, that the top-down approach presents important limitations on the control

of the final object prepared. The complete control on this object and thus on its properties cannot be achieved with the top-down approach and thus, the method should be changed for the bottom-up approach.

1.4. Bottom-Up approach

Conversely to the top-down approach, the bottom-up approach is the strategy that aims to build materials from a small scale system to a larger one. In chemistry or in nanoscience, this means that the material is prepared by assembling in a controlled way small molecules to build larger structures. Therefore, it seems to be a good strategy for a complete control on the final material.

1.4.1. Carbon quantum dots

The research around carbon quantum dots (CQDs) or carbon dots (C-dots) is exploding due to their chemical inertness, tunable emission, low cytotoxicity and excellent biocompatibility.[67] The term C-dots gathers nano-sized particle mainly made of carbon. The principal synthesis method is the treatment of organic precursors using a hydrothermal process or microwave irradiation.[61] The most widely spread organic precursor are citric acid combined with an amino derivative.[99] In 2008, the group of E.P. Giannelis produced C-dots by combining citric acid with sodium 11-aminoundecanoate followed by thermal oxidation at 300°C.[100,101] These kind of carbon quantum dots exhibit strong photoluminescence in the visible light (between *ca.* 450 to 600 nm) depending on their size and composition.[99,102]

C-dots show a huge potential for biological applications, nevertheless the low control on the final structure and the oxidation and edge state of the final structure constitutes the same limitations in terms of properties compared to nanoparticles produced by the top-down approach. Finally to be able to control precisely the structure of graphene quantum dots, the strategy developed by Klaus Müllen seems to be the most promising.[103]

1.4.2. Graphene quantum dots

The complete control of the properties of the final material can only be achieved by the complete control of the size, shape and edges of the GQD. The only way to do so is to use a

synthetic approach based on organic chemistry reactions. The smallest building block for graphene is a phenyl ring and it should be considered as a good starting material for the bottom-up approach.

The structures formed by the addition of phenyl rings to a benzene molecule are called polycyclic aromatic hydrocarbons (PAHs). Starting with naphthalene (10 carbons) and followed by anthracene and phenanthrene (14 carbons), this family includes a myriad of molecules and a few examples are presented in Figure 1.13. By adding in a controllable manner aromatic rings to benzene, one can think synthesizing graphene nanoparticles.

PAHs were first discovered in coal tar in the nineteenth century,[104] however due to their low solubility, large PAHs like coronene or ovalene cannot be extracted from such complex mixture. Therefore, to obtain well-defined structures with no mixture, large PAHs had to be prepared by chemical synthesis.

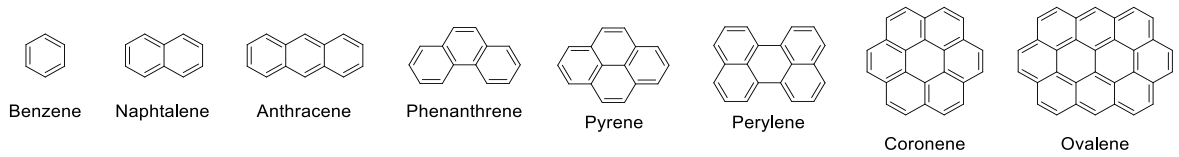

Figure 1.13: The basic structures of the PAHs.

The work of Clar, Scholl and Zander[105–114] on dehydrogenation and polyphenylene coupling allowed the preparation of many new PAHs; however, for applications and characterization, the low solubility of the final compounds remained a problem. The group of Klaus Müllen developed the synthesis of soluble hexa-peri-hexabenzocoronene (HBC) derivatives in the nineties.[103] The synthesis was based on the Diels-Alder reaction: the precursor bearing acetylenic groups reacted with the tetraphenylcyclopentadienone with the extrusion of carbon monoxide to form a polyphenylene dendrimer. Depending on the final product desired, the acetylenic and the tetraphenylcyclopentadienone derivatives could contain solubilizing groups. The dehydrogenation of the polyphenylene dendrimer *via* the Scholl reaction[110] gave rise to a new PAH which can be considered as a nanoparticle of graphene: a graphene quantum dots GQD (Figure 1.14).

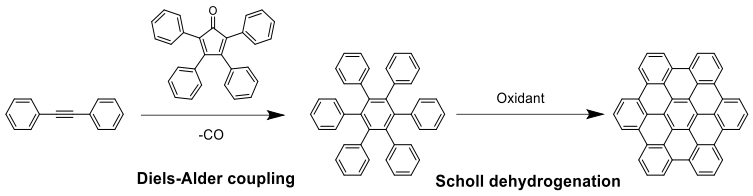

Figure 1.14: General procedure for the synthesis of GQDs; here the synthesis of HBC.

The group of Müllen further explored the synthesis and properties of hexabenzocoronene (HBC) molecules by adding and varying the nature of the peripheral chains,[115–117] in order to solubilize HBCs partially[118] or completely in water[119] and to study their liquid-crystalline properties.[117,120–124]

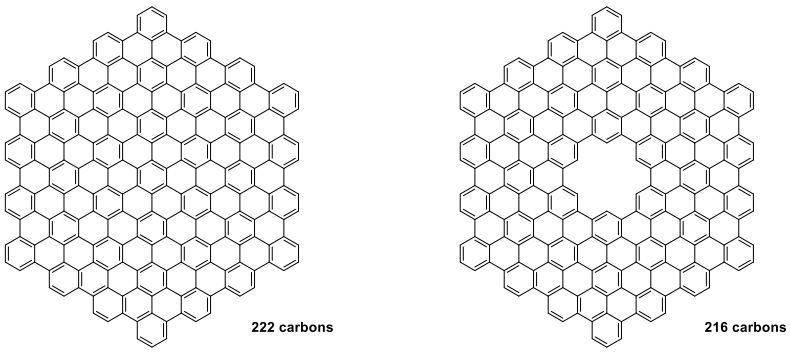

Figure 1.15: Structure of the GQD made of a) 222 carbons[125] and b) 216 carbons.[126]

To create a large variety of structures, Müllen prepared a wide range of precursors bearing acetylenic groups and following an approach based on the divergent synthesis of dendrimer. They were able to obtain GQDs with linear,[127,128] diamond,[129] triangular,[130] propeller[131,132] or rectangular shapes.[133] The biggest fully dehydrogenated GQD that they were able to prepare has the same edge state as HBC but is made of 222 carbons (Figure 1.15a).[125,131] This structure was modified to exhibit a hole in the middle (6 carbon missing in the structure).[126] This GQD made of 216 carbon atoms was prepared from the circular compound 5,5′,5″,5‴,5⁗,5⁗′-Hexa-ethynyl-hexa-*m*-phenylene to demonstrate that as for GNM, the presence of a hole in the regular structure can increase the gap from 1.8 eV for the particles containing 222 carbons to 2.2 eV for 216 carbons (Figure 1.15b). They prepared a bigger structure made of 474 carbons but the increase in size also increased the insolubility of the final product and the

dehydrogenation of the polyphenylene dendrimer was not complete (Figure 1.16). From the interpretation of the mass spectrometry, they suggested that the molecule takes a propeller-like structure.[134]

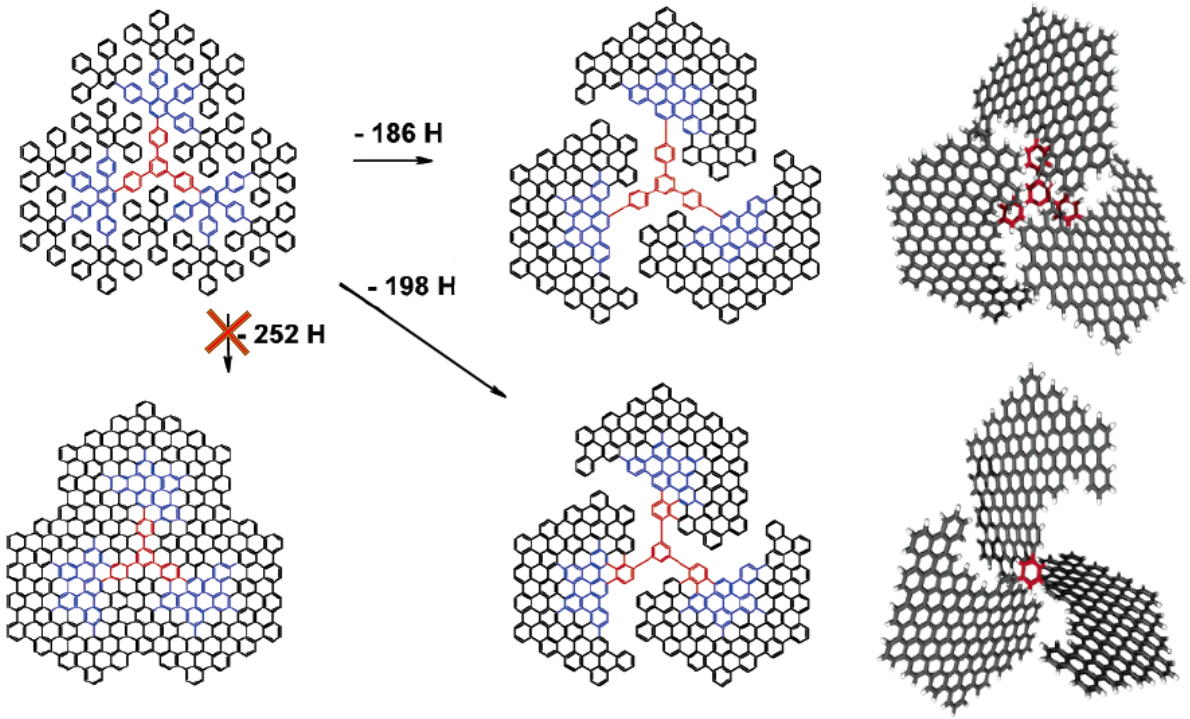

Figure 1.16: Partially dehydrogenated structures identified with 474 carbon atoms.[134]

Considering the low solubility of these compounds, it is necessary to use characterization methods that are different from the usual nuclear magnetic resonance (NMR) and electrospray ionization mass spectrometry (ESI-MS). While the smaller PAHs can be characterized in laser-desorption ionization mass spectrometry (LDI-MS), the ones with more than 96 carbons need matrix assisted laser-desorption ionization mass spectrometry (MALDI-MS).

In 2010, the group of Liang-Shi Li used the strategy developed by Klaus Müllen to produce new GQDs (Figure 1.17).[135,136] To improve the solubility, they introduced three 2,4,6-trialkylylphenyl group so that the alkyl chains prevent stacking between the cores of the GQDs. More importantly, they were able to fabricate nanoparticles with slightly different structures,

for example with a missing part or with two additional carbon atoms (in red on the figure). This precision level on the structure can be reached only by bottom-up synthetic chemistry.

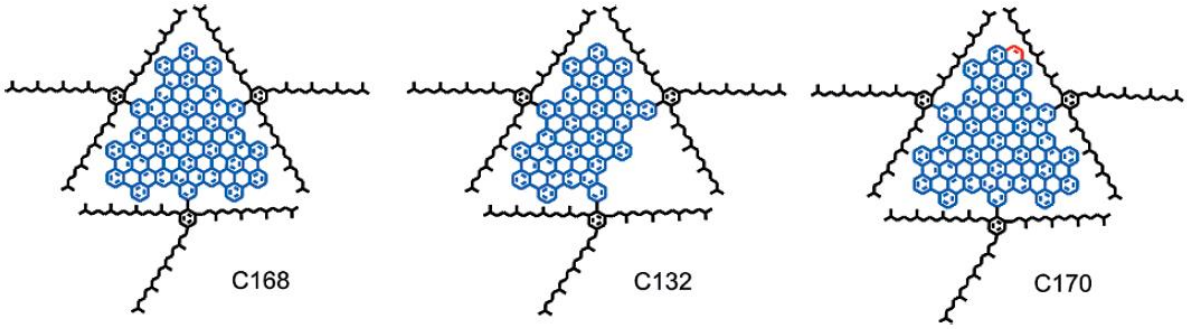

Figure 1.17: L.S. Li structures derived from the C168 structure.[137]

Finally, the group of Müllen modified the periphery of their GQDs with chlorine atoms.[138] Because of the bulkiness of the chlorine atoms, compared to hydrogen which are normally present at the periphery of the molecules, the GQDs are distorted which increases greatly the solubility of the materials. After exploring GQDs for one decade, the group of Müllen used its experience to develop the bottom-up synthesis of GNRs.

1.4.3. Graphene nanoribbons

1.4.3.1. Graphene nanoribbons prepared in solution

The bottom-up synthesis of nanoribbon-like molecules was initiated in the seventies by J.K. Stille who developed conjugated polymers.[139] They prepared a ladder-type polymer consisting of hexagonal and pentagonal aromatic rings using Diels-Alder polycycloaddition (Figure 1.18a). The low solubility of the compound due to π- π interactions was solved in 1994 by the group of D. Schlüter who added flexible alkyl loops to prevent the stacking (Figure 1.18b).[140,141] The first fully conjugated ladder type polymer only made of hexagonal aromatics was done from 1,4-dibromo-2,5-bis(4-decyloxybenzoyl)benzene using Yamomoto coupling followed by an olefination of the carbonyl groups. This polymer was synthesized by the group of U. Scherf in 1993 and it was called “angular polyacene” (Figure 1.18c).[142,143]

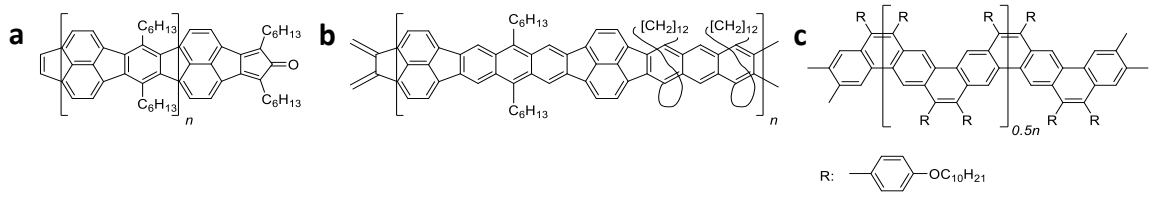

Figure 1.18: First GNR-like structures of a) J.K. Stille[139], d) D. Schlüter[141] and c) U. Scherf.[142]

From this narrow GNR new synthesis were developed to expand the width from a single benzene ring to polyphenylenes with different edges type. In 2000, the group of K. Müllen used the A_2B_2-type Diels-Alder polymerization to prepare the first GNR with a width larger than a single phenyl ring but it resulted in a mixture of randomly kinked GNRs (GNR **1**) (Figure 1.19a).[144] They chose to change of strategy for a A_2B_2-type Suzuki coupling for the synthesis of the GNR **2** (Figure 1.19b);[145] however, the length of those GNRs was limited to *ca.* 10 nm.[146] In 2012, they moved to the AA-type Yamamoto coupling to prepare GNR **3** exhibiting widths between 1.54-1.98 nm and with lengths of *ca.* 20-30 nm and an optical bandgap of 1.1 eV (Figure 1.19c).[147]

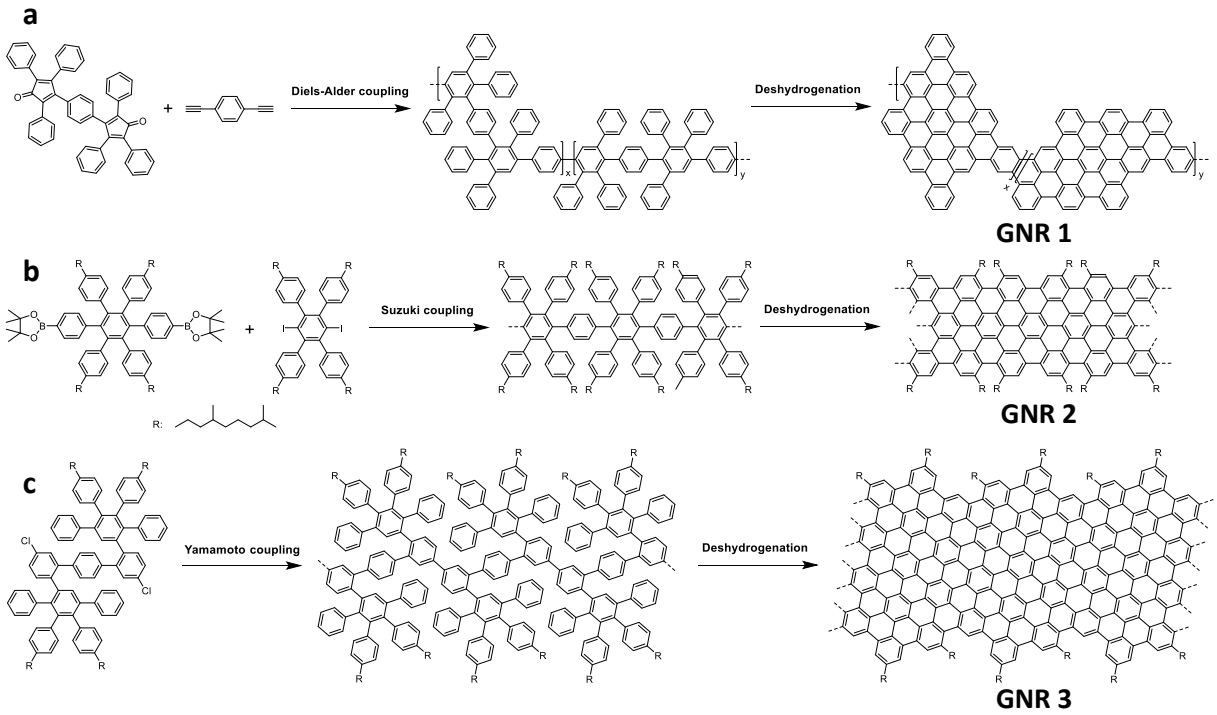

*Figure 1.19: a) A_2B_2-type Diels-Alder coupling between the 1,4-bis(tetraphenylcyclopentadienone-yl)benzene and the 1,4-diethynylbenzene. The polymer was dehydrogenated by $Cu(CF_3SO_3)_2$ and $AlCl_3$ to give GNR **1**.[144] b) A_2B_2-type Suzuki coupling*

between the bis-boronic ester and the 1,4-diiodo-2,3,5,6-tetraphenylbenzene. The polymer was dehydrogenated with $FeCl_3$ in DCM and nitromethane.[145] *c) AA-type Yamamoto coupling of chlorinated monomer in the presence of nickel complexes. The polymer was dehydrogenated with $FeCl_3$ in DCM and nitromethane.*[147]

In 2014, K. Müllen and coworkers applied the Diels-Alder polymerization of a AB-type monomer followed by a treatment with $FeCl_3$ to prepare a "cove-type"[148] edge GNR with unprecedented lengths of 600 nm (Figure 1.20a).[149] The GNR exhibited a width between 0.69-1.13 nm. Later, they also prepared a wider version of this GNR in which two rows of phenyl were added (Figure 1.20b). The new GNR exhibited a width between 1.54-1.98 nm and in accordance with the theory,[150,151] the optical bandgap decreased from 1.9 to 1.2 eV for GNRs **4** and **5**, respectively.[152] They also applied the chlorination method developed on GQDs to the narrow cove-type edges GNR (Figure 1.20c) and found that, as verified by theoretical calculation,[150] the optical bandgap decreased of 0.2 eV to reach 1.7 eV.[138]

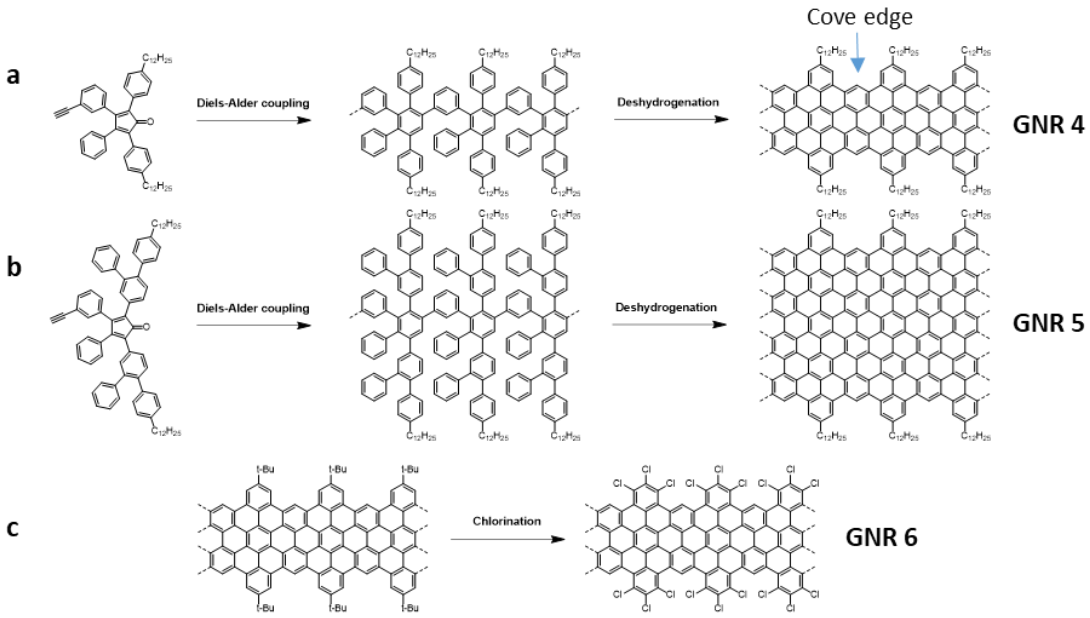

Figure 1.20: Two cove-type edge GNR with width between a) 0.69-1.13nm[149] *and b) 1.54-1.98nm.*[152] *The reaction conditions are the same for both GNR **4** and **5**, the AB-type Diels-Alder coupling is an intramolecular reaction of the cyclopentadienones bearing an acetylenic bond.*

*c) The GNR bearing tert-Butyl groups is subjected to $AlCl_3$ and ICl in CCl_4 to give the corresponding chlorinated GNR **6**.*[138]

While the K. Müllen group focused on the control of the witdh, other groups like the group of J. F. Morin have explored new structure like helically coiled GNRs (Figure 1.21). Their work is based on the use of photochemical cyclodehydrochlorination of chlorinated precursors.[153] Depending on the precursor they were able to prepare nanocoils with various helical pitch and doping.[154,155]

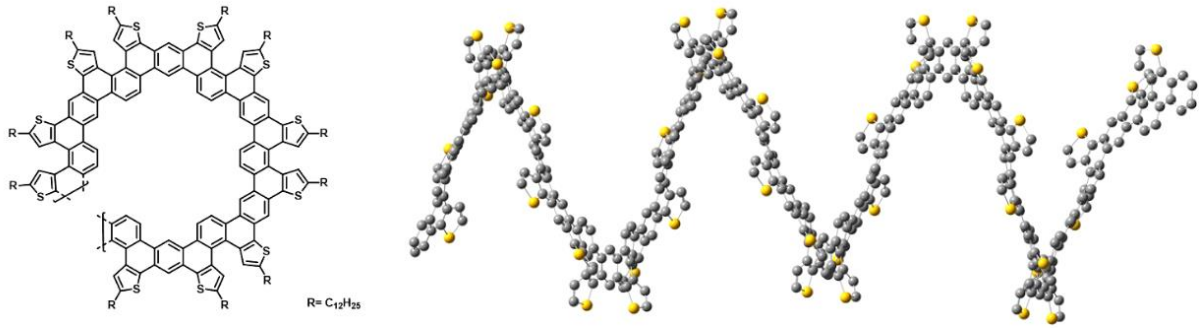

Figure 1.21: Structure of the doped helical GNR of J.F. Morin.[154]

In 2014 the group of Sinitskii prepared a more than 100 nm long chevron-type GNR in solution.[156] After the synthesis, the GNR was deposited on Au crystal and imaged by STM. It is worth mentioning that the fabrication of the same chevron-type GNR was reported previously directly on Au(111) by Müllen and Fasel in their seminal article of 2010.[157] In the case of Sinitskii and coworkers, it is remarkable that they obtained very well defined defect-free structures in solution. Another approach based on the cyclization of alkyne substituents on a linear poly(2,6-dialkynyl-p-phenylene) was developed by Chalifoux in 2016 however, it is limited to narrow width and length of about 35nm.[158]

1.4.3.2. Graphene nanoribbons prepared on surface

For the synthesis of GNRs in the Ultra-High Vacuum (UHV) chamber of a STM, the surface realizes both the coupling of aryl halides as for the synthesis of molecular wires[159] and catalyzes the dehydrogenation. The first example of GNR synthesized on surface was reported in 2010 by the groups of Müllen and Fasel *via* surface-assisted Ullmann[160] coupling (Figure

1.22).[157] It was shown that upon heating, the carbon halogen bond was cleaved and a biradical intermediate is formed.[161] These radicals then recombined to form a carbon-carbon bond that led to the formation of a linear polymer. After heating at higher temperature, the polyphenylene polymer was dehydrogenated to form a fully delocalized GNR.

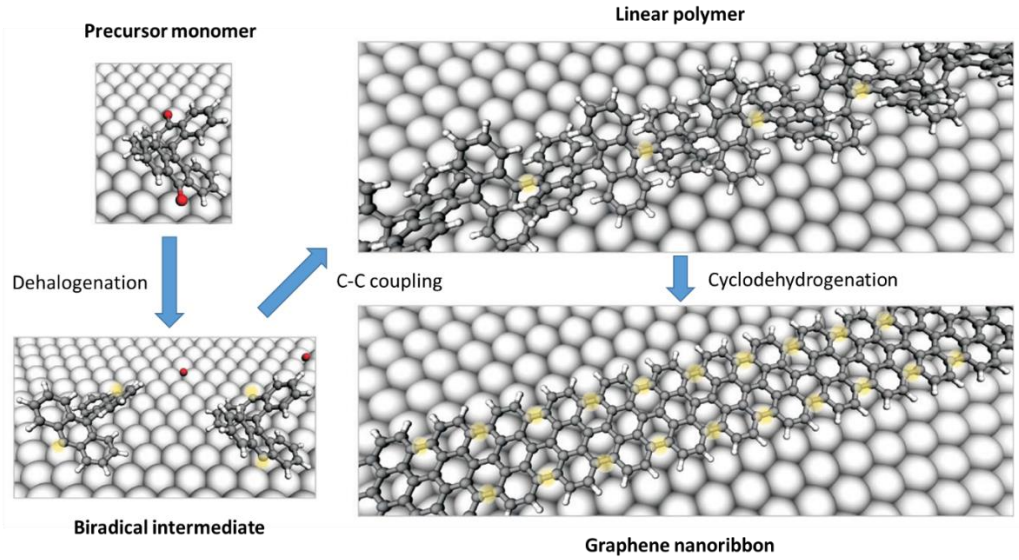

Figure 1.22: Principle of the surface preparation of GNR (adapted from ref 157*)*

This procedure allowed the preparation of the armchair edges GNRs with several rows of carbon atoms *N*=5,[162] 6,[163] 7,[157,164] 13,[165] 14[166] and 15[167] (Figure 1.23). For a long time, only armchair GNRs were available due to the usual synthetic route which used aryl-aryl coupling along the armchair direction rather than the zig-zag direction. In 2016, the group of Müllen synthesized a new U-shaped precursor which was used by R. Fasel to prepare a *N*=6 zigzag GNR in a STM chamber.[168] The structure of the precursor can be tuned with groups like phenyls in the edges to control the band structure of the edge states. These structures may confirm the theoretical predictions that showed promising properties for spintronic like spin confinement[169] and filtering.[170,171]

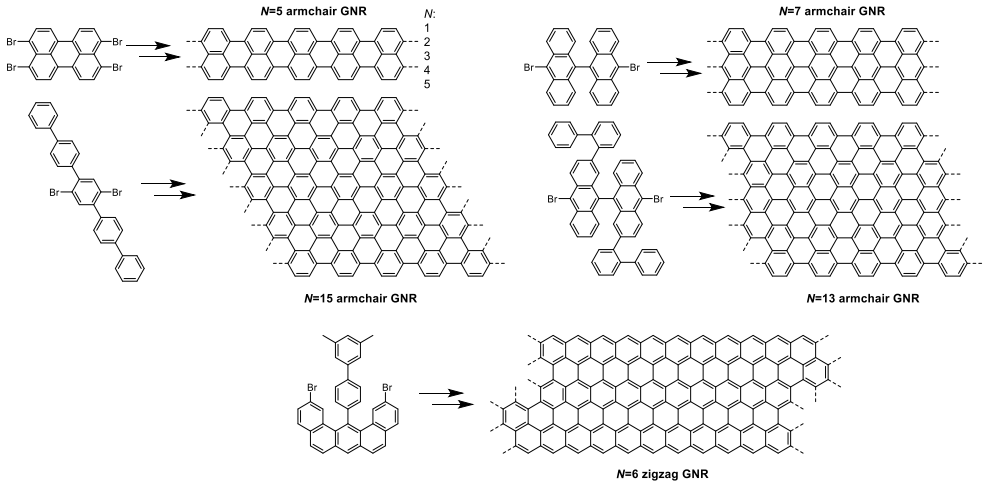

Figure 1.23: Structures of armchair GNRs prepared under UHV in a STM with N=5,[162] *7,*[157,164] *13*[165] *and 15*[167] *and zigzag GNR*[168] *and the corresponding brominated precursors.*

The combination of solution chemistry and surface chemistry gave rise to many interesting 1D structures and a wide range of GNRs with various edge states, width and length are now available. These works on 1D structures and the developments made on surface chemistry allowed the transfer of this knowledge for the development of 2D structures on surface.

1.4.4. 2D structures: graphene nanomesh

The bottom-up synthesis of 2D structures is based on the use of an organic precursor bearing non-linearly oriented functional groups that are evaporated in a STM chamber on a metallic substrate. This precursor should react with the surface and be mobile to reach other precursors. The synthesis of polyphenylene networks on surface were reported almost simultaneously by Lackinger and by Müllen and Fasel in 2009.[172,173] In the first case, the synthesis was based on the surface polymerization of 1,3,5-tris-(4-bromophenyl)benzene on Cu(111) (Figure 1.24a) however, the network produced showed pentagonal, hexagonal or heptagonal structures which led to a great irregularity in the network. A more controlled network could be obtained with the Müllen and Fasel method using the polymerization of an hexaiodo-substituted cyclohexa-*m*-phenylene macrocycle on Ag(111) (Figure 1.24b).[173] The covalent bonds between the molecules were formed *via* the Ullmann reaction as in the case of the formation of GNRs.

The same type of structure was reported by Müllen and Fasel using cyclotrimerization of the 1,3,5- tris-(4'-ethynylphenyl)benzene. The cyclotrimerization was done on Au(111) and it formed a phenyl ring between each precursor to create the 2D polyphenylene dendrimer (Figure 1.24c).[174]

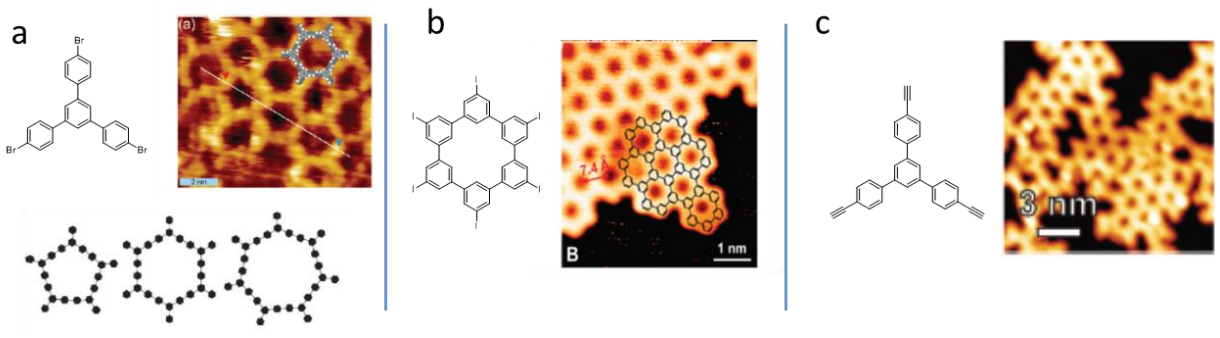

Figure 1.24: Chemical structure and STM images of 2D networks of polyphenylenes from: a) 1,3,5-tris-(4'-bromophenyl)benzene,[172] b) cyclohexa-m-phenylene[173] and c) 1,3,5-tris-(4'-ethynylphenyl)benzene.[174]

The preparation of 2D covalent networks on surface has been widely investigated during the last decades; in some aspect these networks are related to GNMs. In the following section I will report briefly some examples of realization.

The first example was described in 2007 by Leonhard Grill and Stephan Hecht who reported the realization of a covalent porphyrin network on Au(111) surface.[175] The size of the network was limited and contained defect; however, this work opened the route of the realization of 2D networks on surface. In 2013, Cardenas et *al.* prepared a 2D network containing doping from the tetrabromotetrathienoanthracene (TBTTA).[176] The precursor was annealed at 300°C on a Ag(111) surface and the resulting network was well extended but some irregularities arised due to the rotational disorder of the precursor (Figure 1.25a). In 2017 Liu et *al.* fabricated *N*-doped network using the 2,7,13,18-tetrabromodibenzo[a,c]dibenzo[5,6:7,8]quinoxalino-[2,3-i]phenazine (2-TBQP) as the precursor (Figure 1.25b).[177] They annealed the precursor at 250°C on an Au(111) surface and observed both the expected network where each molecule reacted with 4 others and the

linear structure where the molecule only reacts with 2 others to form a ribbon. Those two mechanisms create a lot of irregularities in the resulting network. S. Clair and M. Abel developed 2D networks based on organometallic structures.[178] They used the co-evaporation of iron and 1,2,4,5-tetracyanobenzene on a Ag(111) or Au(111) surface with a 2:1 stoichiometry. Once the molecules were on the surface, they reacted to form a polymeric iron phthalocyanine network (Figure 1.25c).

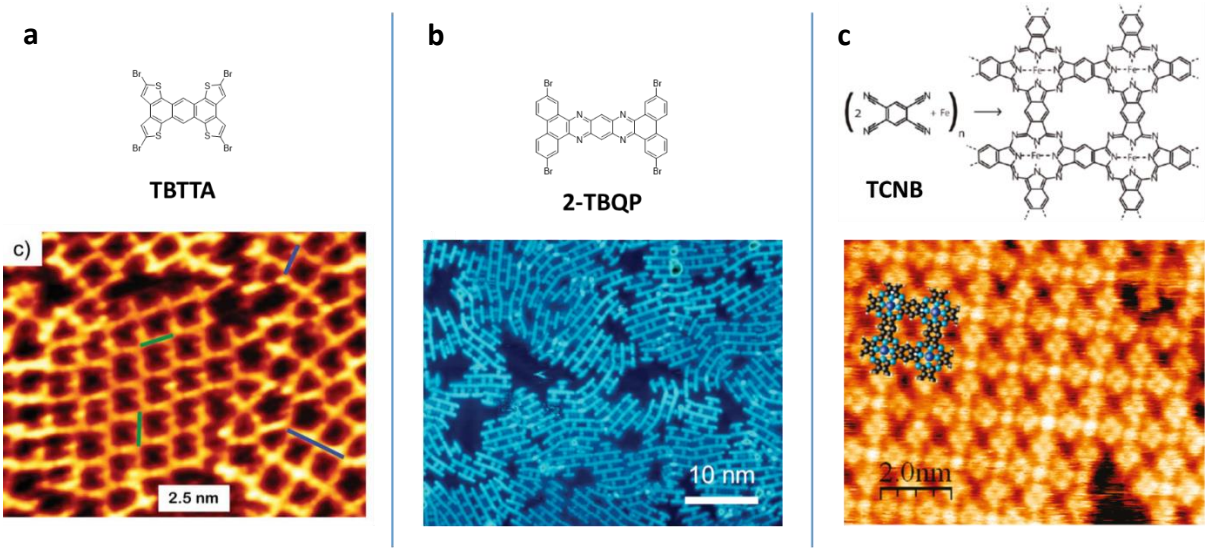

Figure 1.25: Chemical structure and STM images of doped 2D networks of polyphenylenes a) tetrabromotetrathienoanthracene,[176] b) 2-TBQP[177] and c) TCNB.[178]

Finally, other examples of 2D networks based on triphenylamine cores appeared in literature recently.[179,180] Despite their interest, only a limited number of nanomesh-like structures have been reported and in all examples reported so far the "graphene necks" are constituted by a single C-C bond between two phenyl rings which reduces significantly the delocalization of electrons and decreases the conductivity. To increase the conductivity while keeping a decent bandgap, it is necessary to develop new precursors that lead to structures with bigger width as it was done from the first conjugated ladder type polymers up to the current GNRs.

In this part I tried to review the different approaches to synthesize "gaped" graphene materials. While the top-down approach is a powerful method for the mass production of graphene based materials, the low control on the final structures (edge states, oxidation states

and sizes and shapes) makes this method not suitable for some applications in optics or electronics. For applications that require a precise control of the structure, the best approach is the bottom-up approach; however, this approach is much more complicated and time consuming, making it less suitable for mass production.

During my PhD, I focused on the synthesis of graphene quantum dots for applications in optics. After the description of the fabrication of the materials; in the following section, I will give an overview of the techniques used for the optical characterization of these materials and particularly for the detection of single photon emission.

1.5. Optical properties

1.5.1. Absorption and photoluminescence

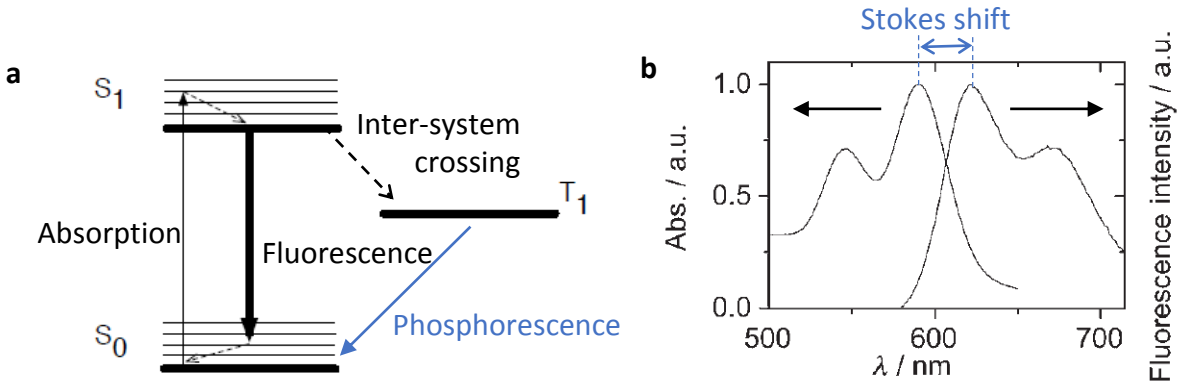

Figure 1.26: a) Jablonski diagram and b) example of normalized absorption and fluorescence of a perylene bisimide dye.[181]

The properties of a dye that absorbs and emits light are described by the energetic levels schematically represented in the Jablonski diagram (Figure 1.26a).[182] Three levels are represented, two singlet state levels (S_0 and S_1) and a triplet state level (T_1). As the dye absorbs a photon, an electron from the ground state S_0 goes to the excited state S_1. The wavelength of this absorption is defined by the gap between S_0 and S_1, only wavelengths that correspond to energy equal or greater than this gap will be absorbed. Once the electron is in the excited state, it can go back to the ground state with two mechanisms of PL, the fluorescence and the phosphorescence.

Chapter 1: Introduction

Fluorescence is the direct transition from the lowest energy level of the excited state S_1 to the ground state S_0. An electron that was excited at a higher level than the lowest level of the excited state can undergo an energy and momentum relaxation towards this level through non-radiative mechanisms like Coulomb scattering and interaction with phonons. Fluorescence is a radiative mechanism where the wavelength of the emitted photon depends on the gap between S_0 and S_1. This emission is most of the time at higher wavelength than the absorption due to the relaxation through non-radiative mechanisms that decreases the energy of the photon emitted (Figure 1.26a). This induces a shift between absorption and emission called Stokes shift (Figure 1.26b).

The phosphorescence phenomenon is caused by the intersystem crossing: an electron can go from the excited state S_1 to the triplet state T_1. Once in this state, the electron is trapped with only “forbidden” transitions available to return to lower states. Whereas the transitions are kinetically unfavorable, they can still happen and give rise to phosphorescence. Whereas the typical decay times for fluorescence are within the range of 0.5 to 20 ns, the decay times for phosphorescence can go from milliseconds up to hours.

Both Fluorescence and phosphorescence can be interrupted definitely or randomly by extinction phenomena like photobleaching or photoblinking. The photobleaching is the irreversible extinction caused by the overexposure of dyes to light (Figure 1.27a). This phenomenon is caused by light-induced chemical degradation that quench the emitted light. Photobleaching is a big issue for the optical study of low quantities of dyes since it will prevent extended experiment time. The photoblinking is the reversible extinction of the emitted light caused by the transition into non- or low-emissive states (Figure 1.27b). This a random phenomenon that can disrupt an experiment inducing uncontrolled extinctions. Both photobleaching and photoblinking are properties that depend mostly on the stability and band structure of the material. Therefore, it is important for optical application to have a material with a high chemical stability.

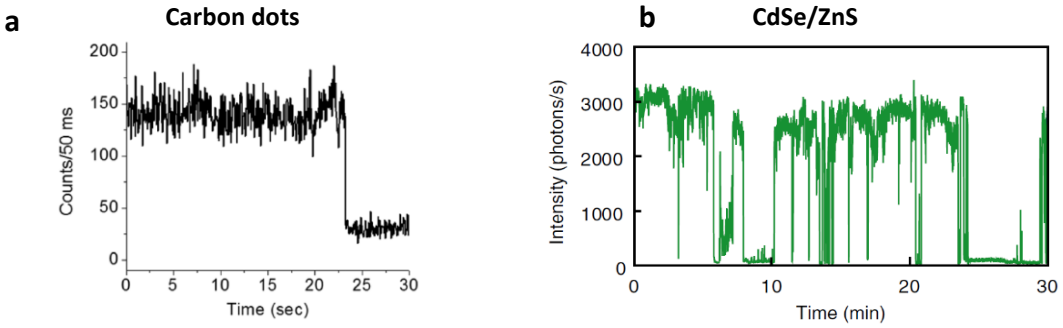

Figure 1.27: Fluorescence intensity traces as the function of time showing for different emitters a) photobleaching in reduced carbon dots[183] *and b) photoblinking in CdSe/ZnS QDs.*[184]

The chemical stability of graphene led to the realization of graphene quantum dots for optical application. In particular, the fundamental optical properties of GQDs synthesized *via* the bottom-up approach is supposed to enable important developments toward the use of such materials for a large range of application from biology to cryptography. However, due to the low solubility of GQD, their dispersion is a key point to observe the single molecule properties.

1.5.2. Dispersion and optical properties of PAHs

The absorption[185] and PL[186] of PAHs has been widely investigated theoretically. The study by Cocchi et *al.* on the difference between coronene and HBC and HBC and bigger structures with the same edge type demonstrated the influence of respectively the edge type and the size on the PL (Figure 1.28).

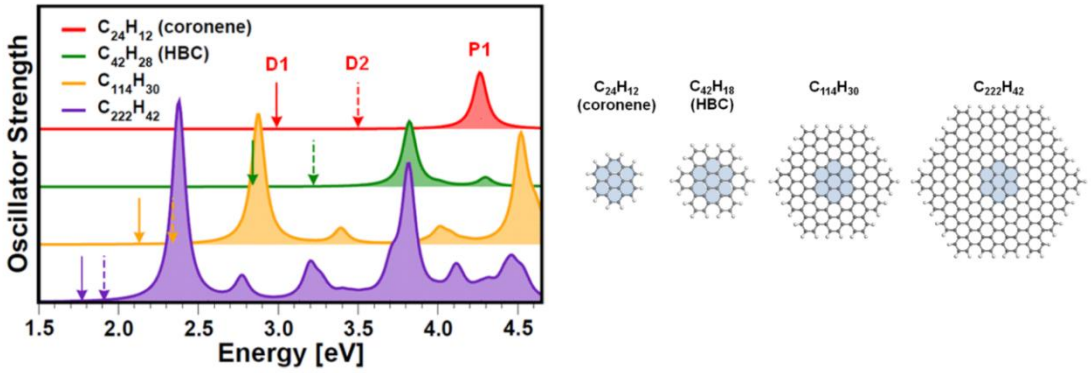

Figure 1.28: Theoretical calculation for the emission of coronene, HBC and bigger GQDs ($C_{114}H_{30}$ and $C_{222}H_{42}$).[186]

The optical study of large PAHs started with the study of the absorption and emission of HBC.[187] This compound exhibits a large emission band at 500 nm but its low solubility (especially when the molecule is not functionalized with alkyl chains) makes difficult the identification of the intrinsic emission properties of HBC versus the emission properties of aggregates necessarily present in solution. In 2012, J. N. Coleman studied the dispersion of HBC in organic solvents like *N*-cyclohexylpyrrolidone (CHP) and tetrahydrofurane (THF).[188] They verified the quality of the dispersion by measuring the absorption, the emission and performing the photoluminescence excitation (PLE) map (Figure 1.29). The map is done by measuring the emission spectra for every excitation. The PL intensity is coded with color from blue to red. For the PL and the PLE, narrow peaks are typical of a good dispersion because aggregation tends to broaden the peaks due to the inter-molecular energy and/or electron transfers. The result in Figure 1.29 on organic solvents clearly shows that CHP is a better solvent for HBC than THF.

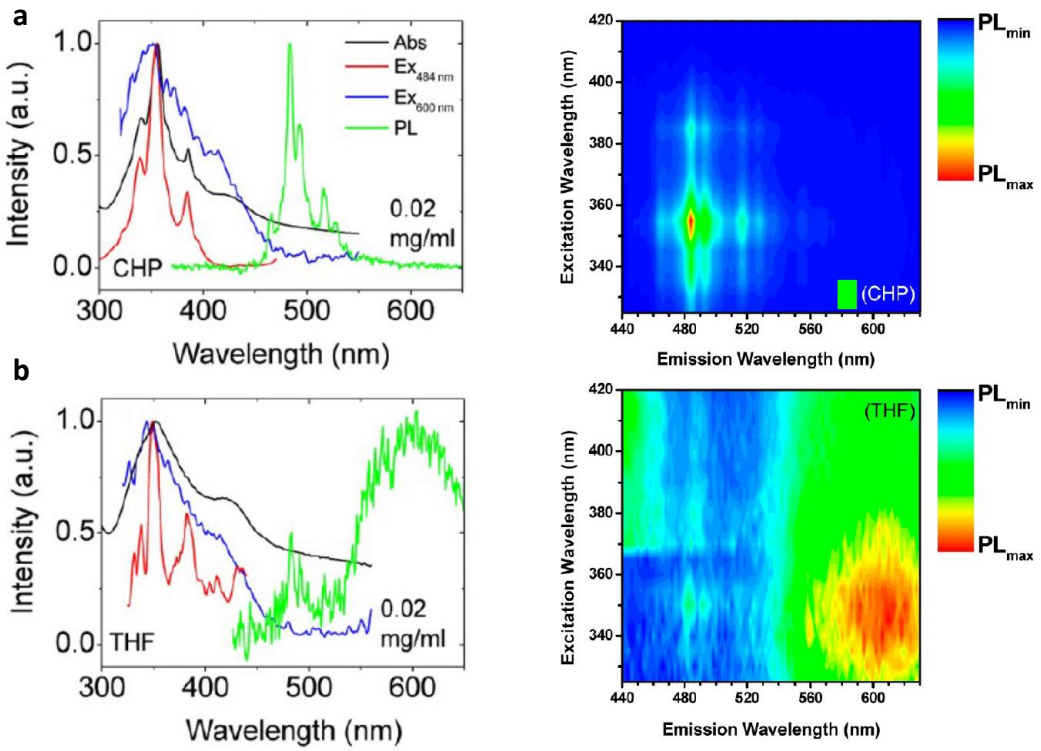

Figure 1.29: Absorption and emission spectra and PLE map of HBC in a) CHP and b) THF. (adapted from ref [188])

A similar study was performed by the group of A. Hirsch in water using surfactants to stabilize the HBC.[189] The surfactant studied were sodium cholate (SC), sodium deoxycholate (SDC) and sodium dodecylbenzenesulfonate (SDBS) and as for organic solvents, they measured the absorption, the PL and the PLE map (Figure 1.30). The results for these surfactant showed that SDC is the better surfactant to disperse HBC in water while SC was decent and SDBS a poor surfactant. They also studied the lifetime of the photoluminescence in the three surfactants and they could fit the lifetime with triexponantial decay functions.

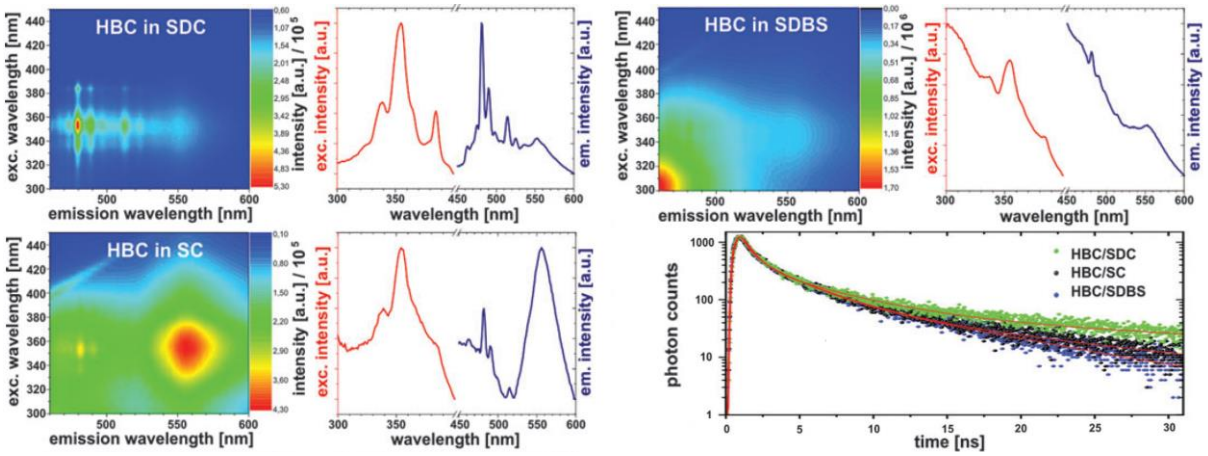

Figure 1.30: Absorption and PL spectra, PLE map and PL lifetime of HBC in SDC, SDBS and SC. (adapted from ref [189])

The quality of the dispersion clearly has an influence on the optical properties measured. For single photon emission properties, it is mandatory to look at single molecule level and therefore, to disperse and individualize molecules properly in solution.

1.5.3. Single photon emitters

A key step for the study of single photon emitters is the control of the uniqueness of the emitting molecule. This control is done measuring the temporal correlations of the photons collected.

If the light source is an usual thermal light source, photons are emitted by groups, this is the bunching effect. It means that for "short" times τ (compared to the lifetime of the excited state) there are more than one photon emitted (Figure 1.31 bottom). For coherent light like

laser, the probability of emission for each photon is independent which means that the emission of a photon does not increase the chance that another photon is emitted at the same time like in thermal light. This does not lead to any bunching or anti-bunching effect; the photons are uncorrelated. In the case of a single photon emitter, photons can only be emitted one by one and for "short" times there should be a gap between two photons, this phenomenon is called antibunching.[190]

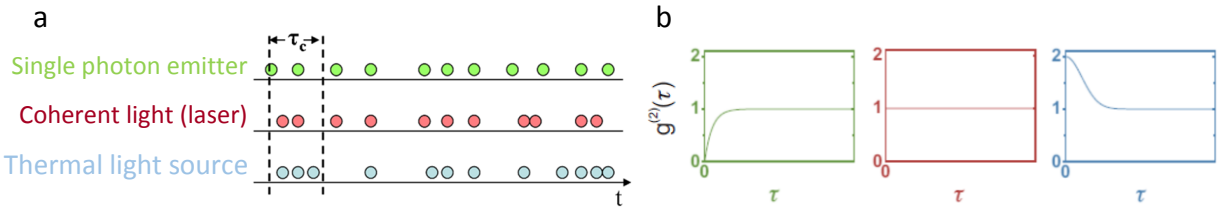

Figure 1.31: a) Schematic of the photoemission for various light sources and b) example of corresponding second order correlation function.

However, experimentally, the direct value of this time period cannot be determined with only one detector since detectors need a down-time of about 30 ns.[182] The setup used is the Hanbury Brown-Twiss arrangement[191] with two detectors and a 50:50 beam splitter (Figure 1.32). In this setup, one detector acts as the "start" for the measurement and the second one as the "stop" and this gives the continuous time difference between two photons. This can be registered and converted from time to amplitude and with the proper normalization,[192] the amplitude is proportional to the second order coherence function $g^{(2)}(\tau) \equiv \frac{<I(t)I(t+\tau)>}{<I(t)>^2}$. The $g^{(2)}(\tau)$ functions for each type of light are represented Figure 1.31b and show that each one of them can be discriminated at low values of the time difference τ.

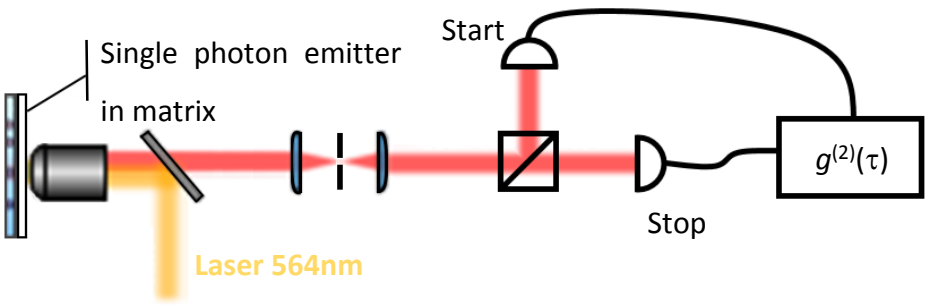

Figure 1.32: Schematic representation of the Hanbury Brown-Twiss setup.

The first single molecules emission measurements were achieved on pentacene dispersed in *para*-terphenyl in the nineties by M. Orrit[193] and W.E. Moerner[194] at cryogenic temperatures. They launched a wide range of new experiments and applications but they were limited by the complicated conditions they had to use for their experiments. However, this was overcome in 1996 with ambient temperature single molecules observation of $DiIC_{12}$ (a cyanine dye commonly used in biology)[195] and it was soon followed by the NV color centers in diamond[192,196,197] and nanocrystals of semiconductor CdSe.[198–200] While all these structures have interesting single photon emission properties, they suffer from both photoblinking and photobleaching and as a result they are unpractical for experiments of more than a few minutes (Figure 1.33).

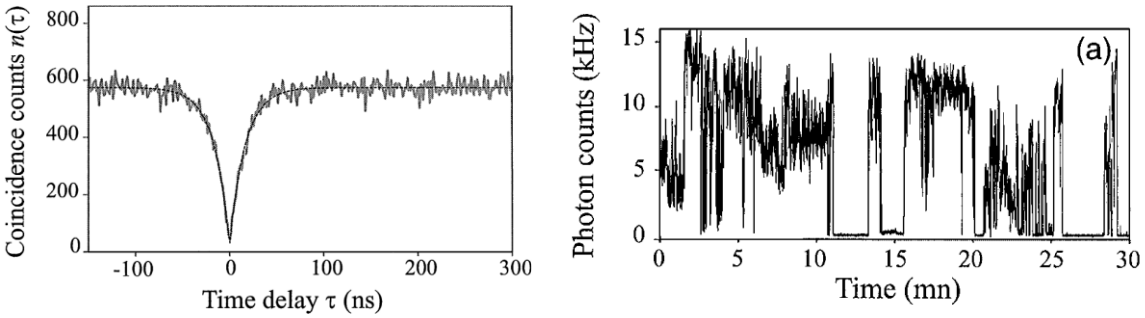

Figure 1.33: Coincidence counts and time trace of a CdSe QD.[200]

1.6. Aim of this work

This work results from the collaboration between the Laboratoire d'Innovation en Chimie des Surfaces Et Nanosciences (LICSEN) and the Laboratoire Aimé Cotton (LAC), it started in 2014. The work at LICSEN is focused on the chemical synthesis of the materials and the LAC studies the dispersion in matrix and the optical properties of the materials. The objective of this collaboration is to investigate the intrinsic properties of the graphene quantum dots made by the bottom-up approach.

The first objective of this project was to re-synthesize GQDs previously described by the group of K. Müllen and investigate the advanced optical properties of these compounds. With the wide range of structures available, it was interesting to see the effect of various parameters

like the size, shape or edge states on the properties. The first part is centered on triangular-shaped GQD made of 96 carbon atoms (C_{96}).

From the experience gained on the C_{96} family, we decided to explore, in the second part of this manuscript, new types of graphene materials which is an intermediate between GQDs and GNRs. This material should have a 1D structure but with a controlled length to see the impact of the length variation on the electronic properties. In fact, the characterization of the optical properties for GNRs is hardly conclusive due to the large variations of length caused by the polymeric approach. This intermediate material between a GQD and a GNR is designated as Graphene Nanorods (GNRods).

Finally, after the exploration of 0D and 1D structures, we turned to 2D structures in the last part of this work. Currently, GNMs are mostly made by the top-down approach and the bottom-up synthesis of 2D structures is limited to small width and reduced delocalization of the electrons. To expand this width there is a need for new organic precursors that should self-organize on surfaces and be reactive to self-assemble upon heating. To explore structures that were already theoretically predicted, there are needs for specific precursors to have specific necks/holes width ratio.

1.7. References

(1) Wallace, P. R. The Band Theory of Graphite. *Phys. Rev.* **1947**, *71*, 622–634.

(2) McClure, J. W. Diamagnetism of Graphene. *Phys. Rev.* **1956**, *104*, 666–671.

(3) Slonczewski, J. C.; Weiss, P. R. Band Structure of Graphite. *Phys. Rev.* **1958**, *109*, 272–279.

(4) Peierls, R. Quelques Propriétés Typiques Des Corps Solides. *Ann. l'I.H.P.* **1935**, *5*, 177–222.

(5) Landau, L. Zur Theorie Der Phasenumwandlungen II. *Phys. Z. Sowjet* **1937**, *11*, 26–35.

(6) Novoselov, K. S.; Geim, A. K.; Morozov, S. V; Jiang, D.; Zhang, Y.; Dubonos, S. V; Grigorieva, I. V; Firsov, A. A. Electric Field in Atomically Thin Carbon Films. *Science* **2004**, *306*, 666–669.

(7) DiVincenzo, D. P.; Mele, E. J. Self-Consistent Effective-Mass Theory for Intralayer Screening in Graphite Intercalation Compounds. *Phys. Rev. B* **1984**, *29*, 1685–1694.

(8) Bolotin, K. I.; Sikes, K. J.; Jiang, Z.; Klima, M.; Fudenberg, G.; Hone, J.; Kim, P.; Stormer, H. L. Ultrahigh Electron Mobility in Suspended Graphene. *Solid State Commun.* **2008**, *146*, 351–355.

(9) Zhao, Q.; Nardelli, M. B.; Bernholc, J. Ultimate Strength of Carbon Nanotubes: A Theoretical Study. *Phys. Rev. B* **2002**, *65*, 144105.

(10) Schulz, B. J.; Dünweg, B.; Binder, K.; Müller, M. Suppression of Capillary Wave Broadening of Interfaces in Binary Alloys Due to Elastic Interactions. *Phys. Rev. Lett.* **2005**, *95*, 096101.

(11) Peres, N.; Lopes dos Santos, J.; Stauber, T. Phenomenological Study of the Electronic Transport Coefficients of Graphene. *Phys. Rev. B* **2007**, *76*, 073412.

(12) Saito, K.; Nakamura, J.; Natori, A. Ballistic Thermal Conductance of a Graphene Sheet. *Phys. Rev. B* **2007**, *76*, 115409.

(13) Zheng, Y.; Ando, T. Hall Conductivity of a Two-Dimensional Graphite System. *Phys. Rev. B* **2002**, *65*, 245420.

(14) Gusynin, V. P.; Sharapov, S. G. Unconventional Integer Quantum Hall Effect in Graphene. *Phys. Rev. Lett.* **2005**, *95*, 146801.

(15) Peres, N. M. R.; Guinea, F.; Castro Neto, A. H. Electronic Properties of Two-Dimensional Carbon. *Ann. Phys.* **2006**, *321*, 1559–1567.

(16) Zhang, Y. B.; Tan, Y. W.; Stormer, H. L.; Kim, P. Experimental Observation of the Quantum Hall Effect and Berry's Phase in Graphene. *Nature* **2005**, *438*, 201–204.

(17) Lee, C.; Wei, X.; Kysar, J. W.; Hone, J. Measurement of the Elastic Properties and Intrinsic Strength of Monolayer Graphene. *Science* **2008**, *321*, 385–388.

(18) Balandin, A. A.; Ghosh, S.; Bao, W.; Calizo, I.; Teweldebrhan, D.; Miao, F.; Lau, C. N. Superior Thermal Conductivity of Single-Layer Graphene. *Nano Lett.* **2008**, *8*, 902–907.

(19) Castro Neto, A. H.; Guinea, F.; Peres, N. M. R.; Novoselov, K. S.; Geim, A. K. The Electronic Properties of Graphene. *Rev. Mod. Phys.* **2009**, *81*, 109–162.

(20) Yang, X.; Cheng, C.; Wang, Y.; Qiu, L.; Li, D. Liquid-Mediated Dense Integration of Graphene Materials for Compact Capacitive Energy Storage. *Science* **2013**, *341*, 534–537.

(21) Huang, C.; Li, C.; Shi, G. Graphene Based Catalysts. *Energy Environ. Sci.* **2012**, *5*, 8848–8868.

(22) Chen, D.; Tang, L.; Li, J. Graphene-Based Materials in Electrochemistry. *Chem. Soc. Rev.* **2010**, *39*, 3157–3180.

(23) Bonaccorso, F.; Sun, Z.; Hasan, T.; Ferrari, A. C. Graphene Photonics and Optoelectronics. *Nat. Photonics* **2010**, *4*, 611–622.

(24) Schwierz, F. Graphene Transistors. *Nat. Nanotechnol.* **2010**, *5*, 487–496.

(25) Lin, Y. M.; Dimitrakopoulos, C.; Jenkins, K. A.; Farmer, D. B.; Chiu, H. Y.; Grill, A.; Avouris, P. 100-GHz Transistors from Wafer-Scale Epitaxial Graphene. *Science* **2010**, *327*, 662–662.

(26) Kim, K.; Choi, J. Y.; Kim, T.; Cho, S. H.; Chung, H. J. A Role for Graphene in Silicon-Based Semiconductor Devices. *Nature* **2011**, *479*, 338–344.

(27) Kedzierski, J.; Hsu, P.-L. H. P.-L.; Healey, P.; Wyatt, P. W.; Keast, C. L.; Sprinkle, M.; Berger, C.; Heer, W. a. De. Epitaxial Graphene Transistors on SiC Substrates. *IEEE Trans. Electron Devices* **2008**, *55*, 2007–2008.

(28) Berashevich, J.; Chakraborty, T. Tunable Band Gap and Magnetic Ordering by Adsorption of Molecules on Graphene. *Phys. Rev. B* **2009**, *80*, 033404.

(29) Yavari, F.; Kritzinger, C.; Gaire, C.; Song, L.; Gulapalli, H.; Borca-Tasciuc, T.; Ajayan, P. M.; Koratkar, N. Tunable Bandgap in Graphene by the Controlled Adsorption of Water Molecules. *Small* **2010**, *6*, 2535–2538.

(30) Dong, X.; Fu, D.; Fang, W.; Shi, Y.; Chen, P.; Li, L. J. Doping Single-Layer Graphene with Aromatic Molecules. *Small* **2009**, *5*, 1422–1426.

(31) Georgakilas, V.; Tiwari, J. N.; Kemp, K. C.; Perman, J. A.; Bourlinos, A. B.; Kim, K. S.; Zboril, R. Noncovalent Functionalization of Graphene and Graphene Oxide for Energy Materials, Biosensing, Catalytic, and Biomedical Applications. *Chem. Rev.* **2016**, *116*, 5464–5519.

(32) Kozlov, S. M.; Viñes, F.; Görling, A. On the Interaction of Polycyclic Aromatic Compounds with Graphene. *Carbon* **2012**, *50*, 2482–2492.

(33) Kozlov, S. M.; Viñes, F.; Görling, A. Bandgap Engineering of Graphene by Physisorbed Adsorbates. *Adv. Mater.* **2011**, *23*, 2638–2643.

(34) Yang, H.; Mayne, A. J.; Comtet, G.; Dujardin, G.; Kuk, Y.; Sonnet, P.; Stauffer, L.; Nagarajan, S.; Gourdon, A. STM Imaging, Spectroscopy and Manipulation of a Self-Assembled PTCDI Monolayer on Epitaxial Graphene. *Phys. Chem. Chem. Phys.* **2013**, *15*, 4939.

(35) Kong, L.; Enders, A.; Rahman, T. S.; Dowben, P. A. Molecular Adsorption on Graphene. *J. Phys. Condens. Matter* **2014**, *26*, 443001.

(36) Sofo, J. O.; Chaudhari, A. S.; Barber, G. D. Graphane: A Two-Dimensional Hydrocarbon. *Phys. Rev. B* **2007**, *75*, 153401.

(37) Elias, D. C.; Nair, R. R.; Mohiuddin, T. M. G.; Morozov, S. V.; Blake, P.; Halsall, M. P.; Ferrare, A. C.; Boukhvalov, D. W.; Katsnelson, M. I.; Geim, A. K.; et al. Control of Graphene's Properties by Reversible Hydrogenation: Evidence for Graphane. *Science* **2009**, *323*, 610–613.

(38) Pulci, O.; Gori, P.; Marsili, M.; Garbuio, V.; Del Sole, R.; Bechstedt, F. Strong Excitons in Novel Two-Dimensional Crystals: Silicane and Germanane. *EPL* **2012**, *98*, 37004.

(39) Zhao, Y.; Dai, Z.; Zhang, C. A First Principles Method to Simulate Electron Mobilities in 2D Materials Related Content Intrinsic Electronic Transport and Thermoelectric Power Factor in N-Type Doped Monolayer MoS2. *New J. Phys.* **2014**, *16*, 105009.

(40) Son, J.; Lee, S.; Kim, S. J.; Park, B. C.; Lee, H. K.; Kim, S.; Kim, J. H.; Hong, B. H.; Hong, J. Hydrogenated Monolayer Graphene with Reversible and Tunable Wide Band Gap and Its Field-Effect Transistor. *Nat. Commun.* **2016**, *7*, 13261.

(41) Nair, R. R.; Ren, W.; Jalil, R.; Riaz, I.; Kravets, V. G.; Britnell, L.; Blake, P.; Schedin, F.; Mayorov, A. S.; Yuan, S.; et al. Fluorographene: A Two-Dimensional Counterpart of Teflon. *Small* **2010**, *6*, 2877–2884.

(42) Jeon, K. J.; Lee, Z.; Pollak, E.; Moreschini, L.; Bostwick, A.; Park, C. M.; Mendelsberg, R.; Radmilovic, V.; Kostecki, R.; Richardson, T. J.; et al. Fluorographene: A Wide Bandgap Semiconductor with Ultraviolet Luminescence. *ACS Nano* **2011**, *5*, 1042–1046.

(43) Niyogi, S.; Bekyarova, E.; Hong, J.; Khizroev, S.; Berger, C.; de Heer, W.; Haddon, R. C. Covalent Chemistry for Graphene Electronics. *J. Phys. Chem. Lett.* **2011**, *2*, 2487–2498.

(44) Bekyarova, E.; Sarkar, S.; Wang, F.; Itkis, M. E.; Kalinina, I.; Tian, X.; Haddon, R. C. Effect of Covalent Chemistry on the Electronic Structure and Properties of Carbon Nanotubes and Graphene. *Acc. Chem. Res.* **2013**, *46*, 65–76.

(45) Chua, C. K.; Pumera, M. Covalent Chemistry on Graphene. *Chem. Soc. Rev.* **2013**, *42*, 3222–3233.

(46) Niyogi, S.; Bekyarova, E.; Itkis, M. E.; Zhang, H.; Shepperd, K.; Hicks, J.; Sprinkle, M.; Berger, C.; Lau, C. N.; Deheer, W. A.; et al. Spectroscopy of Covalently Functionalized Graphene. *Nano Lett.* **2010**, *10*, 4061–4066.

(47) Choi, J.; Kim, K. J.; Kim, B.; Lee, H.; Kim, S. Covalent Functionalization of Epitaxial Graphene by Azidotrimethylsilane. *J. Phys. Chem. C* **2009**, *113*, 9433–9435.

(48) Wang, H.; Zhou, Y.; Wu, D.; Liao, L.; Zhao, S.; Peng, H.; Liu, Z. Synthesis of Boron-Doped Graphene Monolayers Using the Sole Solid Feedstock by Chemical Vapor Deposition. *Small* **2013**, *9*, 1316–1320.

(49) Panchakarla, L. S.; Subrahmanyam, K. S.; Saha, S. K.; Govindaraj, A.; Krishnamurthy, H. R.; Waghmare, U. V.; Rao, C. N. R. Synthesis, Structure, and Properties of Boron- and Nitrogen-Doped Graphene. *Adv. Mater.* **2009**, *21*, 4726–4730.

(50) Liu, L.; Ryu, S.; Tomasik, M. R.; Stolyarova, E.; Jung, N.; Hybertsen, M. S.; Steigerwald, M. L.; Brus, L. E.; Flynn, G. W. Graphene Oxidation: Thickness-Dependent Etching and Strong Chemical Doping. *Nano Lett.* **2008**, *8*, 1965–1970.

(51) Wei, D.; Liu, Y.; Wang, Y.; Zhang, H.; Huang, L.; Yu, G. Synthesis of N-Doped Graphene by Chemical Vapor Deposition and Its Electrical Properties. *Nano Lett.* **2009**, *9*, 1752–1758.

(52) Joucken, F.; Tison, Y.; Lagoute, J.; Dumont, J.; Cabosart, D.; Zheng, B.; Repain, V.; Chacon, C.; Girard, Y.; Botello-Méndez, A. R.; et al. Localized State and Charge Transfer in Nitrogen-Doped Graphene. *Phys. Rev. B* **2012**, *85*, 161408.

(53) Some, S.; Kim, J.; Lee, K.; Kulkarni, A.; Yoon, Y.; Lee, S.; Kim, T.; Lee, H. Highly Air-Stable Phosphorus-Doped n-Type Graphene Field-Effect Transistors. *Adv. Mater.* **2012**, *24*, 5481–5486.

(54) Wang, H. M.; Wang, H. X.; Chen, Y.; Liu, Y. J.; Zhao, J. X.; Cai, Q. H.; Wang, X. Z. Phosphorus-Doped Graphene and (8, 0) Carbon Nanotube: Structural, Electronic, Magnetic Properties, and Chemical Reactivity. *Appl. Surf. Sci.* **2013**, *273*, 302–309.

(55) Casolo, S.; Martinazzo, R.; Tantardini, G. F. Band Engineering in Graphene with Superlattices of Substitutional Defects. *J. Phys. Chem. C* **2011**, *115*, 3250–3256.

(56) Usachov, D.; Vilkov, O.; Grüneis, A.; Haberer, D.; Fedorov, A.; Adamchuk, V. K.; Preobrajenski, A. B.; Dudin, P.; Barinov, A.; Oehzelt, M.; et al. Nitrogen-Doped Graphene: Efficient Growth, Structure, and Electronic Properties. *Nano Lett.* **2011**, *11*, 5401–5407.

(57) Alivisatos, A. P. Semiconductor Clusters, Nanocrystals, and Quantum Dots. *Science* **1996**, *271*, 933–937.

(58) Pietryga, J. M.; Park, Y. S.; Lim, J.; Fidler, A. F.; Bae, W. K.; Brovelli, S.; Klimov, V. I. Spectroscopic and Device Aspects of Nanocrystal Quantum Dots. *Chem. Rev.* **2016**, *116*, 10513–10622.

(59) Hildebrandt, N.; Spillmann, C. M.; Russ Algar, W.; Pons, T.; Stewart, M. H.; Oh, E.; Susumu, K.; Díaz, S. A.; Delehanty, J. B.; Medintz, I. L. Energy Transfer with Semiconductor Quantum Dot Bioconjugates: A Versatile Platform for Biosensing, Energy Harvesting, and Other Developing Applications. *Chem. Rev.* **2017**, *117*, 536–711.

(60) Pedersen, T. G.; Flindt, C.; Pedersen, J.; Mortensen, N. A.; Jauho, A. P.; Pedersen, K. Graphene Antidot Lattices: Designed Defects and Spin Qubits. *Phys. Rev. Lett.* **2008**, *100*, 136804.

(61) Li, L.; Wu, G.; Yang, G.; Peng, J.; Zhao, J.; Zhu, J.-J. Focusing on Luminescent Graphene Quantum Dots: Current Status and Future Perspectives. *Nanoscale* **2013**, *5*, 4015–4039.

(62) Ye, R.; Xiang, C.; Lin, J.; Peng, Z.; Huang, K.; Yan, Z.; Cook, N. P.; Samuel, E. L. G.; Hwang, C. C.; Ruan, G.; et al. Coal as an Abundant Source of Graphene Quantum Dots. *Nat. Commun.* **2013**, *4*, 2943.

(63) Sun, X.; Liu, Z.; Welsher, K.; Robinson, J. T.; Goodwin, A.; Zaric, S.; Dai, H. Nano-Graphene Oxide for Cellular Imaging and Drug Delivery. *Nano Res.* **2008**, *1*, 203–212.

(64) Hummers, W. S.; Offeman, R. E. Preparation of Graphitic Oxide. *J. Am. Chem. Soc.* **1958**, *80*, 1339–1339.

(65) Li, L. L.; Ji, J.; Fei, R.; Wang, C. Z.; Lu, Q.; Zhang, J. R.; Jiang, L. P.; Zhu, J. J. A Facile Microwave Avenue to Electrochemiluminescent Two-Color Graphene Quantum Dots. *Adv. Funct. Mater.* **2012**, *22*, 2971–2979.

(66) Chen, S.; Liu, J.-W.; Chen, M.-L.; Chen, X.-W.; Wang, J.-H. Unusual Emission Transformation of Graphene Quantum Dots Induced by Self-Assembled Aggregation. *Chem. Commun.* **2012**, *48*, 7637–7639.

(67) Shen, J.; Zhu, Y.; Yang, X.; Li, C. Graphene Quantum Dots: Emergent Nanolights for Bioimaging, Sensors, Catalysis and Photovoltaic Devices. *Chem. Commun.* **2012**, *48*, 3686–3699.

(68) Lu, J.; Yang, J. X.; Wang, J.; Lim, A.; Wang, S.; Loh, K. P. One-Pot Synthesis of Fluorescent Carbon Nanoribbons, Nanoparticles, and Graphene by the Exfoliation of Graphite in Ionic Liquids. *ACS Nano* **2009**, *3*, 2367–2375.

(69) Zhang, M.; Bai, L.; Shang, W.; Xie, W.; Ma, H.; Fu, Y.; Fang, D.; Sun, H.; Fan, L.; Han, M.; et al. Facile Synthesis of Water-Soluble, Highly Fluorescent Graphene Quantum Dots as a Robust Biological Label for Stem Cells. *J. Mater. Chem.* **2012**, *22*, 7461.

(70) Lu, J.; Yeo, P. S. E.; Gan, C. K.; Wu, P.; Loh, K. P. Transforming C 60 Molecules into Graphene Quantum Dots. *Nat. Nanotechnol.* **2011**, *6*, 247–252.

(71) Zhuo, S.; Shao, M.; Lee, S. T. Upconversion and Downconversion Fluorescent Graphene Quantum Dots: Ultrasonic Preparation and Photocatalysis. *ACS Nano* **2012**, *6*, 1059–1064.

(72) Xu, Q.; Zhou, Q.; Hua, Z.; Xue, Q.; Zhang, C.; Wang, X.; Pan, D.; Xiao, M. Single-Particle Spectroscopic Measurements of Fluorescent Graphene Quantum Dots. *ACS Nano* **2013**, *7*, 10654–10661.

(73) Han, M. Y.; Özyilmaz, B.; Zhang, Y.; Kim, P. Energy Band-Gap Engineering of Graphene Nanoribbons. *Phys. Rev. Lett.* **2007**, *98*, 206805.

(74) Son, Y. W.; Cohen, M. L.; Louie, S. G. Energy Gaps in Graphene Nanoribbons. *Phys. Rev. Lett.* **2006**, *97*, 216803.

(75) Barone, V.; Hod, O.; Scuseria, G. E. Electronic Structure and Stability of Semiconducting Graphene Nanoribbons. *Nano Lett.* **2006**, *6*, 2748–2754.

(76) Nakada, K.; Fujita, M.; Dresselhaus, G.; Dresselhaus, M. S. Edge State in Graphene Ribbons: Nanometer Size Effect and Edge Shape Dependence. *Phys. Rev. B* **1996**, *54*, 17954–17961.

(77) Li, X.; Wang, X.; Zhang, L.; Lee, S.; Dai, H. Chemically Derived, Ultrasmooth Graphene Nanoribbon Semiconductors. *Science* **2008**, *319*, 1229–1232.

(78) Wang, X.; Ouyang, Y.; Li, X.; Wang, H.; Guo, J.; Dai, H. Room-Temperature All-Semiconducting Sub-10-Nm Graphene Nanoribbon Field-Effect Transistors. *Phys. Rev. Lett.* **2008**, *100*, 206803.

(79) Chen, Z.; Lin, Y. M.; Rooks, M. J.; Avouris, P. Graphene Nano-Ribbon Electronics. *Phys. E Low-Dimensional Syst. Nanostructures* **2007**, *40*, 228–232.

(80) Yang, L.; Park, C. H.; Son, Y. W.; Cohen, M. L.; Louie, S. G. Quasiparticle Energies and Band Gaps in Graphene Nanoribbons. *Phys. Rev. Lett.* **2007**, *99*, 186801.

(81) Jiao, L.; Zhang, L.; Wang, X.; Diankov, G.; Dai, H. Narrow Graphene Nanoribbons from Carbon Nanotubes. *Nature* **2009**, *458*, 877–880.

(82) Kosynkin, D. V; Higginbotham, A. L.; Sinitskii, A.; Lomeda, J. R.; Dimiev, A.; Price, B. K.; Tour, J. M. Longitudinal Unzipping of Carbon Nanotubes to Form Graphene Nanoribbons. *Nature* **2009**, *458*, 872–876.

(83) Oswald, W.; Wu, Z. Energy Gaps in Graphene Nanomeshes. *Phys. Rev. B* **2012**, *85*, 115431.

(84) Fischbein, M. D.; Drndić, M. Electron Beam Nanosculpting of Suspended Graphene Sheets. *Appl. Phys. Lett.* **2008**, *93*, 113107.

(85) Standop, S.; Lehtinen, O.; Herbig, C.; Lewes-Malandrakis, G.; Craes, F.; Kotakoski, J.; Michely, T.; Krasheninnikov, A. V; Busse, C. Ion Impacts on Graphene/Ir(111): Interface Channeling, Vacancy Funnels, and a Nanomesh. *Nano Lett.* **2013**, *13*, 1948–1955.

(86) Bai, J.; Zhong, X.; Jiang, S.; Huang, Y.; Duan, X. Graphene Nanomesh. *Nat. Nanotechnol.* **2010**, *5*, 190–194.

(87) Kim, M.; Safron, N. S.; Han, E.; Arnold, M. S.; Gopalan, P. Fabrication and Characterization of Large-Area, Semiconducting Nanoperforated Graphene Materials. *Nano Lett.* **2010**, *10*, 1125–1131.

(88) Liang, X.; Jung, Y. S.; Wu, S.; Ismach, A.; Olynick, D. L.; Cabrini, S.; Bokor, J. Formation of Bandgap and Subbands in Graphene Nanomeshes with Sub-10 Nm Ribbon Width Fabricated via Nanoimprint Lithography. *Nano Lett.* **2010**, *10*, 2454–2460.

(89) Sinitskii, A.; Tour, J. M. Patterning Graphene through the Self-Assembled Templates: Toward Periodic Two-Dimensional Graphene Nanostructures with Semiconductor Properties. *J. Am. Chem. Soc.* **2010**, *132*, 14730–14732.

(90) Zeng, Z.; Huang, X.; Yin, Z.; Li, H.; Chen, Y.; Li, H.; Zhang, Q.; Ma, J.; Boey, F.; Zhang, H. Fabrication of Graphene Nanomesh by Using an Anodic Aluminum Oxide Membrane as a Template. *Adv. Mater.* **2012**, *24*, 4138–4142.

(91) Liu, J.; Cai, H.; Yu, X.; Zhang, K.; Li, X.; Li, J.; Pan, N.; Shi, Q.; Luo, Y.; Wang, X. Fabrication of Graphene Nanomesh and Improved Chemical Enhancement for Raman Spectroscopy. *J. Phys. Chem. C* **2012**, *116*, 15741–15746.

(92) Akhavan, O. Graphene Nanomesh by ZnO Nanorod Photocatalysts. *ACS Nano* **2010**, *4*, 4174–4180.

(93) Berrada, S.; Hung Nguyen, V.; Querlioz, D.; Saint-Martin, J.; Alarcón, A.; Chassat, C.; Bournel, A.; Dollfus, P. Graphene Nanomesh Transistor with High on/off Ratio and Good Saturation Behavior. *Appl. Phys. Lett.* **2013**, *103*, 183509.

(94) Yang, Y.; Yang, X.; Zou, X.; Wu, S.; Wan, D.; Cao, A.; Liao, L.; Yuan, Q.; Duan, X. Ultrafine Graphene Nanomesh with Large On/Off Ratio for High-Performance Flexible Biosensors. *Adv. Funct. Mater.* **2017**, *27*, 1604096.

(95) Cagliani, A.; Mackenzie, D. M. A.; Tschammer, L. K.; Pizzocchero, F.; Almdal, K.; Bøggild, P. Large-Area Nanopatterned Graphene for Ultrasensitive Gas Sensing. *Nano Res.* **2014**, *7*, 743–754.

(96) Hung Nguyen, V.; Chung Nguyen, M.; Nguyen, H. V.; Dollfus, P. Disorder Effects on Electronic Bandgap and Transport in Graphene-Nanomesh-Based Structures. *J. Appl. Phys.* **2013**, *113*, 013702.

(97) Power, S. R.; Jauho, A. P. Electronic Transport in Disordered Graphene Antidot Lattice Devices. *Phys. Rev. B* **2014**, *90*, 115408.

(98) Ji, X.; Zhang, J.; Wang, Y.; Qian, H.; Yu, Z. Influence of Edge Imperfections on the Transport Behavior of

Graphene Nanomeshes. *Nanoscale* **2013**, *5*, 2527–2531.

(99) Strauss, V.; Margraf, J. T.; Dolle, C.; Butz, B.; Nacken, T. J.; Walter, J.; Bauer, W.; Peukert, W.; Spiecker, E.; Clark, T.; et al. Carbon Nanodots: Toward a Comprehensive Understanding of Their Photoluminescence. *J. Am. Chem. Soc.* **2014**, *136*, 17308–17316.

(100) Bourlinos, A. B.; Stassinopoulos, A.; Anglos, D.; Zboril, R.; Karakassides, M.; Giannelis, E. P. Surface Functionalized Carbogenic Quantum Dots. *Small* **2008**, *4*, 455–458.

(101) Bourlinos, A. B.; Stassinopoulos, A.; Anglos, D.; Zboril, R.; Georgakilas, V.; Giannelis, E. P. Photoluminescent Carbogenic Dots. *Chem. Mater.* **2008**, *20*, 4539–4541.

(102) Krysmann, M. J.; Kelarakis, A.; Dallas, P.; Giannelis, E. P. Formation Mechanism of Carbogenic Nanoparticles with Dual Photoluminescence Emission. *J. Am. Chem. Soc.* **2012**, *134*, 747–750.

(103) Ito, S.; Wehmeier, M.; Brand, J. D.; Kübel, C.; Epsch, R.; Rabe, J. P.; Müllen, K. Synthesis and Self-Assembly of Functionalized Hexa-Peri-Hexabenzocoronenes. *Chem. - A Eur. J.* **2000**, *6*, 4327–4342.

(104) Fetzer, J. C.; Kershaw, J. R. Identification of Large Polycyclic Aromatic Hydrocarbons in a Coal Tar Pitch. *Fuel* **1995**, *74*, 1533–1536.

(105) Clar, E.; Ironside, C. . T.; Zander, M. ASYMMETRIC AND SYMMETRIC ANNELLATION EFFECTS--III* BENZOCORONENES. *Tetrahedron* **1959**, *6*, 358–363.

(106) Clar, E.; Zander, M. 1 : 2-Benxocoronene and Naphtho(2' : 3'-1 : 2)Coronene. *J. Chem. Soc.* **1958**, *0*, 1577–1579.

(107) Clar, E.; Zander, M. 927. Syntheses of Coronene and 1 : 2-7 : 8-Dibenzocoronene. *J. Chem. Soc.* **1957**, *0*, 4616–4619.

(108) Clar, E. Zur Kenntnis Mehrkerniger Aromatischer Kohlenwasserstoffe Und Ihrer Abkömmlinge, IV. Mitteil.: Naphthophenanthrene Und Ihre Chinone. *Berichte der Dtsch. Chem. Gesellschaft* **1929**, *62*, 1574–1582.

(109) Scholl, R.; Seer, C.; Weitzenböck, R. Perylen, Ein Hoch Kondensierter Aromatischer Kohlenwasserstoff C20H12. *Berichte der Dtsch. Chem. Gesellschaft* **1910**, *43*, 2202–2209.

(110) Scholl, R.; Mansfeld, J. Meso-Benzdianthron (Helianthron), Meso-Naphthodianthron, Und Ein Neuer Weg Zum Flavanthren. *Berichte der Dtsch. Chem. Gesellschaft* **1910**, *43*, 1734–1746.

(111) Scholl, R.; Seer, C. Einführung Mehrerer Phthalsäure-Reste in Aromatische Verbindungen. III. Versuche Mit Thianthren, Dimethyl-Thianthren, Thiodiphenylamin UndN-Methyl-Thiodiphenylamin. *Berichte der Dtsch. Chem. Gesellschaft* **1911**, *44*, 1233–1249.

(112) Scholl, R.; Seer, C. Abspaltung Aromatisch Gebundenen Wasserstoffs Und Verknüpfung Aromatischer Kerne Durch Aluminiumchlorid. *Justus Liebigs Ann. Chem.* **1912**, *394*, 111–177.

(113) Zander, M. Neueres Über Polycyclische Aromatische Kohlenwasserstoffe. *Angew. Chemie* **1960**, *72*, 513–521.

(114) Zander, M.; Franke, W. Dicoronyl Und Dicoronylen. *Chem. Ber.* **1958**, *91*, 2794–2797.

(115) Wu, J.; Fechtenkötter, A.; Gauss, J.; Watson, M. D.; Kastler, M.; Fechtenkötter, C.; Wagner, M.; Müllen, K. Controlled Self-Assembly of Hexa-Peri-Hexabenzocoronenes in Solution. *J. Am. Chem. Soc.* **2004**, *126*, 11311–11321.

(116) Wu, J.; Baumgarten, M.; Debije, M. G.; Warman, J. M.; Müllen, K. Arylamine-Substituted Hexa-Peri-Hexabenzocoronenes: Facile Synthesis and Their Potential Applications as "Coaxial" Hole-Transport Materials. *Angew. Chemie - Int. Ed.* **2004**, *43*, 5331–5335.

(117) Wu, J.; Watson, M. D.; Müllen, K. The Versatile Synthesis and Self-Assembly of Star-Type Hexabenzocoronenes. *Angew. Chemie Int. Ed.* **2003**, *42*, 5329–5333.

(118) Lee, M.; Kim, J.-W.; Peleshanko, S.; Larson, K.; Yoo, Y.-S.; Vaknin, D.; Markutsya, S.; Tsukruk, V. V. Amphiphilic Hairy Disks with Branched Hydrophilic Tails and a Hexa-Peri-Hexabenzocoronene Core. *J. Am. Chem. Soc.* **2002**, *124*, 9121–9128.

(119) Wu, J.; Li, J.; Kolb, U.; Müllen, K. A Water-Soluble Hexa-Peri-Hexabenzocoronene: Synthesis, Self-Assembly and Role as Template for Porous Silica with Aligned Nanochannels. *Chem. Commun.* **2006**, *0*, 48–50.

(120) Schmidt-Mende, L.; Fechtenkötter, A.; Müllen, K.; Moons, E.; Friend, R. H.; MacKenzie, J. D. Self-Organized Discotic Liquid Crystals for High-Efficiency Organic Photovoltaics. *Science* **2001**, *293*, 1119–1122.

(121) Fleming, A. J.; Coleman, J. N.; Dalton, A. B.; Fechtenko, A.; Watson, M. D.; Mu, K.; Byrne, H. J.; Blau, W. J. Optical Spectroscopy of Isolated and Aggregate Hexabenzocoronene Derivatives: A Study of Self-Assembling Molecular Nanowires. *J. Phys. Chem. B* **2003**, *107*, 37–43.

(122) Pisula, W.; Tomović, Ž.; El Hamaoui, B.; Watson, M. D.; Pakula, T.; Müllen, K. Control of the Homeotropic Order of Discotic Hexa-Peri-Hexabenzocoronenes. *Adv. Funct. Mater.* **2005**, *15*, 893–904.

(123) Pisula, W.; Kastler, M.; Wasserfallen, D.; Pakula, T.; Mullen, K. Exceptionally Long-Range Self-Assembly of Hexa-Peri-Hexabenzocoronene with Dove-Tailed Alkyl Substituents. *J. Am. Chem. Soc.* **2004**, *126*, 8074–8075.

(124) Shklyarevskiy, I. O.; Jonkheijm, P.; Stutzmann, N.; Wasserberg, D.; Wondergem, H. J.; Christianen, P. C. M.; Schenning, A. P. H. J.; Leeuw, D. M. De; Wu, J.; Mu, K.; et al. High Anisotropy of the Field-Effect Transistor Mobility in Magnetically Aligned Discotic Liquid-Crystalline Semiconductors. *J. Am. Chem. Soc.* **2005**, *127*, 16233–16237.

(125) Simpson, C. D.; Brand, J. D.; Berresheim, A. J.; Przybilla, L.; Räder, H. J.; Müllen, K. Synthesis of a Giant 222 Carbon Graphite Sheet. *Chem. - A Eur. J.* **2002**, *8*, 1424–1429.

(126) Beser, U.; Kastler, M.; Maghsoumi, A.; Wagner, M.; Castiglioni, C.; Tommasini, M.; Narita, A.; Feng, X.; Müllen, K. A C216-Nanographene Molecule with Defined Cavity as Extended Coronoid. *J. Am. Chem. Soc.* **2016**, *138*, 4322–4325.

(127) Böhme, T.; Simpson, C. D.; Müllen, K.; Rabe, J. P. Current-Voltage Characteristics of a Homologous Series

of Polycyclic Aromatic Hydrocarbons. *Chemistry* **2007**, *13*, 7349–7357.

(128) Müller, M.; Iyer, V. S.; Kübel, C.; Enkelmann, V.; Müllen, K. Polycyclic Aromatic Hydrocarbons by Cyclodehydrogenation and Skeletal Rearrangement of Oligophenylenes. *Angew. Chemie (International Ed. English)* **1997**, *36*, 1607–1610.

(129) Muller, M.; Mauermann-Düll, H.; Wagner, M.; Enkelmann, V.; Müllen, K. A Cycloaddition - Cyclodehydrogenation Route from Stilbenoids to Extended Aromatic Hydrocarbons. *Angew. Chemie - Int. Ed.* **1995**, *34*, 1583–1586.

(130) Feng, X.; Wu, J.; Ai, M.; Pisula, W.; Zhi, L.; Rabe, J. P.; Müllen, K. Triangle-Shaped Polycyclic Aromatic Hydrocarbons. *Angew. Chemie - Int. Ed.* **2007**, *46*, 3033–3036.

(131) Iyer, V. S.; Wehmeier, M.; Diedrich, J.; Keegstra, M. A.; Müllen, K. From Hexa-Peri-Hexabenzocoronene to "Superacenes." *Angew. Chemie - Int. Ed.* **1997**, *36*, 1603–1607.

(132) Wu, J.; Enkelmann, V.; Müllen, K. From Branched Hydrocarbon Propellers to C 3 -Symmetric Graphite Disks. *J. Org. Chem.* **2004**, *69*, 5179–5186.

(133) Morgenroth, F.; Reuther, E.; Müllen, K. Polyphenylene Dendrimers: From Three-Dimensional to Two-Dimensional Structures. *Angew. Chemie - Int. Ed.* **1997**, *36*, 631–634.

(134) Simpson, C. D.; Mattersteig, G.; Martin, K.; Gherghel, L.; Bauer, R. E.; Räder, H. J.; Müllen, K. Nanosized Molecular Propellers by Cyclodehydrogenation of Polyphenylene Dendrimers. *J. Am. Chem. Soc.* **2004**, *126*, 3139–3147.

(135) Yan, X.; Cui, X.; Li, L. S. Synthesis of Large , Stable Colloidal Graphene Quantum Dots with Tunable Size. *J. Am. Chem. Soc.* **2010**, *132*, 5944–5945.

(136) Yan, X.; Cui, X.; Li, B.; Li, L. S. Large, Solution-Processable Graphene Quantum Dots as Light Absorbers for Photovoltaics. *Nano Lett.* **2010**, *10*, 1869–1873.

(137) Yan, X.; Cui, X.; Li, L.; V, I. U. Synthesis of Large , Stable Colloidal Graphene Quantum Dots with Tunable Size. *J. Am. Chem. Soc.* **2010**, *132*, 5944–5945.

(138) Tan, Y. Z.; Yang, B.; Parvez, K.; Narita, A.; Osella, S.; Beljonne, D.; Feng, X.; Müllen, K. Atomically Precise Edge Chlorination of Nanographenes and Its Application in Graphene Nanoribbons. *Nat. Commun.* **2013**, *4*, 3646.

(139) Stille, J. K.; Noren, G. K.; Green, L. Hydrocarbon Ladder Aromatics from a Diels-Alder Reaction. *J. Polym. Sci. Part A-1* **1970**, *8*, 2245–2254.

(140) Sclüter, A.-D.; Löffler, M.; Enkeimann, V. Synthesis of a Fully Unsaturated All-Carbon Ladder Polymer. *Nature* **1994**, *368*, 831–834.

(141) Löffler, M.; Schlüter, A. -D; Gessler, K.; Saenger, W.; Toussaint, J. -M; Brédas, J. -L. Synthesis of a Fully Unsaturated "Molecular Board." *Angew. Chemie Int. Ed. English* **1994**, *33*, 2209–2212.

(142) Chmil, K.; Scherf, U. A Simple Two-Step Synthesis of a Novel, Fully Aromatic Ladder-Type Polymer. *Die Makromol. Chemie, Rapid Commun.* **1993**, *14*, 217–222.

(143) Chmil, K.; Scherf, U. Conjugated All-Carbon Ladder Polymers: Improved Solubility and Molecular Weights. *Acta Polym.* **1997**, *48*, 208–211.

(144) Shifrina, Z. B.; Averina, M. S.; Rusanov, A. L.; Wagner, M.; Müllen, K. Branched Polyphenylenes by Repetitive Diels-Alder Cycloaddition. *Macromolecules* **2000**, *33*, 3525–3529.

(145) Yang, X.; Dou, X.; Rouhanipour, A.; Zhi, L.; Räder, H. J.; Müllen, K. Two-Dimensional Graphene Nanoribbons. *J. Am. Chem. Soc.* **2008**, *130*, 4216–4217.

(146) Carothers, W. H. Polymers and Polyfunctionality. *Trans. Faraday Soc.* **1936**, *32*, 39–49.

(147) Schwab, M. G.; Narita, A.; Hernandez, Y.; Balandina, T.; Mali, K. S.; De Feyter, S.; Feng, X.; Müllen, K. Structurally Defined Graphene Nanoribbons with High Lateral Extension. *J. Am. Chem. Soc.* **2012**, *134*, 18169–18172.

(148) Dötz, F.; Brand, J. D.; Ito, S.; Gherghel, L.; Müllen, K. Synthesis of Large Polycyclic Aromatic Hydrocarbons: Variation of Size and Periphery. *J. Am. Chem. Soc.* **2000**, *122*, 7707–7717.

(149) Narita, A.; Feng, X.; Hernandez, Y.; Jensen, S. A.; Bonn, M.; Yang, H.; Verzhbitskiy, I. A.; Casiraghi, C.; Hansen, M. R.; Koch, A. H. R.; et al. Synthesis of Structurally Well-Defined and Liquid-Phase-Processable Graphene Nanoribbons. *Nat. Chem.* **2014**, *6*, 126–132.

(150) Villegas, C. E. P.; Mendonça, P. B.; Rocha, A. R. Optical Spectrum of Bottom-up Graphene Nanoribbons: Towards Efficient Atom-Thick Excitonic Solar Cells. *Sci. Rep.* **2014**, *4*, 6579.

(151) Osella, S.; Narita, A.; Schwab, M. G.; Hernandez, Y.; Feng, X.; Müllen, K.; Beljonne, D. Graphene Nanoribbons as Low Band Gap Donor Materials for Organic Photovoltaics: Quantum Chemical Aided Design. *ACS Nano* **2012**, *6*, 5539–5548.

(152) Narita, A.; Verzhbitskiy, I. A.; Frederickx, W.; Mali, K. S.; Jensen, S. A.; Hansen, M. R.; Bonn, M.; De Feyter, S.; Casiraghi, C.; Feng, X.; et al. Bottom-up Synthesis of Liquid-Phase-Processable Graphene Nanoribbons with near-Infrared Absorption. *ACS Nano* **2014**, *8*, 11622–11630.

(153) Daigle, M.; Picard-Lafond, A.; Soligo, E.; Morin, J. F. Regioselective Synthesis of Nanographenes by Photochemical Cyclodehydrochlorination. *Angew. Chemie - Int. Ed.* **2016**, *55*, 2042–2047.

(154) Daigle, M.; Morin, J.-F. F. Helical Conjugated Ladder Polymers: Tuning the Conformation and Properties through Edge Design. *Macromolecules* **2017**, *50*, 9257–9264.

(155) Daigle, M.; Miao, D.; Lucotti, A.; Tommasini, M.; Morin, J. F. Helically Coiled Graphene Nanoribbons. *Angew. Chemie - Int. Ed.* **2017**, *56*, 6213–6217.

(156) Vo, T. H.; Shekhirev, M.; Kunkel, D. A.; Morton, M. D.; Berglund, E.; Kong, L.; Wilson, P. M.; Dowben, P. A.; Enders, A.; Sinitskii, A. Large-Scale Solution Synthesis of Narrow Graphene Nanoribbons. *Nat. Commun.* **2014**, *5*, 3189.

(157) Cai, J.; Ruffieux, P.; Jaafar, R.; Bieri, M.; Braun, T.; Blankenburg, S.; Muoth, M.; Seitsonen, A. P.; Saleh, M.; Feng, X.; et al. Atomically Precise Bottom-up Fabrication of Graphene Nanoribbons. *Nature* **2010**, *466*, 470–473.

(158) Yang, W.; Lucotti, A.; Tommasini, M.; Chalifoux, W. A. Bottom-Up Synthesis of Soluble and Narrow Graphene Nanoribbons Using Alkyne Benzannulations. *J. Am. Chem. Soc* **2016**, *138*, 51.

(159) Lafferentz, L.; Ample, F.; Yu, H.; Hecht, S.; Joachim, C.; Grill, L. Conductance of a Single Conjugated Polymer as a Continuous Function of Its Length. *Science* **2009**, *323*, 1193–1197.

(160) Xi, M.; Bent, B. E. Mechanism of the Ullmann Coupling Reactions in Adsorbed Monolayers. *J. Am. Chem. Soc.* **1993**, *115*, 7426–7433.

(161) Treier, M.; Pignedoli, C. A.; Laino, T.; Rieger, R.; Müllen, K.; Passerone, D.; Fasel, R. Surface-Assisted Cyclodehydrogenation Provides a Synthetic Route towards Easily Processable and Chemically Tailored Nanographenes. *Nat. Chem.* **2011**, *3*, 61–67.

(162) Zhang, H.; Lin, H.; Sun, K.; Chen, L.; Zagranyarski, Y.; Aghdassi, N.; Duhm, S.; Li, Q.; Zhong, D.; Li, Y.; et al. On-Surface Synthesis of Rylene-Type Graphene Nanoribbons. *J. Am. Chem. Soc.* **2015**, *137*, 4022–4025.

(163) Basagni, A.; Sedona, F.; Pignedoli, C. A.; Cattelan, M.; Nicolas, L.; Casarin, M.; Sambi, M. Molecules-Oligomers-Nanowires-Graphene Nanoribbons: A Bottom-up Stepwise on-Surface Covalent Synthesis Preserving Long-Range Order. *J. Am. Chem. Soc.* **2015**, *137*, 1802–1808.

(164) Ruffieux, P.; Cai, J.; Plumb, N. C.; Patthey, L.; Prezzi, D.; Ferretti, A.; Molinari, E.; Feng, X.; Müllen, K.; Pignedoli, C. A.; et al. Electronic Structure of Atomically Precise Graphene Nanoribbons. *ACS Nano* **2012**, *6*, 6930–6935.

(165) Chen, Y. C.; De Oteyza, D. G.; Pedramrazi, Z.; Chen, C.; Fischer, F. R.; Crommie, M. F. Tuning the Band Gap of Graphene Nanoribbons Synthesized from Molecular Precursors. *ACS Nano* **2013**, *7*, 6123–6128.

(166) Huang, H.; Wei, D.; Sun, J.; Wong, S. L.; Feng, Y. P.; Neto, A. H. C.; Wee, A. T. S. Spatially Resolved Electronic Structures of Atomically Precise Armchair Graphene Nanoribbons. *Sci. Rep.* **2012**, *2*, 983.

(167) Abdurakhmanova, N.; Amsharov, N.; Stepanow, S.; Jansen, M.; Kern, K.; Amsharov, K. Synthesis of Wide Atomically Precise Graphene Nanoribbons from Para-Oligophenylene Based Molecular Precursor. *Carbon* **2014**, *77*, 1187–1190.

(168) Ruffieux, P.; Wang, S.; Yang, B.; Sanchez-Sanchez, C.; Liu, J.; Dienel, T.; Talirz, L.; Shinde, P.; Pignedoli, C. A.; Passerone, D.; et al. On-Surface Synthesis of Graphene Nanoribbons with Zigzag Edge Topology. *Nature* **2016**, *531*, 489–492.

(169) Topsakal, M.; Sevinçli, H.; Ciraci, S. Spin Confinement in the Superlattices of Graphene Ribbons. *Appl. Phys. Lett.* **2008**, *92*, 173118.

(170) Wimmer, M.; Adagideli, I.; Berber, S.; Tománek, D.; Richter, K. Spin Currents in Rough Graphene Nanoribbons: Universal Fluctuations and Spin Injection. *Phys. Rev. Lett.* **2008**, *100*, 177207.

(171) Son, Y. W.; Cohen, M. L.; Louie, S. G. Half-Metallic Graphene Nanoribbons. *Nature* **2006**, *444*, 347–349.

(172) Gutzler, R.; Walch, H.; Eder, G.; Kloft, S.; Heckl, W. M.; Lackinger, M. Surface Mediated Synthesis of 2D Covalent Organic Frameworks: 1,3,5-Tris(4-Bromophenyl)Benzene on Graphite(001), Cu(111), and Ag(110). *Chem. Commun.* **2009**, *0*, 4456–4458.

(173) Bieri, M.; Treier, M.; Cai, J.; Aït-Mansour, K.; Ruffieux, P.; Gröning, O.; Gröning, P.; Kastler, M.; Rieger, R.; Feng, X.; et al. Porous Graphenes: Two-Dimensional Polymer Synthesis with Atomic Precision. *Chem. Commun.* **2009**, *0*, 6919–6921.

(174) Liu, J.; Ruffieux, P.; Feng, X.; Müllen, K.; Fasel, R. Cyclotrimerization of Arylalkynes on Au(111). *Chem. Commun.* **2014**, *50*, 11200–11203.

(175) Grill, L.; Dyer, M.; Lafferentz, L.; Persson, M.; Peters, M. V.; Hecht, S. Nano-Architectures by Covalent Assembly of Molecular Building Blocks. *Nat. Nanotechnol.* **2007**, *2*, 687–691.

(176) Cardenas, L.; Gutzler, R.; Lipton-Duffin, J.; Fu, C.; Brusso, J. L.; Dinca, L. E.; Vondráček, M.; Fagot-Revurat, Y.; Malterre, D.; Rosei, F.; et al. Synthesis and Electronic Structure of a Two Dimensional π-Conjugated Polythiophene. *Chem. Sci.* **2013**, *4*, 3263–3268.

(177) Liu, W.; Luo, X.; Bao, Y.; Liu, Y. P.; Ning, G. H.; Abdelwahab, I.; Li, L.; Nai, C. T.; Hu, Z. G.; Zhao, D.; et al. A Two-Dimensional Conjugated Aromatic Polymer via C-C Coupling Reaction. *Nat. Chem.* **2017**, *9*, 563–570.

(178) Abel, M.; Clair, S.; Ourdjini, O.; Mossoyan, M.; Porte, L. Single Layer of Polymeric Fe-Phthalocyanine: An Organometallic Sheet on Metal and Thin Insulating Film. *J. Am. Chem. Soc.* **2011**, *133*, 1203–1205.

(179) Bieri, M.; Blankenburg, S.; Kivala, M.; Pignedoli, C. A.; Ruffieux, P.; Müllen, K.; Fasel, R. Surface-Supported 2D Heterotriangulene Polymers. *Chem. Commun.* **2011**, *47*, 10239–10241.

(180) Steiner, C.; Gebhardt, J.; Ammon, M.; Yang, Z.; Heidenreich, A.; Hammer, N.; Görling, A.; Kivala, M.; Maier, S. Hierarchical On-Surface Synthesis and Electronic Structure of Carbonyl-Functionalized One- and Two-Dimensional Covalent Nanoarchitectures. *Nat. Commun.* **2017**, *8*, 14765.

(181) Chen, Z.; Baumeister, U.; Tschierske, C.; Würthner, F. Effect of Core Twisting on Self-Assembly and Optical Properties of Perylene Bisimide Dyes in Solution and Columnar Liquid Crystalline Phases. *Chem. - A Eur. J.* **2007**, *13*, 450–465.

(182) Treussart, F. Lumière Issue d'émetteurs Individuels, Applications., Université Pierre et Marie Curie - Paris VI, 2004.

(183) Das, S. K.; Liu, Y.; Yeom, S.; Kim, D. Y.; Richards, C. I. Single-Particle Fluorescence Intensity Fluctuations of Carbon Nanodots. *Nano Lett.* **2014**, *14*, 620–625.

(184) Brokmann, X.; Messin, G.; Desbiolles, P.; Giacobino, E.; Dahan, M.; Hermier, J. P. Colloidal CdSe/ZnS Quantum Dots as Single-Photon Sources. *New J. Phys.* **2004**, *6*, 99.

(185) Li, Y.; Shu, H.; Wang, S.; Wang, J. Electronic and Optical Properties of Graphene Quantum Dots: The Role of Many-Body Effects. *J. Phys. Chem. C* **2015**, *119*, 4983–4989.

(186) Cocchi, C.; Prezzi, D.; Ruini, A.; Caldas, M. J.; Molinari, E. Anisotropy and Size Effects on the Optical Spectra of Polycyclic Aromatic Hydrocarbons. *J. Phys. Chem. A* **2014**, *118*, 6507–6513.

(187) Zhu, S.; Wang, L.; Li, B.; Song, Y.; Zhao, X.; Zhang, G.; Zhang, S.; Lu, S.; Zhang, J.; Wang, H.; et al. Investigation of Photoluminescence Mechanism of Graphene Quantum Dots and Evaluation of Their Assembly into Polymer Dots. *Carbon* **2014**, *77*, 462–472.

(188) Hughes, J. M.; Hernandez, Y.; Aherne, D.; Doessel, L.; Müllen, K.; Moreton, B.; White, T. W.; Partridge, C.; Costantini, G.; Shmeliov, A.; et al. High Quality Dispersions of Hexabenzocoronene in Organic Solvents. *J. Am. Chem. Soc.* **2012**, *134*, 12168–12179.

(189) Englert, J. M.; Hauke, F.; Feng, X.; Müllen, K.; Hirsch, A. Exfoliation of Hexa-Peri-Hexabenzocoronene in Water. *Chem. Commun.* **2010**, *46*, 9194–9196.

(190) Kimble, H. J.; Dagenais, M.; Mandel, L. Photon Antibunching in Resonance Fluorescence. *Phys. Rev. Lett.* **1977**, *39*, 691–695.

(191) Hanbury Brown, R.; Twiss, R. Q. A Test of a New Type of Stellar Interferometer on Sirius. *Nature* **1956**, *178*, 1046–1048.

(192) Brouri, R.; Beveratos, A.; Poizat, J.-P.; Grangier, P. Photon Antibunching in the Fluorescence of Individual Color Centers in Diamond. *Opt. Lett.* **2000**, *25*, 1294–1296.

(193) Orrit, M.; Bernard, J. Single Pentacene Molecules Detected by Fluorescence Excitation in a P-Terphenyl Crystal. *Phys. Rev. Lett.* **1990**, *65*, 2716–2719.

(194) Moerner, W.; Kador, L. Optical Detection and Spectroscopy of Single Molecules in a Solid. *Phys. Rev. Lett.* **1989**, *62*, 2535–2538.

(195) Macklin, J. J.; Trautman, J. K.; Harris, E. D.; Brus, L. E. Imaging and Time-Resolved Spectroscopy of Single Molecules at an Interface. *Science* **1996**, *272*, 255–258.

(196) Gruber, A.; Dräbenstedt, A.; Tietz, C.; Fleury, L.; Wrachtrup, J.; Von Borczyskowski, C. Scanning Confocal Optical Microscopy and Magnetic Resonance on Single Defect Centers. *Science* **1997**, *276*, 2012–2014.

(197) Kurtsiefer, C.; Mayer, S.; Zarda, P.; Weinfurter, H. Stable Solid-State Source of Single Photons. *Phys. Rev. Lett.* **2000**, *85*, 290–293.

(198) Empedocles, S. A.; Norris, D. J.; Bawendi, M. G. Photoluminescence Spectroscopy of Single CdSe Nanocrystallite Quantum Dots. *Phys. Rev. Lett.* **1996**, *77*, 3873–3876.

(199) Lounis, B.; Bechtel, H. A.; Gerion, D.; Alivisatos, P.; Moerner, W. E. Photon Antibunching in Single CdSe/ZnS Quantum Dot Fluorescence. *Chem. Phys. Lett.* **2000**, *329*, 399–404.

(200) Messin, G.; Hermier, J. P.; Giacobino, E.; Desbiolles, P.; Dahan, M. Bunching and Antibunching in the Fluorescence of Semiconductor Nanocrystals. *Opt. Lett.* **2001**, *26*, 1891–1893.

Chapter 2: Graphene Quantum Dots

Chapter 1: Introduction

Chapter 2: Graphene Quantum Dots

2.1. Synthesis of the Quantum Dots

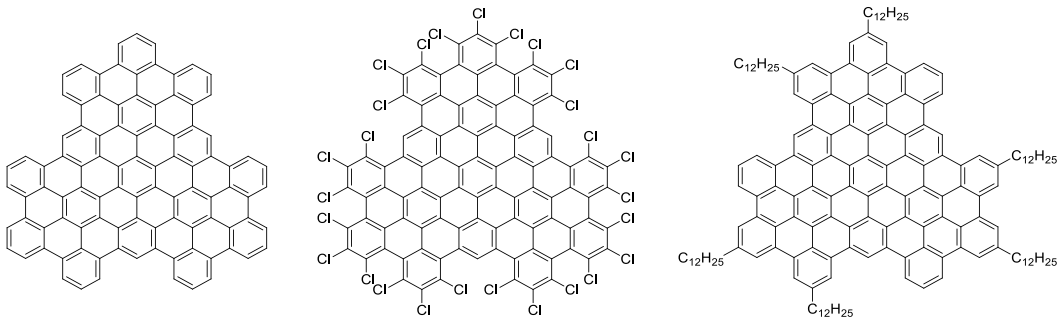

*Figure 2.1: Structures of $C_{96}H_{30}$ **1**, $C_{96}Cl_{27}H_3$ **2** and $C_{168}H_{210}$ **3**.*

The synthesis of GQDs has been widely investigated by the group of K. Müllen in the early nineties and in the beginning of the 2000s. Many structures have been developed exhibiting various sizes, shapes and edge states. The most studied GQDs are hexabenzocoronene (HBC)[1,2] followed by superphenalene $C_{96}H_{30}$ **1** (C96)[3,4] (Figure 2.1). Actually, the C96 GQD can be functionalized with various chemical groups to form what we called the C96 "family" and therefore tune the solubility and optical properties of the nanoparticles. At the beginning of my PhD, in order to be familiar with the chemistry and manipulation of GQDs, and also to be able to provide rapidly interesting structures to the group of Prof. Jean-Sébastien Lauret, we decided to reproduce the synthesis of the C96 GQDs.[4,5]

2.1.1. The Scholl reaction

The first synthesis of this GQD was developed in 1997 by Müllen et *al.*[3] and it was based on the Diels-Alder reaction of an acetylenic compound with a cyclopentadienone derivative followed by the extrusion of CO to form a polyphenylene dendrimer. The reaction was followed by the Scholl reaction,[6,7] an oxidation step known to dehydrogenate polyphenylene to form carbon-carbon bounds. The dehydrogenation of the C96 dendrimer was initially performed with copper(II) trifluoromethanesulfonate and $AlCl_3$;[3] however, these conditions are not suitable for the dehydrogenation of the C96 dendrimer containing solubilizing $C_{12}H_{25}$

alkyl chains since the reaction often leads to unwanted chlorination and/or removal of peripheral alkyl chains. Alternative oxidation procedures based on 2,3-dichloro-5,6-dicyano-1,4-benzoquinone (DDQ) in the presence of triflic acid only lead to partial dehydrogenation product.[8] The most efficient procedure is based on the use of $FeCl_3$ as the oxidant which gives better results in term of oxidative strength and low chlorination.

The Scholl reaction proceeds *via* a radical mechanism and consequently, it requires non-stabilized dichloromethane (DCM) since ethanol or amylene which are commonly used to stabilize DCM are free radical scavengers. Finally to prevent uncontrolled chlorination of the GQD, the reaction is done with a special setup in which argon is first bubbling in a round-bottom flask filled with DCM and then a canula transfers the argon flow from this flask to the reaction solution (Figure 2.2).

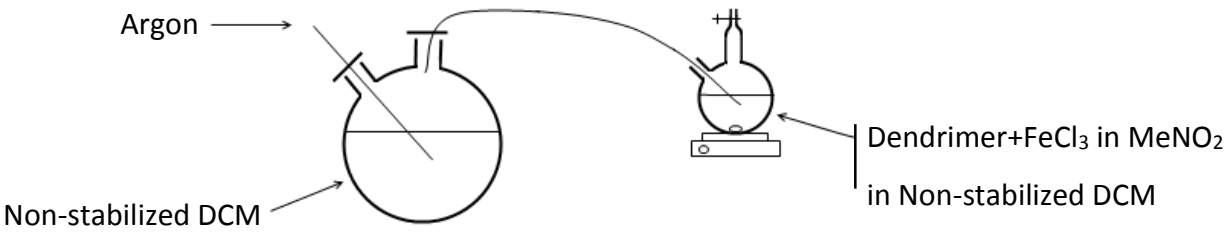

Figure 2.2: Setup for the Scholl reaction.

This setup allows a high flow of argon to bubble in the reaction flask to remove HCl from the solution before it can react with the GQD and without evaporating too quickly the DCM from the reaction flask.

2.1.2. The structures of the C96 family

The synthesis of the C96 GQD starts with the Diels-Alder reaction between 1,3,5-triethynylbenzene and tetraphenylcyclopentadienone in diphenyl ether at 180°C overnight (Scheme 2.1). It is followed by the Scholl reaction in the presence of $FeCl_3$ in nitromethane to dehydrogenate polyphenylene **4** and form GQD **1**. With the setup presented in the previous part, the reaction is conducted at room temperature overnight with a very good yield (95%).

Chapter 2: Graphene Quantum Dots

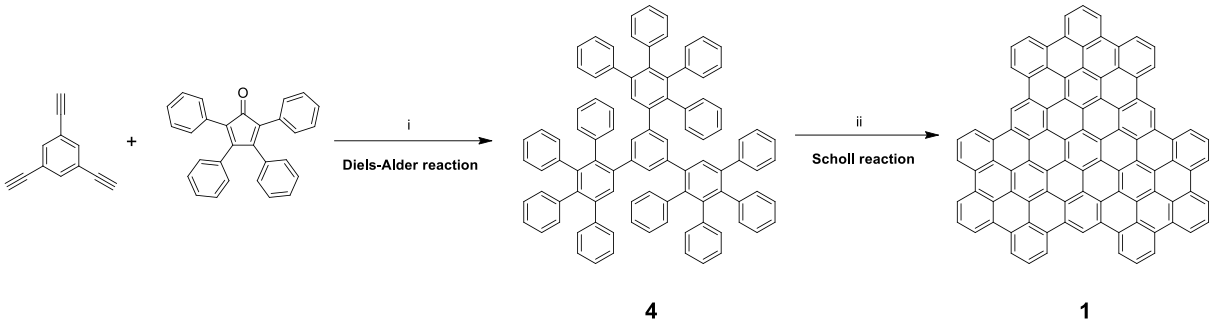

Scheme 2.1: i) Ph_2O, 180°C, overnight, 40% ; ii) $FeCl_3$, $MeNO_2$, DCM, R.T., overnight, 95%.

The reaction is quenched with methanol and GQD **1** is purified by filtration and washing since it is insoluble in the usual organic solvent. However, the low solubility of **1** in usual solvents is a huge drawback for optics experiments that need individual molecule dispersions. To face this issue, we decided to functionalize the edge by chlorination or by adding alkyl chains.[4,5]

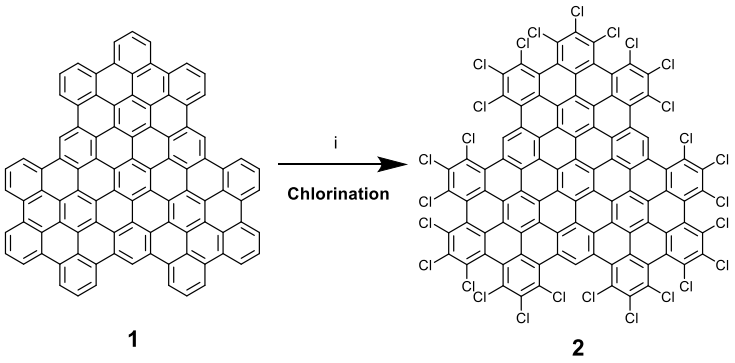

Scheme 2.2: i) $AlCl_3$, ICl, CCl_4, 80°C, 48h, 73%.

Because of the large size of chlorine compared to the hydrogen atoms, the chlorination of the edge of the particles forces the molecule to bend and thus prevents π- π stacking and improves solubility.[5] This synthesis starts directly from C96 **1** and proceeds with $AlCl_3$ and ICl in CCl_4 to replace almost every hydrogen and form $C_{96}Cl_{27}H_3$ **2** (also named C96Cl) (Scheme 2.2).[5] Three of the hydrogens are left due to the strong steric hindrance of the neighboring chlorines. The resulting molecule is highly soluble in chlorinated and usual organic solvents. The purification is done by column chromatography with chloroform as the eluent and product **2** is collected at solvent front.

The functionalization of the GQD with dodecyl chains is preformed to increase the solubility of the GQD with organic solvents. The synthesis follows the same synthetic procedure as the synthesis of C96 GQD **1**; however, cyclopentadienone **9** containing two dodecyl chains has to be synthesized in four steps (Scheme 2.3).[4]

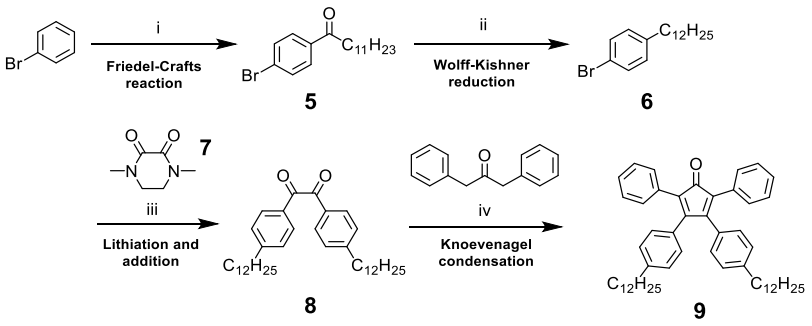

Scheme 2.3: i) $AlCl_3$, $CH_3(CH_2)_{10}COCl$, 50°C, 1h30, 73%; ii) KOH, N_2H_4, triethylene glycol, 130°C, 3H40, 74%; iii) n-BuLi, THF, R.T., overnight, 33%; iv) KOH, EtOH, 90°C, 30min, 51%.

The starting material for this synthesis is bromobenzene which undergoes a Friedel-Crafts reaction with dodecanoyl chloride. The *para*-substituted product **5** is isolated with a good yield (73%) and subjected to the Wolf-Kishner reduction with hydrazine and potassium hydroxide in triethylene glycol. This is the key step for this synthesis since the reaction is very sensitive. In fact, if the temperature is a few degrees too low, the ketone is not reduced and on the contrary, if the solution is heated too much or for a too long time, the product is degraded. After optimization of the process we found that the best conditions to perform the reaction is to heat at 130°C for 3h40 and in the same time remove water by distillation. With these conditions, the yield can go up to 74%. Dione **8** is synthesized *via* the lithiation of the 4-bromododecylbenzene **6** followed by the addition on 1,4-dimethylpiperazine-2,3-dione **7** prepared as described in litterature.[9] The final step is the formation of cyclopentadienone **9** by a double Knoevenagel condensation of dione **8** on 1,3-diphenylpropan-2-one.[10,11] This reaction is done in the presence of potassium hydroxide in ethanol for 30 min at reflux and has a yield of 51%.

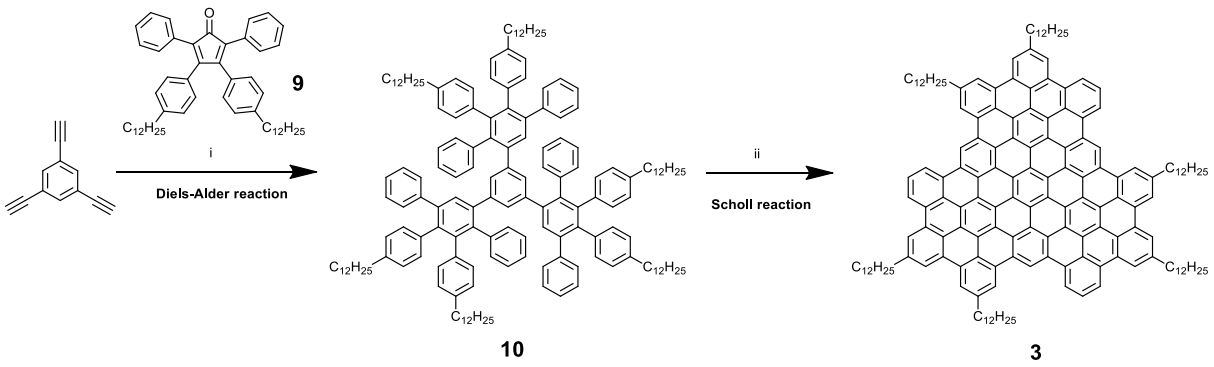

Scheme 2.4: i) Ph_2O, 180°C, overnight, 57% ; ii) $FeCl_3$, $MeNO_2$, DCM, T.A., overnight, 95%.

After the preparation of cyclopentadienone **9**, the Diels-Alder reaction is conducted for the synthesis of the nanoparticle with dodecyl chains **3** (C96C12) with the same conditions as for C96 GQD (Scheme 2.4). However, for this compound, the dehydrogenation step is harder to control due to the possible chlorination of the alkyl chains caused by HCl in solution. Therefore, the reaction progress should be monitored by MALDI-TOF mass spectrometry to make sure that the molecule is fully dehydrogenated with no chlorination. After reaction, the product is purified with filtration and washing with methanol to obtain the pure product with 95% yield.

2.1.3. Chemical characterization

The different molecules were characterized with various methods mostly depending on their solubility. For small molecules like the ones prepared in the synthesis of cyclopentadienone **9**, the main characterization tool was ^{1}H-NMR. The spectrum of cyclopentadienone **9** presented in Figure 2.3 exhibits two sets of signal in the aliphatic and aromatic regions. In the aliphatic region, the protons of the alkyl chains resonate at 0.86, 1.26 and 2.57 ppm. The *CH_2* near the aromatics are more deshielded. In the aromatic part of the spectrum, the protons of the phenyl rings bearing the chain appear as an AB system (two doublets) at 6.80 and 6.96 ppm. The two last phenyl rings close to the carbonyl group appear as a multiplet at higher chemical shifts (between 7.22 to 7.25 ppm).

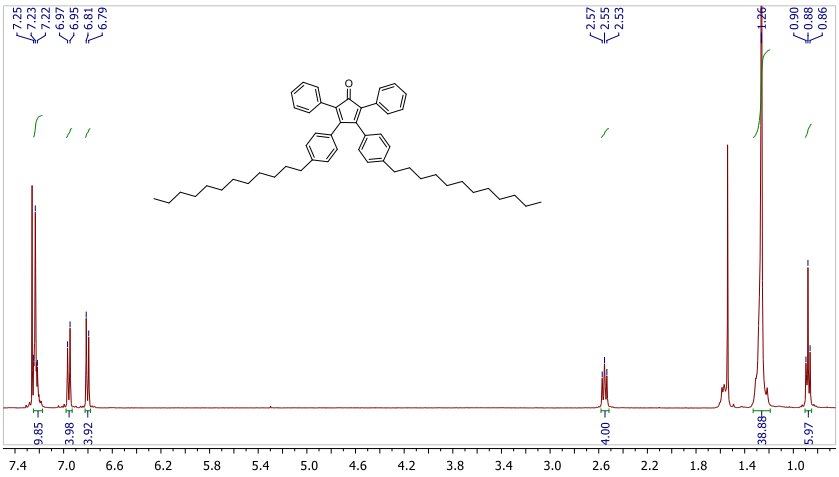

*Figure 2.3: ^{1}H-NMR spectrum of cyclopentadienone **9** in $CDCl_3$*

When cyclopentadienone **9** undergoes the Diels-Alder reaction, the shape of the ^{1}H-NMR spectrum obtained is slightly changed (Figure 2.4). The protons from the alkyl chains still exhibit low chemical shifts between 0.88 and 2.32 ppm depending on their proximity to the aromatic core and the protons in this aromatic core are still highly deshielded and show chemical shifts between 6.52 and 7.15 ppm. The aromatic part is now extremely difficult to interpret since many protons with similar environment are superimposed. It is interesting to note that in the 2.25-2.50 ppm region that the CH_2 in benzylic position (close to the phenyl rings) are slightly different and appear as two triplet centered at 2.32 and 2.36 ppm.

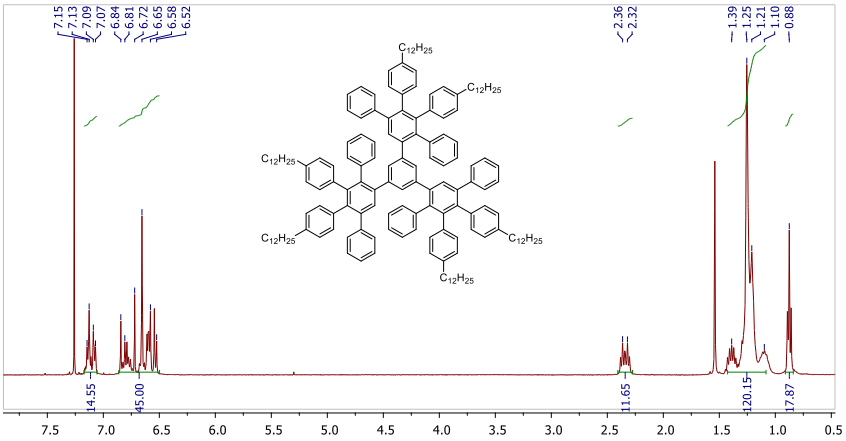

*Figure 2.4: ^{1}H-NMR spectrum of dendrimer **10** in $CDCl_3$*

For dendrimer **4** (without alkyl chains), the interpretation of the ^{1}H-NMR spectrum is even more complicated and the characterization by mass spectrometry (MS) makes more sense to confirm the structure of the final product. In fact, the starting product undergoes a high molecular weight change that is easily followed by MS. The MALDI-TOF mass spectrum of dendrimer **4** (Figure 2.5) clearly exhibits a peak at the expected value for the *m/z* of 1219.54 for the desired tri-substituted compound and there are no traces of the di-substituted compound at *m/z* of 863.12.

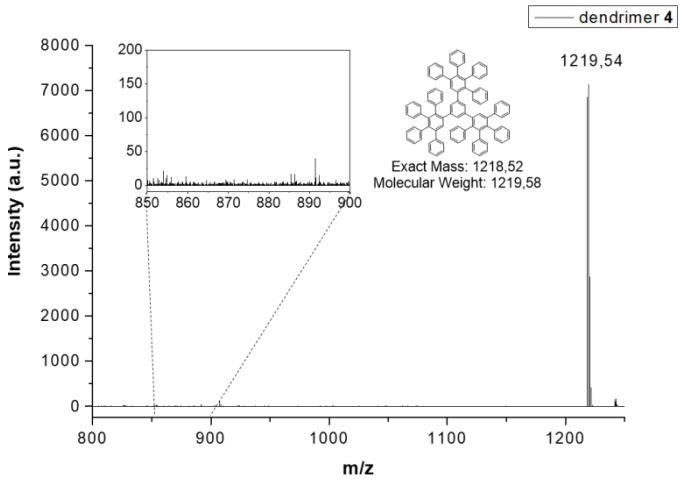

*Figure 2.5: MALDI-TOF MS spectrum of dendrimer **4**.*

For the characterization of the dehydrogenated compounds **1** and **2**, it is impossible to perform NMR because of the low solubility of the compounds. Consequently, the characterization is done by MALDI-TOF MS. For the preparation of the samples, we used two procedures depending on the solubility of the molecule. In the first one, the GQD is dispersed in a solvent (DCM for example) and 10 µl of this solution is mixed with 90 µl of a solution of *trans*-2-[3-(4-*tert*-butylphenyl)-2-methyl-2-propenylidene]malononitrile (DCTB) (10 mg in 1 ml of THF). 1 µl of this mixture is deposited on the MALDI plate and analyzed. In the second method, 0.5 mg of the sample is directly crushed with 50 equivalents of tetracyanoquinodimethane (TCNQ) in a crucible. This mixture is either directly deposited on a conducting tape on the MALDI plate or dispersed in a non-solvent (water or cyclohexane) and then deposited.[12] While C96Cl **2** and C96C12 **3** are soluble enough in solvents and can be

characterized with the process in solution with DCTB, C96 **1** has to be characterized with the solid process with TCNQ. In fact, the use of a matrix helps the ionization of the molecule allowing a better transfer of the energy from the laser to the molecules.

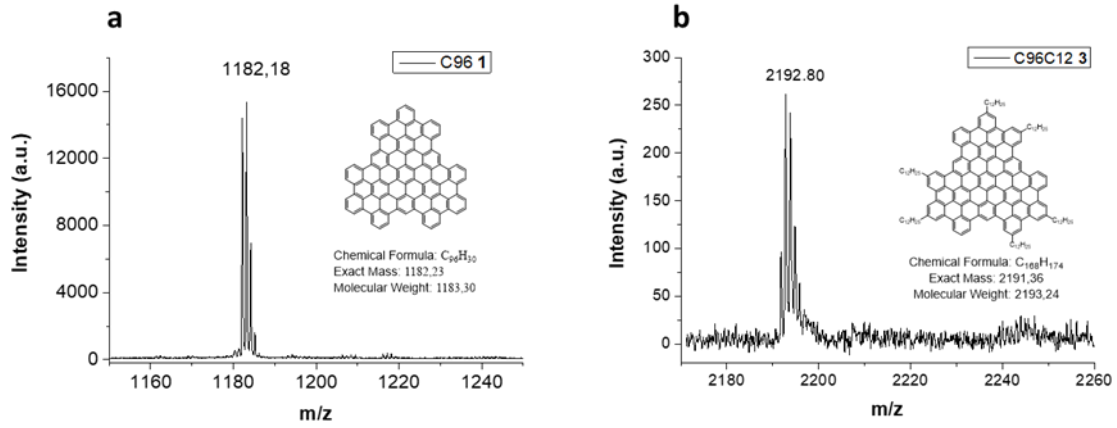

*Figure 2.6: MALDI-TOF MS spectra of a) C96 **1** b) C96C12 **3***

The MALDI-TOF spectrum for **1** (Figure 2.6a) only shows the fully dehydrogenated compound with no trace of the dendrimer at *m/z* 1182.18. The spectrum of C96C12 **3** exhibits peaks at *m/z* 2192.80 (M+H) for an expected exact mass of 2191.36 g/mol (Figure 2.6b).

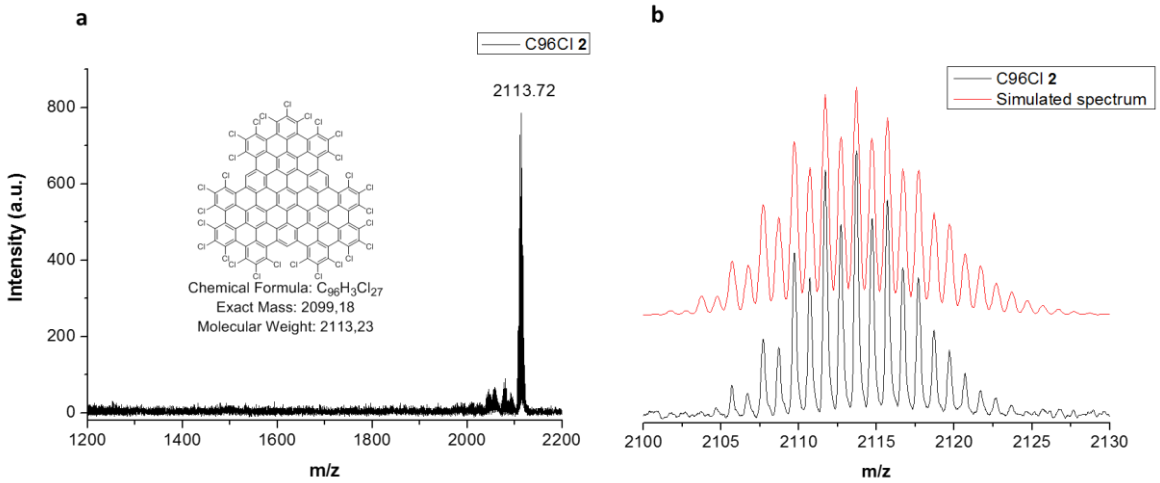

*Figure 2.7: a) MALDI-TOF MS spectrum of C96Cl **2** and b) comparison of the spectrum obtained and the one simulated for C96Cl **2**.*

The MALDI-TOF spectrum of GQD **2** shows the fully chlorinated compound with *m/z* of 2113.72 (Figure 2.7). The monoisotopic peak reflecting the exact mass at *m/z* 2099.18 cannot be observed because it represents a negligible part of the sample. The simulated mass spectrum obtained from the website: www.chemcalc.org (with molecular formula $C_{96}H_3Cl_{27}$ and FWHM 0.5) is fully consistent with the experimental data. Finally, on the full spectrum, one can observe unavoidable traces of partially chlorinated compounds at lower *m/z*.

2.1.4. Microscopy analysis of GQD 3

Both for the physical and optical properties, we mainly focused on GQD **3** since it has the same 2D aromatic core as C96 GQD **1** but a much better solubility thanks to the dodecyl chains. This GQD exhibits a size of about 1.5 nm for the core and 1.5 nm for the chains which was confirmed by High-Resolution Transmission Electron Microscopy (HRTEM) in the images in Figure 2.8 made by Dr. Hanako Okuno from the "Institut Nanosciences et Cryogénie" of the CEA-Grenoble. GQDs **3** also tend to stack to form columns as shown on the TEM image.

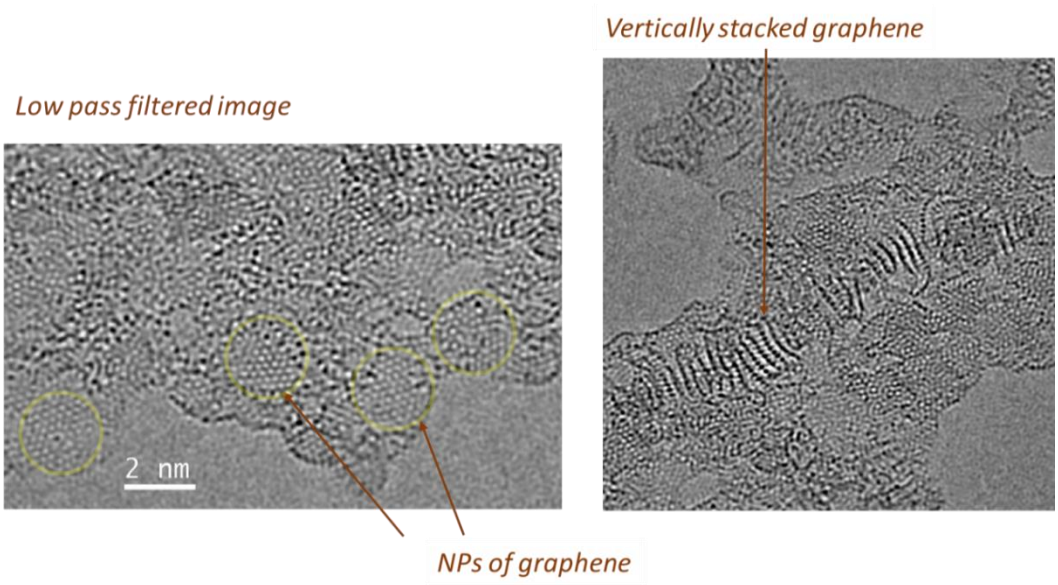

*Figure 2.8: HRTEM images of GQD **3** realized at INAC CEA-Grenoble by Dr. H. Okuno.*

We also tried to perform STM at the solid liquid interface in order to characterize the organization of the nanoparticles on surface. The STM images were realized by Dr. Fabien Silly from our Institute at CEA-Saclay for GQD **3** in 1-phenyloctane on HOPG (highly oriented

pyrolytic graphite) (Figure 2.9). Unfortunately, no organization of individual molecules was observed and only columnar structures were visualized.

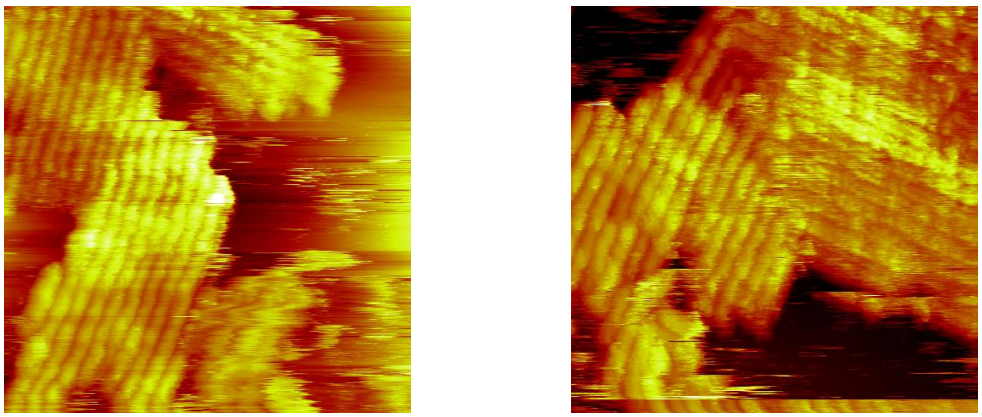

*Figure 2.9: STM images of the columnar structures of C96C12 GQD **3** performed at the Service de Physique de l'Etat Condensé (SPEC) (CEA-Saclay) by Dr. F. Silly.*

As it is shown on the TEM and STM images, C96C12 GQD **3** tends to aggregate and form columnar structures. For the characterization of their properties at the single molecule level it is therefore mandatory to find a way to separate the aggregates and more importantly when the nanoparticles are individualized to keep them isolated from each other.

2.2. Optical properties

2.2.1. Absorption

When working with carbon nanomaterials (carbon nanotubes and graphene), one of the main challenge is the dispersion and the preparation of stable solutions. We face the same problems with the nanoparticles of graphene, especially for bare (non-functionalized) nanoparticles. In order to disperse these particles, we have tested different solvent such as toluene, *N*-methylpyrrolidone (NMP), 1,2,4-trichlorobenzene (TCB) and surfactants like sodium cholate (SC) or sodium deoxycholate (SDC). We conclude that the best dispersants are TCB and SDC so, for the rest of the study, we will use spectrophotometric grade TCB to disperse GQDs. It is worth mentioning that when the GQDs contain functional groups like chlorine atoms or alkyl chains (GQD **2** and **3**), they exhibit an apparent good solubility in usual solvents like dichloromethane, chloroform, toluene and tetrahydrofuran; however, the

particles still form aggregates in solution.[4,13] Therefore for functionalized nanoparticles we also choose to work in TCB. The solutions of GQDs are prepared at 0.1 mg/ml in TCB, sonicating in an ultrasonic bath for 30 seconds and stirring for 24 hours.

We first determined the absorption spectra of GQDs **1**, **2** and **3** in TCB (Figure 2.10). The difference in the intensity of absorption can be seen immediately and is mostly due to the poor solubility of GQD **1** compared to GQD **2** and **3**. The spectrum of **1** shows a weak absorption band around 450 and 500 nm with a shoulder around 650 nm. The spectrum of **3** shows a large band at *ca.* 450 nm with shoulders at around 575 and 650 nm. The spectrum of **2** is relatively different and shows major peaks at 510 and 540 nm and the maximum absorption is red-shifted of *ca.* 20 nm and 40 nm compared to those of GQD **1** and **3**, respectively. This behavior is attributed to a better dispersion of the molecules in solution.[5]

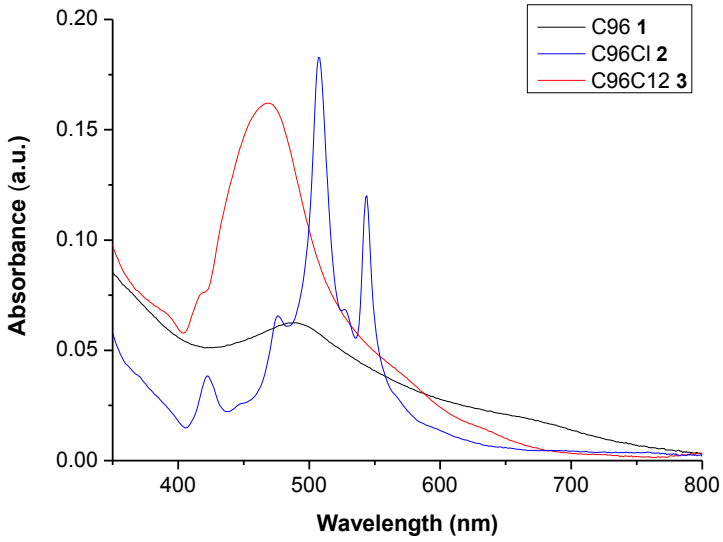

*Figure 2.10: UV-Vis absorption spectra of GQDs **1**, **2** and **3** in TCB*

In order to gain more insight in the optical properties of the particles, we performed photoluminescence (PL) and photoluminescence excitation (PLE) spectroscopies and we evaluated the single emission properties of the particles in collaboration with a group of physicists. For the rest of this chapter, we will focus on C96C12 GQD **3**.

2.2.2. Photoluminescence

The PL measurements are done on a custom setup at the Laboratoire Aimé Cotton (LAC) of the University Paris-Sud in Orsay. The setup is made of a supercontinuum laser source and two monochromators to control the wavelength of the excitation light. The PL is collected by a convergent lens and the excitation wavelength is excluded by a filter ahead of the monochromator and the CCD camera (Figure 2.11).

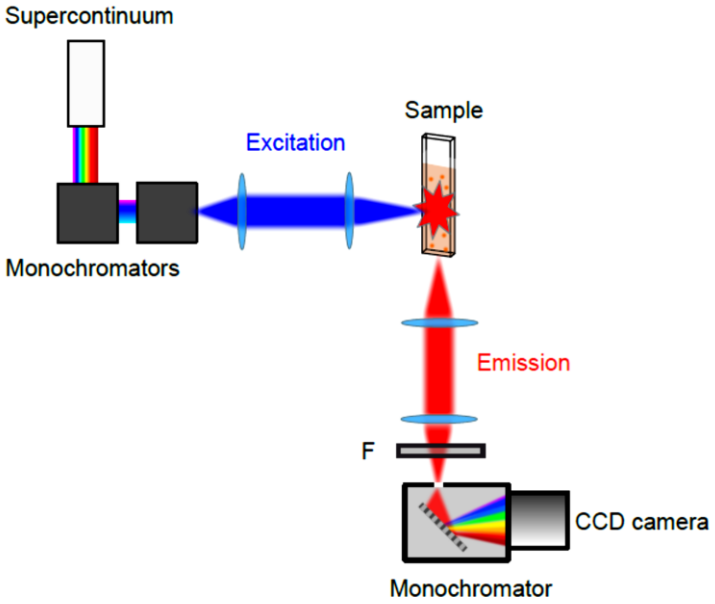

Figure 2.11: Setup for the PL measurement

In the usual conditions, the PL spectra are recorded with an excitation at 400 nm at a power of 110 µW. To prevent the saturation of the detector by the excitation light, the filter installed before the CCD camera suppresses the light with wavelength smaller than 405 nm. The PL spectrum of GQD **3** showed a large Stokes shift of the PL of 230 nm with the largest emission band at 648 nm and smaller emissions at 704, 575 and 520 nm (Figure 2.12). Those emissions are corresponding to the bumps observed in the absorption spectrum, which shows that the levels involved in both mechanisms are connected.

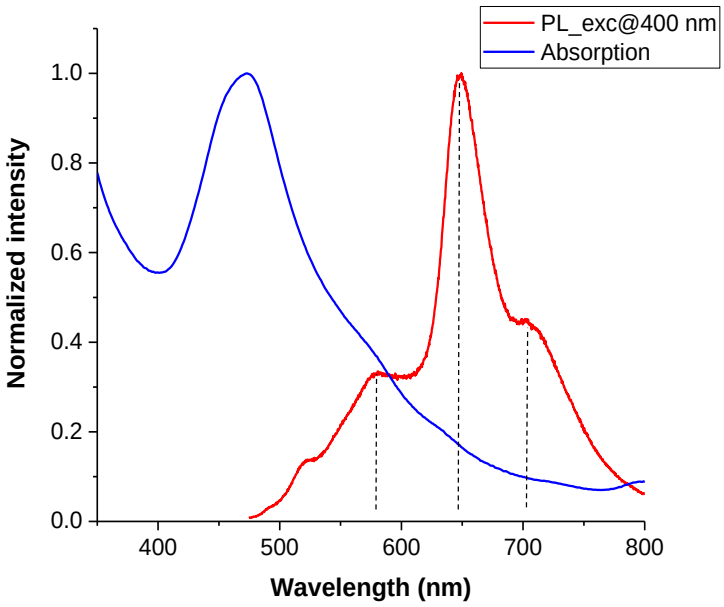

*Figure 2.12: Absorption and PL of a solution of GQD **3** in TCB (0.01 mg/ml)*

The shape of the PL and the presence of several bands cannot be explained only with this measurement and it is necessary perform other analysis like time resolved photoluminescence to discriminate the transitions involved and determine if this emission comes from individual molecules or aggregates.

2.2.3. Time-resolved photoluminescence

The time-resolved PL is done with the same setup as presented in Figure 2.11 but now the CCD camera is replaced by an avalanche photodiode, the laser is linked to a start-stop counter and the intensity of PL signal is monitored as a function of time at a given wavelength. The fluorescence decay of GQD **3** is monitored at 520, 575, 648 and 704 nm (Figure 2.13).

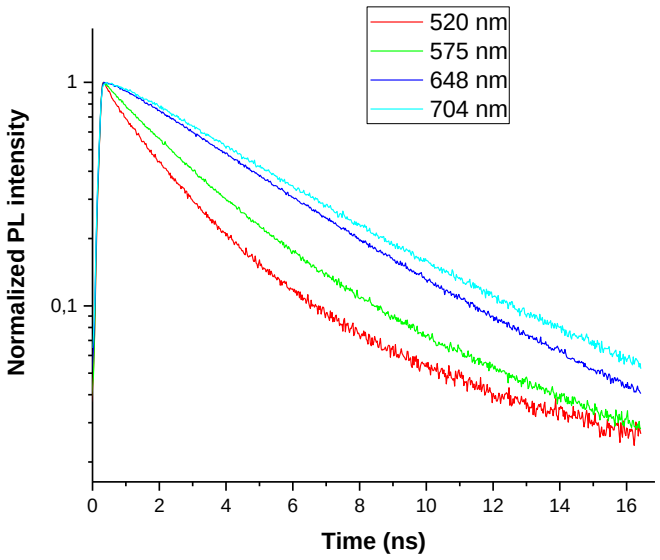

*Figure 2.13: PL decay over time of a solution of **3** (0.01g/ml) for various wavelength*

The lower energy transitions (648 and 704nm) show mono-exponential decay with lifetimes of about 5 ns while the higher energy transitions show multi-exponential decay. The mutli-exponential behavior means that more than one level is involved in the de-excitation. It is impossible to discriminate whether this multi-step de-excitation involves different levels in the same molecule or in small aggregates. Nevertheless, the mono-exponential decays observed at lower energy show that only one level is involved and it is a good indication that these transitions correspond to transition of individualized molecules in solutions. The fact that the molecules are individualized is extremely important for the characterization of the single photon emission properties.

To complete this experiment and be able to conclude on the quality of the dispersion, PLE map is a powerful tool, as we showed in the introduction (paragraph 1.4.2) for the dispersion of HBC.

2.2.4. Photoluminescence-excitation map

The PLE map of the GQD **3** is made by measuring the PL spectra for every wavelength of excitation and combining them (Figure 2.14b). The resulting map represents the excitation

wavelength as a function of the emission wavelength with a variation of color representing the intensity of the PL.

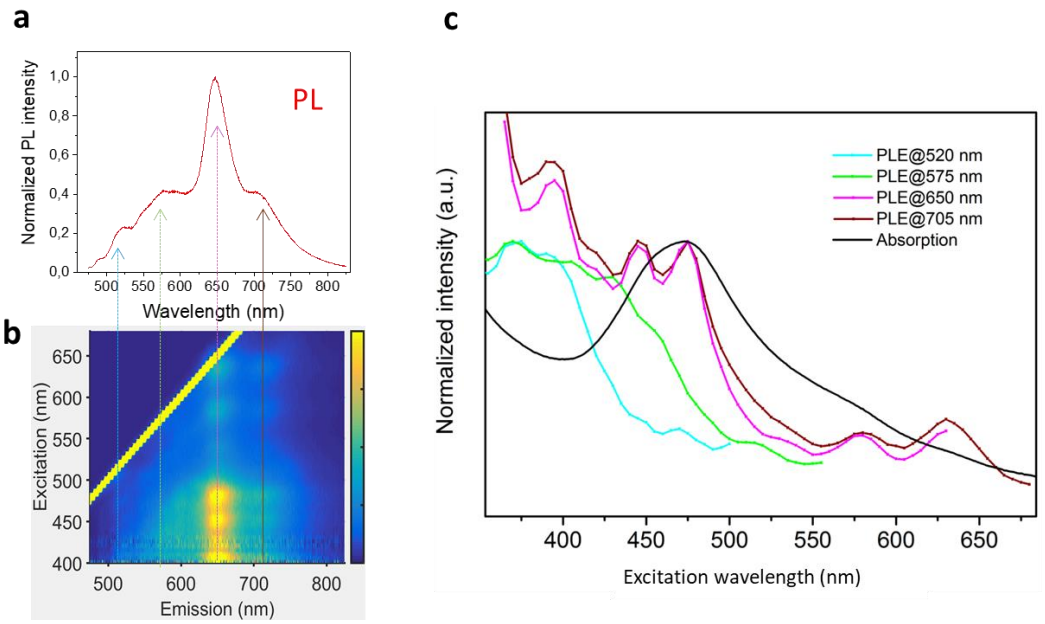

*Figure 2.14: Spectra of a solution of C96C12 **3** (0.01 mg/ml): a) photoluminescence spectrum, b) photoluminescence excitation map and c) normalized photoluminescence excitation spectra extracted from the PLE map at wavelength indicated by the colored arrows (blue, green, pink and brown) and superimposed absorption spectrum (black) of the solution.*

This map confirms that the main emission is at 650 nm with one resonance at higher wavelength (705 nm) and two at lower wavelength (575 and 520 nm). The main emission peak seems to be caused by the relaxation of multiple excitation levels and these levels also seem to relax in the emission at lower energy (705 nm). The photoluminescence excitation curves are extracted from this map by selecting spectra at the wavelength of the PL spectrum (520, 575, 650 and 705 nm). These excitation curves are compared to the absorption (Figure 2.14c) and show that for low energy emission (650 and 705 nm), the spectra exhibit a well-defined structure with some peaks corresponding to bumps in the absorption spectrum. This means that the energy levels involved in the absorption in solution are indeed the levels that relax into the low energy PL.

2.3. Single molecule properties

2.3.1. Sample preparation

To study single molecule properties, the molecules of the GQDs need to be isolated from each other in a polymer matrix and deposited on a surface. The matrix is also useful to minimize the quenching and the blinking of the PL due to the contact with the environment: substrate, air, charges, etc. The single molecule photoluminescence setup is presented in Figure 2.15. A laser source at 594 nm passes through an objective and excites the sample. The light emitted by the GQDs is collected by the same objective and is separated from the incident light with a dichroic mirror before passing through a pinhole to increase the spatial resolution of the image at the spectrograph. The objective is motorized in order to perform the mapping of the substrate to determine the source of the emission and therefore see if it comes from aggregates or single molecules.

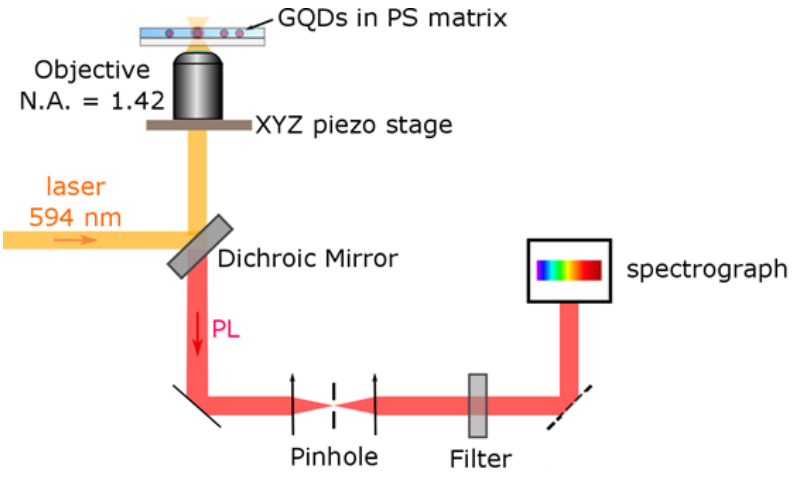

Figure 2.15: PL mapping setup

To prepare the samples for single molecule measurements, the previously prepared solution of GQD **3** at 0.1 mg/ml (about 5.10^{-5} M) is diluted 10 times and 100 times to achieve three different solutions at 5.10^{-5} M, 5.10^{-6} M and 5.10^{-7} M. 2 ml of these solutions of GQD **3** were mixed with 2 ml of a solution of purified polystyrene[14] in TCB (0.075 mg/ml) and sonicated in an ultrasonic bath for 10 seconds. Approximately 20 µl of these mixtures were spin-coated at 2000 rpm for 180 seconds[15] on a glass coverslip previously treated with oxygen plasma for 5

min to remove any organic contaminant. The sample is then dried at 90°C for one hour and imaged in the PL mapping setup described in Figure 2.15.

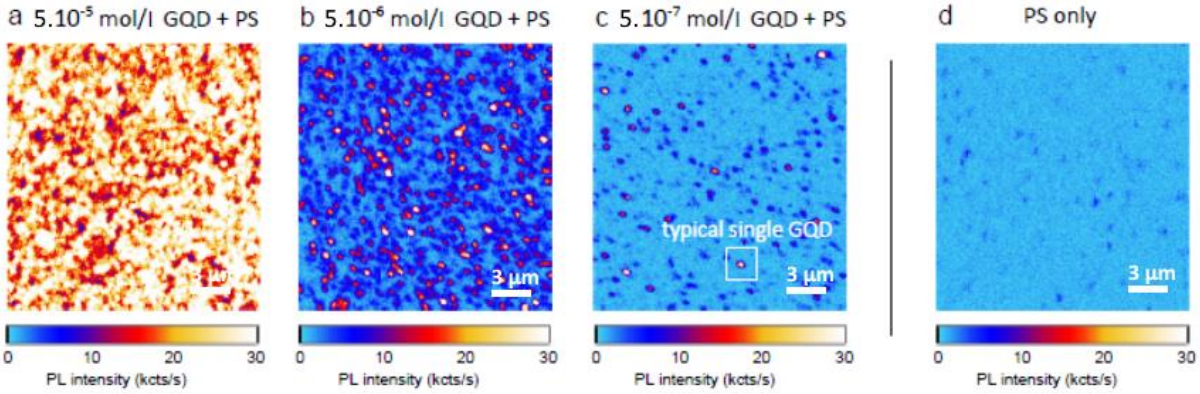

*Figure 2.16: PL images of the various dispersions prepared from GQD **3** solutions at a) 5.10^{-5} M, b) 5.10^{-6} M and c) 5.10^{-7} M and d) PL image of PS only.*

Figure 2.16 shows the photoluminescence images of the three samples prepared from solution of GQD **3** at 5.10^{-5}, 5.10^{-6} and 5.10^{-7} M in TCB and, as a reference, the PL response of the polystyrene film alone. While, the solution at 5.10^{-4} and 5.10^{-5} M seem too concentrated because we observe a large number of non-individualized PL signals; on Figure 2.16c, we observed small isolated spots which may correspond to a single molecule. The purified polystyrene analyzed confirmed that the PL was not coming from impurities left in the matrix since it did not show any significant photoluminescence signals.

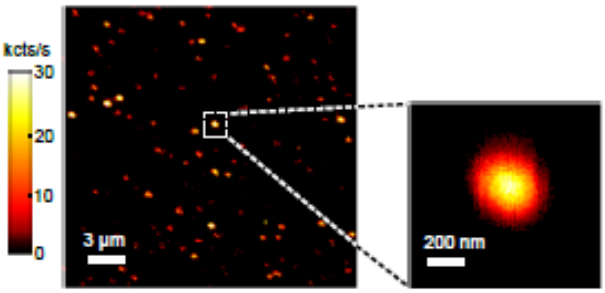

Figure 2.17: PL map and enlargement on a diffraction limited spot.

Figure 2.17 shows the signal observed on another sample; this technique is limited by diffraction and the minimal spot size is about 200-300 nm. These small spots indicate that the

emitter is made of a limited number of molecules but it does not ensure that it is due to a single GQD. To have an idea of the number of molecules in this spot, we examined the stability of its photoluminescence.

2.3.2. Single molecule discrimination

The photobleaching of the molecules under the beam can be used to determine the number of emitters. In fact, in the case of multiple molecules under illumination, the molecules will be turned off one after the others. This phenomenon will give rise to a decrease of the PL intensity over time with discrete jumps as the number of molecules becomes close to one (Figure 2.18).

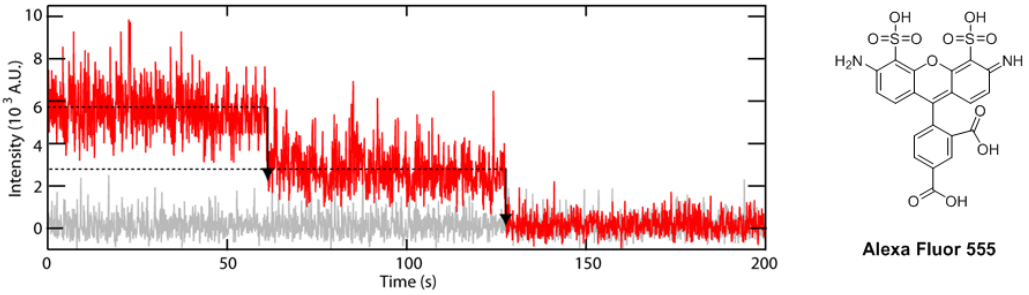

Figure 2.18: Spectrum of the PL intensity over time for the Alexa Fluor 555 dye (red) compared to the background (grey)[16]

In the case of a single emitter, this intensity should exhibit a single step from a constant intensity down to zero. This means that the only light source is a GQD and when it turns off, the PL is extinguished. In our case, the objective is focused on a spot and the PL is recorded to trace the spectrum of the intensity over time (Figure 2.19).

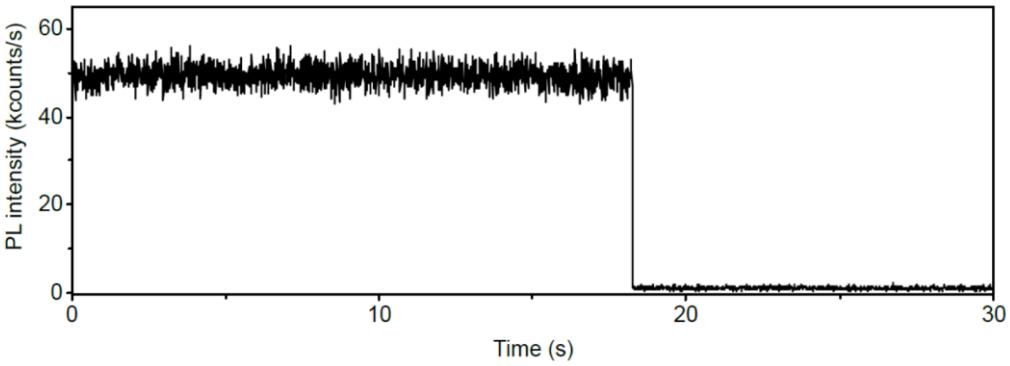

*Figure 2.19: PL intensity evolution as a function of time for a diffraction limited spot of GQD **3***

The PL intensity trace presented in Figure 2.19 was observed for multiple spots, it confirms that the spots are made of a single GQD (or of very few molecules which all turned off simultaneously, which is unlikely) and it allowed us to ensure that the PL obtained is intrinsic to the C96C12 GQD **3**. In term of stability, GQD **3** is stable for hours with no blinking at a usual power of 200 nW (Figure 2.20).

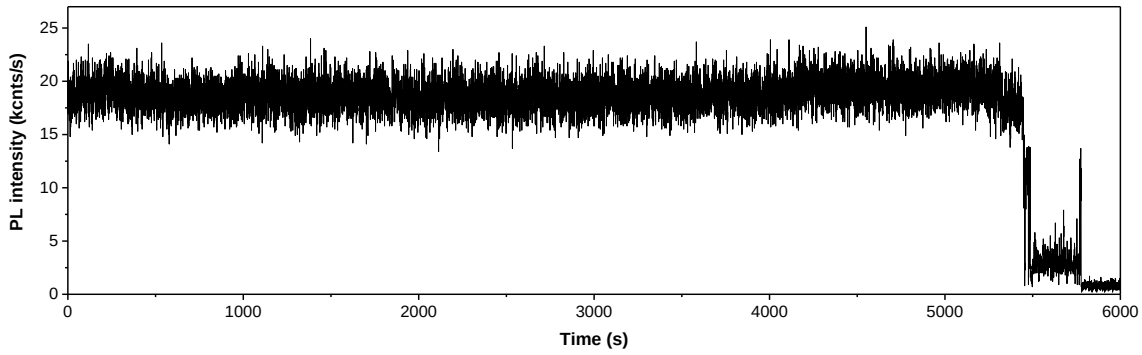

*Figure 2.20: Typical photostability of C96C12 GQD **3** over time*

The high photostability of the sample is a promising result for the optical study and the applications of the GQDs. The confirmation of the uniqueness of the emitter permits the study of the single photon emission starting with the PL of a single molecule.

2.3.1. Photoluminescence

The confirmation of the single molecule characteristic of our sample allows us to look at the intrinsic PL of the GQD **3**. The overall shape of the PL (Figure 2.21) is very similar to the one obtained in solution (Figure 2.12) which confirms the good dispersion of the GQDs.

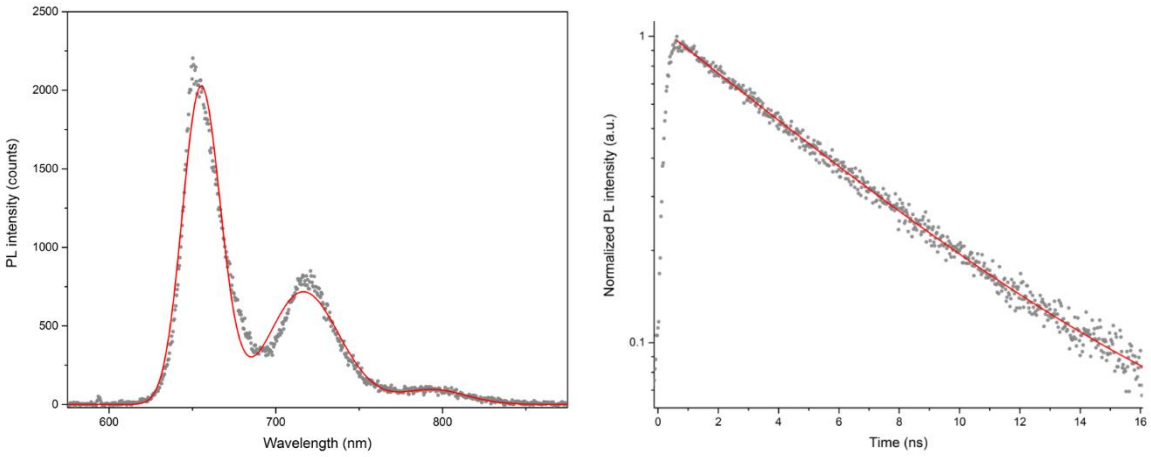

*Figure 2.21: PL spectrum and time-resolved PL of a single C96C12 GQD **3***

The main peak is still located at 653 nm with peaks at lower energy at 719 and 797 nm. The time-resolved PL is in good agreement with the results in solution and shows a mono-exponential decay with a life-time of about 4.7 ns.

2.3.2. Single photon emitter

The single photon emission properties were introduced in chapter 1.4. and we showed that this unique property was characterized by the evolution of the second order correlation function $g^{(2)}(\tau)$. In theory for a single photon emitter, this function should go down to zero when $\tau = 0$ however, experimentally, the emitter is considered a single photon emitter if $g^{(2)}(0) < 0.5$. The setup for the measurement of $g^{(2)}(\tau)$ is the same as for PL mapping but this time the emitted light is collected into the Hanbury Brown-Twiss setup made of a 50:50 beam splitter and two detectors (Figure 2.22).

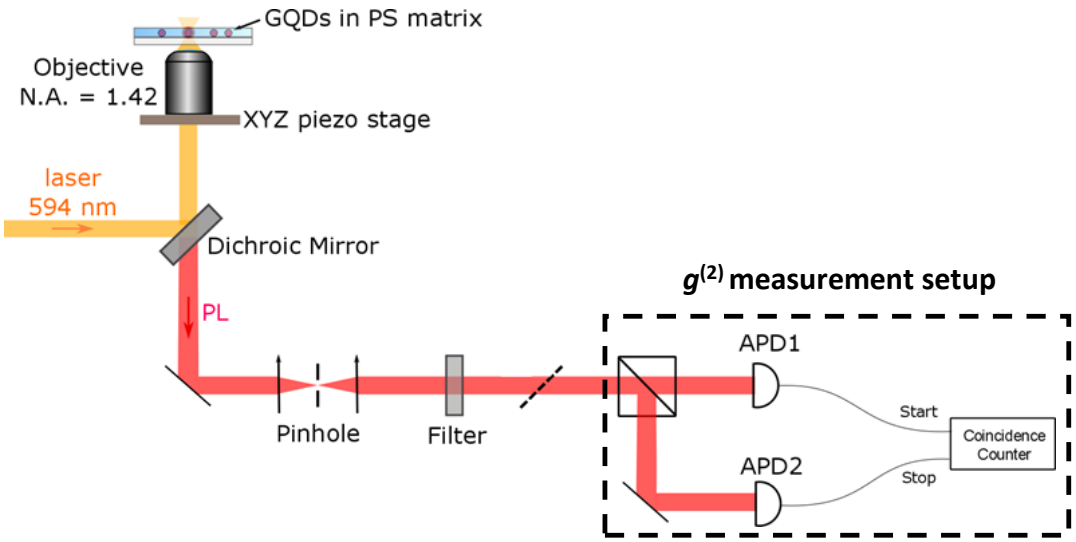

Figure 2.22: Schematic representation of the experimental setup for the measurement of the $g^{(2)}$ function

In our case, the correlation function plotted in Figure 2.23a exhibits a $g^{(2)}(0) = 0.05$. This result is in strong contrast with the results of such experiments performed on "top-down" GQDs made from graphene oxide where no antibunching was observed.[17] In this study, the absence of antibunching was interpreted as a consequence of the extrinsic nature of the states at the origin of the luminescence: multidefect sites emitting in an uncorrelated manner. In our case, we have performed measurements on more than 30 specimens of GQD **3**, all of them leading to $g^{(2)}(0) < 0.1$. Moreover, the weak value observed for the $g^{(2)}(0)$ is an indication of the good purity of single photon emission associated with the single graphene quantum dots. This result strongly suggests that GQDs synthesized *via* the "bottom-up" approach constitute interesting alternatives to other single emitters, such as defects in WSe2,[18–22] in *h*-BN[23–25] or to carbon nanotubes.[26] Indeed, the emission wavelength of GQDs can be tuned thank to their size and/or functionalities. In addition, water soluble GQDs could find important applications in biology as stable, bright and non-toxic dyes. These results have been summarized in a paper deposited on ArXiv[27] and have been accepted for publication in Nature Communications.[28]

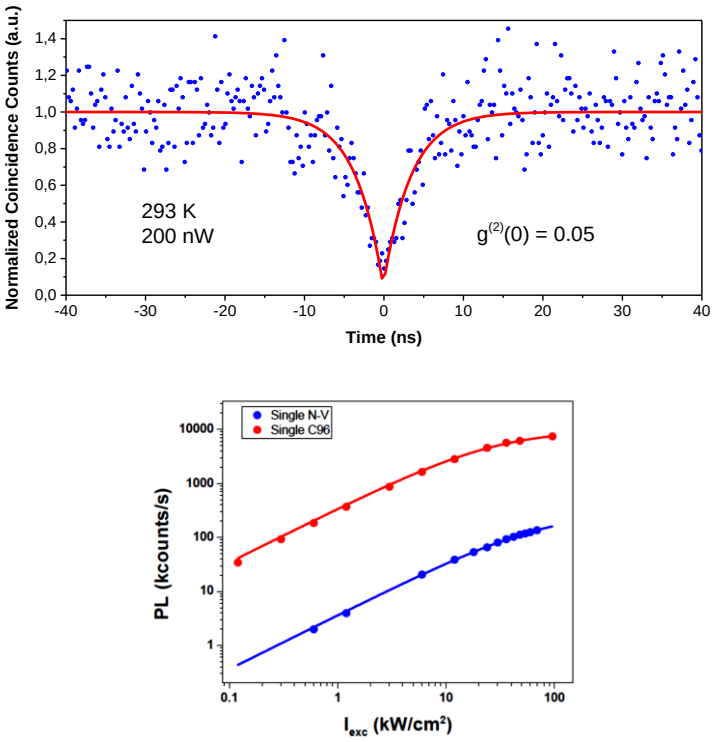

*Figure 2.23: a) $g^{(2)}$ function for GQD **3** and b) comparison between the saturation curve for GQD **3** (red) and NV center (blue); the experiments were realized on the same setup.*

The confirmation of the character of single photon emitter allowed us to explore other important characteristics like brightness. The brightness is extracted from the saturation curve (Figure 2.23b) measured increasing the power of excitation and plotting the intensity of the PL. The intensity of the PL in this case is fitted by: $R = R_{sat}/(1 + \frac{I_{sat}}{I_{exc}})$

With R_{sat} the count rate at saturation, I_{sat} the incident power at saturation and I_{exc} the incident power. The fit leads to R_{sat}~9.7 Mcounts/s and I_{sat}= 28 kW.cm^{-2}. These results were compared with the widely used NV centers in diamond and particularly with a NV center in 111-diamond on the same setup. This emitter led to a R_{sat}~0.3 Mcounts/s which is coherent with the values of the literature[29] but this value is 30 times lower than the one obtained for GQD **3**.

2.3.3. Optical study of C96Cl

The advantage of GQDs compared to the current single photon emitters is that the doping, the functionalization or the change of the size or edge states could allow us to tune the optical properties of the GQDs. The chlorination of nanoparticle induces a red shift of the absorption and emission compared to the bare or alkyl-functionalized GQDs **1** and **3**.[5] To this end, GQD **2** was dispersed in TCB and polystyrene and then spin-coated on glass coverslips. The procedure was the same than the one established for GQD **3**: a dispersion of **2** in TCB at 0.01 mg/ml is mixed with purified polystyrene in TCB (0.075 mg/ml) and sonicated in an ultrasonic bath for 10 seconds. Approximately 20 µl of the mixture is spin-coated at 2000 rpm for 180 seconds[15] on a glass coverslip previously treated with oxygen plasma for 5min to remove any organic contaminant and the sample is then dried at 90°C for 1h.

We were able to obtain the PL spectrum of a single C96Cl GQD **2** and a red-shift of *ca.* 100 nm compared to the PL of GQD **3** was observed (Figure 2.24a). C96Cl GQD **2** also exhibited single photon emission properties (Figure 2.24b).

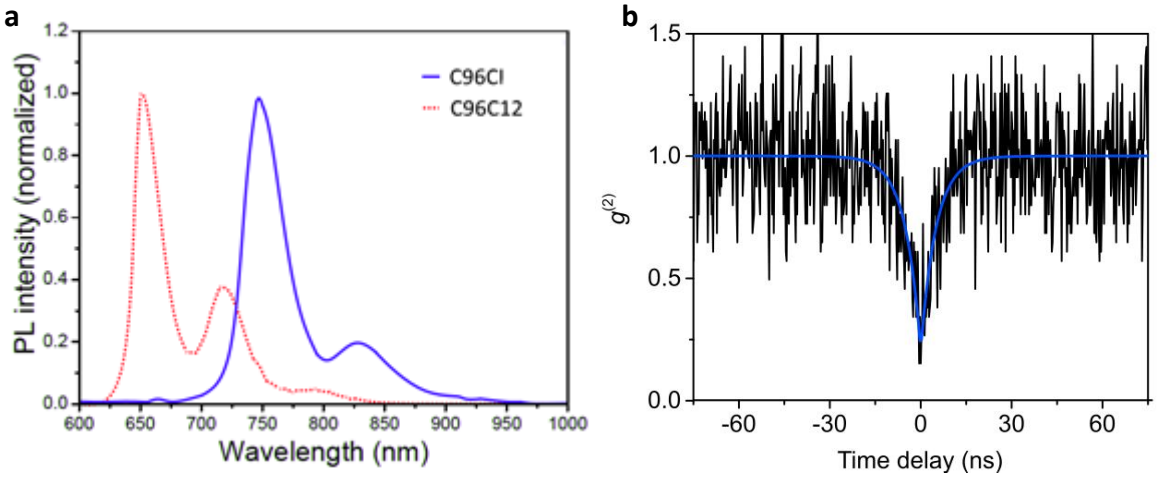

*Figure 2.24: a) PL spectra of C96Cl **2** (blue line) and C96C12 **3** (red dot line) and b) $g^{(2)}$ function for C96Cl **2**.*

2.4. Conclusion

To sum up, we were able to reproduce the synthesis of three GQDs containing 96 sp^2 carbon atoms in their aromatic cores: one without any functional groups at the periphery (GQD **1**),

one containing 27 chlorine atoms (GQD **2**) and one containing six $C_{12}H_{25}$ alkyl chains (GQD **3**). The solubility of the GQDs is increased depending on the edge functionalization and this allowed dispersion of the functionalized GQDs in TCB for optical studies. The optical properties were further explored for C96C12 GQD **3** with the study of its properties at the single molecule level. GQD **3** exhibited a single photon emission with a photostability of hours with no blinking and an intensity of saturation 30 times better than NV centers in diamond. Moreover, we proved that the functionalization of GQD **1** with chlorine to form C96Cl **2** can tune the bandgap while keeping the single photon emission properties. To further explore the properties of those materials, we decided to focus on one parameter, the length variation, while keeping the atomically controlled structure; this gave rise to graphene nanorods (GNRods) which will be detailed in Chapter 3.

2.5. References

(1) Grimsdale, A. C.; Müllen, K. The Chemistry of Organic Nanomaterials. *Angew. Chemie - Int. Ed.* **2005**, *44*, 5592–5629.

(2) Herwig, P.; Kayser, C. W.; Müllen, K.; Spiess, H. W. Columnar Mesophases of Alkylated Hexa-Peri-Hexabenzocoronenes with Remarkably Large Phase Widths. *Adv. Mater.* **1996**, *8*, 510–513.

(3) Iyer, V. S.; Wehmeier, M.; Diedrich, J.; Keegstra, M. A.; Müllen, K. From Hexa-Peri-Hexabenzocoronene to "Superacenes." *Angew. Chemie - Int. Ed.* **1997**, *36*, 1603–1607.

(4) Tomović, Ž.; Watson, M. D.; Müllen, K. Superphenalene-Based Columnar Liquid Crystals. *Angew. Chemie - Int. Ed.* **2004**, *43*, 755–758.

(5) Tan, Y. Z.; Yang, B.; Parvez, K.; Narita, A.; Osella, S.; Beljonne, D.; Feng, X.; Müllen, K. Atomically Precise Edge Chlorination of Nanographenes and Its Application in Graphene Nanoribbons. *Nat. Commun.* **2013**, *4*, 3647.

(6) Scholl, R.; Mansfeld, J. Meso-Benzdianthron (Helianthron), Meso-Naphthodianthron, Und Ein Neuer Weg Zum Flavanthren. *Berichte der Dtsch. Chem. Gesellschaft* **1910**, *43*, 1734–1746.

(7) Scholl, R.; Seer, C.; Weitzenböck, R. Perylen, Ein Hoch Kondensierter Aromatischer Kohlenwasserstoff C20H12. *Berichte der Dtsch. Chem. Gesellschaft* **1910**, *43*, 2202–2209.

(8) Mattioli, C. Design, Synthesis and Study of Molecules for Graphene Functionalization., 'Université Toulouse III Paul Sabatier, 2014.

(9) Mohr, B.; Enkelmann, V.; Wegner, G. Synthesis of Alkyl- and Alkoxy-Substituted Bends and Oxidative Coupling to Tetraalkoxyphenanthrene-9,10-Diones. *J. Org. Chem.* **1994**, *59*, 635–638.

(10) Shapiro, E.; Becker, E. Steric Effects and Spectra in the Tetracyclones. *Tetrahedron* **1953**, *857*, 4769–4775.

(11) Ito, S.; Wehmeier, M.; Brand, J. D.; Kübel, C.; Epsch, R.; Rabe, J. P.; Müllen, K. Synthesis and Self-Assembly of Functionalized Hexa-Peri-Hexabenzocoronenes. *Chem. - A Eur. J.* **2000**, *6*, 4327–4342.

(12) Przybilla, L.; Brand, J.; Yoshimura, K.; Rader, H.; Mullen, K. MALDI-TOF Mass Spectrometry of Insoluble Giant Polycyclic Aromatic Hydrocarbons by a New Method of Sample Preparation. *Anal. Chem.* **2000**, *72*, 4591–4597.

(13) Debije, M. G.; Piris, J.; De Haas, M. P.; Warman, J. M.; Tomović, Ž.; Simpson, C. D.; Watson, M. D.; Müllen, K. The Optical and Charge Transport Properties of Discotic Materials with Large Aromatic Hydrocarbon Cores. *J. Am. Chem. Soc.* **2004**, *126*, 4641–4645.

(14) Tian, Y.; Sheinin, V.; Kulikova, O.; Mamardashvili, N.; Scheblykin, I. G. Improving Photo-Stability of Conjugated Polymer MEH-PPV Embedded in Solid Matrices by Purification of the Matrix Polymer. *Chem. Phys. Lett.* **2014**, *599*, 142–145.

(15) Fleury, L.; Segura, J. M.; Zumofen, G.; Hecht, B.; Wild, U. P. Nonclassical Photon Statistics in Single-Molecule Fluorescence at Room Temperature. *Phys. Rev. Lett.* **2000**, *84*, 1148–1151.

(16) Bumb, A.; Sarkar, S. K.; Wu, X. S.; Brechbiel, M. W.; Neuman, K. C. Quantitative Characterization of Fluorophores in Multi-Component Nanoprobes by Single-Molecule Fluorescence. *Biomed. Opt. Express* **2011**, *2*, 2761–2769.

(17) Xu, Q.; Zhou, Q.; Hua, Z.; Xue, Q.; Zhang, C.; Wang, X.; Pan, D.; Xiao, M. Single-Particle Spectroscopic Measurements of Fluorescent Graphene Quantum Dots. *ACS Nano* **2013**, *7*, 10654–10661.

(18) Koperski, M.; Nogajewski, K.; Arora, A.; Cherkez, V.; Mallet, P.; Veuillen, J. Y.; Marcus, J.; Kossacki, P.; Potemski, M. Single Photon Emitters in Exfoliated WSe2 Structures. *Nat. Nanotechnol.* **2015**, *10*, 503–506.

(19) Srivastava, A.; Sidler, M.; Allain, A. V.; Lembke, D. S.; Kis, A.; Imamoglu, A. Optically Active Quantum Dots in Monolayer WSe2. *Nat. Nanotechnol.* **2015**, *10*, 491–496.

(20) Chakraborty, C.; Kinnischtzke, L.; Goodfellow, K. M.; Beams, R.; Vamivakas, A. N. Voltage-Controlled Quantum Light from an Atomically Thin Semiconductor. *Nat. Nanotechnol.* **2015**, *10*, 507–511.

(21) He, Y. M.; Clark, G.; Schaibley, J. R.; He, Y.; Chen, M. C.; Wei, Y. J.; Ding, X.; Zhang, Q.; Yao, W.; Xu, X.; et al. Single Quantum Emitters in Monolayer Semiconductors. *Nat. Nanotechnol.* **2015**, *10*, 497–502.

(22) Tonndorf, P.; Schmidt, R.; Schneider, R.; Kern, J.; Buscema, M.; Steele, G. A.; Castellanos-Gomez, A.; van der Zant, H. S. J.; Michaelis de Vasconcellos, S.; Bratschitsch, R. Single-Photon Emission from Localized Excitons in an Atomically Thin Semiconductor. *Optica* **2015**, *2*, 347–352.

(23) Li, X.; Shepard, G. D.; Cupo, A.; Camporeale, N.; Shayan, K.; Luo, Y.; Meunier, V.; Strauf, S. Nonmagnetic Quantum Emitters in Boron Nitride with Ultranarrow and Sideband-Free Emission Spectra. *ACS Nano* **2017**, *11*, 6652–6660.

(24) Martínez, L. J.; Pelini, T.; Waselowski, V.; Maze, J. R.; Gil, B.; Cassabois, G.; Jacques, V. Efficient Single Photon Emission from a High-Purity Hexagonal Boron Nitride Crystal. *Phys. Rev. B* **2016**, *94*, 121405.

(25) Tran, T. T.; Bray, K.; Ford, M. J.; Toth, M.; Aharonovich, I. Quantum Emission from Hexagonal Boron Nitride Monolayers. *Nat. Nanotechnol.* **2016**, *11*, 37–41.

(26) He, X.; Htoon, H.; Doorn, S. K.; Pernice, W. H. P.; Pyatkov, F.; Krupke, R.; Jeantet, A.; Chassagneux, Y.; Voisin, C. Carbon Nanotubes as Emerging Quantum-Light Sources. *Nat. Mater.* **2018**.

(27) Zhao, S.; Lavie, J.; Rondin, L.; Orcin-Chaix, L.; Diederichs, C.; Roussignol, P.; Chassagneux, Y.; Voisin, C.; Müllen, K.; Narita, A.; et al. Single Photon Emission from Graphene Quantum Dots at Room Temperature. **2018**.

(28) Zhao, S.; Lavie, J.; Rondin, L.; Orcin-Chaix, L.; Diederichs, C.; Roussignol, P.; Chassagneux, Y.; Voisin, C.; Müllen, K.; Narita, A.; et al. Single Photon Emission from Graphene Quantum Dots at Room Temperature. *Nat. Commun.* **2018**.

(29) Lesik, M.; Tetienne, J. P.; Tallaire, A.; Achard, J.; Mille, V.; Gicquel, A.; Roch, J. F.; Jacques, V. Perfect Preferential Orientation of Nitrogen-Vacancy Defects in a Synthetic Diamond Sample. *Appl. Phys. Lett.* **2014**, *104*, 113107.

Chapter 3 : Graphene Nanorods

Chapter 2: Graphene Quantum Dots

Chapter 3: Graphene Nanorods

3.1. Introduction

The optical characterization of the intrinsic properties of GNRs is complicated due to their low solubility and their polydispersity. To be able to discriminate the effects of the width, the edge state and of the length on the properties it is necessary to control those parameters. While for GNRs the control of the width and the edge state is done by the choice of the precursor, the control of the length is impossible due to the polymerization. Therefore, the development of a new type of 1D materials with controlled width, edge state and length is mandatory to understand the impact of this parameter on the optical properties observed.

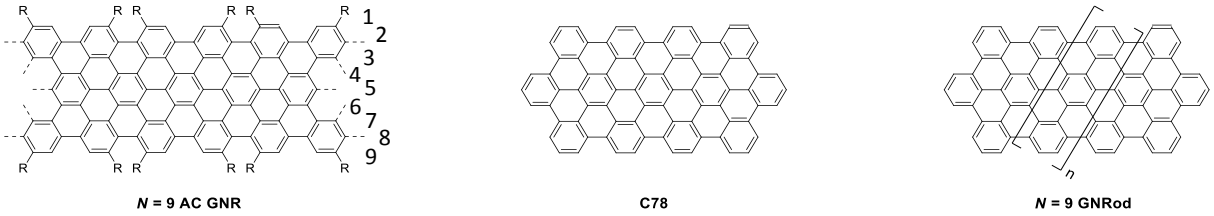

Figure 3.1: Structures of the N = 9 AC GNR, C78 GNRod and N = 9 GNRod.

By analogy with "gold nanorods", an intermediate object between round-shaped gold nanoparticles and gold nanowires, we called this new type of graphene material "graphene nanorods" (GNRods). The first structure we studied is based on the *N* = 9 AC GNR[1] (Figure 3.1) and is made of 78 carbon atoms (C78). This rod-shaped graphene quantum dots, of formula $C_{78}H_{26}$, exhibits a width of about 0.9 nm and a length of about 2.5 nm; it has already been reported by Klaus Müllen.[2] The variation of length of the GNRod can be achieved *via* the controlled addition of a rows of phenyls to the structure to give rise to the *N* = 9 GNRod family. In this study we focused on the addition of a single row of phenyls to form the first member of this family. In the case of the graphene particle **11**, the addition of this row gives rise to a linear structure, $C_{96}H_{30}$ **12** (C96L) (Figure 3.2). It is interesting to notice that this nanoparticle constitutes an isomer of the triangle-shaped GQD **1** described in Chapter 2.

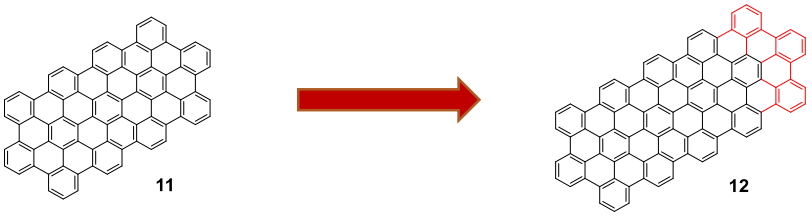

*Figure 3.2: Length variation of C78 graphene nanoparticles **11.***

The second structure we studied is based on the *N* = 15 GNR and the corresponding GNRod is $C_{132}H_{34}$ (C132) (Figure 3.3).[3] This structure has the same length of about 2.5 nm but it has a width of about 1.5 nm. The addition of multiple rows of phenyl gives rise to the *N*=15 GNRods.

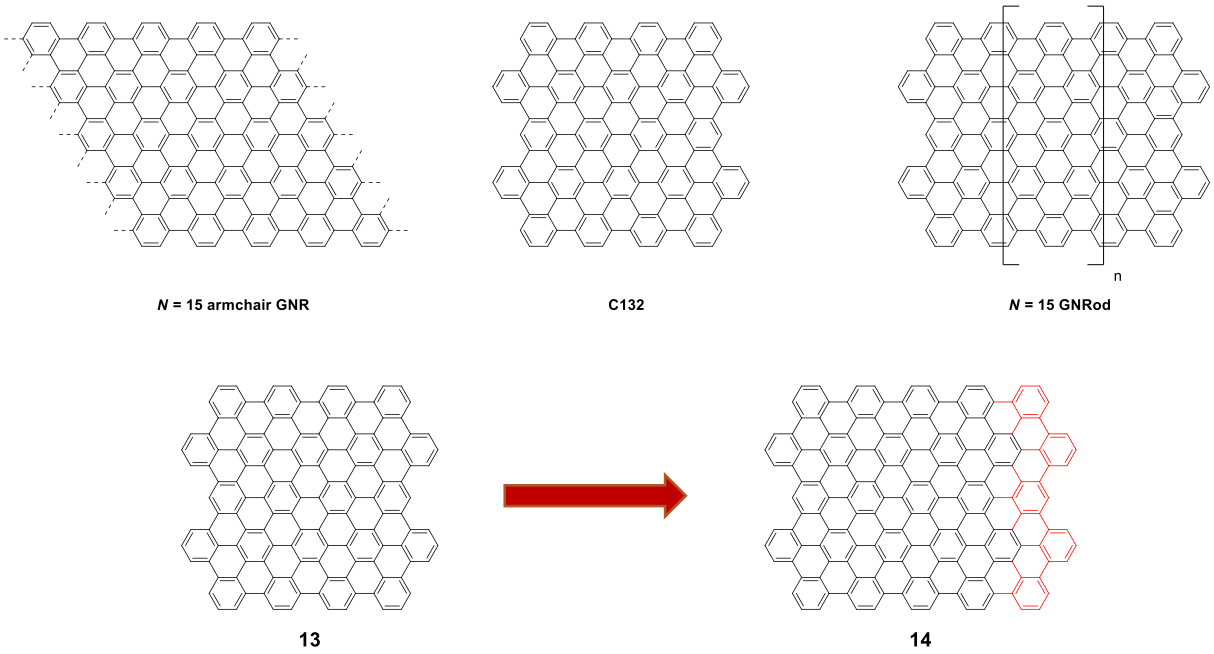

*Figure 3.3: Structures of the N = 15 GNR, C132 GNRod and N = 15 GNRod and schematic representation of the extension of the C132 graphene nanoparticles **13***

Similarly to C78 **11**, the C132 GNRod **13** was also prepared with an additional row of phenyl rings and it gave a new structure, $C_{162}H_{38}$ **14** (C162) (Figure 3.3).

Like the graphene quantum dots described in Chapter 2, the structure and the properties of these GNRods can be tuned either by the addition of alkyl chains of chlorine atoms and therefore this creates a wide range of structure variation that we synthesized (Figure 3.4).

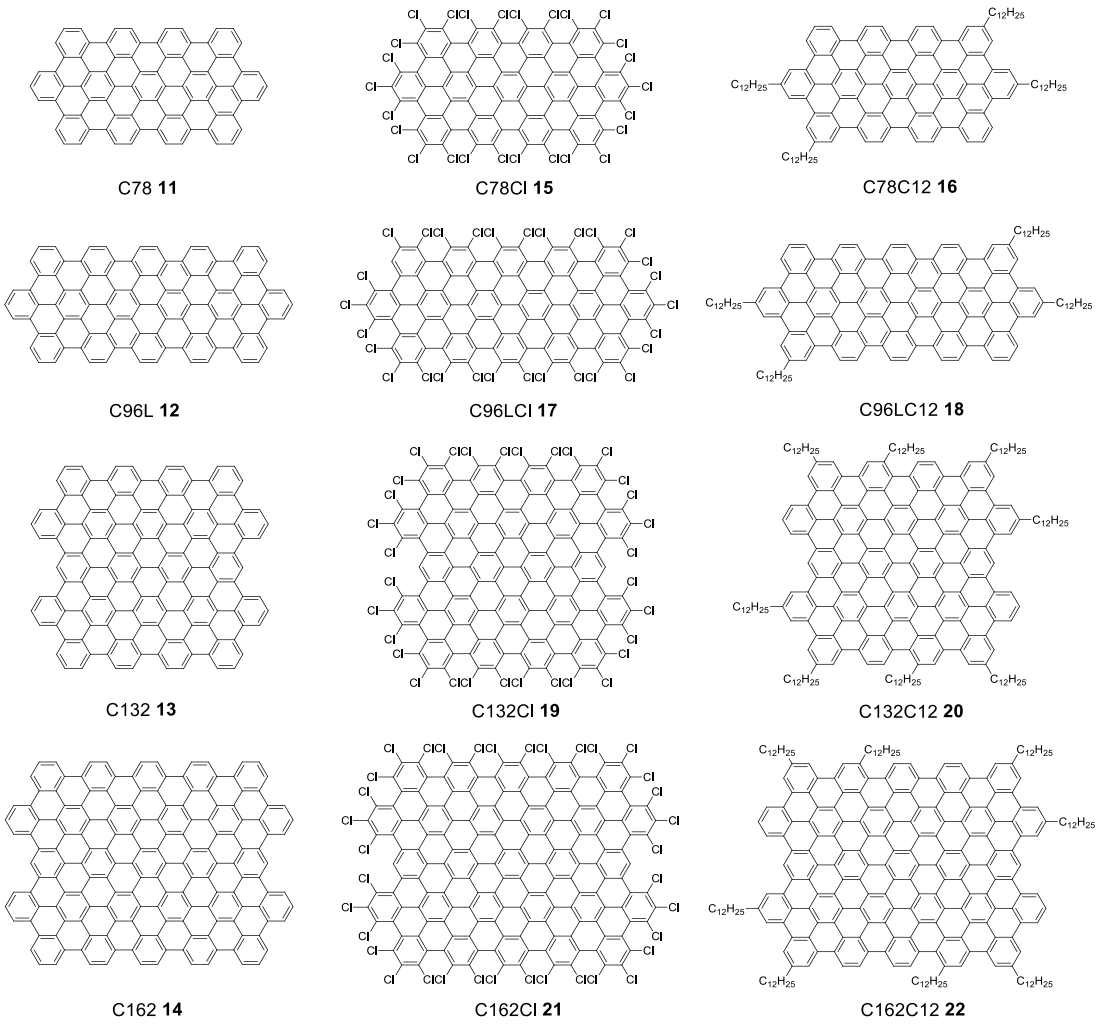

Figure 3.4: Structures of the GNRods synthesized in this Chapter

3.2. *N* = 9 graphene nanorods

The synthetic methods of the GNRods are the same as those presented for GQDs in the previous chapter. The first step is a Diels-Alder reaction with an acetylenic precursor to form a polyphenyl dendrimer which is oxidized and eventually chlorinated. The first synthetic route, described by Müllen, for the preparation of C78 GNRod was based on the reaction of 1,3-di(phenyl-ethynyl)benzene **23** with tetraphenylcyclopentadienone (Figure 3.5).[2]

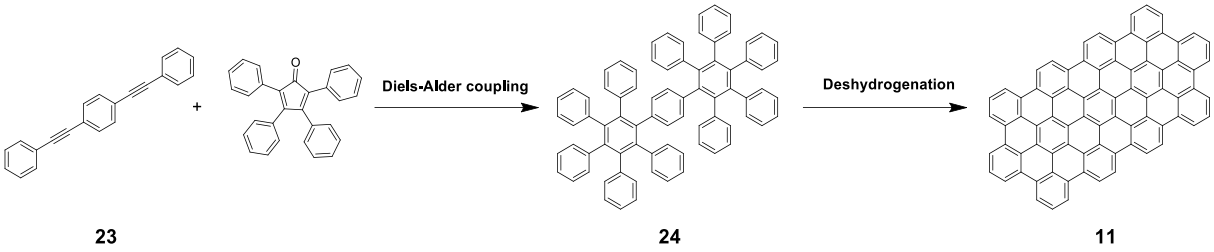

Figure 3.5: First synthetic route for the preparation of C78.[2]

However, to increase the length of the GNRod in one direction, we have decided to explore another approach based on the use of 2',5'-diethynyl-*para*-terphenyl core and tune the number of terphenyl in the core to gradually increase the number of terphenyl units in the core (see below paragraph 3.2.1.). Most of the syntheses presented in this chapter are based on two palladium catalyzed reactions: the Suzuki coupling and the Sonogashira coupling; the mechanism of these reactions are described in Figure 3.6.

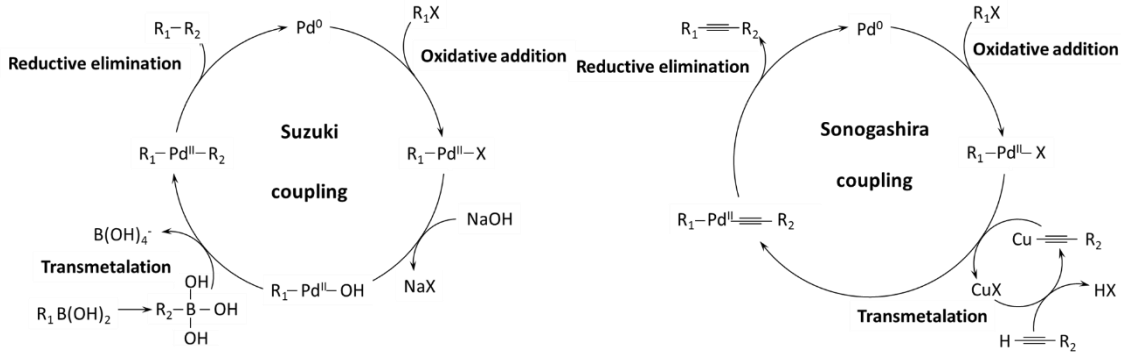

Figure 3.6: Representation of the Suzuki and Sonogashira catalytic cycles.

Each palladium coupling is made of three steps, the oxidative addition, the transmetalation and the reductive elimination. In the case of the Sonogashira coupling, an additional step is needed involving the metalation of the alkyne group with copper (I) before the transmetalation. These reactions should be carried out under argon to prevent the inhibition of the palladium (0) catalyst by oxygen and therefore, the solvent used are distillated and subsequently degassed with "freeze-pump-thaw" technique. This technique consists in the freezing of the solvent with liquid nitrogen followed by the slow heating up to room temperature under vacuum to remove gases from the solution.

3.2.1. Synthesis and characterization of the C78 family

The synthesis of the desired 2',5'-diethynyl-*para*-terphenyl **29** started with the disylilation of 1,4-diiodobenzene with trimethylsilyl chloride in the presence of lithium di-*iso*-propylamide (LDA) (

Scheme 3.1)[4] to give 1,4-diiodo-2,5-bis(trimethylsilyl)benzene **25** with a decent yield of 64%. It was followed by a Suzuki coupling with two equivalents of phenylboronic acid. The Suzuki reaction was performed with $Pd(PPh_3)_2Cl_2$ catalyst in the presence of K_2CO_3 in a mixture of THF, EtOH and water and the *para*-terphenyl derivative **26** was obtained with 97% yield. The product was iodinated directly with 4 equivalents of ICl (1M in CH_2Cl_2) (2 equivalents *per* TMS group) to give 2',4'-diiodo-*para*-terphenyl **27**. The final step was the Sonogashira coupling of two equivalents of ethynyltrimethylsilane on diiodo-*para*-terphenyl **27**. The resulting protected compound **28** was deprotected with tetra-*n*-butylammonium fluoride (TBAF) to give precursor **29** right before the Diels-Alder reaction.

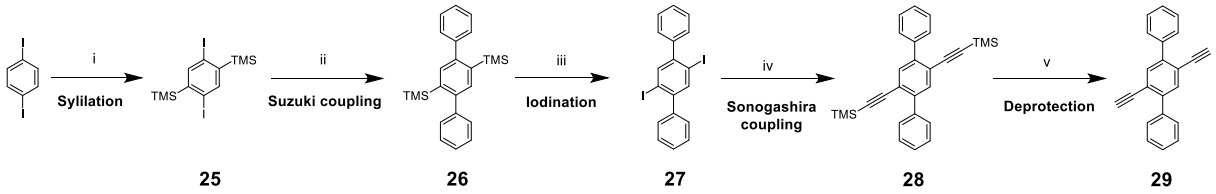

Scheme 3.1: i) TMSCl, LDA, -78°C, 1h, 64%; ii) $PhB(OH)_2$, $Pd(PPh_3)_2Cl_2$, K_2CO_3, THF/EtOH/H_2O, 60°C, overnight, 97%; iii) ICl, DCM, R.T., overnight, 40%; iv) ethynyltrimethylsilane, $Pd(PPh_3)_2Cl_2$, CuI, 80°C, 24h, 96%; v) TBAF, R.T., 2h, 91%.

The protected precursor **28** was characterized by ^{1}H-NMR spectroscopy. The NMR spectrum exhibited a singlet at 7.61 ppm for the two aromatic protons of the central phenyl, a mutiplet from 7.66 to 7.63 ppm for the four protons of the external phenyl in *ortho* position of the central phenyl and a multiplet between 7.43 and 7.35 ppm for the other protons of the external phenyls. Finally the eighteen protons of the TMS groups appear as a singlet at 0.13 ppm (Figure 3.7).

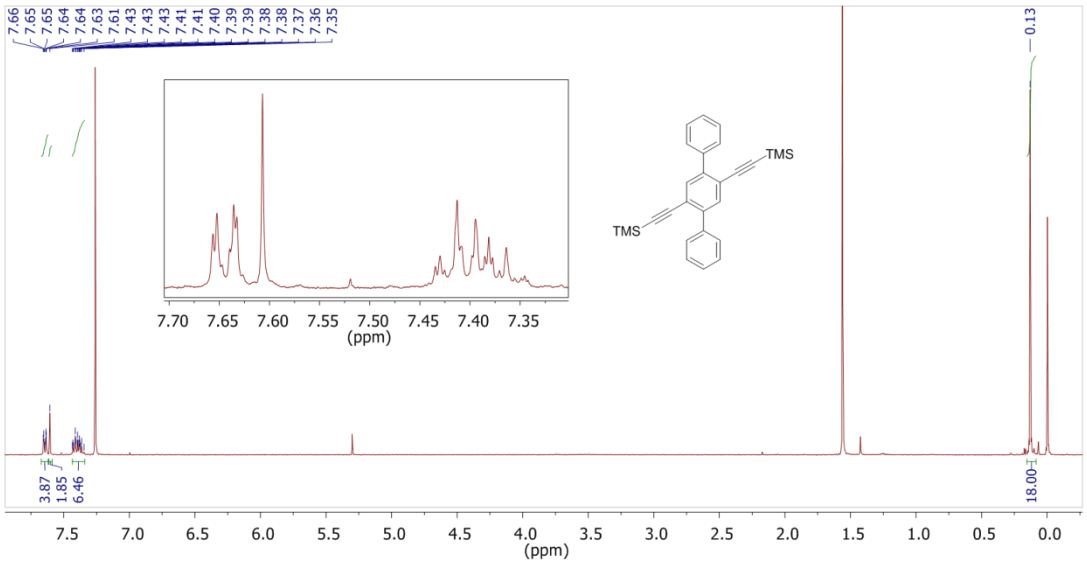

*Figure 3.7: ^{1}H-NMR spectrum of the protected precursor **28** in $CDCl_3$.*

To prepare GNRod **11**, precursor **29** underwent a Diels-Alder reaction with tetraphenylcyclopentadienone and the resulting polyphenylene dendrimer **30** was dehydrogenated with $FeCl_3$ to give the C78 GNRod **11** (Scheme 3.2).

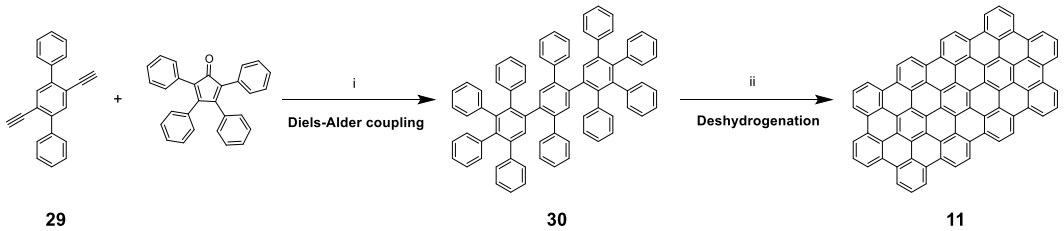

Scheme 3.2: i) o-xylene, 180°C, overnight, 51%; ii) $FeCl_3$, $MeNO_2$, DCM, R.T., overnight, 90%.

The MALDI-TOF mass spectrum of dendrimer **30** was done by solubilizing the molecule in DCM and mixing it with the DCTB matrix. Figure 3.8a showed the di-substituted compound at *m/z* of 990.43 (M^+) and 1013.42 $(M+Na)^+$. The completely dehydrogenated GNRod had a low solubility in the usual organic solvents and therefore, as for GQD **1**, the characterization of this product was only possible using the mixing of the sample with TCNQ matrix as presented in 2.1.2 for C96 **1**. The spectrum of GNRod **11** exhibited a main peak at *m/z* of 962.26 (M^+) and a second peak corresponding to $(M+Na)^+$ at 985.63 (Figure 3.8b).

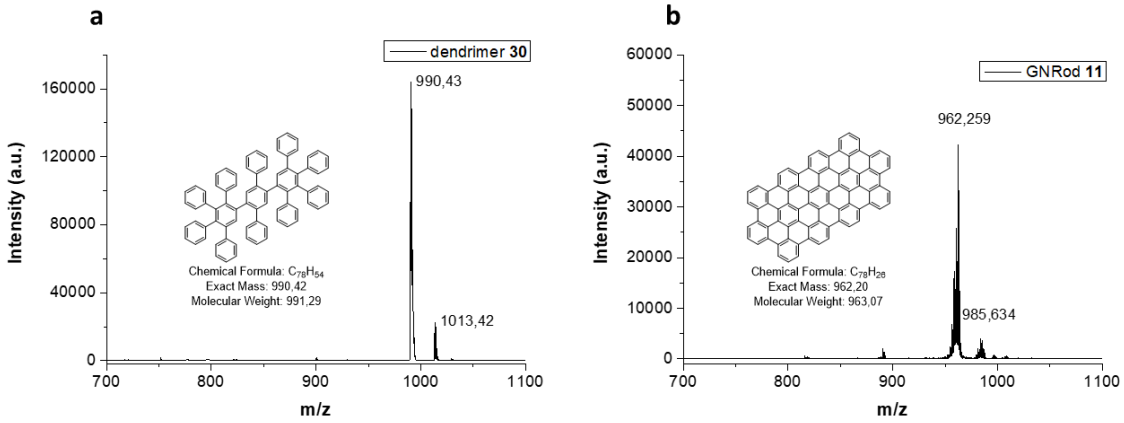

*Figure 3.8: MALDI-TOF mass spectra of a) dendrimer **30** and b) GNRod **11.***

GNRod **11** can be functionalized with chlorine and alkyl chains like to form a complete family. For the chlorination, the condition was similar to the one used for GQD **2**, $AlCl_3$ and ICl in CCl_4 at 80°C for 30 hours (Scheme 3.3). However, despite changes in the reaction time, (up to 72 h) and $AlCl_3$ and ICl equivalents, the product was always obtained as a mixture of partially chlorinated compounds. Similarly to GQD **3**, the C78C12 **16** GNRod was prepared *via* Diels-Alder reaction of precursor **29** with alkyl-substituted tetraphenylcyclopentadienone **9** and the dehydrogenation of the resulting dendrimer **31** was performed with $FeCl_3$.

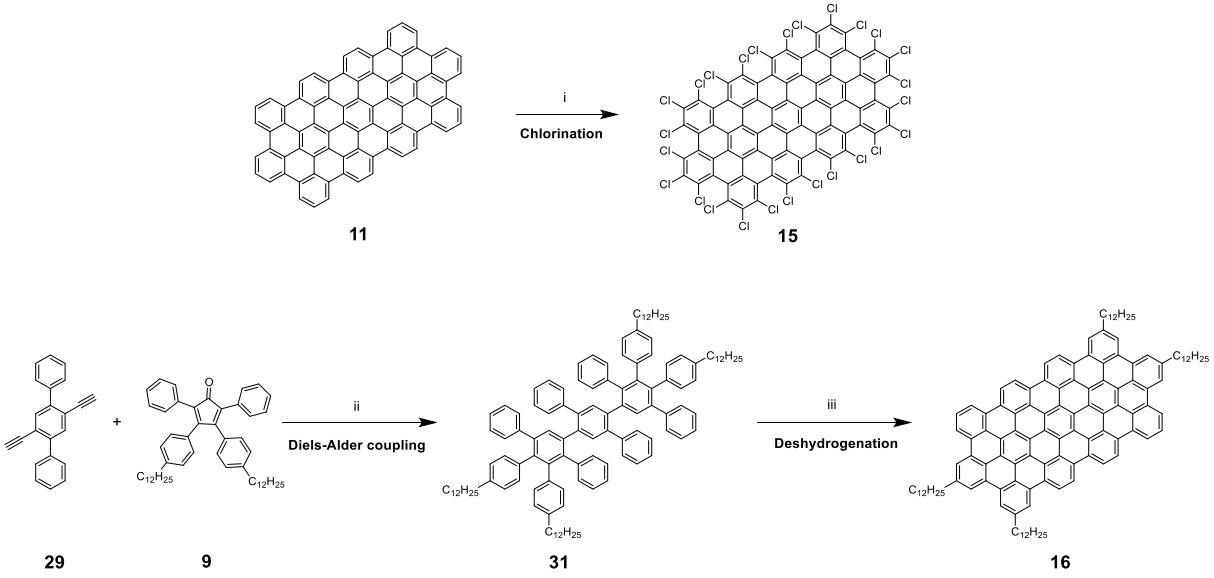

Scheme 3.3: i) $AlCl_3$, ICl, CCl_4, 80°C, 72h, 10%; ii) o-xylene, 180°C, overnight, 98%; iii)$FeCl_3$, $MeNO_2$, DCM, R.T., 5h, 66%.

The product of the synthesis of GNRod **15** was characterized with MALDI-TOF spectrometry and the spectrum exhibits a mixture of chlorinated compounds with the GNRod missing two chlorine as the main product at *m/z* of 1788.15 (Figure 3.9a). This powder cannot be purified due to the low difference in polarity between the fully chlorinated compound and the ones missing few chlorines. The spectrum of GNRod **16** shown Figure 3.9b exhibited two peaks of the desired product at *m/z* of 1635.11 (M^+) and 1657.98 $(M+Na)^+$ with no traces of the chlorinated compound at 1668.92.

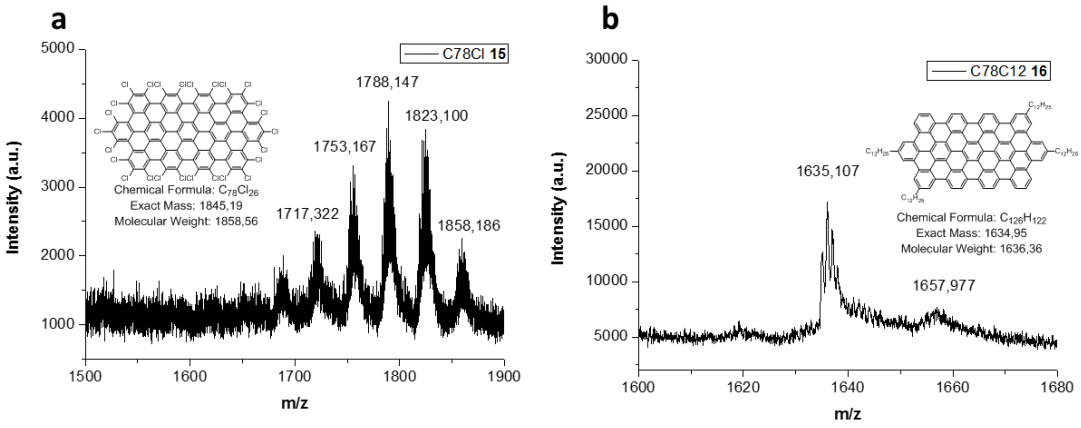

*Figure 3.9: MALDI-TOF of a) GNRod **15** and b) GNRod **16**.*

After preparing these first GNRods, we extended the length in one direction while keeping the same edge state changing the precursor used.

3.2.2. Synthesis and characterization of the linear C96 family

The preparation of the linear C96 structure (C96L) is based on the same principle as the preparation of C78 **11**. Considering the shape of the molecule, the deduction of the precursor needed is straightforward from the synthesis of GNRod **11**, C96L polyphenylene dendrimer **33** should be prepared from bis(terphenyl) core **32** (Figure 3.10).

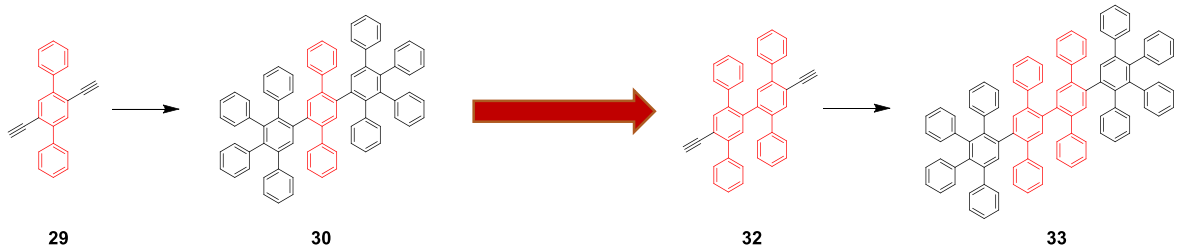

*Figure 3.10: Determination of the precursor for C96L **12**.*

To determine the synthetic route for the preparation of the acetylenic precursor **32**, we performed a retrosynthetic study (Figure 3.11). The ethynyl groups will be added by Sonogashira coupling on the dihalogenated-diterphenyl derivative which will be prepared from the di(TMS)-diterphenyl derivative. The latter will be obtained from monohalogenated-terphenyl which will be synthesized from the terphenyl **26**.

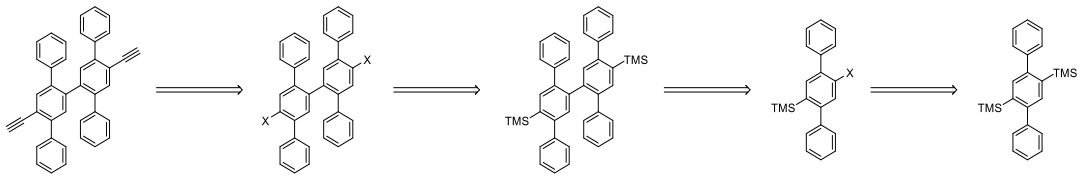

*Figure 3.11: Retrosynthesis for the preparation of precursor **32.***

To perform this synthesis, *para*-terphenyl **26** was mono-iodinated in the presence 0.9 equivalents of $AgBF_4$ and ICl (1M in CH_2Cl_2) to give the mono-iodo terphenyl derivative **34** (Scheme 3.4).[5] The addition of ICl was done at 0°C and the reaction was left 1 h at room temperature. The reaction did not form the di-iodoterphenyl derivative but led to a mixture of terphenyl **26** and monoiodo-terphenyl **34**. The iodoterphenyl **34** was purified partially by column chromatography since a part of the terphenyl **26** can be removed and a part remains in mixture with **34**. The presence of *para*-terphenyl **26** is not an issue for the next reaction since the TMS groups are not reactive.

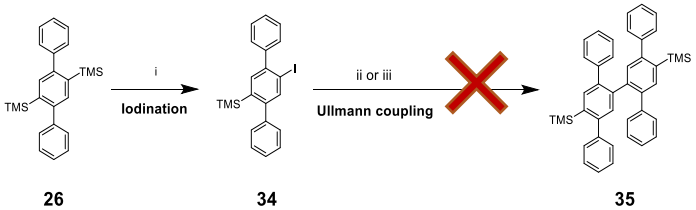

Scheme 3.4: i) ICl, $AgBF_4$, R.T., 1h, 76%; ii) $Pd(OAc)_2$, Cu, DMSO, 50°C, 4h, 0%; iii) Pd/C, Zn, Acetone/water, R.T., overnight, 0%.

We tried to synthesize the bis(terphenyl) **35** with the Ullmann coupling of two iodoterphenyl **34**. In our case, due to the sensitivity of the protective group (TMS) it was impossible to use the usual conditions with copper as the catalyst and heating at high temperature (above 200°C).[6] Therefore, milder methods should be used based on palladium catalyst like $Pd(OAc)_2$ combined with copper[7] or Pd/C combined with zinc.[8] Unfortunately, the conditions tested did not permit to achieve the desired bis(terphenyl) **35**.

The Suzuki coupling was adopted to solve this problem; it required first the preparation of the boronic derivative **36** (Scheme 3.5).[5] Iodoterphenyl **34** reacted with *n*-BuLi followed by the addition on *iso*-(propoxy)boronpinacol (*i*-PrOBpin), then **36** reacted with the iodoterphenyl **34** in the presence of $Pd(OAc)_2$ and SPhos in a mixture of toluene and water (6:1) at 60°C and gave the bis(terphenyl) derivative **35** with 53% yield.

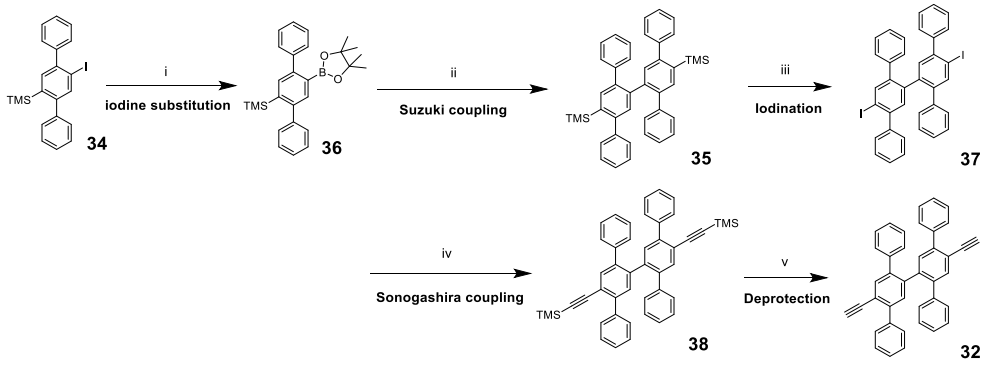

*Scheme 3.5: i) n-BuLi, i-PrOBpin, THF, -78°C, overnight, 90%; ii) **34**, $Pd(OAc)_2$, SPhos, K_3PO_4, toluene/water, 60°C, overnight, 53%; iii) ICl, DCM, R.T., overnight, 61%; iv) ethynyltrimethylsilane, $Pd(PPh_3)_2Cl_2$, CuI, toluene/Et_3N, 80°C, overnight, 60%; v) TBAF, THF, R.T., 2h.*

The bis(terphenyl) **35** was then iodinated *via* the usual iodination conditions with 4 equivalents of ICl in CH_2Cl_2 to give diiobo-bis(terphenyl) **37** with 61% yield. The Sonogashira coupling of the diiodo-bis(terphenyl) **37** with ethynyltrimethylsilane was carried out using $Pd(PPh_3)_2Cl_2$ as the catalyst and CuI as the co-catalyst. After one night at 80°C the protected

precursor **38** was obtained with 60% yield. The final step was the deprotection, which was done right before the Diels-Alder reaction, with TBAF in THF for 2 hours and it resulted in precursor **32** with 91% yield.

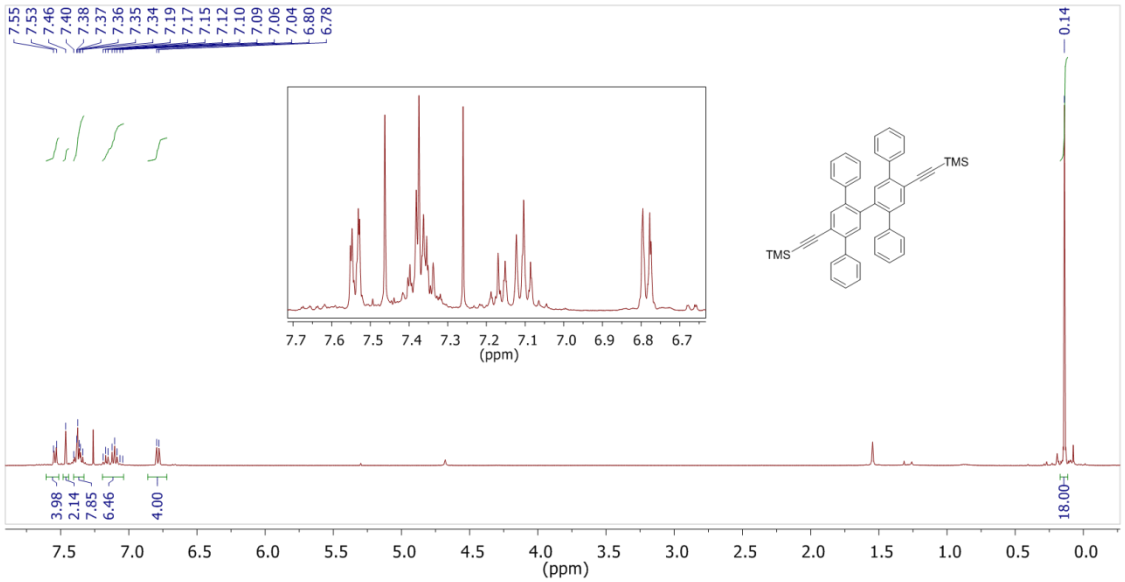

*Figure 3.12: ^{1}H-NMR spectrum of bis(terphenyl) **38** in $CDCl_3$.*

The bis(terphenyl) **38** was characterized by ^{1}H-NMR spectroscopy. The NMR spectrum showed two singlets for the four protons of the central phenyls at 7.55 and 7.53 ppm. Sixteen protons from the outside phenyls showed shifts from 7.46 to 7.04 ppm while the four protons in *para* of the central phenyls appeared as two singlets at 6.80 and 6.78 ppm and the peak of the eighteen protons from the TMS groups was located at 0.14 ppm.

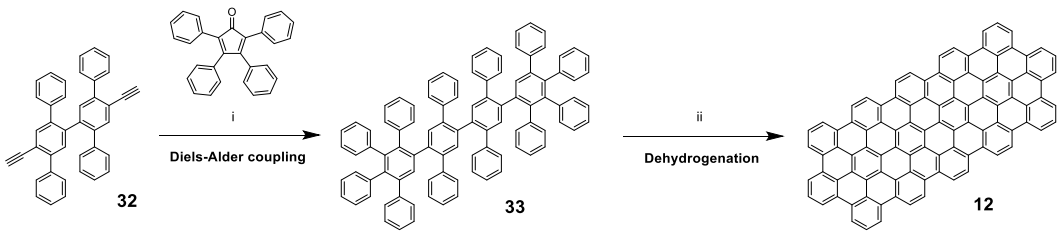

Scheme 3.6: i) o-xylene, 180°C, overnight, 92%; ii) $FeCl_3$, DCM, overnight, 80%.

The new precursor **32** underwent a Diels-Alder reaction with tetraphenylcyclopentadienone to give dendrimer **33** (Scheme 3.6)**.** The dehydrogenation *via* the Scholl reaction achieved the

preparation of C96L GNRods **12**. Both dendrimer **33** and GNRod **12** were characterized with MALDI-TOF spectrometry. The spectrum of dendrimer **33** exhibited the peaks of the pure products at *m/z* of 1218.53 (M^+) (Figure 3.13a) and similarly, the spectrum of GNRod **12** showed a single peak at *m/z* of 1182.28 (M^+) (Figure 3.13b).

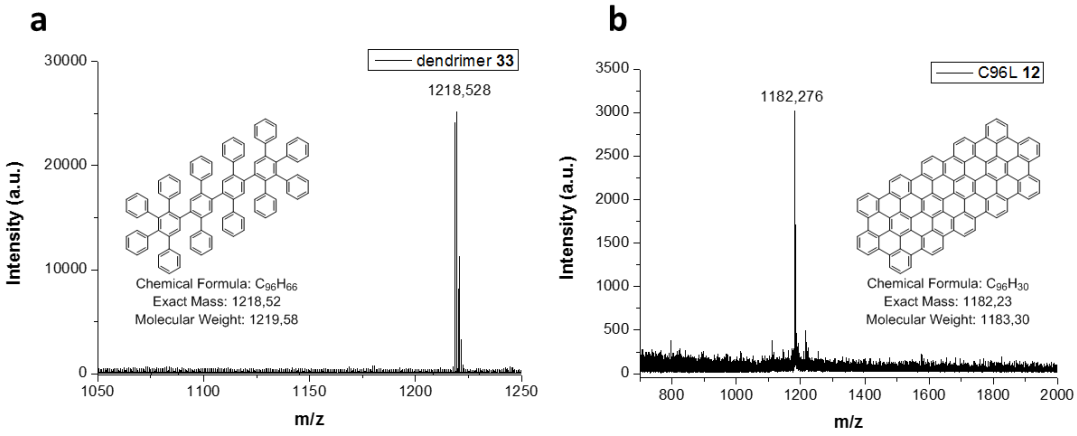

*Figure 3.13: MALDI-TOF mass spectra of a) dendrimer **33** and b) GNRod **12**.*

The C96L structure could undergo the same edge variation as C96 GQD **1** and be chlorinated but since the edge structure is different, the structure obtained is not partially but completely chlorinated which means that we obtained the $C_{96}Cl_{30}$ **17** (C96LCl) (Scheme 3.7). The chlorination of **14** is done in the presence of $AlCl_3$ and ICl to give **17** however, as for C78Cl **15**, the resulting powder is made of a mixture of fully and partially chlorinated compound. It is possible to add alkyl chains but since the precursor for C96L reacted with two tetraphenylcyclopentadienone, dendrimer **39** possessed only 4 dodecyl chains. The reaction of the bis-terphenyl **32** with the alkyl-substituted tetraphenylcyclopentadienone **9** gave dendrimer **39** which was oxidized by $FeCl_3$ to give to the C96LC12 GNRods **18**. However, while the conditions used for this last step are the same that were used for C96C12 **3**, they could not achieve the fully dehydrogenated compound. This means that besides being dependent on the number of bonds that need to be formed, the dehydrogenation conditions are also dependent on the shape of the molecule. These conditions are still getting optimized to achieve the fully dehydrogenated GNRod **18**.

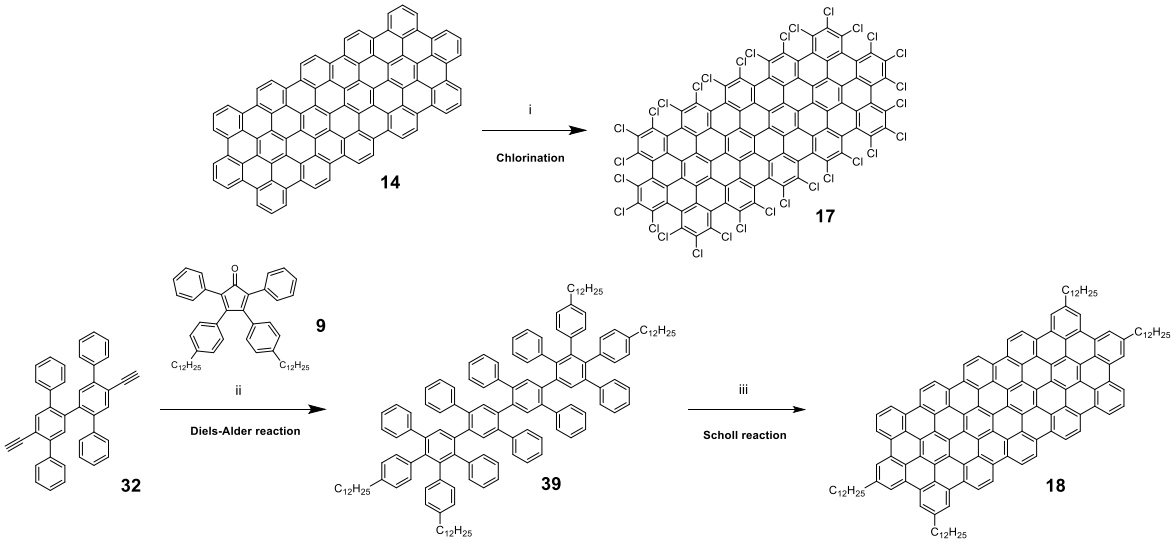

Scheme 3.7: i) $AlCl_3$, ICl, CCl_4, 80°C, 72h, 35%; ii) o-xylene, 180°C, overnight, 66%; iii) $FeCl_3$, $MeNO_2$, DCM, R.T..

The MALDI-TOF spectrum of GNRod **17** exhibits the peak of the fully chlorinated GNRod at *m/z* of 2216.25 but the compound missing one chlorine is the main product at *m/z* of 2182.25 with traces of the one missing two chlorines at *m/z* of 2147.28. We are still investigating the reasons why the main product is the one missing one chloride. The edge state should not be a problem since it is the same as for the $C_{60}H_{22}$ prepared by Müllen[9] and $AlCl_3$ and ICl are both introduced in excess. The GNRod **18** was also characterized with MALDI-TOF spectrometry and it exhibited a single peak for the compound missing 5 carbon-carbon bonds at *m/z* 1865.25.

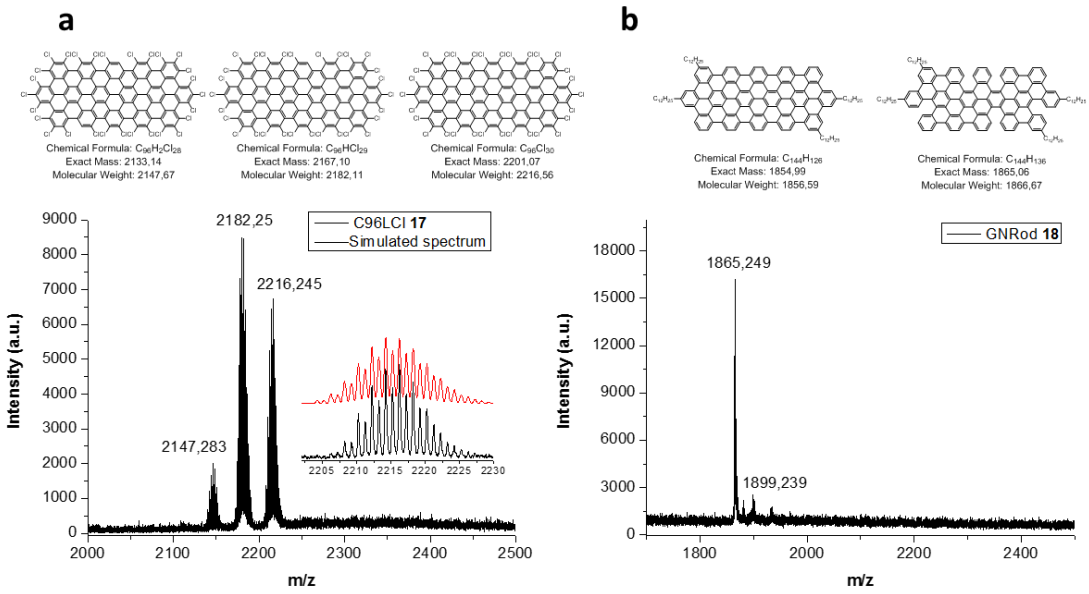

*Figure 3.14: MALDI-TOF spectra of a) the GNRod **17** and b) the GNRod **18**.*

3.3. *N* = 15 graphene nanorods

The C132 GQD **13** was first prepared by Müllen in 1997.[3] From this structure, we decided to expand the length of the nanoparticle similarly to the *N* = 9 nanorod family.

3.3.1. Synthesis and characterization of the C132 family

The synthesis of the square-shaped graphene nanoparticle **13** started with the synthesis of the protected tetraethynylbiphenyl core **40** which was prepared *via* the Sonogashira coupling of 4 equivalents of ethynyltrimethylsilane on 3,3',5,5'-tetrabromobiphenyl. The deprotection of **40** before the Diels-Alder reaction with TBAF gave the tetraethynyl derivative **41** (Scheme 3.8). The reaction of **41** with the tetraphenylcyclopentadienone gave the polyphenylene dendrimer **42** which was dehydrogenated *via* the usual conditions with $FeCl_3$ to give the graphene nanoparticle **13**.

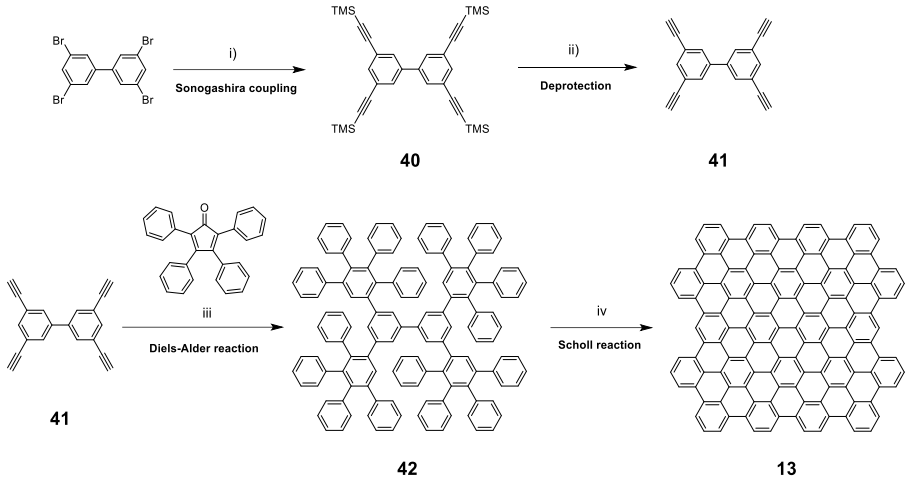

Scheme 3.8: i) Ethynyltrimethylsilane, $Pd(PPh_3)_2Cl_2$, CuI, Toluene/Et_3N, 80°C, overnight, 45%; ii) TBAF, THF, R.T., 2h, 50%; iii) Ph_2O, 180°C, overnight, 75%; iv) $FeCl_3$, DCM, R.T., 18h, 51%.

The MALDI-TOF spectrum (Figure 3.15a) of the dendrimer **42** showed the expected peak at *m/z* of 1674.79 with no traces of the tri-substituted derivative. After the dehydrogenation reaction, the MALDI-TOF spectrum showed a complete dehydrogenation at *m/z* of 1618.34 (Figure 3.15b).

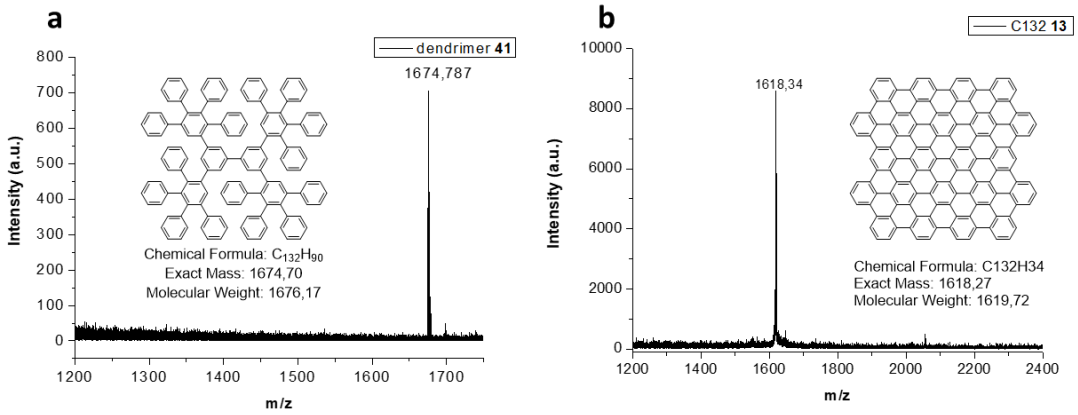

*Figure 3.15: MALDI-TOF mass spectra of dendrimer **42** and GNRod **13**.*

The C132 GQD was chlorinated to give the C132Cl nanoparticles **19** ($C_{132}Cl_{32}H_2$) (Scheme 3.9). As for C96Cl **2**, some positions could not undergo the chlorination due to the edge conformation. Similarly to what was done above, the biphenyl precursor **41** reacted with the

tetraphenylcyclopentadienone **9** to give the dendrimer with eight dodecyl chains **43** (Scheme 3.9). The dendrimer **43** was dehydrogenated in the presence of $FeCl_3$ to give **20**.

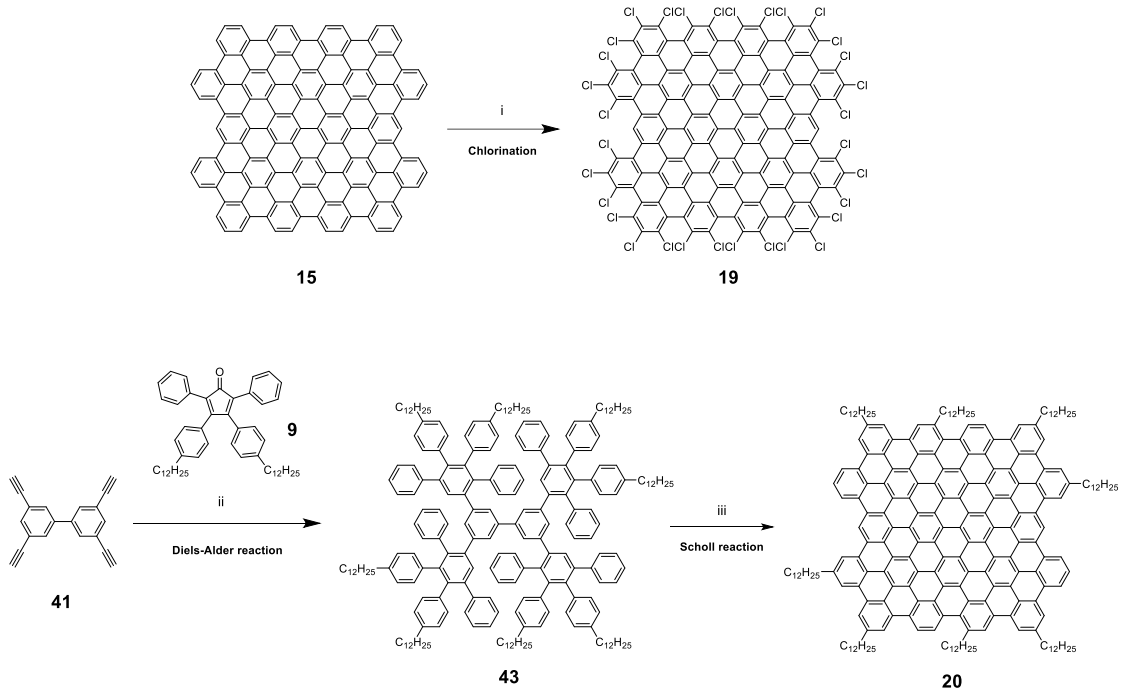

Scheme 3.9: i) $AlCl_3$, ICl, CCl_4, 80°C, 48h, 36%; ii) o-xylene, 180°C, overnight, 63%; iii) $FeCl_3$, DCM, R.T., overnight, 92%.

The MALDI-TOF spectrum of C132Cl **19** shown in Figure 3.16a exhibited a peak distribution coherent with the one expected for this type of chlorinated compound with a major peak at a m/z of 2721.02. Traces of compounds missing one or two chlorine were found at *m/z* of 2687.10 and 2653.13. The spectrum for C132C12 **20** showed a major peak corresponding to the expected product at *m/z* of 2963.84 $(M)^+$ (Figure 3.16b).

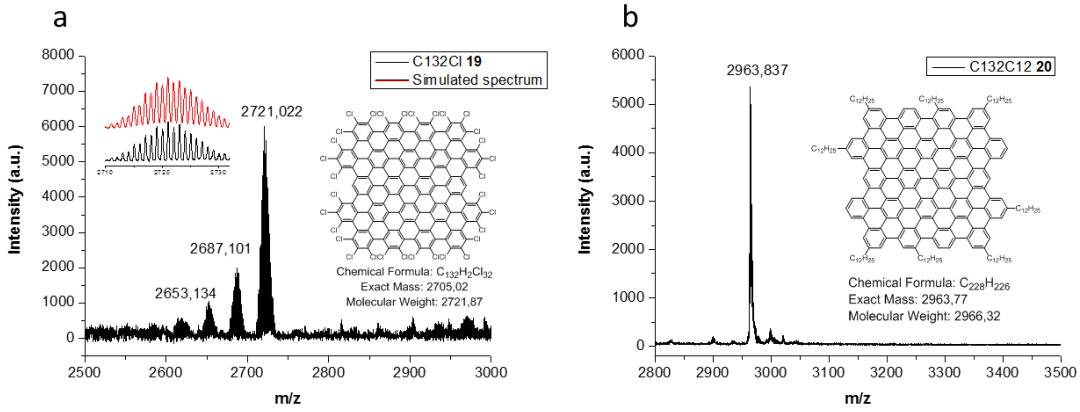

*Figure 3.16: MALDI-TOF mass spectra of a) GNRod **19** and b) GNRod **20**.*

3.3.2. Synthesis and characterization of the C162 family

For the extension of the C132 particles, we decided to follow the same strategy as for the linear C96 GNRods with the extension of the central core. Consequently, biphenyl **41** used for the preparation of dendrimer **42** should be replaced by bis(diethynylphenyl)pentaphenyl **44** to produce polyphenylene dendrimer **45** (Figure 3.17).

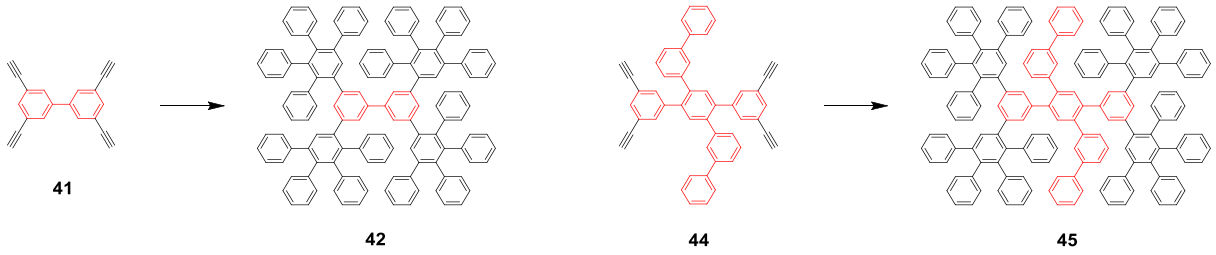

*Figure 3.17: Determination of the precursor for C162 **14**.*

The precursor **44** was synthesized in two blocks starting from 1,3,5-tribromobenzene for the first block and from 2,5-diiodo-1,4-phenylenebistrimethylsilane **26** for the second block (Scheme 3.10). 1,3,5-tribromobenzene reacted with 2 equivalents of ethynyltrimethysilane in the presence of $PdCl_2(PPh_3)_2$ and CuI to give the monobromodiacetylene compound **46** which was converted to boronic acid derivative **47** by treatment with n-BuLi and *iso*-(propoxy)boronpinacol.

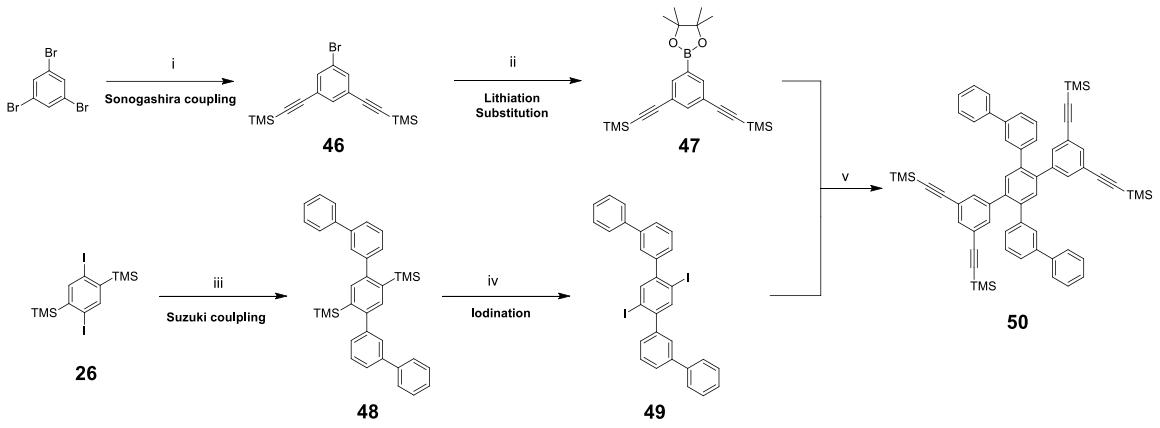

Scheme 3.10: i) Ethyltrimethylsilane, $Pd(PPh_3)_2Cl_2$, CuI, Toluene/Et_3N, 80°C, overnight, 45%; ii) n-BuLi, i-PrOBpin, Et_2O, -50°C, overnight, 85%; iii) meta-biphenylboronic acid, $Pd(OAc)_2$, SPhos, Toluene/water, 80°C, overnight, 68%; iv) ICl, DCM, R.T., overnight, 66%; v) $Pd_2(dba)_3$, SPhos, K_2CO_3 Toluene/EtOH/water, 80°C, overnight, 57%.

The second building block was synthesized in two steps by reaction of 2,5-diiodo-1,4-phenylenebistrimethylsilane **26** with *meta*-biphenylboronic acid. The TMS groups of the pentaphenyl derivative **48** were converted into iodo groups by treatment with 4 equivalents of ICl (1M in CH_2Cl_2) to give the diiodopentaphenyl derivative **49**. Finally, the protected core **50** was synthesized by Suzuki coupling between **47** and **49** in the presence of $Pd_2(dba)_3$, SPhos and K_2CO_3 in a mixture of toluene, ethanol and water at 80°C. The catalyst for this last Suzuki coupling was changed because of the low reproducibility of the reaction with $Pd(OAc)_2$ in this case.

The ^{1}H-NMR spectra of the two building blocks **47** and **49** and the protected core **50** are presented in Figure 3.18. The ^{1}H-NMR spectrum of the boronic ester **47** exhibited two singlets for the three aromatic protons at 7.84 and 7.64 ppm, a singlet at 1.33 ppm for the twelve protons on the boronic ester and a singlet at 0.22 ppm for the eighteen protons on the TMS groups. The ^{1}H-NMR spectrum of the diiodopentaphenyl **49** exhibited a singlet for two aromatic protons of the central phenyl at 7.96 ppm and a multiplet for eighteen protons of the external phenyls between 7.68 and 7.36 ppm. The ^{1}H-NMR spectrum of the dendritic core **50** exhibited a singlet for 2 protons of the central phenyl at 7.52 ppm, a multiplet for twenty-

four protons of the external phenyls between 7.52 and 7.30 ppm and a singlet for eighteen protons of the TMS groups at 0.19 ppm

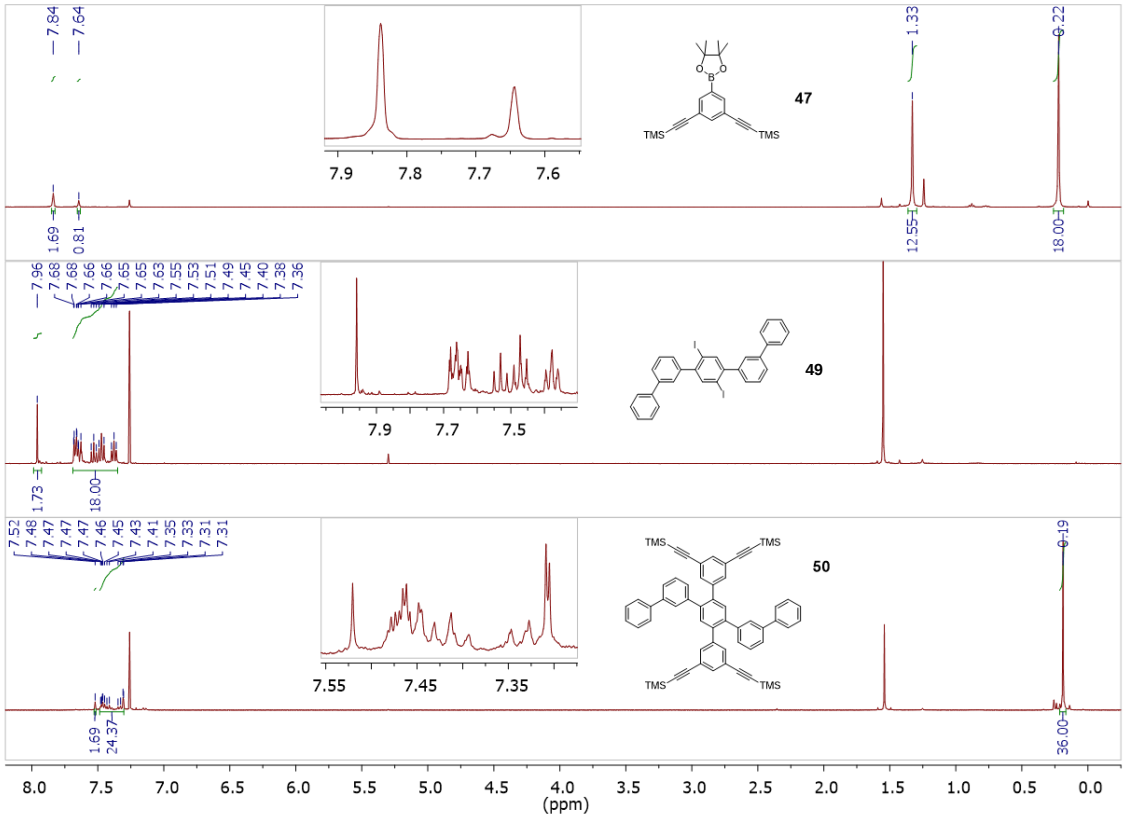

*Figure 3.18: ^{1}H-NMR spectrum of boronic ester **47**, pentaphenyl **49** and dendritic core **50** in $CDCl_3$.*

The family of C162 GNRods (*i.e.*, the bare C162, C162Cl and C162C12) was synthesized according the synthetic scheme described previously (Scheme 3.11). The ethynyl groups of the core of the dendrimer were deprotected using TBAF before the Diels Alder reaction. Precursor **44** reacted with tetraphenylcyclopentadienone to give dendrimer **45** which was oxidized to form the expected C162 GNRod **14**. The latter GNRod was chlorinated in the presence of ICl and $AlCl_3$ in CCl_4 to give C162Cl GNRod **21**.

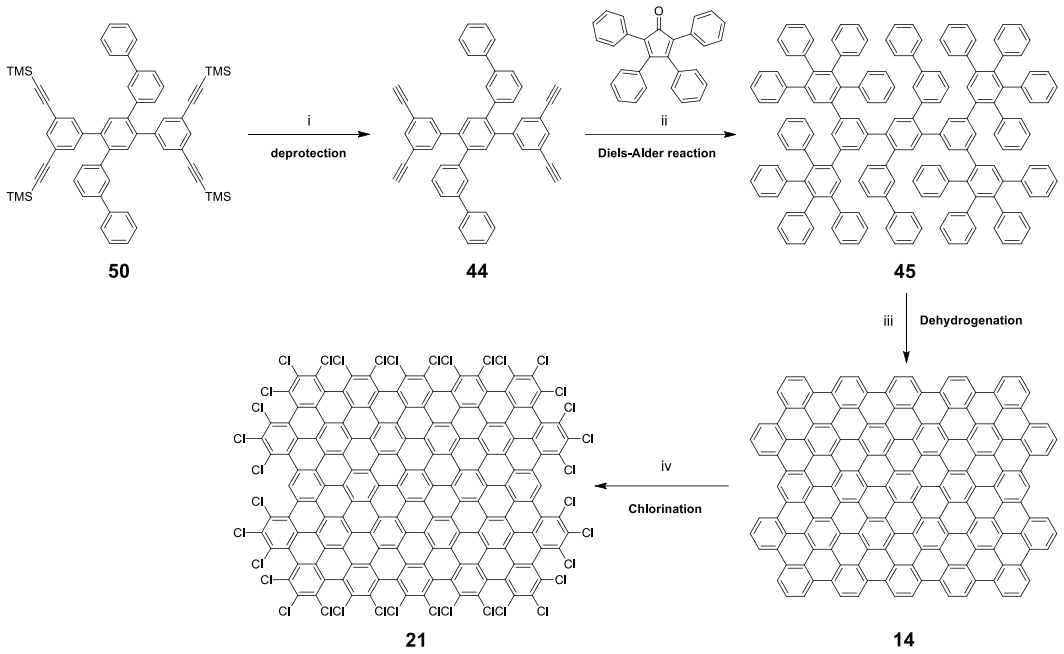

Scheme 3.11: i) TBAF, THF, 0°C, 1h, 94%, ii) o-xylene, 180°C, overnight, 39%; iii) $FeCl_3$, $MeNO_2$, DCM, R.T., overnight, 73%; iv) $AlCl_3$, ICl, CCl_4, 80°C, 72h, 49%

Like for the previous GNRods, C162 dendrimer **45** and GNRod **14** were characterized by MALDI-TOF mass spectrometry using the classical preparation in solution with DCTB matrix for **45** and the solid mixing of the sample with TCNQ matrix for **14** (Figure 3.19). The spectrum of dendrimer **45** showed two peaks at *m/z* 2054.65 (M^+) and 2077.69 $(M+Na)^+$ and the spectrum of GNRod **14** showed a peak at *m/z* 1962.43 (M^+).

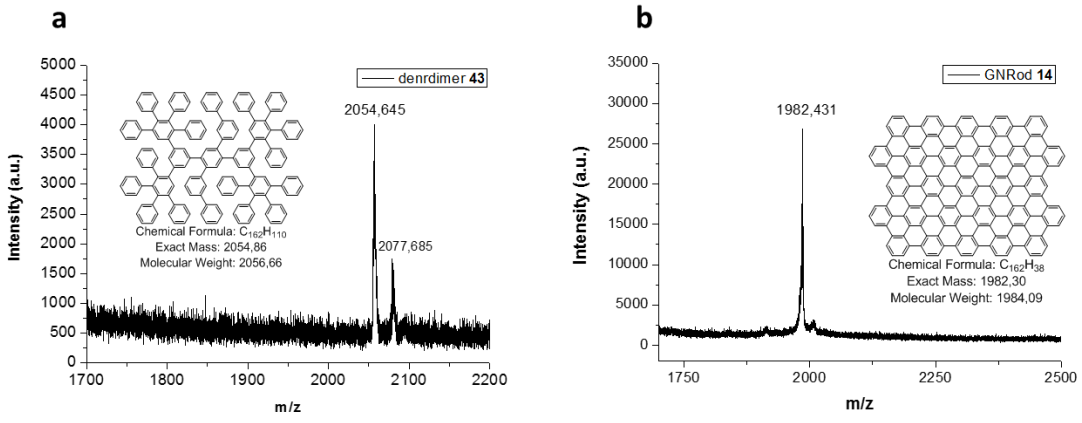

*Figure 3.19: MALDI-TOF mass spectra of a) dendrimer **45** and b) GNRod **14**.*

The characterization the GNRod **21** is problematic since neither the expected peaks corresponding to the chlorinated particles at 3204.89 (exact mass) or 3224.06 (molecular weight) nor the peak of the starting material can be found in the final blue powder (Figure 3.20). The mass spectra only showed noisy signals containing two maxima at *m/z* of 1830 and *m/z* of 3777 which did not correspond to any expected structure.

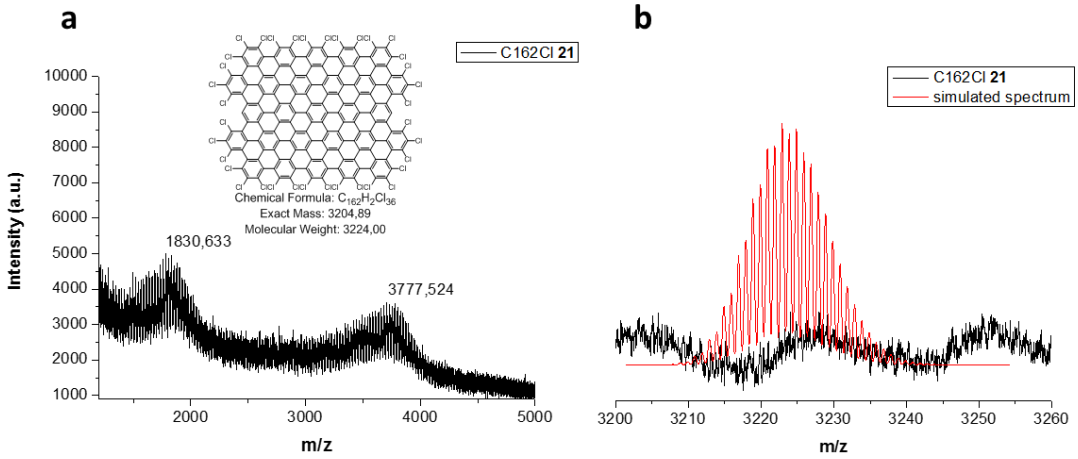

*Figure 3.20: a) MALDI-TOF mass spectra of the GNRod **21** and b) comparison of the obtained spectrum for GNRod **21** with the simulated one.*

While this characterization by mass spectrometry was impossible yet, the compound obtained after the chlorination exhibited a good solubility in chlorinated solvent like chloroform and it was even purified by high-performance liquid chromatography (HPLC) on Hypersil GOLD™ silica column. In addition, the absorption spectrum of this compound is coherent with the expected spectra for C162Cl; this study is developed in the following section. Therefore, we strongly believe that we obtained the desired compound and we are currently working on its characterization. The experience we have with this reaction shows that the graphene nanoparticles do not degrade during the chlorination, the latter always proceeds and the only byproducts observed are due to incomplete chlorination.

Finally, the C162C12 GNRod **22** was synthesized by reaction of **44** with **9**, the dendrimer **51** was dehydrogenated in the presence of $FeCl_3$.

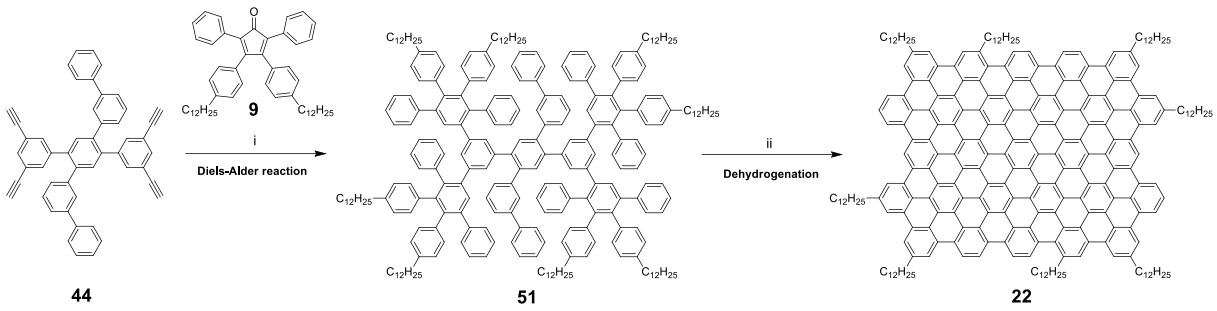

Scheme 3.12: i) o-xylene, 80°C, overnight, 68%; ii) $FeCl_3$, $MeNO_2$, DCM, R.T., overnight, 34%.

The GNRod **22** exhibits the same difficulty of characterization as GNRod **21** and while the product was characterized with MALDI-TOF spectrometry, neither the expected peak corresponding to the fully dehydrogenated compound at 3321.80 (exact mass) nor the peak of the starting material (3400.49) can be found in the final powder.

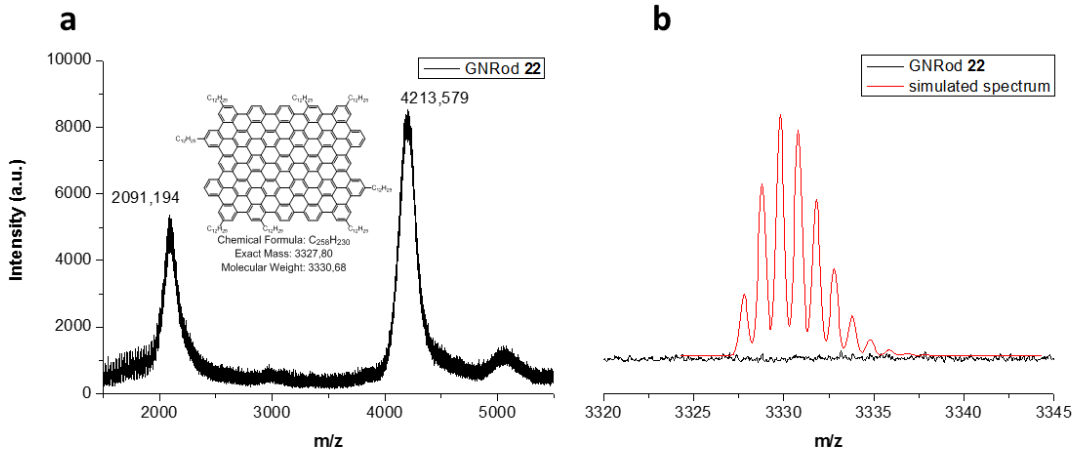

*Figure 3.21: a) MALDI-TOF spectrum of the GNRod **22** and b) comparison of the obtained spectrum for GNRod **22** with the simulated one.*

The organic synthesis of several GNRods allowed us to have access to a wide range of structures. Despite the current problems with the dehydrogenation step of the new GNRod containing alkyl chains (C96LC12 **18**), the partial chlorination of some GNRods (**15**, **17** and **19**) and the problems with the characterization of the doped C162 (**21** and **22**), the optical study of the effect of the size variation can still be explored. In fact, we studied the effect of the size

and width variation in the narrow GNRods C78 **11** and C96L **12** and the wider GNRods C132 **13** and C162 **14**.

3.4. Optical properties

3.4.1. The C78 based GNRods

The first optical study was the comparison between the GNRods C78 **11** and C96L **12**. For this study, we chose to disperse the GNRods in SDS due to the flaws of TCB. In fact, if TCB contains traces of air, it degrads for a sonication carried out for more than 5 min with an ultrasonic bath or with an ultrasonic probe. Moreover, the high density of TCB (1.45 g/cm^3) made centrifugation impossible. Those two points were huge drawbacks for compounds with a poor solubility since optical experiments need a clear solution without non-soluble aggregates. On the contrary, SDS solutions are stable to sonication and allow higher power and time of sonication with no issues regarding centrifugation. The solutions were prepared at 0.1 mg/ml in a solution of SDS (2%) before sonication during 1 hour in an ultrasonic bath and stirring overnight. The resulting solutions for GNRods **11** and **12** are presented in Figure 3.22 and exhibit pale yellow and pale orange colors.

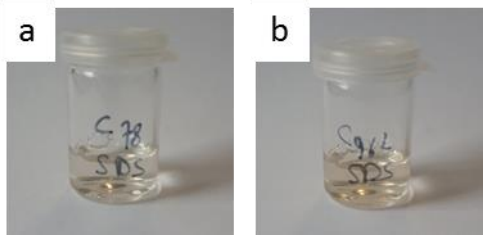

*Figure 3.22: Pictures of the dispersions of a) C78 **11** and b) C96L **12** in SDS.*

The absorption spectra of the solutions of GNRods **11** and **12** were measured and the first result is that the low solubility of the bare GNRods induces a low intensity of the absorption (Figure 3.23). The spectrum for C78 **11** shows a broad absorption band at *ca.* 400 nm with lower absorptions at 540, 589 and 640 nm. The spectrum for C96L **12** is very similar with a broad absorption band around 425 nm and two lower at 575 and 645 nm. The red-shift of

about 25 nm between GNRods **11** and **12** confirms that absorption can be tuned with length variation without changing the edge state.

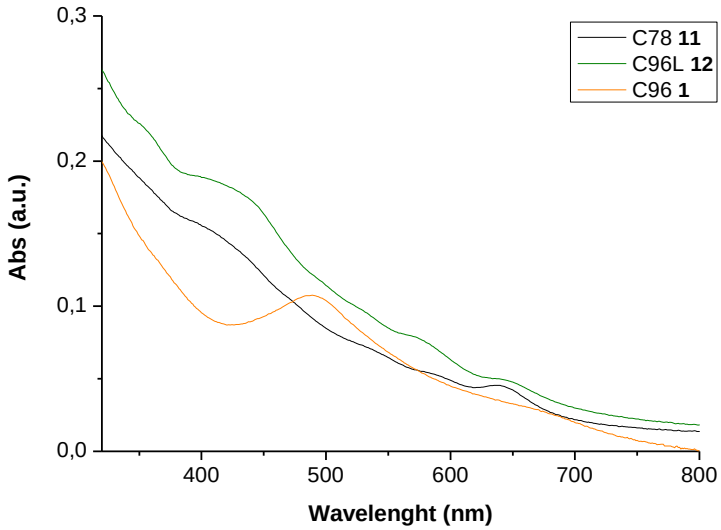

*Figure 3.23: Absorption spectra of C78 **11** and C96L **12** GNRods and GQD **1**.*

GNRod **12** and GQD **1** are both made of 96 carbon atoms but exhibit different shapes; while GNRod **12** is linear, GQD **1** is triangular. These structures were compared to see the impact of a shape variation on the optical properties. The spectra Figure 3.23 show that there is a difference of about 50 nm between the two main absorption peaks. This confirms that optical properties of graphenic materials are mainly governed by the shape and edge state of the material. While these parameters slightly change between C78 **11** and C96L **12**, they drastically change between C96L **12** and C96 **1**, it results in a much bigger shift in the second case.

3.4.2. The C132 based GNRods

The C132 GNRods are dispersed in TCB following the method presented for GQDs and the resulting dispersions are shown in Figure 3.24. The solution of C132 **13** exhibits a pale pink color due to its low solubility, C132Cl **19** is highly soluble with a clear blue color and C132C12 **20** is also soluble with a purple color.

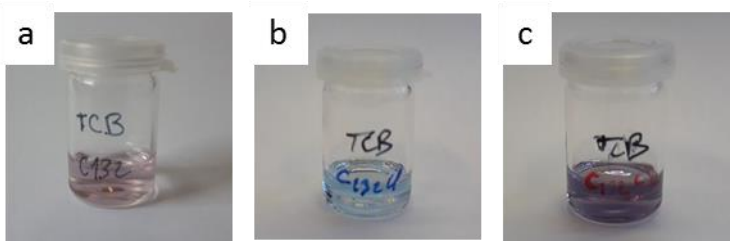

*Figure 3.24: Pictures of the dispersions of a) C132 **13**, b) C132Cl **19** and c) C132C12 **20** in TCB.*

The absorption spectra of these GNRods showed low shifts of the absorption with differences in the intensity of absorption mostly due to the poor solubility of GNRod **13** compared to GNRod **19** and **20**. The spectra of C132 **13** and C132C12 **20** exhibited broad absorption band at about 570 nm with additional weak absorption bands for GNRod **20** at 440, 640, 700 and 740 nm (Figure 3.25). The main absorption band of the spectrum of C132Cl **19** is located at 585 nm with weaker absorptions at 360, 390, 425, 650 and 700 nm. The shift of *ca.* 15 nm between C132 **13** and C132Cl **19** was coherent with the shift observed between C96 **1** and C96Cl **2** (*ca.* 20 nm), this confirms the red-shifting effect of chlorination.

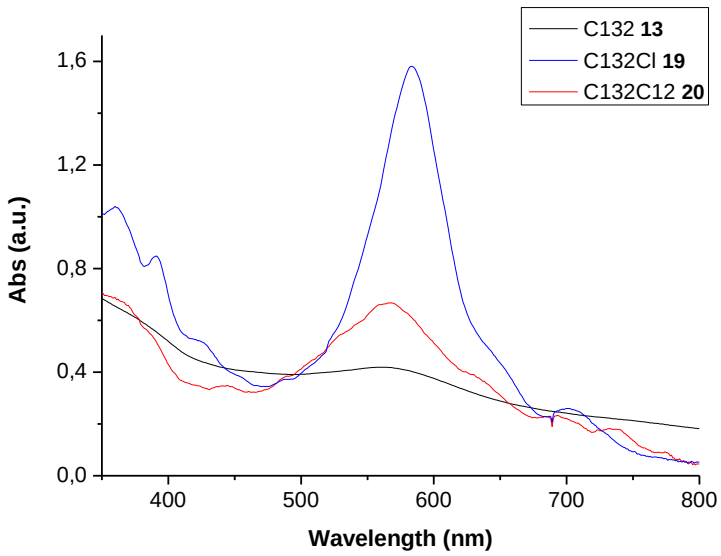

Figure 3.25: Absorption spectra of the C132 family in TCB.

The absorption spectrum of C132 **13** was compared with the one of C162 **14**, the GNRod with an additional row of phenyls (Figure 3.26). The spectrum of GNRod **14** exhibited a broad

absorption band at *ca.* 590 nm with a weaker absorption at 410 nm. The red-shift of *ca.* 20 nm observed between the main absorption bands of C132 **13** and C162 **14** confirmed the results of GNRods C78 **11** and C96 **12** showing that an increase in length induces a red-shift of the absorption.

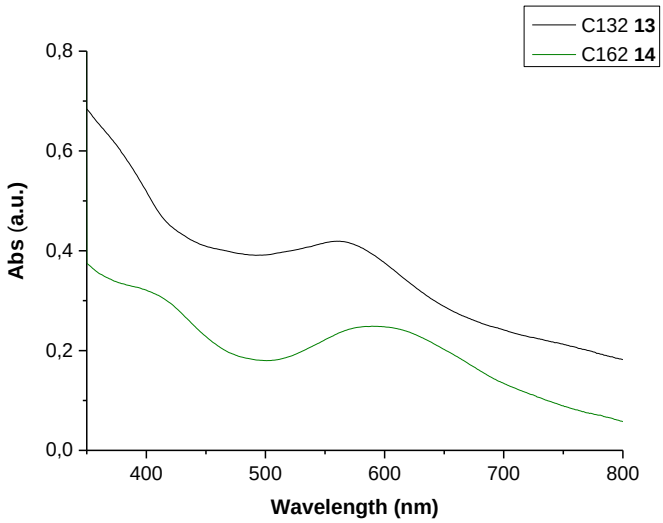

*Figure 3.26: Comparison of the absorption spectra of C132 **13** and C162 **14** in TCB.*

The spectrum of GNrod **14** was then compared with the spectra of the functionalized C162 GNRods (chlorinated and with alkyl chains) using SDS for the dispersion (Figure 3.27). The shape of the spectra for the C162 family were very similar to the ones obtained for the C132 family. The spectra of C162 **14** and C162C12 **22** exhibited a main absorption bands at 590 nm with an additional weaker band for GNRod **22** at 420 nm. The spectrum of GNRods C162Cl **21** showed a broad absorption band at 605 nm which corresponds to a shift of *ca.* 15 nm. This absorption value is intermediate between the one of C132Cl **19** and the absorption of the chlorinated GQD made of 222 carbons ($C_{222}Cl_{42}$) reported in the literature (*ca.* 700 nm).[9] While this did not give any information on the chlorination state or the purity, it confirmed that the product of the chlorination of C162 **21** was a chlorinated GNRod with an intermediate size between C132Cl **21** and $C_{222}Cl_{42}$.

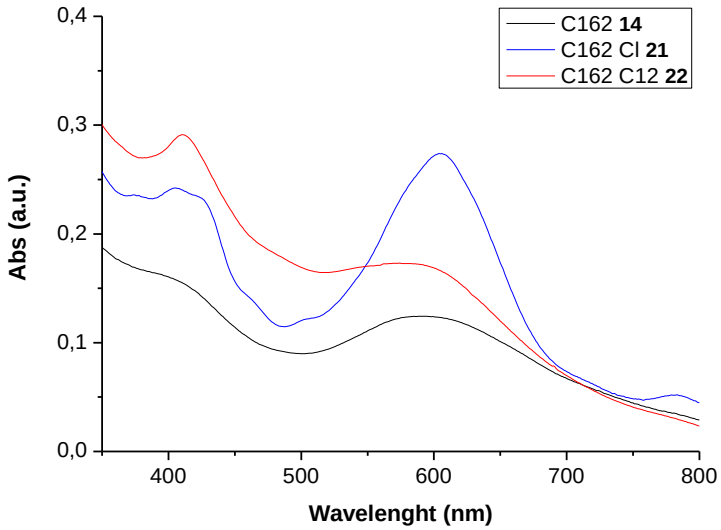

Figure 3.27: Absorption spectra of the C162 family GNRods in SDS.

3.1. Conclusion

To conclude, we were able to prepare a new series of GNRod adding a row of phenyl to the precursor of existing GNRods. These new GNRods (**12** and **14**) exhibited absorption bands with a red-shift of *ca.* 20 nm compared to their shorter counterparts (**11** and **13**). This method could be used to further extend the length of the GNRods. The only limit to this length increase is the solubility of the needed acetylenic precursor. However, the comparison between C96L **12** and C96 **1** showed that large shifts can be achieved changing the shape of the graphenic structures. Chlorination is another method able to increase the solubility and tune the optical properties inducing a shift of *ca.* 15 nm compared to the bare molecule. All these results showed that one can select the optical properties of graphenic structures tuning them at the atomic level.

(1) Schwab, M. G.; Narita, A.; Hernandez, Y.; Balandina, T.; Mali, K. S.; De Feyter, S.; Feng, X.; Müllen, K. Structurally Defined Graphene Nanoribbons with High Lateral Extension. *J. Am. Chem. Soc.* **2012**, *134* (44), 18169–18172.

(2) Müller, M.; Iyer, V. S.; Kübel, C.; Enkelmann, V.; Müllen, K. Polycyclic Aromatic Hydrocarbons by Cyclodehydrogenation and Skeletal Rearrangement of Oligophenylenes. *Angew. Chemie (International Ed. English)* **1997**, *36* (15), 1607–1610.

(3) Morgenroth, F.; Reuther, E.; Müllen, K. Polyphenylene Dendrimers: From Three-Dimensional to Two-Dimensional Structures. *Angew. Chemie - Int. Ed.* **1997**, *36* (6), 631–634.

(4) Luliński, S.; Serwatowski, J. Bromine as the Ortho-Directing Group in the Aromatic Metalation/Silylation of Substituted Bromobenzenes. *J. Org. Chem.* **2003**, *68* (24), 9384–9388.

(5) Golling, F. E.; Quernheim, M.; Wagner, M.; Nishiuchi, T.; Müllen, K. Concise Synthesis of 3D π-Extended Polyphenylene Cylinders. *Angew. Chemie - Int. Ed.* **2014**, *53* (6), 1525–1528.

(6) Ullmann, F.; Bielecki, J. Ueber Synthesen in Der Biphenylreihe I. *Berichte der Dtsch. Chem. Gesellschaft* **1901**, *34* (2), 2174–2185.

(7) Banwell, M. G.; Kelly, B. D.; Kokas, O. J.; Lupton, D. W. Synthesis of Indoles via Palladium[0]-Mediated Ullmann Cross-Coupling of o-Halonitroarenes with α-Halo-Enones or -Enals. *Org. Lett.* **2003**, *5* (14), 2497–2500.

(8) Venkatraman, S.; Li, C. J. Carbon - Carbon Bond Formation via Palladium-Catalyzed Reductive Coupling in Air. *Org. Lett.* **1999**, *1* (7), 1133–1135.

(9) Tan, Y. Z.; Yang, B.; Parvez, K.; Narita, A.; Osella, S.; Beljonne, D.; Feng, X.; Müllen, K. Atomically Precise Edge Chlorination of Nanographenes and Its Application in Graphene Nanoribbons. *Nat. Commun.* **2013**, *4*, 3647.

Chapter 4 : Graphene Nanomesh

Chapter 3: Graphene Nanorods

Chapter 4: Graphene Nanomeshes

4.1. Introduction

The processes of deposition and activation of small molecules on metal surfaces in a STM chamber developed for the formation of 2D covalent networks[1] and graphene nanoribbons[2] can be applied to the formation graphene nanomesh. Despite their interest, only a limited number of graphene nanomesh-like structures have been reported (Figure 4.1).[3–8] It is important to notice that in all examples reported so far the "graphene necks" are constituted of a single C-C bond between 2 phenyl rings. In such structures, because of the free rotation along the single bond and of the steric hindrance between the hydrogen atoms in *ortho* of the C-C bond, the phenyl rings are not coplanar which reduces significantly the delocalization of electrons and decreases of the conductivity. This phenomenon is well-known in biphenyl derivatives.[9]

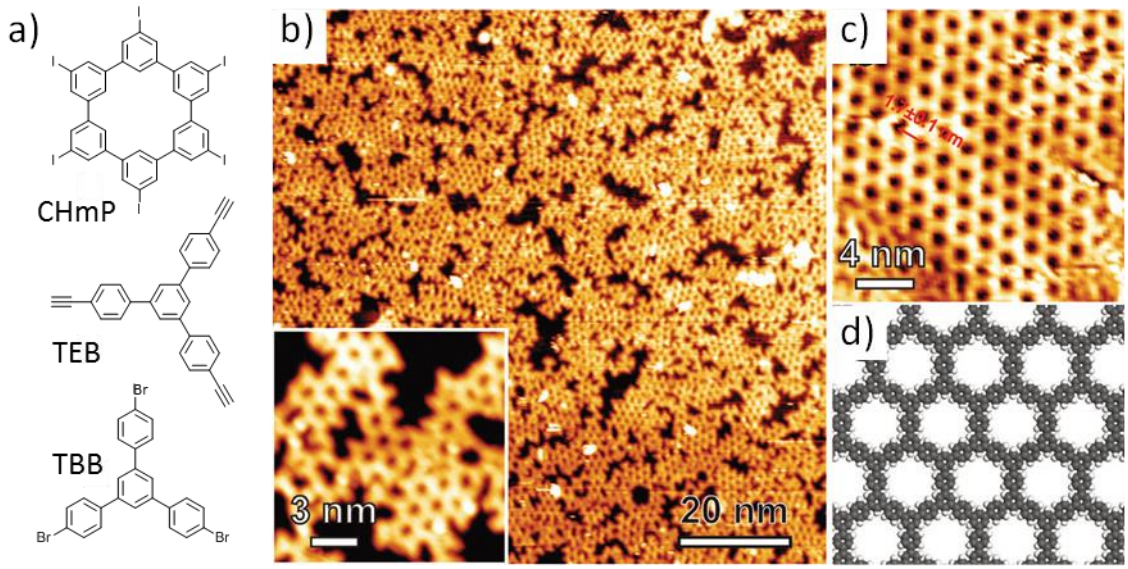

Figure 4.1: a) Chemical structure of typical GNM precursors, hexaiodocyclohexa-m-phenylene (CHmP),[5] 1,3,5-tris-(4'-ethynylphenyl)benzene (TEB)[4] and 1,3,5-tris-(4'-bromophenyl)benzene (TBB);[3] b) the STM images of the resulting network for TEB[4] and c) the simulated structure for TEB.

During my PhD, we wanted to fabricate graphene nanomeshes in which the graphene neck is composed of several benzene rings and not only of a single C-C bond as it is the case in the

examples described in Figure 4.1. To this end, we synthesized two precursors: the 2,2',2"-triiodotriphenylene **52** and the 1,3,5-tris(4'-iodo-*para*-terphenyl)benzene **53** which exhibit a C_3 symmetry and contain 3 iodine atoms (Figure 4.2).

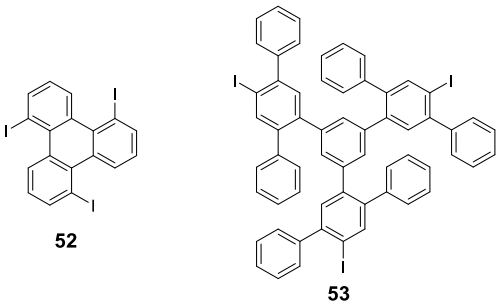

*Figure 4.2: Chemical structure of 2,2',2"-triiodotriphenylene **52** and 1,3,5-tris(4'-iodo-para-terphenyl)benzene **53.***

We expected these compounds to give rise to the formation of GNMs in which the graphene necks are constituted of two or three phenyl rings with holes corresponding to a phenyl (6 carbon atoms) or a hexabenzocoronene (42 carbon atoms) missing (Figure 4.3). The neck widths and the hole diameters are respectively of 0.6 and 0.7 nm for the GNM from **52** and 0.9 and 1.0 nm for the GNM from **53**.

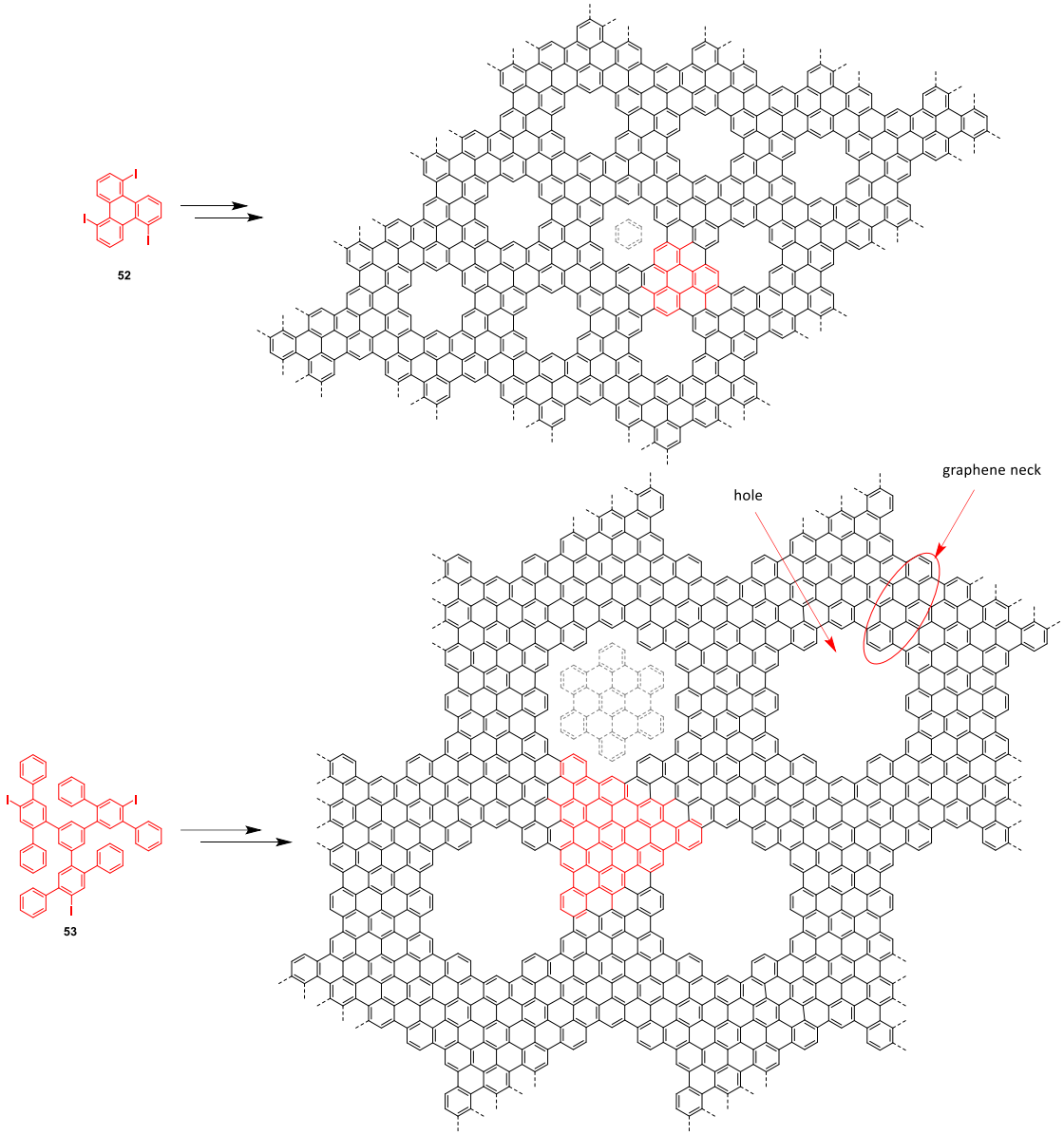

*Figure 4.3: Structure of the GNMs made from triiodotriphenylene **52** and tris(para-terphenyl)benzene **53**.*

The group of Philippe Dollfus at the "Insitut d'Electronique Fondamentale" (IEF) of the University of Orsay, investigated by numerical simulation the electrical properties of graphene nanomesh devices with hole and neck sizes in the typical range of what can be obtained by the bottom-up approach.[10,11] This part of my project based on well-controlled graphene objects may offer the unique opportunity to compare simulation to measurements and to

orient the chemical synthesis towards the best structures. Both the precursor **52** and **53** are not commercial, so they have to be synthesized.

4.2. Synthesis of the precursors for the graphene nanomesh

4.2.1. Triphenylene

The first GNM precursor (2,2',2"-triiodotriphenylene **52**) was prepared following procedures previously reported by Bin Xu and co-workers.[12,13] 2,3-Dichloronitrobenzene underwent a trimerization catalyzed by copper in *N*,*N*-dimethylformamide (DMF) at 160°C overnight to give the 2,2',2"-trinitrotriphenylene **54** (Scheme 4.1). The nitro groups were reduced into amine groups by hydrogenation in the presence of Pd/C in a mixture of ethyl acetate and ethanol. The amine groups of **55** were converted into diazonium salts which were transformed into iodine groups by a Sandmeyer reaction in the presence of potassium iodide to give the triiodotriphenylene **52**.

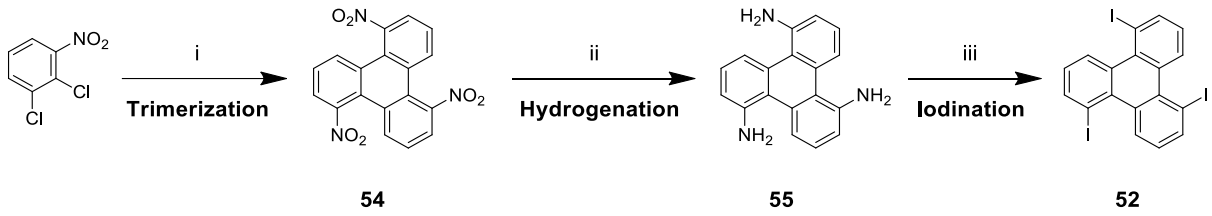

Scheme 4.1: i) Cu, DMF, 160°C, overnight, 34%; ii) Pd/C, EtOAc/EtOH, R.T., overnight, 73%; iii) KI, HCl, $NaNO_2$, water, 0°C to R.T., 1h, 26%.

The precursor **52** was characterized with ^{1}H-NMR, it exhibited a doublet highly deshielded for the protons in *ortho* of the iodine at 9.20 ppm, a doublet for the protons in *para* of the iodine at 8.23 ppm and a doublet of doublet centered at 7.15 ppm for the protons in *meta* of the iodine (Figure 4.4).

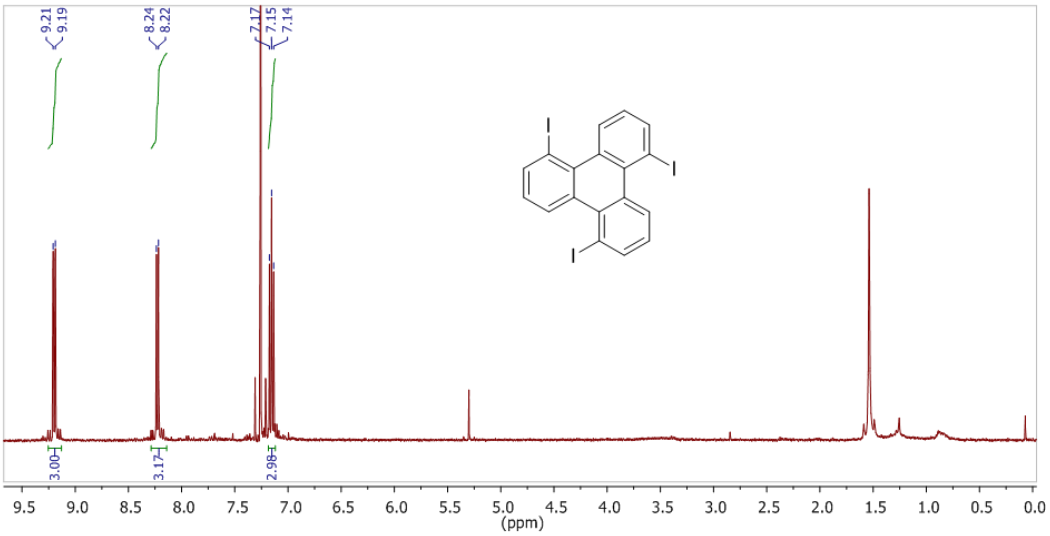

*Figure 4.4: ^{1}H-NMR spectrum of the precursor **52** in $CDCl_3$.*

4.2.2. Tris(terphenyl)benzene

For the second GNM precursor, we wanted to prepare two precursors bearing either bromine or iodine atoms to be able to tune the reactivity on surface. Indeed, for the CVD growth of the GNM, depending on the halogen, the coupling reaction can be performed at different temperature.[14] The carbon-bromine bond is more stable compared to the carbon-iodine bond due to a higher dissociation energy (336 and 272 kJ/mol respectively in the gas phase) and therefore, the activation temperature for the coupling is higher for bromine compared to iodine (around 120°C for iodine and at least 200°C for bromine).[14]

We first tried to prepare the brominated precursor **57**; the reaction started from the already prepared mono-iodo-*para*-terphenyl **34** which underwent a Suzuki coupling reaction with 1,3,5-phenyltriboronic acid tris(pinacol) ester (Scheme 4.2). The coupling was tested using $Pd(PPh_3)_4$ as the catalyst and K_2CO_3 as the base in a mixture of ethanol, water and THF. However, due to the high steric hindrance and despite changes in the reaction time, temperature or base (for example Cs_2CO_3) the pure product could not be isolated and the reaction gave a mixture of the mono-, di- and tri-substituted compound with partial loss of the trimethylsilyl groups. We changed the catalyst for $Pd(OAc)_2$ using SPhos as an electon-rich ligand with K_3PO_4 as the base in a mixture of toluene and water. These conditions were used

to force the reaction toward the formation of the tri-substituted compound and attained the desired product **56** with a 62% yield.

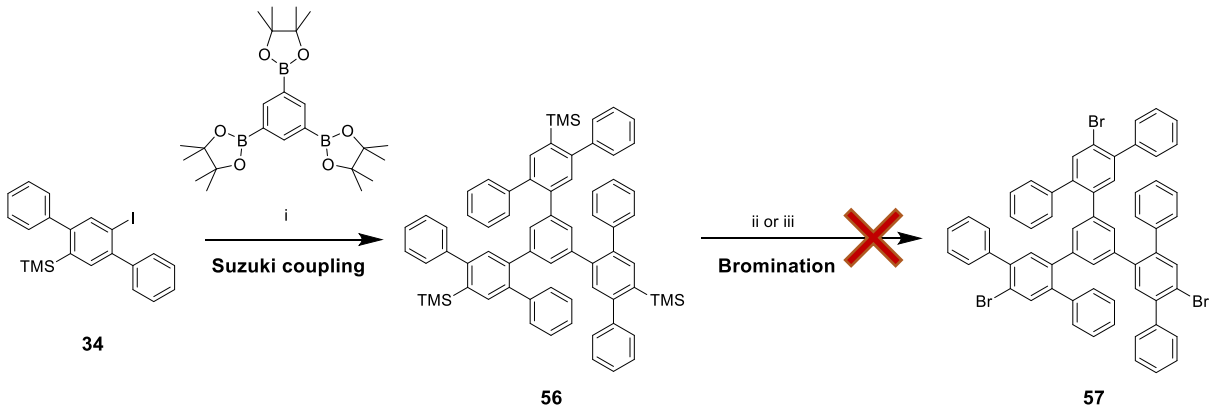

Scheme 4.2: i) $Pd(OAc)_2$, SPhos, K_3PO_4, toluene/water, 100°C, overnight, 62%; ii) NBS, NaBr or LiBr, MeOH/THF or DCM, R.T., overnight, 0%; iii) Br_2, NaOAc, THF, R.T., 24h, 0%.

In the next step, we studied the transformation of the TMS groups into bromine. The first attempts were made using purified *N*-bromosuccinimide (NBS) with sodium bromide in a mixture of methanol and THF[15] but these conditions could not permit to achieve the brominated compound. Similarly, the reaction with lithium bromide and DCM could not permit to isolate the fully brominated compound. We also tested the direct bromination with Br_2 and sodium acetate[16] but once again we were not able to achieve the desired product. Consequently, we changed strategy and tested the iodination reaction.

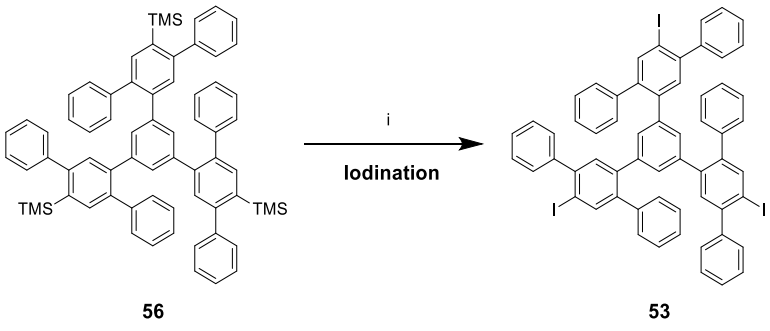

Scheme 4.3: i) ICl, DCM, R.T., overnight, 98%.

The iodination was carried out with the conventional procedure used also in Chapter 3 with two equivalents of iodine monochloride *per* TMS group in DCM; the desired precursor **53** was

obtained with a 98% yield (Scheme 4.3). The precursor **53** was characterized with ^{1}H-NMR, it exhibited a distinct signal around 7.92 ppm for the three protons of the core phenyl and a multiplet from 7.46 to 6.49 ppm for the 36 other protons (Figure 4.5).

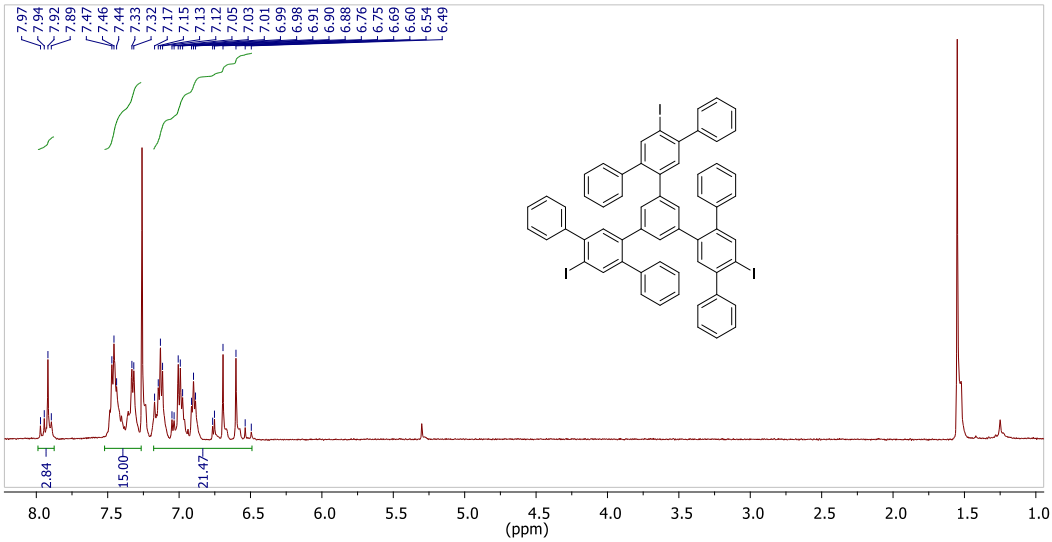

*Figure 4.5: ^{1}H-NMR spectrum of precursor **53** in $CDCl_3$.*

4.3. Simulation

The GNMs have been a growing field of interest for theoretical calculation;[10,11,17–21] however, the structures simulated so far did not fit perfectly with the structures that we are developing. Consequently, it was necessary to perform specific theoretical calculations with our precursors and the foreseen structures to extract the properties like the band structures and the gap of the GNMs. The theoretical calculations were performed by Dr Sylvain Latil at the Service de Physique de l'Etat Condensé (SPEC) from CEA-Saclay using density functional theory (DFT) with the autocoherent tight-binding code "DFTB+" after validation of the method on a model GNM.

To construct the band structures and estimate the gap in GNMs, it was first necessary to define the structure of the unit cells. Graphene nanomeshes are defined as a periodical network of holes in the 2-dimensional structure of graphene. Considering $\overrightarrow{\mathbf{a_1}}$ and $\overrightarrow{\mathbf{a_2}}$ the two base vectors of the hexagonal lattice of graphene, the holes are arranged following the vectors $\overrightarrow{\mathbf{A_1}}$ and $\overrightarrow{\mathbf{A_2}}$

defined as: $\overrightarrow{\mathbf{A_1}} = m_{11}.\overrightarrow{\mathbf{a_1}} + m_{12}.\overrightarrow{\mathbf{a_2}}$ and $\overrightarrow{\mathbf{A_2}} = m_{21}.\overrightarrow{\mathbf{a_1}} + m_{22}.\overrightarrow{\mathbf{a_2}}$ with m_{ij} defined as integers (Figure 4.7). Therefore, a network is defined by its matrix:

$$\mathrm{M} = \begin{bmatrix} m_{11} & m_{12} \\ m_{21} & m_{22} \end{bmatrix}.$$

One can note that both triiodotriphenylene **52** and triiodotris(*para*-terphenyl)benzene **53** molecules are prochiral. This means that they will form two stereoisomers on a surface; these stereoisomers cannot react with each-other to give defect-free GNMs (Figure 4.6). On surface, depending on which face precursor **52** will adsorb, it will give rise to two different GNMs while precursor **53** will give rise to the same network (Figure 4.7).

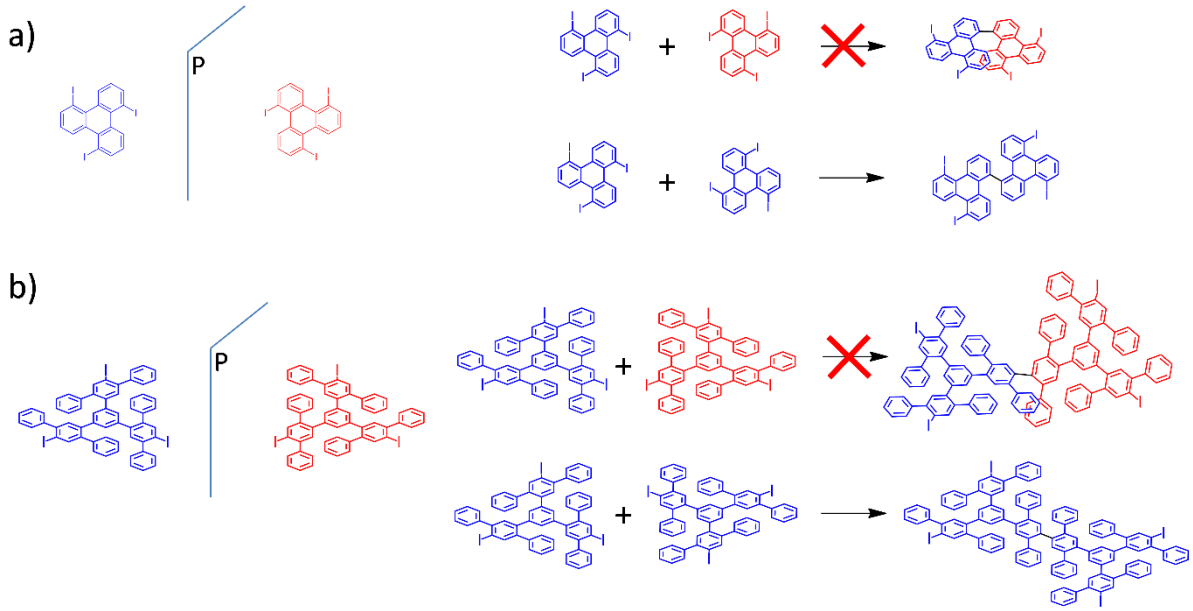

*Figure 4.6: Representation of the mirror images and resulting reactions of the prochirals a) precursor **52** and b) precursor **53.***

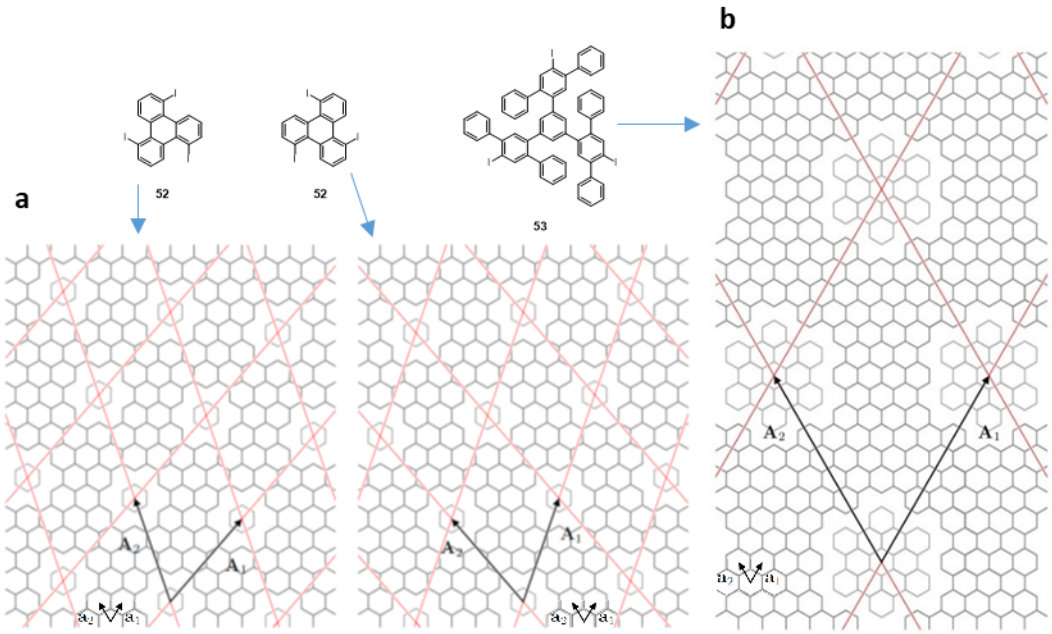

*Figure 4.7: a) Precursor **52** and its resulting GNM and b) precursor **53** and its resulting GNM. The pale grey structures represent the removed atoms.*

Finally for the GNMs obtained from precursor **52**, the two matrices of the networks can be expressed as: and $\mathrm{M} = \begin{bmatrix} 5 & -1 \\ 4 & 1 \end{bmatrix}$ and $\mathrm{M} = \begin{bmatrix} 4 & 1 \\ 5 & -1 \end{bmatrix}$ and for the GNM obtained from precursor **53**, the matrix of the network can be expressed as: $\mathrm{M} = \begin{bmatrix} 9 & 0 \\ 0 & 9 \end{bmatrix}$. GNMs obtained from precursor **52** belong to the group of symmetry *p6* and the GNMs obtained from precursor **53** to group of symmetry *p6m*.

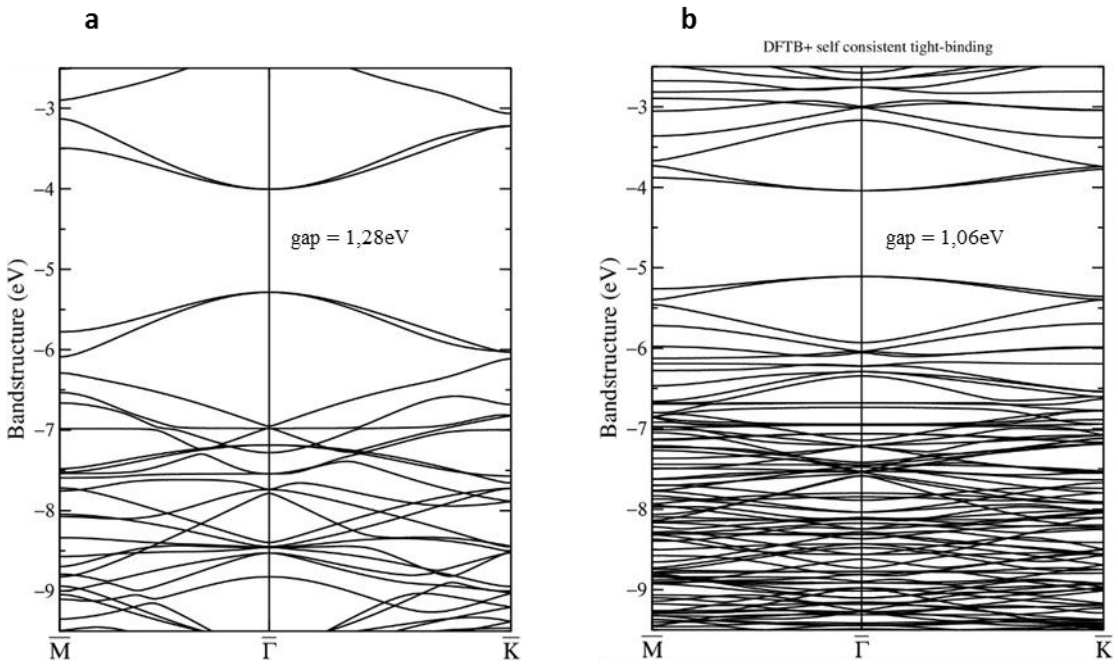

*Figure 4.8: Band structures for the GNMs from a) precursor **52** and b) precursor **53**.*

The band structures were obtained from the DFTB+ calculations; the networks exhibit a direct bandgap of 1.28 eV for precursor **52** and 1.06 eV for precursor **53** (Figure 4.8). These values of bandgap permit to envision electronics applications; in addition the fact that the bandgaps are direct leads us to envision interesting optical properties.

4.4. On surface synthesis

The work on GNR polymerization on metallic surfaces[2,22–29] paved the way for the creation of 2D covalent networks and it was expected that GNMs were grown on metallic surface during the course of the PhD, unfortunately our colleagues at the University of Orsay faced problems with their microscope and then their Institute moved on top of the "Plateau de Saclay" last year. They are now setting up their new laboratory and as soon as the STM will be operative, they will test growth of GNMs with the precursors already prepared.

In the meantime, we decided to test the organization of the 2,2',2"-triiodotriphenylene **52** at the solid-liquid interface on HOPG (Highly Oriented Pyrolytic Graphite) in collaboration with Dr Yoshihiro Kikkawa at the National Institute of Advanced Industrial Science and Technology

(AIST) in Tsukuba (Japan). Indeed the formation of halogen bonds is valuable approach to the realization of a well-ordered covalent networks.[30,31] The determination of the conditions to observe stable crystalline phases would be a huge step toward the realization of a 2D network. So far, while multiple solvents (1-phenyloctane, 1,2,4-trichlorobenzene, 1-octanoic acid) were tested but no stable phase was observed.

4.5. Conclusion

In this chapter, we presented the synthesis of two potential precursors of graphene nanomeshes. The band structures and bandgaps were determined by DFT calculation; unfortunately, the molecules have not been tested yet for the growth of GNMs. As we have seen, the precursors presented in this part are prochirals and while they are interesting for a first proof of concept, the GNMs will certainly exhibit a high level of defect and limited sizes.

To obtain a regular network and prevent any variation of the structure depending on the side the molecule lands on, new non-prochiral precursors or non-influeneced by the chirality should be designed. It is the case of compound **58** (Figure 4.9). This structure can be synthesized and it can be further tuned by the addition of heteroatoms like nitrogen.

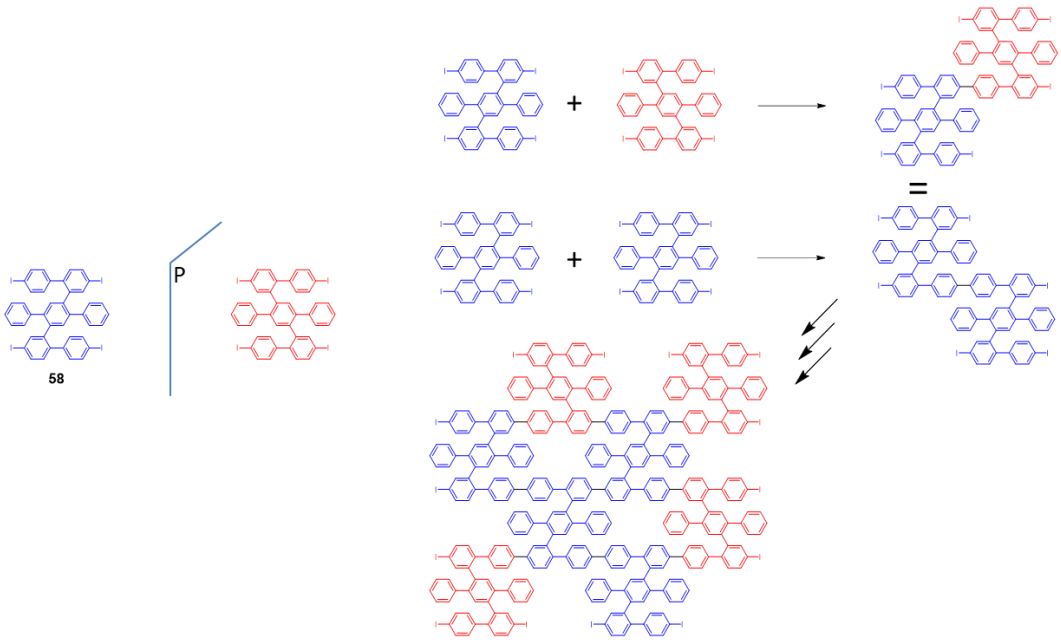

Figure 4.9: Structure of a GNM precursor in which would not be influence by the chirality

4.6. References

(1) Grill, L.; Dyer, M.; Lafferentz, L.; Persson, M.; Peters, M. V.; Hecht, S. Nano-Architectures by Covalent Assembly of Molecular Building Blocks. *Nat. Nanotechnol.* **2007**, *2*, 687–691.

(2) Cai, J.; Ruffieux, P.; Jaafar, R.; Bieri, M.; Braun, T.; Blankenburg, S.; Muoth, M.; Seitsonen, A. P.; Saleh, M.; Feng, X.; et al. Atomically Precise Bottom-up Fabrication of Graphene Nanoribbons. *Nature* **2010**, *466*, 470–473.

(3) Gutzler, R.; Walch, H.; Eder, G.; Kloft, S.; Heckl, W. M.; Lackinger, M. Surface Mediated Synthesis of 2D Covalent Organic Frameworks: 1,3,5-Tris(4-Bromophenyl)Benzene on Graphite(001), Cu(111), and Ag(110). *Chem. Commun.* **2009**, *0*, 4456–4458.

(4) Liu, J.; Ruffieux, P.; Feng, X.; Müllen, K.; Fasel, R. Cyclotrimerization of Arylalkynes on Au(111). *Chem. Commun.* **2014**, *50*, 11200–11203.

(5) Bieri, M.; Treier, M.; Cai, J.; Aït-Mansour, K.; Ruffieux, P.; Gröning, O.; Gröning, P.; Kastler, M.; Rieger, R.; Feng, X.; et al. Porous Graphenes: Two-Dimensional Polymer Synthesis with Atomic Precision. *Chem. Commun.* **2009**, *0*, 6919–6921.

(6) Eichhorn, J.; Strunskus, T.; Rastgoo-Lahrood, A.; Samanta, D.; Schmittel, M.; Lackinger, M. On-Surface Ullmann Polymerization via Intermediate Organometallic Networks on Ag(111). *Chem. Commun.* **2014**, *50*, 7680–7682.

(7) Fan, Q.; Wang, C.; Liu, L.; Han, Y.; Zhao, J.; Zhu, J.; Kuttner, J.; Hilt, G.; Gottfried, J. M. Covalent, Organometallic, and Halogen-Bonded Nanomeshes from Tetrabromo-Terphenyl by Surface-Assisted Synthesis on Cu(111). *J. Phys. Chem. C* **2014**, *118*, 13018–13025.

(8) Moreno, C.; Vilas-Varela, M.; Kretz, B.; Garcia-Lekue, A.; Costache, M. V; Paradinas, M.; Panighel, M.; Ceballos, G.; Valenzuela, S. O.; Peña, D.; et al. Bottom-up Synthesis of Multifunctional Nanoporous Graphene. *Science (80-.).* **2018**, *360*, 199–203.

(9) Pauly, F.; Viljas, J. K.; Cuevas, J. C.; Schön, G. Density-Functional Study of Tilt-Angle and Temperature-Dependent Conductance in Biphenyl Dithiol Single-Molecule Junctions. *Phys. Rev. B* **2008**, *77*, 155312.

(10) Berrada, S.; Hung Nguyen, V.; Querlioz, D.; Saint-Martin, J.; Alarcón, A.; Chassat, C.; Bournel, A.; Dollfus, P. Graphene Nanomesh Transistor with High on/off Ratio and Good Saturation Behavior. *Appl. Phys. Lett.* **2013**, *103*, 183509.

(11) Hung Nguyen, V.; Mazzamuto, F.; Saint-Martin, J.; Bournel, A.; Dollfus, P. Graphene Nanomesh-Based Devices Exhibiting a Strong Negative Differential Conductance Effect. *Nanotechnology* **2012**, *23*, 065201.

(12) Tan, Q.; Chen, H.; Xia, H.; Liu, B.; Xu, B. Parent and Trisubstituted Triazacoronenes: Synthesis, Crystal Structure and Physicochemical Properties. *Chem. Commun.* **2016**, *52*, 537–540.

(13) Tan, Q.; Zhou, D.; Zhang, T.; Liu, B.; Xu, B. Iodine-Doped Sumanene and Its Application for the Synthesis of Chalcogenasumanenes and Silasumanenes. *Chem. Commun.* **2017**, *53*, 10279–10282.

(14) Lafferentz, L.; Eberhardt, V.; Dri, C.; Africh, C.; Comelli, G.; Esch, F.; Hecht, S.; Grill, L. Controlling On-Surface Polymerization by Hierarchical and Substrate-Directed Growth. *Nat. Chem.* **2012**, *4*, 215–220.

(15) Operamolla, A.; Omar, H.; Babudri, F.; Farinola, G. M.; Naso, F. Synthesis of S-Acetyl Oligoarylenedithiols via Suzuki-Miyaura Cross-Coupling. *J. Org. Chem.* **2007**, *72*, 10272–10275.

(16) Patil, S. A.; Uthaisar, C.; Barone, V.; Fahlman, B. D. Synthesis, Characterization and DFT Study of 1-Bromo-4-(3,7-Dimethyloctyl) Benzene. *J. Mol. Struct.* **2012**, *1015*, 41–45.

(17) Lee, J.; Roy, A. K.; Wohlwend, J. L.; Varshney, V.; Ferguson, J. B.; Mitchel, W. C.; Farmer, B. L. Scaling Law for Energy Bandgap and Effective Electron Mass in Graphene Nano Mesh. *Appl. Phys. Lett.* **2013**, *102*, 203107.

(18) Pedersen, T. G.; Flindt, C.; Pedersen, J.; Mortensen, N. A.; Jauho, A. P.; Pedersen, K. Graphene Antidot Lattices: Designed Defects and Spin Qubits. *Phys. Rev. Lett.* **2008**, *100*, 136804.

(19) Ji, X.; Zhang, J.; Wang, Y.; Qian, H.; Yu, Z. Influence of Edge Imperfections on the Transport Behavior of Graphene Nanomeshes. *Nanoscale* **2013**, *5*, 2527–2531.

(20) Hung Nguyen, V.; Chung Nguyen, M.; Nguyen, H. V.; Dollfus, P. Disorder Effects on Electronic Bandgap and Transport in Graphene-Nanomesh-Based Structures. *J. Appl. Phys.* **2013**, *113*, 013702.

(21) Power, S. R.; Jauho, A. P. Electronic Transport in Disordered Graphene Antidot Lattice Devices. *Phys. Rev. B* **2014**, *90*, 115408.

(22) Abdurakhmanova, N.; Amsharov, N.; Stepanow, S.; Jansen, M.; Kern, K.; Amsharov, K. Synthesis of Wide Atomically Precise Graphene Nanoribbons from Para-Oligophenylene Based Molecular Precursor. *Carbon N. Y.* **2014**, *77*, 1187–1190.

(23) Treier, M.; Pignedoli, C. A.; Laino, T.; Rieger, R.; Müllen, K.; Passerone, D.; Fasel, R. Surface-Assisted Cyclodehydrogenation Provides a Synthetic Route towards Easily Processable and Chemically Tailored Nanographenes. *Nat. Chem.* **2011**, *3*, 61–67.

(24) Zhang, H.; Lin, H.; Sun, K.; Chen, L.; Zagranyarski, Y.; Aghdassi, N.; Duhm, S.; Li, Q.; Zhong, D.; Li, Y.; et al. On-Surface Synthesis of Rylene-Type Graphene Nanoribbons. *J. Am. Chem. Soc.* **2015**, *137*, 4022–4025.

(25) Basagni, A.; Sedona, F.; Pignedoli, C. A.; Cattelan, M.; Nicolas, L.; Casarin, M.; Sambi, M. Molecules-Oligomers-Nanowires-Graphene Nanoribbons: A Bottom-up Stepwise on-Surface Covalent Synthesis Preserving Long-Range Order. *J. Am. Chem. Soc.* **2015**, *137*, 1802–1808.

(26) Ruffieux, P.; Cai, J.; Plumb, N. C.; Patthey, L.; Prezzi, D.; Ferretti, A.; Molinari, E.; Feng, X.; Müllen, K.; Pignedoli, C. A.; et al. Electronic Structure of Atomically Precise Graphene Nanoribbons. *ACS Nano* **2012**, *6*, 6930–6935.

(27) Ruffieux, P.; Wang, S.; Yang, B.; Sanchez-Sanchez, C.; Liu, J.; Dienel, T.; Talirz, L.; Shinde, P.; Pignedoli, C. A.; Passerone, D.; et al. On-Surface Synthesis of Graphene Nanoribbons with Zigzag Edge Topology. *Nature* **2016**, *531*, 489–492.

(28) Chen, Y. C.; De Oteyza, D. G.; Pedramrazi, Z.; Chen, C.; Fischer, F. R.; Crommie, M. F. Tuning the Band Gap

of Graphene Nanoribbons Synthesized from Molecular Precursors. *ACS Nano* **2013**, *7*, 6123–6128.

(29) Huang, H.; Wei, D.; Sun, J.; Wong, S. L.; Feng, Y. P.; Neto, A. H. C.; Wee, A. T. S. Spatially Resolved Electronic Structures of Atomically Precise Armchair Graphene Nanoribbons. *Sci. Rep.* **2012**, *2*, 983.

(30) Cavallo, G.; Metrangolo, P.; Milani, R.; Pilati, T.; Priimagi, A.; Resnati, G.; Terraneo, G. The Halogen Bond. *Chem. Rev.* **2016**, *116*, 2478–2601.

(31) Gilday, L. C.; Robinson, S. W.; Barendt, T. A.; Langton, M. J.; Mullaney, B. R.; Beer, P. D. Halogen Bonding in Supramolecular Chemistry. **2015**.

Chapter 5 : Conclusion

Chapter 4: Graphene Nanomeshes

Chapter 5: Conclusion

In this work we realized the synthesis of various GQDs based on Diels-Alder coupling of an acetylenic precursor with a cyclopentadienone followed by a dehydrogenation step *via* Scholl reaction. The structure of the GQDs can be tuned by the addition of either chlorine or dodecyl chain to increase solubility and change the optical properties.

In chapter 1 (Introduction), we gave an overview of the gapped-graphene materials and we presented two approaches: the top-down and the bottom-up approaches that were developed for the fabrication of these materials. Most of the studies on the bottom-up approach are devoted to the synthesis and properties of graphene nanoribbons. GNRs are synthesized by polymerization and therefore GNRs present a certain polydispersity that prevents exploring their intrinsic properties. Finally, despite the large amount of literature on graphene quantum dots and graphene nanoribbons, there is still room for the development of original structures and for the study of their optical properties.

In chapter 2, we reported the synthesis and new characterization on the well-known superphenalene C96 structure. The C96C12 GQD **3** was imaged with STM and HR-TEM and columnar structures were observed. For advanced optical study, it was necessary for find the best conditions for the dispersion of the particles in order to obtain individualized molecules in solution. It was realized with 1,2,4-trichlorobenzene and it was confirmed with the results in PL, PLE and time-resolved PL on GQD **3**. The single photon emission properties of GQD **3** embedded in polystyrene were characterized and we found that this GQD could emit single photon at room temperature with a high brightness and high stability. The saturation rate curves showed that GQD **3** had an intensity of saturation 30 times higher than N-V center in 111-diamond. Finally, the C96Cl GQD **2** was also tested to confirm the possibility to tune the optical properties and it appeared that it is also a good single photon emitter at room temperature. Moreover, the peripheral functionalization with chlorine atoms permitted to shift the maximum emission of *ca.* 100 nm in the red.

Chapter 5: Conclusion

In chapter 3, we synthesized new families of graphene nanoparticles exhibiting elongated shapes. These nanoparticles were named graphene nanorods (GNRods). Using the same final steps as GQDs (Diels-Alder and Scholl reactions), the length of these rods was tuned adding a row of phenyls to the acetylenic precursor. Starting from the C78 **11** and C132 **13**, the change of precursors gave rise to new structures, the C96L **12** and the C162 **14** with the same width and edge morphology than their parent nanoparticles and with only one parameter varying: their length. The four GNRods (**11**-**14**) were also chlorinated and we faced some difficulties to chlorinate totally the C78, C96L and C132 GNRods. Indeed, the analyses by MALDI-TOF mass spectrometry showed a mixture of the desired nanoparticles with particles with 1, 2 or 3 chlorine atoms missing. The synthesis needs to be optimized. For the biggest GNRod **21** (C162Cl), we were not able to characterize properly the materials by MALDI-TOF mass spectrometry; the work is still ongoing. Finally, the polyphenylene dendrimers with dodecyl alkyl chains were also prepared but the dehydrogenation step has to be optimized to get the fully dehydrogenated GNRods without chlorination.

In chapter 4, we have used the bottom-up approach to synthesize two precursors for the preparation of graphene nanomeshes (GNMs). In literature, the GNM structures reported so far, the graphene neck is constituted of a single C−C bond between phenyl rings. We envisioned to form GNM structures with larger conductive graphene necks (between 0.6 and 1 nm, 2 to 4 phenyl rings). The precursors should have been deposited on metallic surfaces in a STM chamber; unfortunately, several problems with STM delayed the experiments. Nevertheless, the precursors are ready and they can be tested as soon as the problems will be solved. The properties of the GNMs were simulated and bandgaps in the order of 1 eV are expected. We also showed that the precursors are prochiral and therefore they may produce irregular networks during the CVD in the STM chamber and that. Moreover, precursor **52** can give rise to two different networks depending on which face they adsorb on surface.

In the future, this project should focus around the in depth study of the already prepared GNRods to see the impact of length variation on the intrinsic optical properties. First, the problem of synthesis should be solved; then to go further in this direction, additional rows of phenyls should be added following the approach developed for precursors **32** and **44** (Figure

5.1). However, this approach will be limited due to the high number of synthetic steps needed, the poor solubility of the resulting precursor and the difficulty of purification.

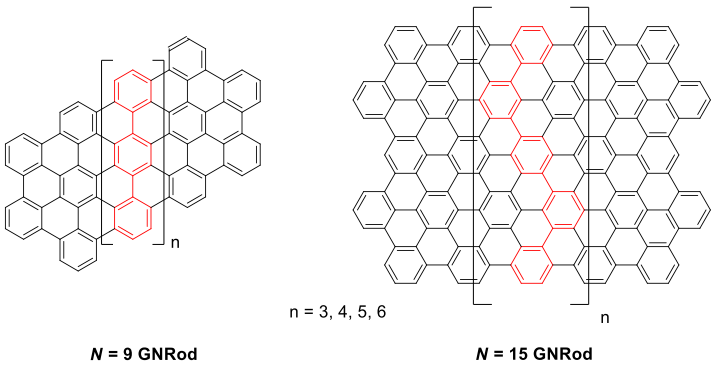

Figure 5.1: The chemical structures of the N = 9 and N = 15 GNRods.

The future GNRods will permit to fully study the influence of the shape and edge morphology of the nanoparticles on their properties. Indeed *N = 9* GNRods with n = 2 and n = 4 contain 96 and 128 sp^2 carbons, respectively. Their properties will be compared to the triangular-shaped C96 (GQD **1**) and to the square-shaped C132 (GQD **13**). The *N = 15* GNRods with n = 3 contain 222 sp^2 carbons. It will be compared to the well-known hexagonal C222 nanoparticles synthesize by Müllen.

Concerning GNMs, to tackle the issue of the prochirality of precursors **52** and **53**, a new precursor will be designed (Figure 5.2). The structure of this precursor and consequently of the final GNM can be further tuned by the addition of nitrogen at both extremities of the central terphenyl by replacement of phenylboronic by 4-pyridinylboronic acid during the synthesis.

Finally, other nitrogen-doped structures based on tetraanthracenylporphyrin are currently developed in the group. We hope that these structures will also give rise to 2D covalent porous networks on surface.

Chapter 5: Conclusion

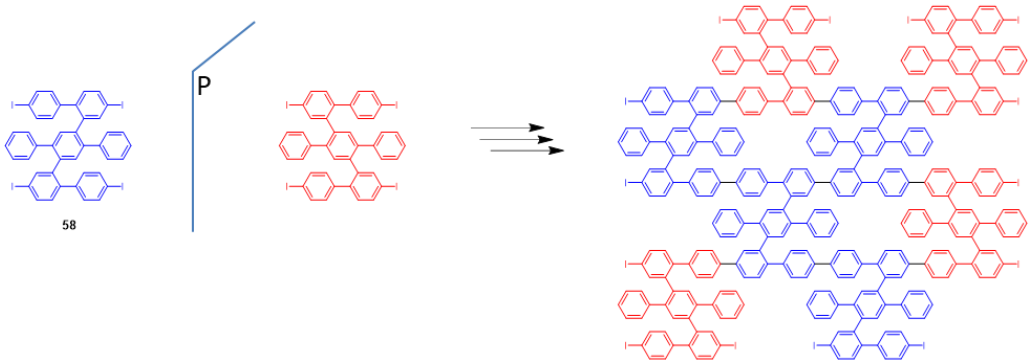

Figure 5.2: The chemical structure of a) the zig-zagging AC GNR[1] and b) the non-prochiral precursor.

Chapter 6 : Experimental Part

Chapter 5: Conclusion

Chapter 6: Experimental Part

6.1. Technics

The UV-vis spectra were recorded in quartz cells of 1 cm in a Perkin Elmer Lambda 900 UV-Vis-NIR spectrophotometer. The photoluminescence spectra are recorded on a custom setup at the LAC. The setup is made of a supercontinuum laser (SC-400-6, Fianium), two monochromators for the excitation (SP2150i, Princeton Instruments), a monochromator for the emission (SP2300i, Princeton Instruments) and a CCD camera (PIXIS100B, Princeton Instruments). For time resolved photoluminescence, the Peletier-cooled CCD camera is replaced by an avalanche photodiode (IDQ100) and the laser is linked to a start-stop counter (TimeHarp 260, PicoQuant). The single photon experiments are done with an oil-immersion microscope objective (PLAPON 60XO, Olympus) using the oil with ref 10976 from Fluka. The excitation is polarized with a Glan-Taylor prism (Thorlabs) and the emission is collected with an avalanche photodiode (APD) (SPCM-AQRH-13, PerkinElmer) in the case of the optical scanning and a liquid-nitrogen-cooled CCD camera (PyLoN-100BRX, Princeton Instruments) in the case of the photoluminescence measurement. For the optical scanning, a *xyz* piezoelectric scanner (Nano-PDQ, Mad City Labs) is also needed with its acquisition card (PCIe-6323, National Instruments). For the second order correlation measurement, the Hanbury-Brown and Twiss interferometer is made of a counter/timer (Picoharp 3009), an 800 nm short-pass filter (03SWP418, Melles Griot) and two APDs (SPCM-AQRH-13, PerkinElmer) connected to a wide-range time digitizer (P7887, FastComtec). The ^{1}H-NMR spectra were recorded with a 400 MHz BRUKER Avance spectrometer. The chemical shifts presented are in ppm (parts *per* million) compared to the solvent signal used as the internal reference ($CDCl_3$: 7.26 ppm). The MALDI-TOF spectra are recorded with a BRUKER Ultraflextreme or a BRUKER Autoflex Speed (for the monitoring of the Scholl reaction). The APPI MS spectra are recorded with an Agilent Technology QTOF 6540. STM imaging of the samples was performed at the liquid/solid interface using a Pico-SPM (Molecular Imaging, Agilent Technology) scanning tunneling microscope. Cut Pt/Ir tips were used to obtain constant current images at room temperature with a bias voltage applied to the sample. STM images were processed and analyzed using the application FabViewer.[1] The HR-TEM images were obtained with a FEI-Titan Ultimate transmission electron microscope operating at 80 kV.

Chapter 6: Experimental part

6.1. Solvents and reagents

The solvents are of technical grade and used as receive from Carlo Erba Reagents or Sigma-Aldrich. For anhydrous synthesis, dichloromethane, carbon tetrachloride, triethylamine and diethyl ether are distillated with calcium hydride under nitrogen, toluene and THF are distillated with potassium/benzophenone under nitrogen. The reagents are used as received from Sigma-Aldrich, TCI or Interchim. The 1,4-dimethylpiperazine-2,3-dione **7** was prepared as described in the litterature.[2]

6.2. Graphene quantum dots

Synthesis of the dendrimer 4[3]:

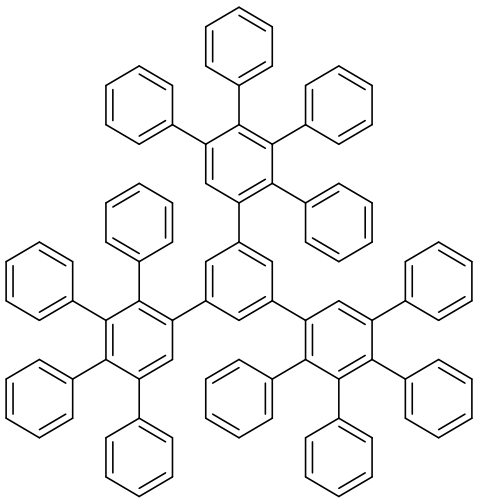

Tetraphenylcyclopentadienone (240 mg, 0.63 mmol) and 1,3,5-triethynylbenzene (26 mg, 0.17 mmol) were introduced in a dry Schlenck flask with diphenyl ether, degassed with two vaccum-argon cycles and heated at 180 °C overnight. The viscous violet product was diluted with 1mL of dichloromethane and added dropwise to cold ethanol (200 ml). The violet product was filtered on PTFE (0.2 µm) and dried under vacuum. The product was first purified with column chromatography with toluene to get rid of Ph_2O. The product was redispersed in hot methanol to solublize the excess of cyclopentadienone, filtered on PTFE membrane and washed with methanol. Finally, 306.4 mg of white powder were obtained (40% yield).

^{1}H NMR (δ in ppm, 400MHz, $CDCl_3$): 7.35-7.32 (m, 3H), 7.16-6.61 (m, 63H).

MALDI-TOF MS: calcd for $C_{96}H_{66}$: 1219.58 found: 1219.54.

Synthesis of GQD 1[3]:

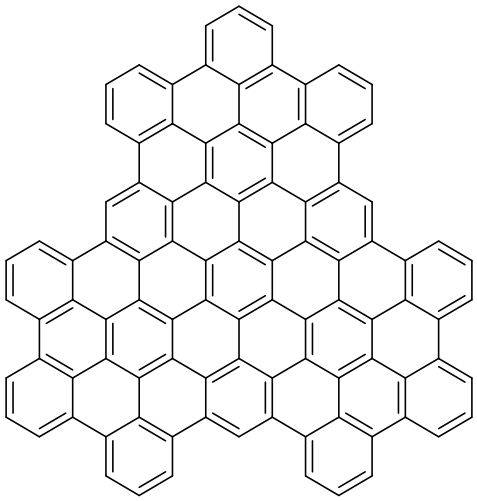

Dendrimer **4** (268 mg, 0.22 mmol) was dispersed in 120 ml of non-stabilized dichloromethane in a two-necked round-bottom flask of 250 ml. Separetly, $FeCl_3$ (4.49 g, 27.6 mmol) was added to 5 ml of anhydrous nitromethane in a glovebox and then added to the solution of dendrimer. The solution was left 18 hours under argon coming from a two necked round-bottom flask filled with Dichloromethane in which argon was bubbling. The evolution of the reaction was followed with MALDI-TOF mass spectrometry after quenching of a small amount of reaction mixture with methanol followed by centrifugation. The solution was quenched with methanol (about 80 ml) and then filtered on PTFE and washed with methanol. The pure product was obtained as 247.7 mg of black powder (95% yield).

MALDI-TOF MS: calcd for $C_{96}H_{30}$: 1182.23, found: 1182.18.

Synthesis of GQD 2[4]:

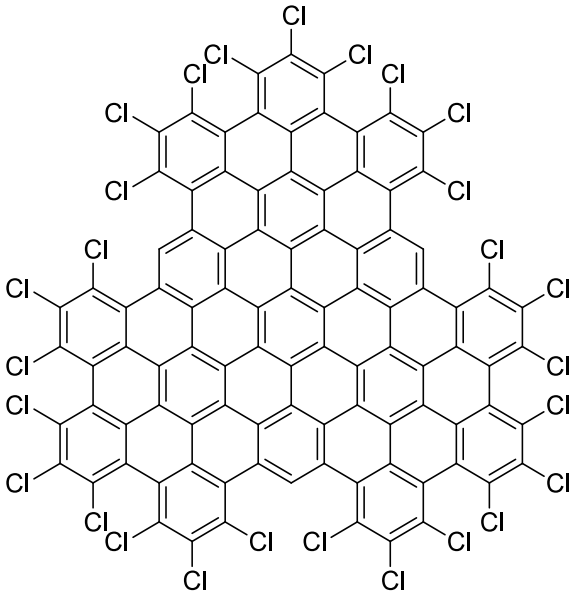

GQD **1** (29 mg, 0.025 mmol) and $AlCl_3$ (13 mg, 0.098 mmol) were introduced in a dry two necked round-bottom flask (100 ml), and dissolved on 20 ml of CCl_4. After 20 min of argon bubbling, ICl (0.74 ml, 14.7 mmol) was added and the reaction was left for 48h at 80°C. The reaction was quenched with ethanol and ICl and CCl_4 were evaporated at about 60°C with a liquid nitrogen trap. The solid obtained after evaporation of the solvents was then washed with ethanol and purified by column chromatography on chloroform. Finally, the product was obtained as 37.2 mg of a violet powder (73% yield). Because of the presence of 27 chlorine atoms, the monoisotopic mass was not detected.

MALDI-TOF MS: calcd for $C_{96}H_3Cl_{27}$: 2099.18 (M_W 2113.28), found: 2113.72.

Synthesis of 4-bromododecanoylbenzene 5[5]:

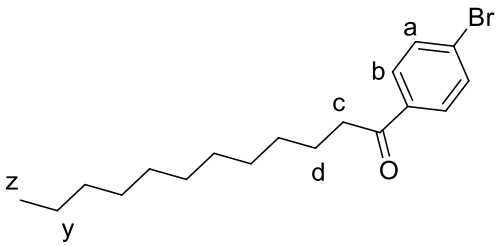

Bromobenzene (21 ml, 210 mmol) and aluminum chloride (16 g, 120 mmol) were introduced under stirring in a two necked round-bottom flask at room temperature. Dodecanoyl chloride (24 ml, 100 mmol) was introduced dropwise and the mixture was heated at 50°C for 1h30. The solution was then cooled down to room temperature and poured on ice. The product was

extracted with dichloromethane and washed with water (500 ml), hydrochloric acid (2 ml of HCl 37% in 400 ml of water) and saturated sodium chloride solution (400 ml) and dried with sodium sulfate. After evaporation of the organic solvent the product was purified by recrystallization in ethanol. The solid was filtered and dried under vacuum overnight to finally obtain 24.74 g of white powder (73% yield).

^{1}H NMR (δ in ppm, 400MHz, $CDCl_3$): 7.83-7.81 (d, *J*=8.4Hz, 2H, b), 7.61-7.59 (d, *J*=8.4Hz, 2H, a), 2.94-2.90 (t, *J*=7.4Hz, 2H, c), 1.74-1.53 (m, 18H, d-y), 0.90-0.86 ppm (t, *J*=6.6Hz, 3H, z).

Synthesis of 4-bromododecylbenzene 6[5]:

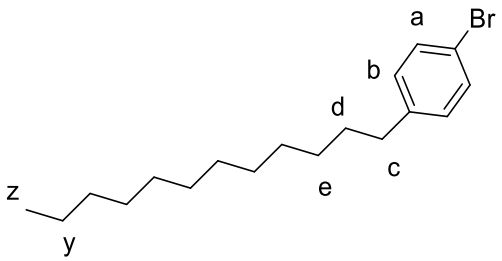

4-bromododecanoylbenzene **5** (10 g, 29.5 mmol), potassium hydroxide (5 g, 89 mmol) and hydrazine monohydrate (3.5 ml, 72 mmol) were introduced in a round-bottom flask with 50 ml of ethylene glycol. The mixture was heated at 130°C and after 3h40, water and hydrazine were distillated at 220°C for 4h30. The mixture was the cooled down and poured in diluted hydrochloric acid. The product was extracted with dichloromethane and washed with water. The organic phase was then dried with sodium sulfate and the solvent was evaporated. The product was purified by column chromatography with petroleum ether. The 4-bromododecylbenzene was obtained as 7.06 g of a colorless liquid (74% yield).

^{1}H NMR (δ in ppm, 400MHz, $CDCl_3$): 7.41-7.39 (d, *J*=8Hz, 2H, a), 7.07-7.05 (d, *J*=8.4Hz, 2H, b), 2.57 (t, *J*=7.6Hz, 2H, c), 1.57 (t, *J*=7.2, 2H, d), 1.28 (m, 20H, e-y), 0.91 (t, *J*=6.8Hz, 3H, z).

Synthesis of 1,2-bis(4-dodecylphenyl)ethane-1,2-dione 8[5]:

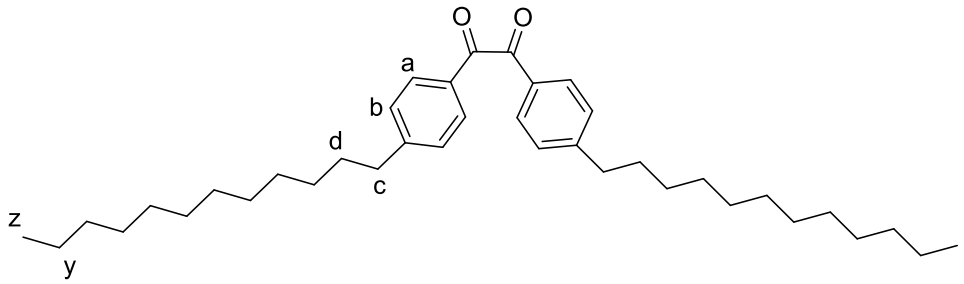

4-bromododecylbenzene **6** (8 g, 24.5 mmol) was introduced under argon in a dried round-bottom flask with anhydrous THF. The mixture was cooled down to -50°C and n-butyllithium (17.5 ml, 24.5 mmol) was added dropwise. The solution was heated up to 0°C in an ice bath and transferred through a cannula in a two-necked round-bottom flask in a suspension of 1,4-dimethylpiperazine-2,3-dione (1.58 g, 11 mmol) in 80 ml of anhydrous THF. The mixture was stirred overnight at room temperature. The reaction was quenched with diluted hydrochloric acid. The product was extracted with dichloromethane and washed with diluted hydrochloric acid and water and dried with sodium sulfate. The organic phase was evaporated and the solid was purified by column chromatography with a mixture of cyclohexane and dichloromethane (2/1). The pure product was obtained as 2.19 g of a yellowish powder (33% yield).

^{1}H NMR (δ in ppm, 400MHz, $CDCl_3$): 7.89-7.87 (d, *J*=8Hz, 4H, a), 7.31-7.29 (d, *J*=8.4Hz, 4H, b), 2.69-2.65 (t, *J*=7.6Hz 4H, c), 1.64-1.30 (m, 40H, d-y), 0.90-0.86 ppm (t, *J*= 4.95Hz, 6H, z).

Synthesis of 3,4-bis(4-dodecylphenyl)-2,5-diphenylcyclopenta-2,4-dienone 9[5]:

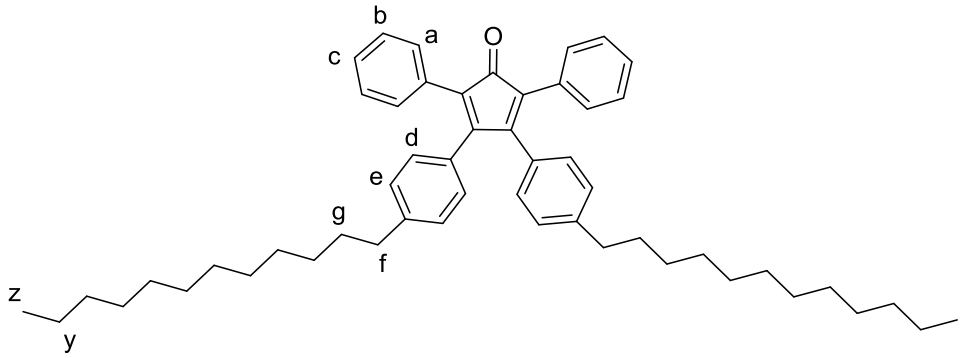

1,2-bis(4-dodecylphenyl)ethane-1,2-dione **8** (2 g, 3.8 mmol) and 1,3-diphenylpropan-2-one (0.72 g, 3.45 mmol) were introduced in 10mL of ethanol and the yellow mixture was heated to 90°C. Potassium hydroxide (0.22 g, 3.9 mmol) was then added and the mixture turns purple. After 30min the solution was cooled down to 0°C and the viscous mixture was added to diluted

hydrochloric acid. The product was extracted with dichloromethane and washed with water. After evaporation of the organic phase the solid was purified by column chromatography with a mixture of cyclohexane and dichloromethane (10/1). The pure product was obtained as 2.49 g a purple powder (51% yield).

^{1}H NMR (δ in ppm, 400MHz, $CDCl_3$): 7.26-7.20 (m, 12H, a, b, c), 6.97-6.95 (d, *J*=6Hz, 4H, d), 6.82-6.80 (d, *J*=6Hz 4H, e), 2.57-2.53 (m, 4H, f), 1.54-1.27 (m, 40H, g-y), 0.90-0.87 ppm (t, *J*= 4.95Hz, 6H, z).

Synthesis of dendrimer 10[5]:

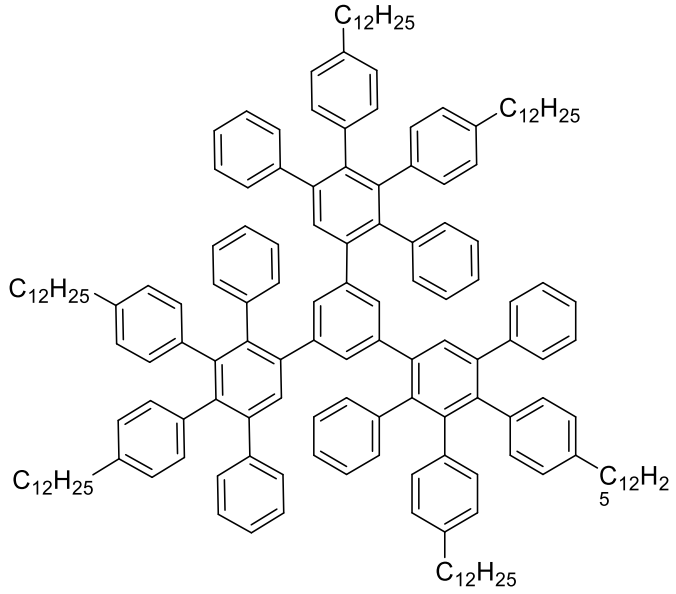

3,4-bis(4-dodecylphenyl)-2,5-diphenylcyclopentadienone **9** (450 mg, 0.62 mmol) and 1,3,5-triethynylbenzene (25 mg, 0.17 mmol) were introduced in a dry Schlenck flask with diphenyl ether (5 ml) and heated at 180 °C overnight. The viscous brown product was diluted with 1mL of dichloromethane and added dropwise to cold ethanol (200 ml). The brown product was filtered on PTFE (0.2 µm) and dried under vacuum. The product was first purified with column chromatography with toluene to get rid of Ph_2O. The product was redispersed in hot methanol to solublize the excess of cyclopentadienone, filtered on PTFE membrane and washed with methanol. Finally, 220 mg of yellowish powder were obtained (57% yield).

^{1}H NMR (δ in ppm, 400MHz, $CDCl_3$): 7.15-6.52 (m, 60H); 2.35 (dt, *J*=17.1, 7.4 Hz, 12H); 1.25 (m, 120H); 0.88 (t, *J*=6.8 Hz, 18H).

MALDI-TOF MS: calcd for $C_{168}H_{210}$: 2227.64, found: 2228.60 (M+H).

Synthesis of GQD 3[5]:

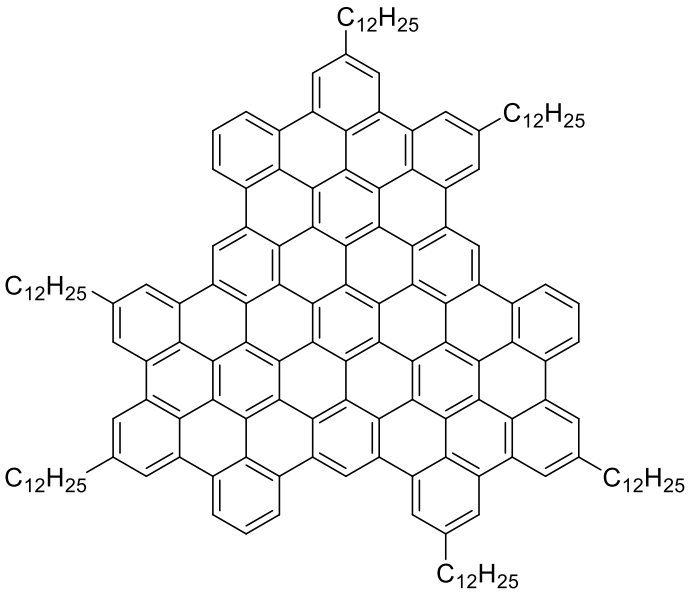

Dendrimer **10** (50 mg, 0.022 mmol) was dispersed in non-stabilized dichloromethane (40 ml) in a two-necked round-bottom flask of 100 ml. Separetly, $FeCl_3$ (458 mg, 2.8 mmol) was dissolved in anhydrous nitromethane in a glove box (2 ml) and added to the solution of dendrimer. The solution was left 18 hours under argon coming from a two necked round-bottom flask filled with dichloromethane in which argon was bubbling. The evolution of the reaction was followed with MALDI-TOF mass spectrometry after quenching of a small amount of reaction mixture with methanol followed by centrifugation. When the reaction wais finished, the solution was quenched with methanol (40 ml) and then filtered on PTFE membrane (0.2 µm). The pure product was obtained as 46mg of a black powder (95% yield).

MALDI-TOF MS: calcd for $C_{168}H_{174}$: 2191.36; found: 2191.80.

6.3. Graphene nanorods

Synthesis of 1,4-diodo-3,6-trimethylsilylbenzene 25[6]:

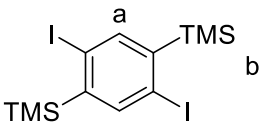

1,4-diiodobenzene (9.9 g, 30 mmol) and chlorotrimethylsilane (8.5 ml, 66 mmol) were introduced in a dry three necked round-bottom flask of 250 ml with 70 ml of dry THF. The solution was cooled down to -70°C and lithium diisopropylamide (LDA) (33 ml, 2 M in THF) was added dropwise. The solution was left an hour under stirring around -50°C and then hydrolysed with H_2SO_4 (1.5 10^{-2} M , about 100 ml). After extraction with ether, the organic phase was washed with water twice and dried. The solide was then dispersed in methanol, filtered and washed with methanol. The product was obtained as 9.04 g of a white powder after drying under vaccum (64% yield).

^{1}H NMR (δ in ppm, 400MHz, $CDCl_3$): 7.39 (s, 2H, a), 0.38ppm (s, 9H, b).

MALDI-TOF MS m/z: calcd for $C_{12}H_{20}I_2Si_2$: 473.93; found: 473.92.

Synthesis of 2',5'- bis(trimethylsilyl)-1,1':4',1''-terphenyl 26:

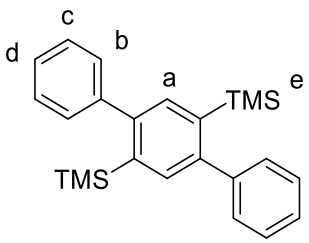

Compound **25** (2 g, 4.2 mmol), phenylboronic acid (1.54 g, 12.6 mmol), potassium carbonate (3.5 g, 25.3 mmol) and $Pd(PPh_3)_2Cl_2$ (0.30 g, 0.4 mmol) were inserted in a dry three necked round-bottom flask. The powders were degassed by 3 vaccum-argon cycles. 50 ml of THF, 40 ml of Ethanol and 20 ml of water were mixed together and degassed by 3 “freeze-pump-thaw”. After addition of the solvents, the reaction was left at 60°C overnight. The dark solution obtained was extracted with DCM, filtered on celite and washed with water twice and brine. The brownish solid was first purified through a pad of silica with cyclohexane and then with flash chromatography with a mixture of cyclohexane and dichloromethane (9/1). The pure product was obtained as 1.54 g of white powder (97% yield).

^{1}H NMR (δ in ppm, 400MHz, $CDCl_3$): 7.44 (s, 2H, a), 7.49-7.37 (m, 10H, b-d), 0.02 (s, 18H, e).

MALDI-TOF MS m/z: calcd for $C_{24}H_{30}Si_2$: 374.67; found: 374.19.

Synthesis of 2',5'- diiodo-1,1':4',1''-terphenyl 27:

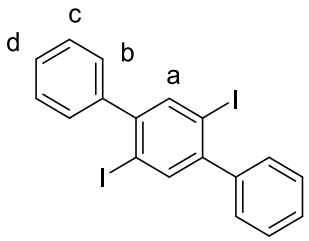

2',5'- bis(trimethylsilyl)-1,1':4',1''-terphenyl **26** (750 mg, 2.0 mmol) was introduced in a dry two necked round-bottom flask with 20 ml of dry dichloromethane. After cooling down to 0°C, ICl (401 µL, 8.0 mmol) was added dropwise. The reaction was left overnight at room temperature under argon. The solution was quenched with sodium thiosulfate (1 M, about 20 ml) and washed with water. The product was purified *via* recrystallization in cyclohexane and filtration to give 383 mg of a white powder (40% yield).

^{1}H NMR (δ in ppm, 400MHz, $CDCl_3$): 7.89 (s, 2H, a), 7.48-7.39 (m, 10H, b-d).

MALDI-TOF MS m/z: calcd for $C_{24}H_{30}I_2$: 481.90; found: 481.90.

Synthesis of 2',5'- bis(ethynyltrimethylsilane)-1,1':4',1''-terphenyl 28:

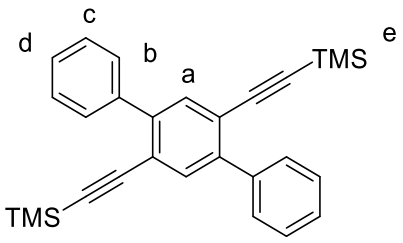

2',5'- diiodo-1,1':4',1''-terphenyl **27** (250 mg, 0.52 mmol), Copper iodide (19.7 mg, 0.10 mmol) and $Pd(PPh_3)_2Cl_2$ (36.3 mg, 0.052 mmol) were introduced in a three necked round-bottom flask and degassed by two vaccum-argon cycles. 60 ml of triethylamine and 40 ml of toluene were introduced and degassed by three "freeze-pump-thaw". The solution was heated up to 80°C and ethynyltrimethylsilane (220 µl, 1.5 mmol) was added dropwise. The reaction was left under argon at 80°C for 24 hours. The solution was filtered on celite and the product was extracted with DCM and washed with water. The organic phase was dried and the solvent was

evaporated. The product was purified with column chromatography with a mixture of cyclohexane and DCM (95/5). The pure product was obtained as 138.9 mg of yellowish powder (96% yield)

^{1}H NMR (δ in ppm, 400MHz, $CDCl_3$): 7.66-7.63 (m, 4H, b), 7.61 (s, 2H, a), 7.41-7.36 (m, 6H, c-d), 0.13 (s, 18H, e).

MALDI-TOF MS m/z: calcd for $C_{28}H_{30}Si_2$: 422.19; found: 422.19.

Synthesis of 2',5'- bis(ethynyl)-1,1':4',1''-terphenyl 29:

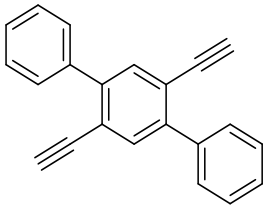

2',5'- bis(ethynyltrimethylsilane)-1,1':4',1''-terphenyl **28** (100 mg, 0.23 mmol) was introduced in a dry Schlenck flask and degassed by two vaccum-argon cycles. The solvent (THF, 6 ml) was added and then Bu_4NF (0.56 ml, 1M in THF, 0.57 mmol) was introduced dropwise and the yellowish solution turned blue. The solution was then left at ambient temperature for two hours. The product was extracted by DCM and washed twice by water. The solvent was evaporated and the final product was obtained as 60 mg of yellow powder (91% yield). The product was directly used in the next reaction without further purification.

Synthesis of dendrimer 30:

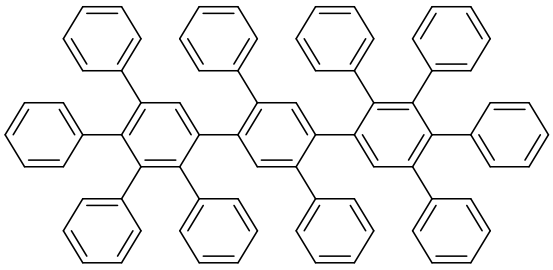

2',5'- bis(ethynyl)-1,1':4',1''-terphenyl **29** (131 mg, 0.47 mmol) and tetraphenylcyclopentadienone (545 mg, 1.4 mmol) were introduced in a dried Schlenck flask and degassed by two vaccum-argon cycles. The o-xylene (5 ml) was then introduced and the solution was heated up to 180°C and left under stirring overnight. About 1 ml of DCM was

added to decrease the viscosity and the solution was poured in about 150 ml of cold methanol. The precipitate was filtered and washed with methanol. The pure product was obtained as 236 mg of a pinkish powder (51% yield).

^{1}H NMR (δ in ppm, 400MHz, $CDCl_3$): 7.56 (s, 2H), 7.31 (s, 2H), 7.20-6.53 (m, 50H).

MALDI-TOF MS m/z: calcd for $C_{78}H_{54}$: 990.42; found: 990.40.

Synthesis of GNRod 11:

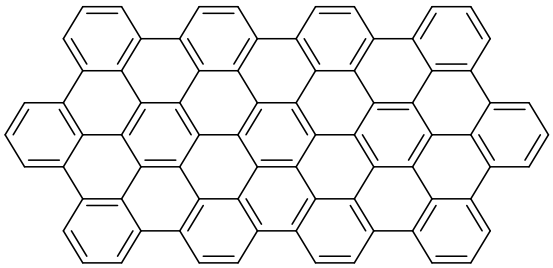

Dendrimer **30** (150 mg, 0.15 mmol) was dispersed in 40 ml of non-stabilized Dichloromethane in a two-necked round-bottom flask of 250 ml. Separetly, $FeCl_3$ (2.4 g, 15 mmol) was added to 5 ml of anhydrous nitromethane in a glove box and then added to the solution. The solution was left 17 hours under argon coming from a two necked round-bottom flask filled with dichloromethane in which argon was bubbling. The evolution of the reaction was monitored with MALDI-TOF mass spectrometry after quenching of a small amount of reaction mixture with methanol followed by centrifugation. The solution was quenched with methanol (about 40 ml) and then filtered on PTFE and washed with methanol. The pur product was obtained as 132 mg of black powder (90% yield).

MALDI-TOF MS m/z: calcd for $C_{78}H_{26}$: 962.20; found: 962.22.

Synthesis of GNRod 15:

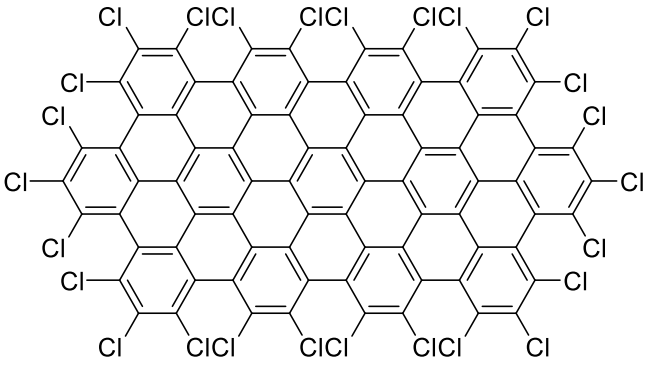

GQD **11** (50.3 mg, 0.052 mmol) and $AlCl_3$ (27.7 mg, 0.21 mmol) were introduced in a dry two necked round-bottom flask (100 ml), and dissolved on 20 ml CCl_4. After 20 min of argon bubbling, ICl (5g, 30.8 mmol) were added and the reaction was left for 72h at 80°C. The reaction was quenched with ethanol and ICl and CCl_4 were evaporated at about 60°C with a liquid nitrogen trap. The solid obtained after evaporation of the solvents was then washed with ethanol and purified by column chromatography with chloroform. After evaporation of the solvent, 10.4 mg of a brown powder were obtained (10% yield). Because of the presence of 26 chlorine atoms, the monoisotopic mass was not detected.

MALDI-TOF MS m/z: calcd for $C_{78}Cl_{26}$: 1845.19 (M_W 1858.56); found: 1788.15. The main product is the compound missing two chlorines.

Synthesis of dendrimer 31:

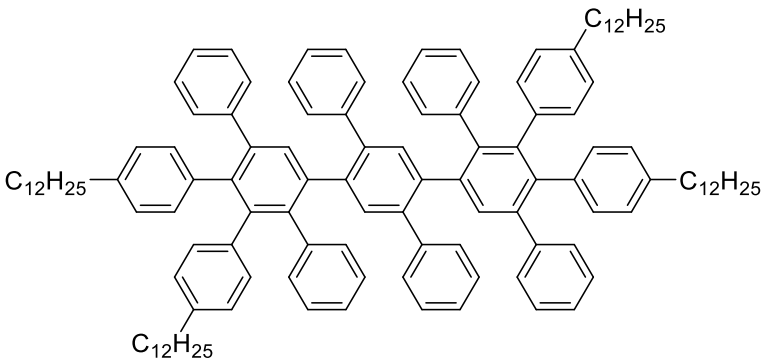

2',5'- bis(ethynyl)-1,1':4',1''-terphenyl **29** (58.9 mg, 0.21 mmol) and 3,4-bis(4-dodecylphenyl)-2,5-diphenylcyclopentadienone (457.8 mg, 0.64 mmol) were introduced in a dried Schlenck flask and degassed by two vaccum-argon cycles. The o-xylene (4 ml) was then introduced and the solution was heated up to 180°C and left under stirring overnight. After evaporation of the

solvent, the product was purified with column chromatography with a mixture of cyclohexane and DCM (70/30). The pure product was obtained as 340 mg of a pale brown powder (98% yield).

^{1}H NMR (δ in ppm, 400MHz, $CDCl_3$): 7.54 (s, 2H), 7.09-6.47(m, 48H), 2.37-2.30 (dt, *J*=26.5, 7.4Hz, 8H), 1.30-1.21 (m, 80H), 0.89-0.86 (m, 12H).

MALDI-TOF MS m/z: calcd for $C_{126}H_{150}$: 1663.17; found: 1664.23 (M+H).

Synthesis of GNRod 16:

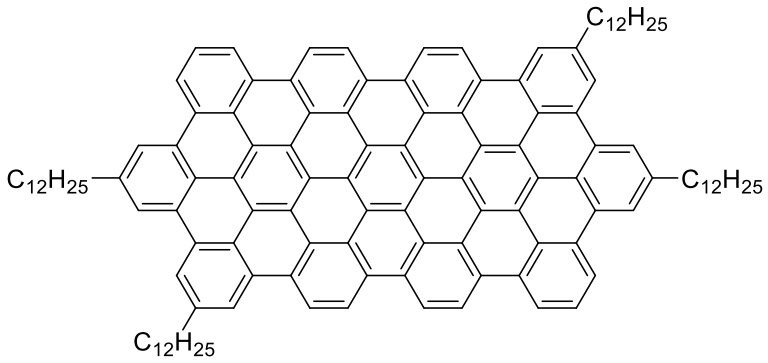

Dendrimer **30** (50 mg, 0.030 mmol) was dispersed in 40 ml of non-stabilized Dichloromethane in a two-necked round-bottom flask of 100 ml. Separetly, $FeCl_3$ (409 mg, 2.52 mmol) was added to 5 ml of anhydrous nitromethane in a glove box and then added to the solution of dendrimer. The solution was left 5 hours under argon coming from a two necked round-bottom flask filled with dichloromethane in which argon was bubbling. The evolution of the reaction was monitored with MALDI-TOF mass spectrometry after quenching of a small amount of reaction mixture with methanol followed by centrifugation. The solution was quenched with methanol (about 40 ml) and then filtered on PTFE and washed with methanol. The product was purified with a column chromatography with THF and a second one with Toluene and obtained as 32.2 mg of black powder (66% yield).

MALDI-TOF MS m/z: calcd for $C_{126}H_{122}$: 1634.95; found: 1635.10.

Synthesis of 2'-Iodo-5'-(trimethylsilyl)-1,1':4',1''-terphenyl 34[7]:

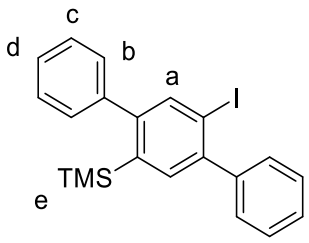

2',5'- bis(trimethylsilyl)-1,1':4',1''-terphenyl **26** (1 mg, 2.7 mmol) and $AgBF_4$ (0.47 mg, 2.4 mmol) were introduced in 14 ml of THF/MeOH (2/1) in a two-necked round-bottom flask. The solution was cooled down to 0°C and 2.67 ml of ICl (1 M in DCM) were added and left 1 hour under stirring at room temperature. After quenching with $Na_2S_2O_3$ (1 M, around 10 ml), the organic phase was separated and washed 3 times with water before evaporation of the solvents. The product is purified with column chromatography with cyclohexane and after evaporation of the solvent, 867 mg of white powder are obtained (76% yield).

^{1}H NMR (δ in ppm, 400MHz, $CDCl_3$): 7.85 (s, 2H, a), 7.49-7.39 (m, 10H, b-d), 0.01 (s, 9H, e).

MALDI-TOF MS m/z: calcd for $C_{21}H_{21}ISi$: 428.39; found: 428.05.

Synthesis of acid -5'-(trimethylsilyl)-1,1':4',1''-terphenyl-2'-boronic ester 36[7]:

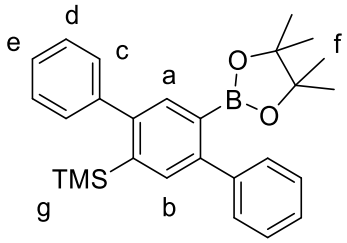

2'-Iodo-5'-(trimethylsilyl)-1,1':4',1''-terphenyl **34** (0.1 g, 0.23 mmol) was introduced in a dry round-bottom flask, degassed by two vaccum-argon cycles and left two hours under vaccum. 15 ml of dry THF were introduced and cooled down to -78°C. The n-BuLi solution (0.175 ml, 0.35 mmol, 1 M in cyclohexane) was added dropwise and the solution turned yellow. After one hour, the solution was heated up to -40°C and 2-Isopropoxy-4,4,5,5-tetramethyl-1,3,2-dioxaborolane (0.14 ml, 0.70 mmol) was added dropwise. The reaction was then left under argon at ambient temperature for three hours. The product was extracted with dichloromethane, washed with water twice and dried with sodium sulfate. After the evaporation of the solvent and purification with column chromatography with a mixture of

cyclohexane and DCM (60/40), the product was obtaiend as 90 mg of a yellowish powder (90% yield).

^{1}H NMR (δ in ppm, 400MHz, $CDCl_3$): 7.61 (s, 1H, a), 7.57 (s, 1H, b), 7.42-7.33 (m, 10H, c-e), 1.19 (s, 12H, f), 0.01 (s, 9H, g).

MALDI-TOF MS m/z: calcd for $C_{27}H_{33}BO_2Si$: 428.23; found: 428.23.

Synthesis of 3,3'-di(trimethylsilyl)-2,5,2',5'- tetraphenylbiphenyl 35:

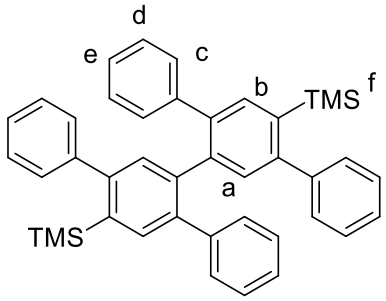

Boronic ester **36** (200 mg, 0.47 mmol), iodo-terphenyl **34** (300 mg, 0.7 mmol), Palladium acetate (55 mg, 0.24 mmol), SPhos (190 mg, 0.47 mmol) and Potassium phosphate tribasic (198 mg, 0.93 mmol) were introduced in a dry round-bottom flask and degassed by three vaccum-argon cycles. 6 ml of Toluene and 1 ml of water were added and degassed by 3 "freeze-pump-thaw" and the reaction was left at 60°C overnight. The dark solution obtained was extracted with DCM, filtered on celite and washed twice with water and brine. The brownish solid was first purified through a pad of silica with cyclohexane and then with flash chromatography with a mixture of cyclohexane and dichloromethane (95/5). The product was obtained as 150 mg of a white powder (53% yield).

^{1}H NMR (δ in ppm, 400MHz, $CDCl_3$): 7.61 (s, 2H, a), 7.57 (s, 2H, b), 7.47-7.32 (m, 20H, c-e), 0.0 (s, 18H, f).

MALDI-TOF MS m/z: calcd for $C_{42}H_{42}Si_2$: 602.28; found: 602.28.

Synthesis of 3,3'-diiodo-2,5,2',5'- tetraphenylbiphenyl 37:

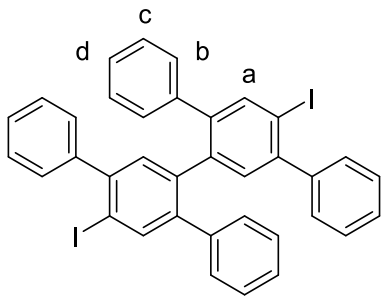

3,3'-di(trimethylsilyl)-2,5,2',5'- tetraphenylbiphenyl **35** (150 mg, 0.25 mmol) was introduced in a dry 25 ml round-bottom flask and dezaged with two vaccum-argon cycles. Then 5 ml of DCM were added and the solution was cooled down to 0°C. Iodine monochloride (50 µL, 1.0 mmol) was added and the reaction was left overnight at room temperature under argon. The reaction was quenched with a saturated solution of sodium thiosulfate, the product was extracted with DCM and washed twice with water. The organic phase was evaporated and the solide was purified by column chromatography with a mixture of cyclohexane and DCM (70/30). The pure product was obtained as 108 mg of a yellowish powder (61% yield).

^{1}H NMR (δ in ppm, 400MHz, $CDCl_3$): 7.81-7.60 (m, 4H, a), 7.52-7.31 (m, 8H, b), 7.23-7.12 (m, 8H, c), 6.79-6.78 (m, 4H, d).

MALDI-TOF MS m/z: calcd: 710.00; found: 710.01.

Synthesis of 3,3'-bis(ethynyltrimethylsilane)-2,5,2',5'- tetraphenylbiphenyl 38:

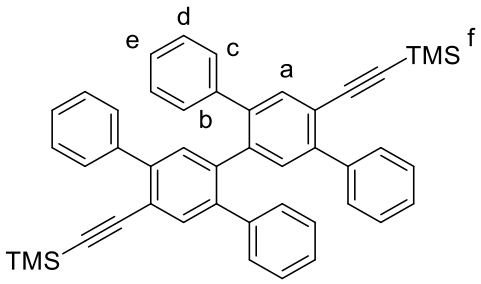

3,3'-diiodo-2,5,2',5'- tetraphenylbiphenyl **37** (100 mg, 0.14 mmol), Copper iodide (27 mg, 0.14 mmol), and $Pd(PPh_3)_2Cl_2$ (49 mg, 0.07 mmol) were introduced in a dry three neck round-bottom flask and degassed with two vacuum-argon cycles. Then 10 ml of toluene and 15 ml of Et_3N were introduced and the solution was degassed with two "freeze-pump-thaw". The ethynyltrimathylsilane (48 µL, 0.34 mmol) was then introduced dropwise and the solution was

left at 80°C overnight. The solution was filtered on celite and the product was extracted with DCM, washed with water twice and dried with sodium sulfate. After purification with column chromatography with a mixture of cyclohexane and DCM (95/5) the final product was obtained as 55.4 mg of a white powder (60% yield).

^{1}H NMR (δ in ppm, 400MHz, $CDCl_3$): 7.55-7.53 (m, 4H, a), 7.46 (s, 2H, b), 7.40-7.34 (m, 8H, c), 7.19-7.04 (m, 8H, d), 6.80-6.78 (m, 4H, e), 0.07 (s, 18H, f).

MALDI-TOF MS m/z: calcd for $C_{46}H_{42}Si_2$: 650.28; found: 650.30.

Synthesis of 3,3'-diethynyl-2,5,2',5'- tetraphenylbiphenyl 32:

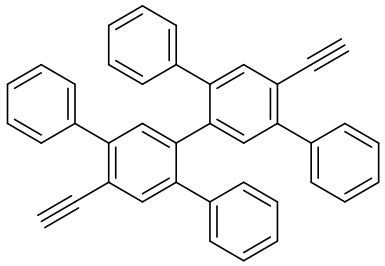

3,3'-bis(ethynyltrimethylsilane)-2,5,2',5'- tetraphenylbiphenyl **38** (50 mg, 0.077 mmol) was introduced in a Schlenck flask and degassed with to vacuum-argon cycles and THF (3 ml) was introduced. The Bu_4NF was then added (184 µL, 0.18 mmol) and the solution was left 2h at ambient temperature. The product was extracted with DCM and washed with water twice before the organic phase was evaporated and the product was obtained as 60 mg of white powder (91% yield). The product was directly used in the next reaction without further purification.

Synthesis of dendrimer 33:

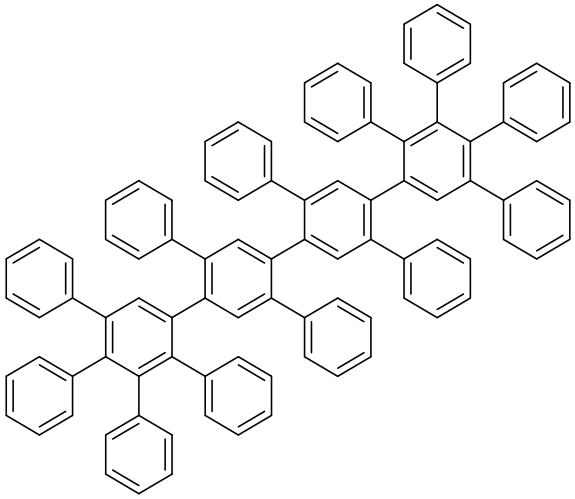

3,3'-diethynyl-2,5,2',5'- tetraphenylbiphenyl **32** (18 mg, 0.035 mmol) and tetraphenylcyclopentadienone (33 mg, 0.085 mmol) were introduced in a Schlenck flask and degassed with two vacuum-argon cycles. The o-xylene (5 ml) was then added and the reaction was left at 180°C overnight. About 1 ml of DCM was then added and the solution was added dropwise to about 100 ml of cold ethanol. The resulting white precipitate was then filtered and washed with ethanol. The product was obtained as 40 mg of a white powder (92% yield).

^{1}H NMR (δ in ppm, 400MHz, $CDCl_3$): 7.45-7.28 (m, 6H), 7.24-6.62(m, 60H).

MALDI-TOF MS m/z: calcd for $C_{96}H_{66}$: 1218.52; found: 1218.53.

Synthesis of GNRod 12:

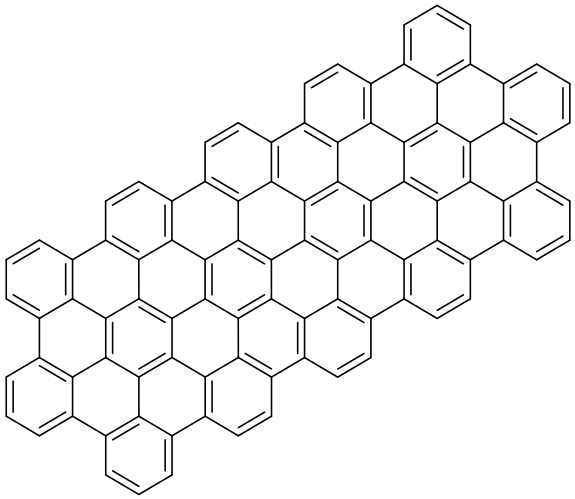

Dendrimer **33** (35 mg, 0.029 mmol) was dispersed in non-stabilized DCM and the solution was degassed with argon for 30 min. Separetly, $FeCl_3$ (587 mg, 3.6 mmol) was added to 5 ml of anhydrous nitromethane in a glove box. After the addition of the $FeCl_3$ solution, the mixture was left 16 hours under argon coming from a two necked round-bottom flask filled with dichloromethane in which argon was bubbling. The evolution of the reaction was monitored with MALDI-TOF mass spectrometry after quenching of a small amount of reaction mixture with methanol followed by centrifugation. The solution was quenched with methanol (about 40 ml) and then filtered on PTFE and washed with methanol. The pur product was obtained as 27 mg of black powder (80% yield).

MALDI-TOF MS m/z: calcd for $C_{96}H_{30}$: 1182.23; found: 1182.28.

Synthesis of GNRod 17:

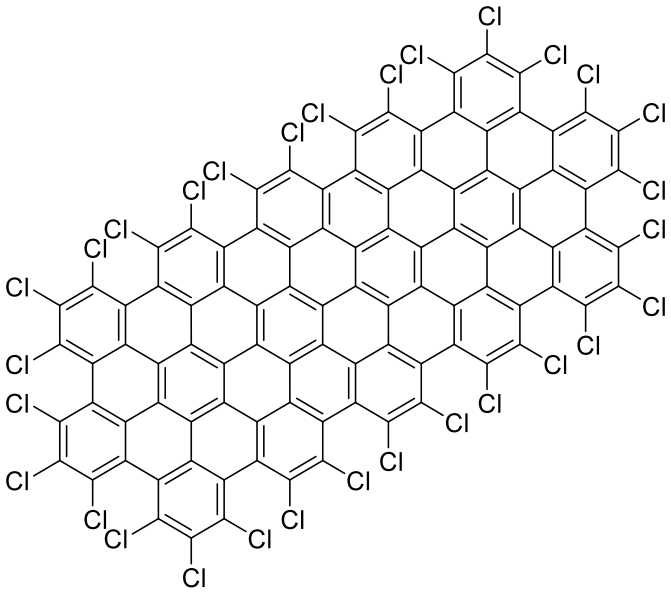

GQD **12** (30 mg, 0.025 mmol) and $AlCl_3$ (13.5 mg, 0.10 mmol) were introduced in a dry two necked round-bottom flask (100 ml), and dissolved in 20 ml of CCl_4. After 20 min of argon bubbling, ICl (5 g, 30.8 mmol) was added and the reaction was left for 48h at 80°C. The reaction was quenched with ethanol and ICl and CCl_4 were evaporated at about 60°C with a liquid nitrogen trap. The solid obtained after evaporation of the solvents was then washed with ethanol and purified by column chromatography with chloroform. After evaporation of the solvent, the product was obtained as 19.8 mg of green powder (35% yield). Because of the presence of 30 chlorine atoms, the monoisotopic mass was not detected.

MALDI-TOF MS m/z: calcd for $C_{96}Cl_{30}$: 2201.07 (M_W 2216.56); found: 2182.25. The main product is the compound missing one chlorine.

Synthesis of dendrimer 39:

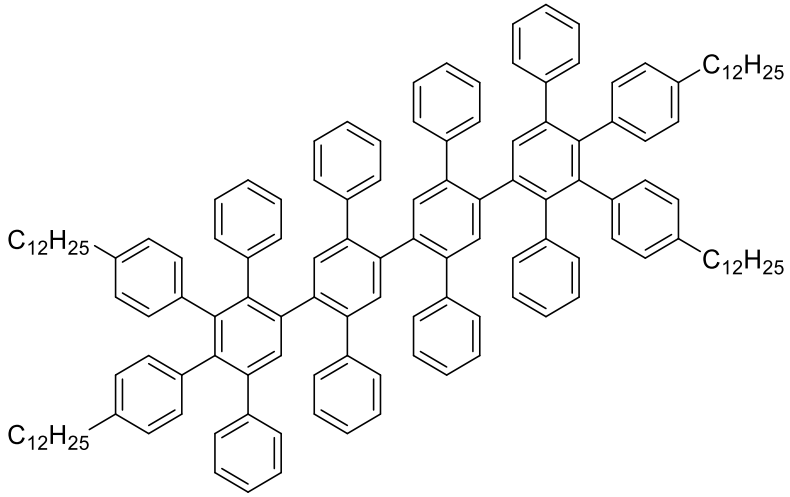

3,3'-diethynyl-2,5,2',5'- tetraphenylbiphenyl **32** (40 mg, 0.079 mmol) and 3,4-bis(4-dodecylphenyl)-2,5-diphenylcyclopentadienone (171 mg, 0.24 mmol) were introduced in a Schlenck flask and degassed with two vacuum-argon cycles. The o-xylene (5 ml) was then added and the reaction was left at 180°C overnight. About 1 ml of DCM was then added and the solution precipitated in about 100 ml of cold ethanol. The resulting white precipitate was then filtered and washed with ethanol. The product was obtained as 99 mg of a white powder (66% yield).

^{1}H NMR (δ in ppm, 400MHz, $CDCl_3$): 7.23-6.79(m, 62H), 2.57-2.53 (m, 8H), 1.26 (s, 80H), 0.88 (t, *J*=6.4Hz, 12H).

MALDI-TOF MS m/z: calcd for $C_{144}H_{162}$: 1891.27; found: 1891.37.

Synthesis of GNRod 18:

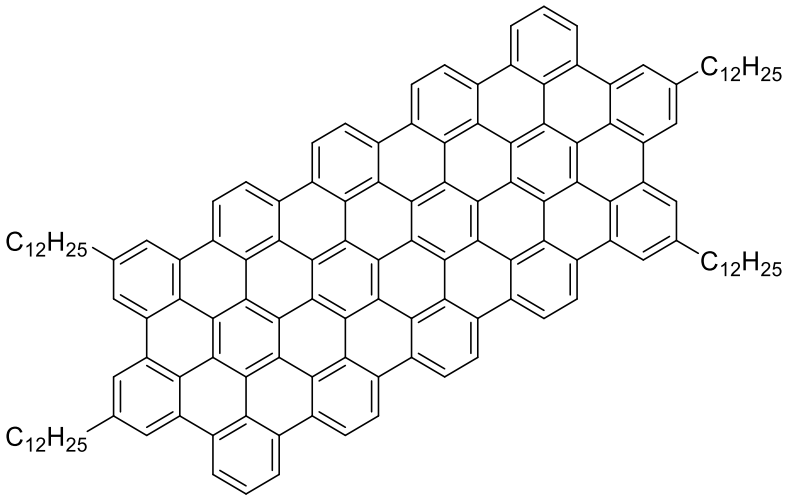

Dendrimer **39** (56 mg, 0.030 mmol) was dispersed in non-stabilized DCM and the solution was degassed with argon for 30min. Separetly, $FeCl_3$ (691 mg, 4.3 mmol) was added to 5 ml of anhydrous nitromethane in a glove box. After the addition of the $FeCl_3$ solution, the mixture was left 8 hours under argon coming from a two necked round-bottom flask filled with DCM in which argon was bubbling. The evolution of the reaction was monitored with MALDI-TOF mass spectroscometry after quenching of a small amount of reaction mixture with methanol followed by centrifugation. The solution was quenched with methanol (about 40 ml) and then filtered on PTFE and washed with methanol. After evaporation of the solvent, 45.7 mg of black powder are obtained (83% yield).

MALDI-TOF MS m/z: calcd for $C_{144}H_{126}$: 1854.99; found: 1865.25. The main peak found is the one of the compound missing 5 carbon-carbon bonds.

Synthesis of 3,3',5,5'-tetra(ethynyltrimethylsilane)-1,1'-biphenyl 40[8]:

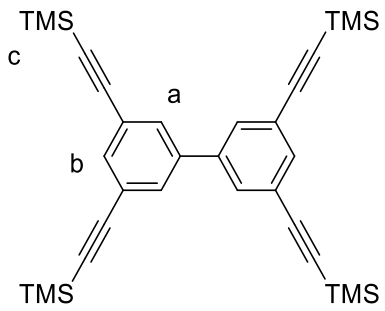

3,3',5,5'-tetrabromo-1,1'-biphenyl (500 mg, 1.06 mmol), copper iodide (81 mg, 0.43 mmol), $Pd(PPh_3)_2Cl_2$ (149 mg, 0.21 mmol) and triphenylphosphine (112 mg, 0.43 mmol) were

introduced in a dry round-bottom flask and degassed by three vacuum-argon cycles. The distillated toluene (7 ml) and triethylamine (12 ml) were added and the orange solution was left 15 min at 60°C under argon. The ethynyltrimethylsilane (0.9 ml, 6.4 mmol) was added and the solution turned black. The mixture was left 5h at 80°C and quenched with diluted hydrochloric acid. The product was extracted with dichloromethane and washed with water. After evaporation of the organic phase, the solid was purified with a mixture of cyclohexane and ethyl acetate (2%). The product was obtained as 254 mg of a white powder (45% yield).

^{1}H NMR (δ in ppm, 400MHz, $CDCl_3$): 7.59-7.57 (m, 6H, a-b), 0.25 (s, 36H, c).

Synthesis of 3,3',5,5'-tetraethynyl-1,1'-biphenyl 41[8]:

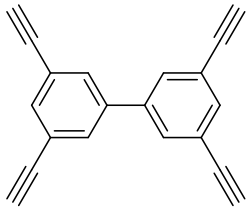

3,3',5,5'-tetra(ethynyltrimethylsilane)-1,1'-biphenyl **40** was introduced (0.13 g, 0.24 mmol) in a solution of Bu_4NF (0.46 ml, 1 M in THF) and THF (7 ml). The solution was stirred for 2 hours at room temperature. The product was extracted with dichloromethane and washed with water. The organic solution was dried with Na_2SO_4 and the solvent was evaporated. The purification was done with column chromatography with a mixture of cyclohexane and toluene (7/1) and gives 30 mg of a white solid (50% yield). The product was directly used in the next reaction without further purification.

Synthesis of dendrimer 42[8]:

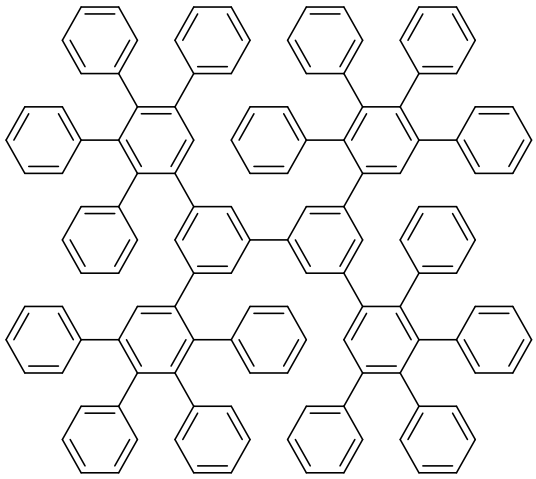

3,3',5,5'-tetraethynyl-1,1'-biphenyl **40** (30 mg; 0,12 mmol) and tetraphenylcyclopentadienone (253 mg; 0,66 mmol) were added to diphenylether (1 ml) in a dry Schlenk flask and heated at 180 °C overnight. The viscous product was diluted with 1 ml of dichloromethane and added dropwise to cold ethanol (200 ml). The product was filtered and dried under vacuum. The powder was first purified with column chromatography with toluene to get rid of Ph_2O. The second purification was done on column chromatography with a mixture of cyclohexane and DCM (7/1). The final product was obtained as 150 mg of a pale brown powder (75% yield).

^{1}H NMR (δ in ppm, 400MHz, $CDCl_3$): 7.17-6.66 (m, 86H), 6.34-6.31 (m, 4H).

MALDI-TOF MS m/z: calcd for $C_{132}H_{90}$: 1674.70, found: 1674.79.

Synthesis of GNRod 13[8]:

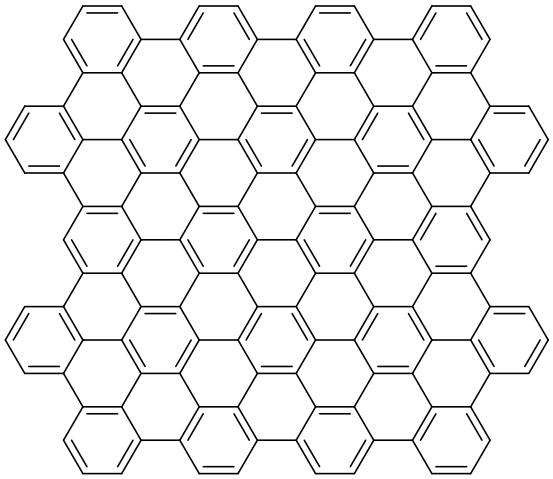

Dendrimer **42** (50 mg, 0.22 mmol) was dispersed in 120 ml of non-stabilized DCM in a two-necked round-bottom flask of 250 ml. Separetly, $FeCl_3$ (4.49 g, 27.6 mmol) was added to 5 ml of anhydrous nitromethane in a glove box. After addition of the $FeCl_3$ solution, the mixture was left 18 hours under argon coming from a two necked round-bottom flask filled with DCM in which argon was bubbling. The evolution of the reaction was monitored with MALDI-TOF mass spectrometry after quenching of a small amount of reaction mixture with methanol followed by centrifugation. The solution was quenched with methanol (about 80 ml) and then filtered on PTFE and washed with methanol. The pure product was obtained as 25 mg of black powder (51% yield).

MALDI-TOF MS m/z: calcd for $C_{132}H_{34}$: 1618.27, found: 1618.34.

Synthesis of GNRod 19[4]:

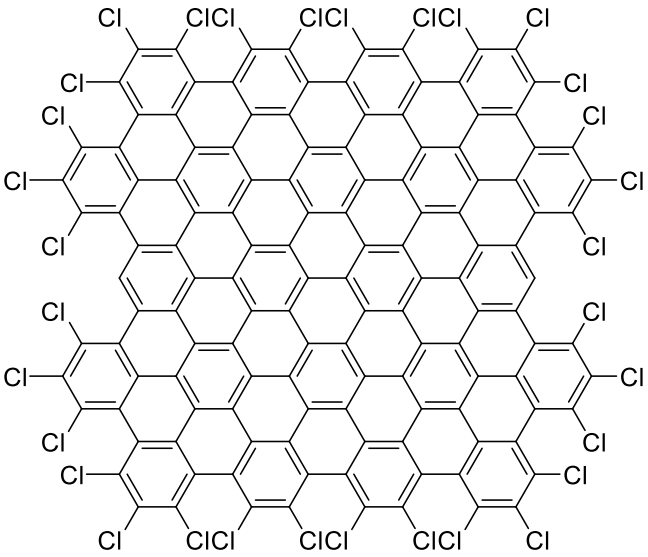

GNRod **13** (20 mg, 0.012 mmol) and AlCl3 (6.6 mg, 0.049 mmol) were introduced in a dry two necked round-bottom flask (100 ml), and dissolved on 20 ml of CCl_4. After 20 min of argon bubbling, ICl (0.37 ml, 7.4 mmol) was added and the reaction was left for 48h at 80°C. The reaction was quenched with ethanol and then ICl and CCl_4 were evaporated at about 60°C with a liquid nitrogen trap. The solid obtained after evaporation of the solvents was washed with ethanol and purified by column chromatography with chloroform. The final product was obtained as 12 mg of a blue powder (36% yield).

MALDI-TOF MS m/z: calcd for $C_{132}H_2Cl_{32}$: 2705.02 (M_W 2721.87), found: 2721.02.

Synthesis of dendrimer 43[9]:

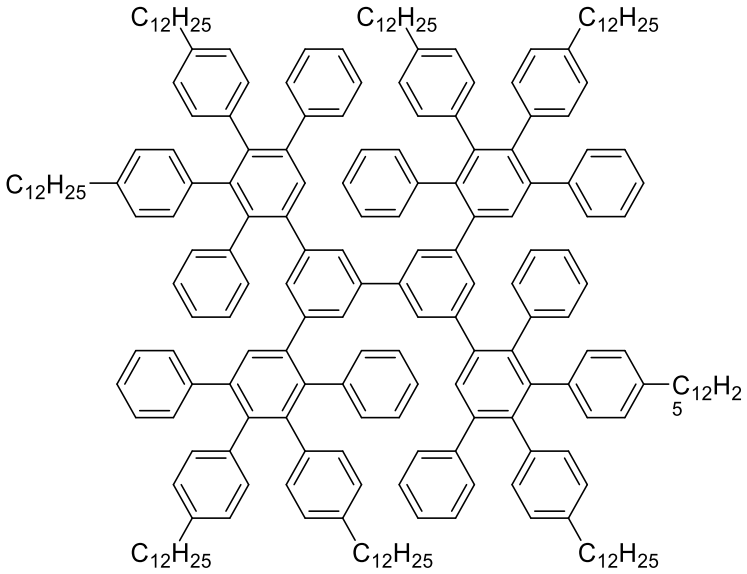

3,3',5,5'-tetraethynyl-1,1'-biphenyl **41** (30 mg; 0,12 mmol) and 3,4-bis(4-dodecylphenyl)-2,5-diphenylcyclopentadienone (253 mg; 0,66 mmol) were added to o-xylene (2 ml) in a dry Schlenk flask and heated at 180 °C overnight. The viscous product was diluted with 1 ml of dichloromethane and added dropwise to cold ethanol (200 ml). The precipitate was filtered and dried under vacuum. The purification was done with column chromatography with a mixture of cyclohexane and DCM (4/1) and the desired product was obtained as 230 mg of brownish powder (63% yield).

^{1}H NMR (δ in ppm, 400MHz, $CDCl_3$): 7.16-6.33 (m, 82H), 2.39-2.30 (m, 16H), 1.41-1.09 (m, 160H), 0.88 (t, *J*=6.8Hz, 24H).

MALDI-TOF MS m/z: calcd for $C_{228}H_{282}$: 3022.76, found: 3022.56.

Synthesis of GNRod 20[9]:

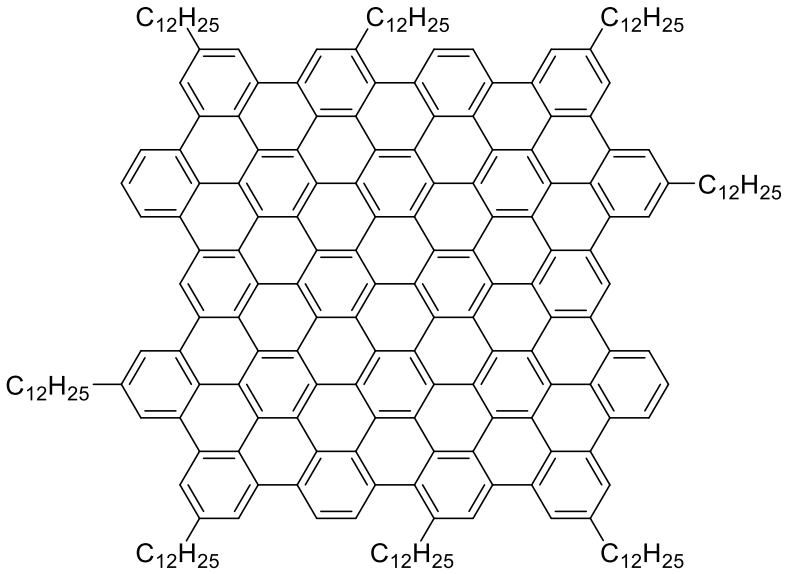

Dendrimer **43** (50 mg, 0.22 mmol) was dispersed in 120 ml of non-stabilized DCM in a two-necked round-bottom flask of 250 ml. Separetly, $FeCl_3$ (4.49 g, 27.6 mmol) was added to 5 ml of anhydrous nitromethane in a glove box. After addition of the $FeCl_3$ solution, the mixture was left 21 hours under argon coming from a two necked round-bottom flask filled with DCM in which argon was bubbling. The evolution of the reaction was monitored with MALDI-TOF mass spectrometry after quenching of a small amount of reaction mixture with methanol followed by centrifugation. The solution was quenched with methanol (about 80 ml) and then filtered on PTFE and washed with methanol. The pure product was obtained as 45 mg of black powder (92% yield).

MALDI-TOF MS m/z: calcd for $C_{228}H_{226}$: 2963.77, found: 2963.84.

Synthesis of 3,5- bis(ethynyltrimetylsilane)-bromobenzene 46[10]:

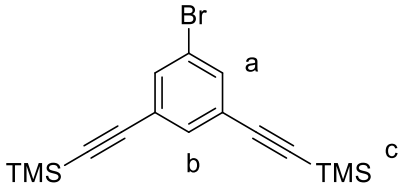

Tribromobenzene (500 mg, 1.6 mmol), Copper iodide (80.4 mg, 0.42 mmol), triphenylphosphin (116 mg, 0.44 mmol) and $Pd(PPh_3)_2Cl_2$ (148.7 mg, 0.21 mmol) were introduced in a three necked round-bottom flask and degassed by two vaccum-argon cycles. 12 ml of triethylamine and 7 ml of toluene were introduced and degassed by three “Freeze-

pump-thaw". The solution was heated up to 80°C and ethynyltrimethylsilane (0.39 ml, 2.74 mmol) was added dropwise. The reaction was left under argon at 80°C overnight. The solution was filtered with celite and the product was extracted by DCM and washed with water. The brown oil obtained after evaporation of the solvent was filtered on silica with DCM and then purified with a mixture of cyclohexane and ethyl acetate (2%). After evaporation of the solvent 235 mg of the oily product were obtained (45% yield).

^{1}H NMR (δ in ppm, 400MHz, $CDCl_3$): 7.53 (2H, m, a), 7.49 (1H, m, b), 0.24 (18H, s, c).

MALDI-TOF MS m/z: calcd for for $C_{16}H_{21}BrSi_2$: 348.04; found: 348.04.

Synthesis of Acid 3,5- bis(ethynyltrimetylsilane)-phenylboronic ester 47:

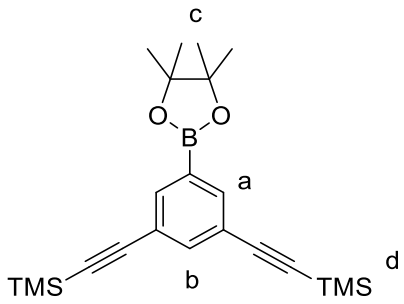

3,5- bis(ethynyltrimetylsilane)-bromobenzene **46** (0.6g, 1.7 mmol) was introduced in a dry round-bottom flask and degassed with two vaccum-argon cycles. The diethylether (about 15 ml) was distilated directly in the reaction flask after drying overnight with CaH_2. The solution was cooled down to -50°C and n-Butyllithium solution (1.28 ml, 2.5 mmol, 2 M in cyclohexane) was added dropwise. After stirring for 5 min, the reaction turned orange and 2-Isopropoxy-4,4,5,5-tetramethyl-1,3,2-dioxaborolane (1.05 ml, 5.1 mmol) was added before stirring again overnight at room temperature. The product was extracted with DCM and washed with water and the organic phase was dried and evaporated. The oily product was purified with column chromatography first with cyclohexane and then with DCM. The product was obtained as 575 mg of a yellow oil (85% yield).

^{1}H NMR (δ in ppm, 400MHz, $CDCl_3$): 7.84 (2H, m, a), 7.64 (1H, m, b), 1.33 (12H, s, c), 0.22 (18H, s, d).

MALDI-TOF MS m/z: calcd for $C_{22}H_{33}BO_2Si_2$: 396.21; found: 393.18.

Synthesis of 2',5'- bis(trimethylsilyl)-3',3''biphenyl-1,1':4',1''-terphenyl 48:

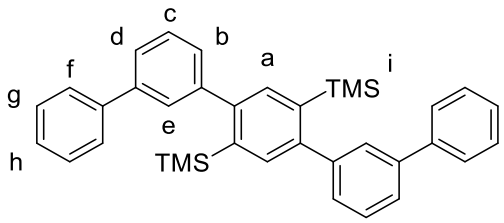

DiiododiTMSbenzene **25** (1 g, 2.1 mmol), 2-biphenylboronic acid (1.25 g, 6.33 mmol), Potassium carbonate (1.34 g, 6.33 mmol), SPhos (170 mg, 0.42 mmol) and $Pd(OAc)_2$ (47 mg, 0.21 mmol) were introduced in a dry three necked round-bottom flask. The powders were degassed by 3 vaccum-argon cycles. 30 ml of toluene and 5 ml of water were mixed and degassed by 3 "freeze-pump-thaw". After addition of the solvents, the reaction was left at 80°C overnight. The dark solution obtained was extracted with DCM, filtered on celite and washed twice with water and brine. The brownish solid was first purified through a pad of silica with cyclohexane and then with flash chromatography with cyclohexane and dichloromethane (9/1). The pure product was obtained as 760mg of white powder (68% yield).

^{1}H NMR (δ in ppm, 400MHz, $CDCl_3$): 7.88 (s, 2H, a), 7.69-7.38 (m, 28H, b-h), 0.05-0.02 (m, 18H, i).

MALDI-TOF MS m/z: calcd: 526.25; found: 526.25.

Synthesis of 2',5'- diiodo-3',3''biphenyl-1,1':4',1''-terphenyl 49:

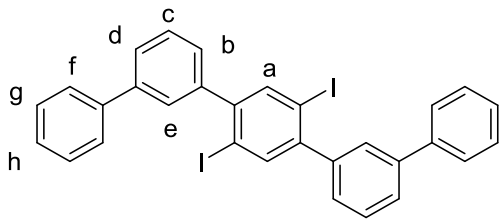

2',5'- bis(trimethylsilyl)-3',3''biphenyl-1,1':4',1''-terphenyl **48** (0.1 g, 0.19 mmol) was introduced in a dry round-bottom flask and degassed by two vaccum-argon cycles. Then 5 ml of DCM were added and the solution was cooled down to 0°C and degassed with argon bubbling for 10min. The ICl solution (0.76 ml, 1M in DCM, 0.76 mmol) was then added dropwise and the reaction was left under stirring at ambient temperature under argon

overnight. The reaction was quenched with a sodium sulfate solution (1 M, about 10 ml) and the product was extracted with DCM and washed twice with water. After evaporation of the solvent and purification with a column chromatography with a mixture of cyclohexane and ethyl acetate (2%), the pure product was obtained as 80 mg of a white powder (66% yield).

^{1}H NMR (δ in ppm, 400MHz, $CDCl_3$): 7.89 (s, 2H, a), 7.68-7.36 (m, 18H, b-h).

MALDI-TOF MS m/z: calcd for $C_{36}H_{38}Si_2$: 633.97; found: 633.96.

Synthesis of 2',5'- bis(3,5- bis(ethynyltrimetylsilane)-phenyl)-3',3''biphenyl-1,1':4',1''-terphenyl 50:

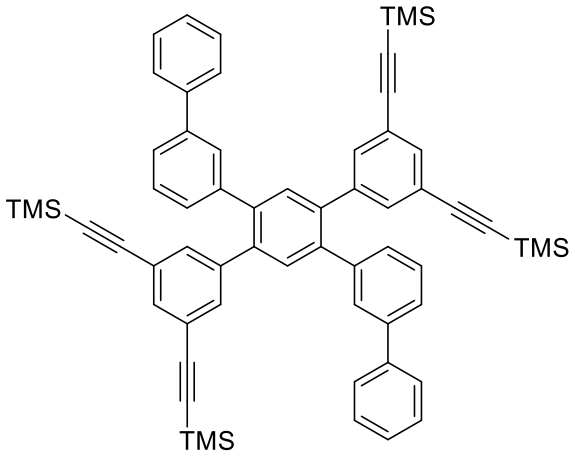

2',5'- diiodo-3',3''biphenyl-1,1':4',1''-terphenyl **47** (830 mg, 1.31 mmol), acid 3,5-bis(ethynyltrimetylsilane)-phenylboronic ester **47** (1.3 g, 3.27 mmol), $Pd_2(dba)_3$ (119 mg, 0.13 mmol), SPhos (215 mg, 0.52 mmol) and potassium carbonate (1.08 g, 7.84 mmol) were introduced in a schlenk flash and degassed with two vaccum-argon cycles. Toluene (18 ml), ethanol (6 ml) and water (3 ml) were added and degassed with three Freeze-pump-thaw. The reaction was left 24 hours at 80°C under argon. The solution was filtered on celite with DCM and washed twice with water. The organic phase was evaporate and purified with column chromatography with a mixture of cyclohexane and DCM (9/1) as eluant. The pure product was obtained as 735 mg of powder (57% yield).

^{1}H NMR (δ in ppm, 400MHz, $CDCl_3$): 7.52 (s, 2H), 7.48-7.30 (m, 24H), 0.19 (s, 36H).

MALDI-TOF MS m/z: calcd for $C_{62}H_{62}Si_4$: 918.39; found: 918.39.

Synthesis of 2',5'- bis(3,5- diethynylphenyl)-3',3''biphenyl-1,1':4',1''-terphenyl 44:

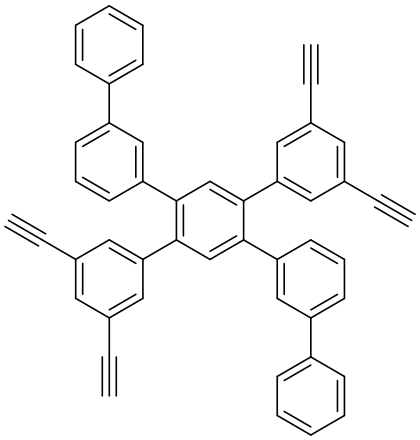

Compound **50** (150 mg, 0.16 mmol) was introduced in a dry schlenk flask and degassed with two vaccum-argon cycles. 20 ml of THF and TBAF (0.82 ml, 0.82 mmol, 1 M in THF) were added and the reaction was left 1 hour at 0°C. The product was extracted with DCM and washed twice with water and the organic phase was evaporated. The product was precipitated in methanol and filtered to obtain 95 mg of powder (94% yield). The product was directly used was the next reaction without further purification.

Synthesis of dendrimer 45:

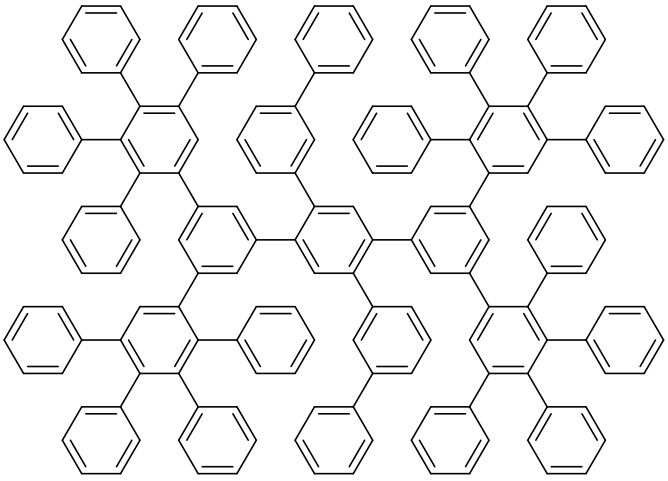

Precursor **44** (150 mg, 0.24 mmol) and tetraphenylcyclopentadienone (400 mg, 1.1 mmol) were introduced in a dry schlenk flask and degassed by two vaccum-argon cycles. The o-xylene (5 ml) was added and the reaction was left at 180°C overnight. The solution was then precipitated dropwise in cold ethanol (about 200 ml) and the precipitate was filtered. This

solide was purified with multiple recrystalisations in methanol. The pure product was obtained as 183 mg of a white solid (39% yield).

^{1}H NMR (δ in ppm, 400MHz, $CDCl_3$): 7.42-7.28 (m, 10H), 7.22-6.64 (m, 100H).

MALDI-TOF MS m/z: calcd for $C_{162}H_{110}$: 2054.86; found: 2054.65.

Synthesis of GNRod 14:

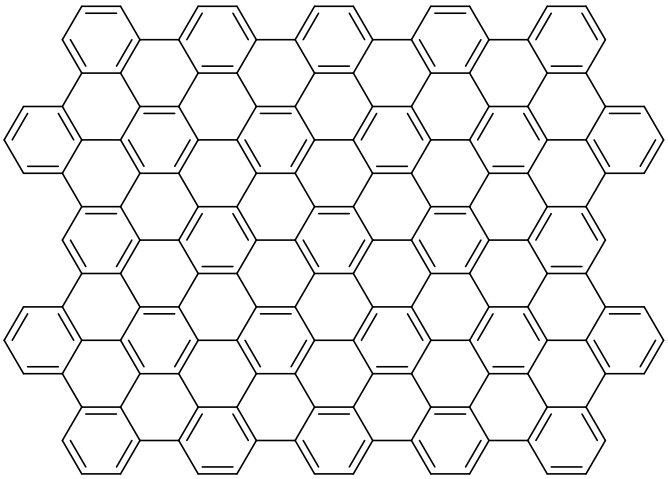

Dendrimer **45** (30 mg, 0.015 mmol) was dispersed in 40 ml of non-stabilized DCM in a two-necked round-bottom flask of 100 ml. Separetly, $FeCl_3$ (0.43 g, 2.6 mmol) was added to 4 ml of anhydrous nitromethane in a glove box. After addition of the $FeCl_3$ solution, the mixture was left 20 hours under argon coming from a two necked round-bottom flask filled with DCM in which argon was bubbling. The solution was quenched with methanol (about 40 ml) and then filtered on PTFE and washed with methanol. The pure product was obtained as 21 mg of black powder (73% yield).

MALDI-TOF MS m/z: calcd for $C_{162}H_{36}$: 1982.30; found: 1982.43.

Synthesis of GNRod 21:

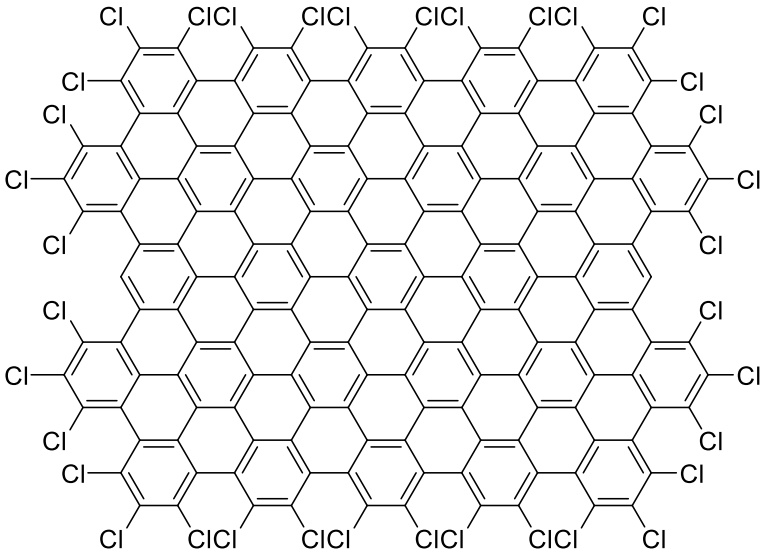

GNRod **14** (15 mg, 0.0076 mmol) and AlCl3 (20 mg, 0.15 mmol) were introduced in a dry two necked round-bottom flask (100 ml), and dissolved on 20 ml CCl_4. After 20 min of argon bubbling, ICl (2.1 g, 13 mmol) were added and the reaction was left for 72h at 85°C. The reaction was quenched with ethanol and ICl and CCl_4 were evaporated at about 60°C with a liquid nitrogen trap. The solid obtained after evaporation of the solvents was solubilized with DCM and precipitated in methanol. The precipitate was then washed with methanol and purified by column chromatography in chloroform. The final product was obtained as 12 mg of a blue powder (49% yield).

MALDI-TOF MS m/z: calcd for $C_{27}H_2Cl_{34}$: 3204.89 (M_W 3224.00); this product could not be characterized with this method.

Synthesis of dendrimer 51:

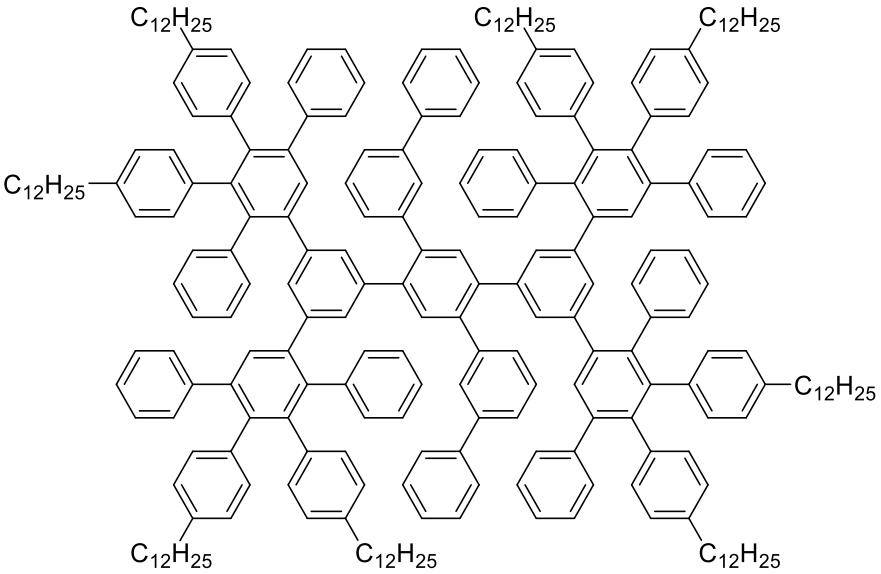

Precursor **50** (15 mg, 0.024 mmol) and tetraphenylcyclopentadienone (82 mg, 0.11 mmol) were introduced in a dry schlenk flask and degassed by two vaccum-argon cycles. The o-xylene (5 ml) was added and the reaction was left at 180°C overnight. The solution was then added dropwise to cold ethanol (about 200 ml) and the precipitate was filtered. This solide was purified with multiple recrystalisations in methanol. The pure product was obtained as 55 mg of a red solid (68% yield).

^{1}H NMR (δ in ppm, 400MHz, $CDCl_3$): 7.40-7.28 (m, 12H), 7.21-6.51 (m, 90), 2.36-2.31 (m, 16), 1.42-1.07 (m, 160H), 0.89-0.86 (m, 24H).

MALDI-TOF MS m/z: calcd for $C_{258}H_{303}$: 3400.36; found: 3400.49.

Synthesis of GNRod 22:

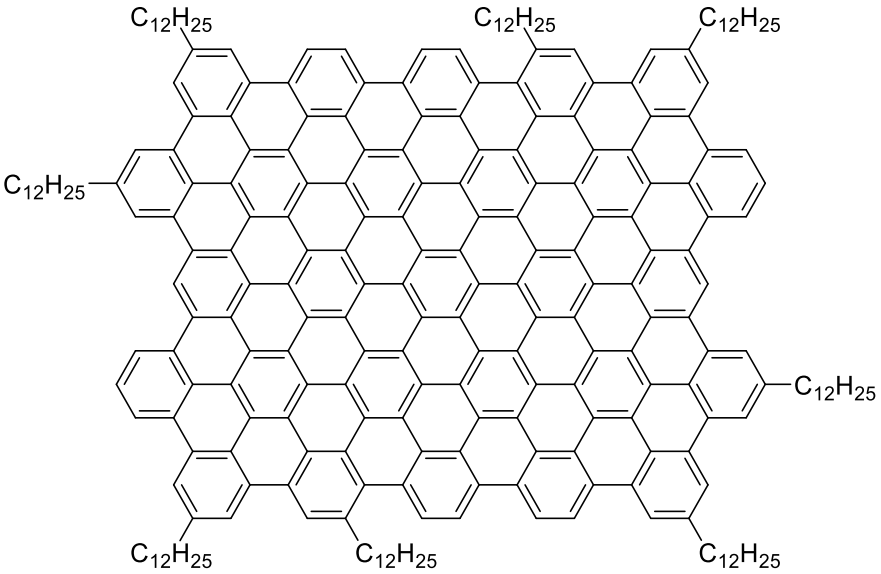

Dendrimer **51** (40 mg, 0.012 mmol) was dispersed in 40 ml of non-stabilized DCM in a two-necked round-bottom flask of 100 ml. Separetly, $FeCl_3$ (1.1 g, 4.2 mmol) was added to 8 ml of anhydrous nitromethane in a glove box. After addition of the $FeCl_3$ solution, the mixture was left 20 hours under argon coming from a two necked round-bottom flask filled with DCM in which argon was bubbling. The solution was quenched with methanol (about 40 ml) and then filtered on PTFE and washed with methanol. The pure product was obtained as 39 mg of black powder (99% yield).

MALDI-TOF MS m/z: calcd for $C_{258}H_{230}$: 3327.80; this product could not be characterized with this method.

6.4. Graphene nanomesh

Synthesis of 1,5,9-trinitrotriphenylene 52[11]:

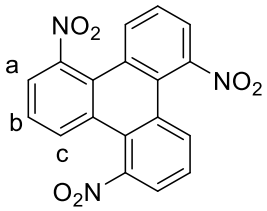

2,3-dichloronitrobenzene (10g, 52.1mmol) was introduced in a round-bottom flask and degassed by 2 vacuum-argon cycles. Anhydrous dimethylformamide (DMF) (200mL) and copper (20g, 312.5mmol) were introduced and the solution was stirred at 160°C overnight. After cooling down to 120°C the solution was filtered on celite. The product was washed 3 times with DMF and the filtrate was then poured in a diluted ammonium solution (1.2 l at 6.5%) under stirring. The black solid was filtered and washed with the diluted ammonium

solution and water. The product was recrystallized in acetone and filtered twice to get 2.12 g of the pure yellowish powder (34% yield).

^{1}H NMR (δ in ppm, 400MHz, $CDCl_3$): 8.16-8.14 (d, *J*=8.3Hz, 3H, a), 7.94-7.92 (d, *J*=7.7Hz, 3H, c), 7.70-7.66 (dd, *J*=8.1, 8.1Hz, 3H, b).

MALDI-TOF MS m/z: calcd for $C_{18}H_9N_3O_6$: 363.05, found: 363.04.

Synthesis of triphenylene-1,5,9-triamine 53[11]:

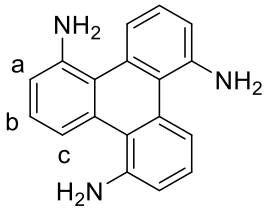

1,5,9-Trinitrotriphenylene **52** (1.5 g, 4.1 mmol) was introduced in a reaction flask with 250 ml of ethyl acetate and 25 ml of ethanol. The solution was degassed bubbling argon 5 min and palladium on carbon (300 mg) was added. The flask was then placed in a shaker hydrogenation apparatus for an hour. The solution was filtered on celite and washed with ethyl acetate and the solvent was evaporated. The pure product was obtained as 820 mg of yellowish powder (73% yield)

^{1}H NMR (δ in ppm, 400MHz, $CDCl_3$): 8.35-8.33 (d, *J*=8.1Hz, 3H, a), 7.31-7.27 (dd, *J*=8.0 , 8.0Hz, 3H, b), 6.88-6.86 (d, *J*=7.7Hz, 3H, c).

MALDI-TOF MS m/z calcd for $C_{18}H_9NH_2$: 273.13, found: 274.13 $(M+H)^+$.

Synthesis of 1,5,9-Triiodotriphenylene 54[12]:

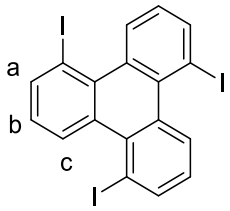

1,5,9-Trinitrotriphenylene **53** (0.2g, 0.73mmol) was introduced in a 25 ml round-bottom flask with 2 ml of HCl (3M) and 2 ml of water. The solution was cooled down to 0°C and a solution of sodium nitrite (1.45 M, 2 ml) was added dropwise under stirring. The resulting solution was added to a solution of sodium iodide (4.45 M, 3 ml) and left under stirring at room

temperature for one hour. The solution was heated to 65°C for 15 min. The solid was filtered and washed with a diluted solution of sodium thiosulfate. The solid was diluted in dichloromethane (about 50 ml) and washed with water three times. The organic phase was dried and evaporated to obtain a dark red powder. This powder was purified with column chromatography with DCM to afford 112 mg of pale yellow powder (26% yield)

^{1}H NMR (δ in ppm, 400MHz, $CDCl_3$): 9.21-9.19 (d, *J*=8.2Hz, 3H, a), 8.24-8.22 (d, *J*=7.7Hz, 3H, c), 7.15 (dd, *J*=8.0, 7.8Hz, 3H, b).

MALDI-TOF MS m/z: calcd for $C_{18}H_9I_2$: 605.78, found: 605.81.

Synthesis of 1,3,5-tris(2'-trimethylsilyl-1,1':4',1''-terphenyl)benzene 55:

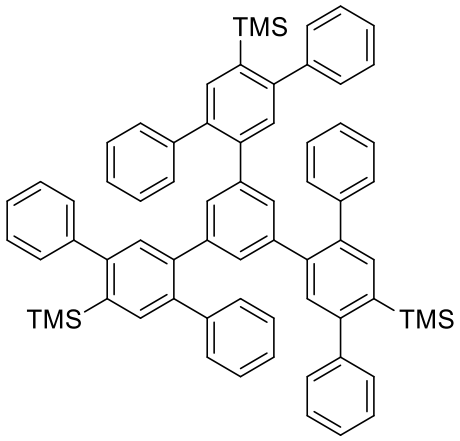

Iodoterphenyltrimethylsilane **34** (1.24 g, 2.89 mmol), Acid phenyltriboronic ester (400 mg, 0.87 mmol), Palladium acetate (6.5 mg, 0.029 mmol), SPhos (23.8 mg, 58 mmol) and Potassium phosphate tribasic (1.23 g, 5.7 mmol) were introduced in a 25 ml Schlenk flask and degassed with three vaccum-argon cycles. The solution was left overnight at 100°C under argon and filtered on celite with DCM before evaporation of the solvents. The product was purified with recrystallisation in cyclohexane and obtained as 530g of a white powder (62% yield).

^{1}H NMR (δ in ppm, 400MHz, $CDCl_3$): 8.36 (s, 6H), 7.52-7.38 (m, 30H), 7 (s, 3H), 0.03 (s, 27H).

MALDI-TOF MS m/z: calcd for $C_{69}H_{66}Si_3$: 978.45, found: 978.43.

Synthesis of 1,3,5-tris(2'-iodo-1,1':4',1''-terphenyl)benzene 56:

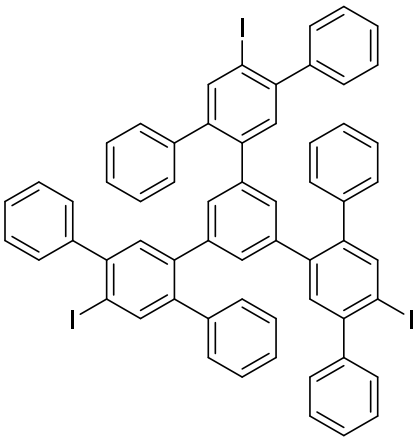

1,3,5-tris(2'-trimethylsilylterphenyl)benzene **55** (350 mg, 0.35 mmol) was introduced in 30 ml of DCM in a two-necked round-bottom flask. The solution was degassed with argon bubbling for 15min and cooled down to 0°C. The ICl (2.1 ml, 2.1 mmol, 1 M in nitromethane) was added dropwise and the solution was left overnight under stirring at room temperature. The reaction was quenched with $Na_2S_2O_3$ (1 M, 20 ml) and the product was extracted with DCM, washed twice with water and brine. After evaporation of the solvent, the product is purified with column chromatography with a mixture of cyclohexane and ethyl acetate (2%). The pure product was obtained as 400 mg of pale yellow powder (98% yield).

^{1}H NMR (δ in ppm, 400MHz, $CDCl_3$): 7.97-7.89 (m, 3H), 7.46-7.32 (m, 15H), 7.17-6.49 (m, 21H).

MALDI-TOF MS m/z: calcd for $C_{69}H_{39}I_2$: 1140.69, found: 1140.03.

(1) Silly, F. A Robust Method for Processing Scanning Probe Microscopy Images and Determining Nanoobject Position and Dimensions. *J. Microsc.* **2009**, *236*, 211–218.
(2) Mohr, B.; Enkelmann, V.; Wegner, G. Synthesis of Alkyl- and Alkoxy-Substituted Bends and Oxidative Coupling to Tetraalkoxyphenanthrene-9,10-Diones. *J. Org. Chem.* **1994**, *59*, 635–638.
(3) Iyer, V. S.; Wehmeier, M.; Diedrich, J.; Keegstra, M. A.; Müllen, K. From Hexa-Peri-Hexabenzocoronene to "Superacenes." *Angew. Chemie - Int. Ed.* **1997**, *36*, 1603–1607.
(4) Tan, Y. Z.; Yang, B.; Parvez, K.; Narita, A.; Osella, S.; Beljonne, D.; Feng, X.; Müllen, K. Atomically Precise Edge Chlorination of Nanographenes and Its Application in Graphene Nanoribbons. *Nat. Commun.* **2013**, *4*, 3646.
(5) Tomović, Ž.; Watson, M. D.; Müllen, K. Superphenalene-Based Columnar Liquid Crystals. *Angew. Chemie - Int. Ed.* **2004**, *43*, 755–758.
(6) Luliński, S.; Serwatowski, J. Bromine as the Ortho-Directing Group in the Aromatic Metalation/Silylation of Substituted Bromobenzenes. *J. Org. Chem.* **2003**, *68*, 9384–9388.
(7) Golling, F. E.; Quernheim, M.; Wagner, M.; Nishiuchi, T.; Müllen, K. Concise Synthesis of 3D π-Extended Polyphenylene Cylinders. *Angew. Chemie - Int. Ed.* **2014**, *53*, 1525–1528.
(8) Morgenroth, F.; Reuther, E.; Müllen, K. Polyphenylene Dendrimers: From Three-Dimensional to Two-Dimensional Structures. *Angew. Chemie - Int. Ed.* **1997**, *36*, 631–634.
(9) Pisula, W.; Tomovi, E.; Simpson, C.; Kastler, M.; Pakula, T.; Müllen, K. Relationship between Core Size, Side Chain Length, and the Supramolecular Organization of Polycyclic Aromatic Hydrocarbons. *Chem. Mater.* **2005**, *17*, 4296–4303.
(10) Cantin, K.; Lafleur-Lambert, A.; Dufour, P.; Morin, J. F. Studies toward the Synthesis of Phenylacetylene Macrocycle Based Rotaxane Precursors as Building Blocks for Organic Nanotubes. *European J. Org. Chem.* **2012**, *2012*, 5335–5349.
(11) Tan, Q.; Chen, H.; Xia, H.; Liu, B.; Xu, B. Parent and Trisubstituted Triazacoronenes: Synthesis, Crystal Structure and Physicochemical Properties. *Chem. Commun.* **2016**, *52*, 537–540.
(12) Tan, Q.; Zhou, D.; Zhang, T.; Liu, B.; Xu, B. Iodine-Doped Sumanene and Its Application for the Synthesis of Chalcogenasumanenes and Silasumanenes. *Chem. Commun.* **2017**, *53*, 10279–10282.

Synthèse et propriétés des points quantiques et nanomeshes de graphène

La modification des propriétés du graphène, notamment l'ouverture d'une bande interdite par la nanostructuration, est un véritable enjeu pour la physique et pour les applications du graphène. Ce travail est le résultat de la collaboration entre le Laboratoire d'Innovation en Chimie des Surfaces et Nanosciences (LICSEN) et le Laboratoire Aimé Cotton (LAC). Le but de cette collaboration est l'exploration des propriétés intrinsèques des points quantiques de graphène préparés par l'approche ascendante. En effet, cette approche permet un contrôle complet de la structure du matériau obtenu et rend possible la modification à l'atome près en vue de décrire complètement les relations structure/propriétés.

Le premier objectif de cette thèse a été de reproduire des synthèses de points quantiques de graphènedéjà existantes dans la littérature afin d'être capable d'en explorer les propriétés optiques avancées. Le grand nombre de structures synthétisables permet de faire varier sélectivement la forme, la taille et les états de bords des points quantiques de graphène. La première partie de cette thèse est donc centrée sur la synthèse organique d'un point quantique de 96 atomes de carbone (C96). Cette synthèse est basée sur le couplage de Diels-Alder d'un composé acétylénique et de la tétraphénylcyclopentadiénone suivi d'une étape de déshydrogénation de Scholl. Ce point quantique peut être fonctionnalisé soit avec six chaines dodécyles (C96C12), soit avec des atomes de chlore (C96Cl). L'étude optique s'est concentrée sur le composé C96C12 qui présente une absorption à 475 nm et une émission à 650 nm dans le solvant 1,2,4-trichlorobenzène. Malgré des problèmes d'agrégation due aux interactions pi, cette molécule a été isolée dans une matrice de polystyrène pour l'observation de ses propriétés optiques intrinsèques. Ces propriétés sont remarquables, en effet, il y a émission de photons uniques avec une grande pureté et une grande brillance. L'émission de photons uniques est conservée dans le cas du C96Cl avec un décalage de 100 nm vers le rouge, ce qui prouve la possibilité de contrôler les propriétés en contrôlant parfaitement la structure.

Grâce à l'expérience accumulée sur la famille des C96, nous avons pu explorer un nouveau type de matériaux graphéniques, intermédiaires entre les points quantiques et les

nanorubans. Ces matériaux ont une structure unidimensionnelle (1D) et une longueur contrôlée. Ce dernier point diffère des nanorubans dont la longueur varie à cause de la préparation *via* une polymérisation, ce qui rend l'étude de l'impact de la longueur sur les propriétés optiques impossible sur ces objets. En partant des structures faites de 78 et 132 carbones (C78 et C132), nous avons ajouté une rangée de phényles en préparant des nouveaux précurseurs acétyléniques. Cette méthode a permis la synthèse de deux nouvelles structures allongées faites de 96 et 162 carbones (C96L et C162) que nous avons appelées « nanorods » de graphène. De la même manière que les points quantiques, ces nanorods ont été préparés avec des chaînes alkyles et des chlores pour former une grande variété de structures. L'étude de l'absorption de ces molécules a montré que l'augmentation de la longueur d'une rangée de phényles (de C78 à C96L et de C132 à C162) engendrait un déplacement de la longueur d'onde d'absorption vers le rouge. Cependant, ce décalage est plus faible que celui engendré par une variation de forme pour un même nombre d'atomes (entre C96 et C96L).

Enfin, après l'exploration de structures à zéro dimension et 1D, nous nous sommes intéressés aux structures à deux dimensions (2D), les nanomeshes. Les nanomeshes de graphène sont des réseaux périodiques de trous dans le graphène. Dans ce matériau, la taille et l'organisation des trous dans la structure ainsi que la taille des partie graphéniques restantes entre les trous (appelées « neck ») vont être responsables de ces propriétés. Actuellement, ces réseaux sont principalement faits par approche descendante à partir de graphène exfolié *via* des étapes d'oxydation partielle ; les tailles des trous sont de l'ordre d'une cinquantaine de nm et ceux de la partie graphénique (« neck ») de l'ordre d'une dizaine de nanomètre. Cette méthode offre peu de contrôle sur le type de structures obtenues et sur leur état d'oxydation, il faut donc lui préférer l'approche ascendante. Les premières tentatives pour réaliser des réseaux 2D covalents graphéniques par l'approche ascendante sont limitées à des largeurs de « neck » d'un seul phényle entre les trous, réduisant ainsi la délocalisation des électrons dans le plan. Nous avons donc préparé deux nouveaux précurseurs organiques dont l'assemblage et la réaction sur surface dans une chambre de STM devrait permettre de réaliser des réseaux avec une largeur de « neck » de deux à trois phényles soit environ 1 nm.

Molecules Glossary

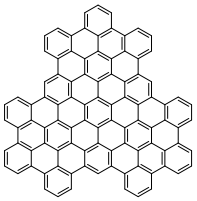

1

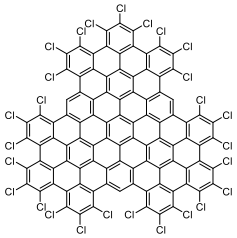

2

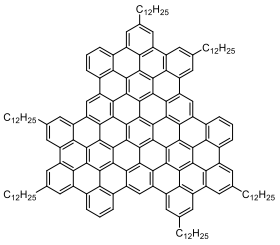

3

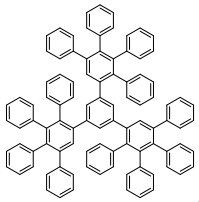

4

5

6

7

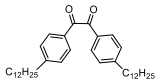

8

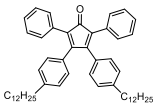

9

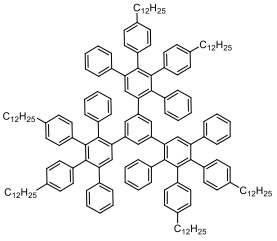

10

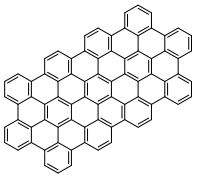

11

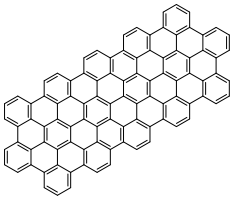

12

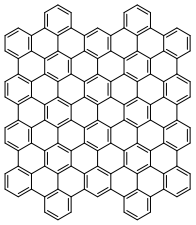

13

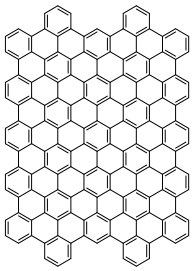

14

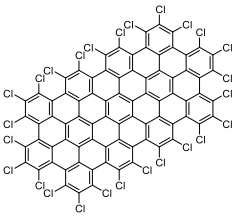

15

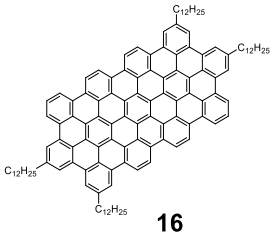

16

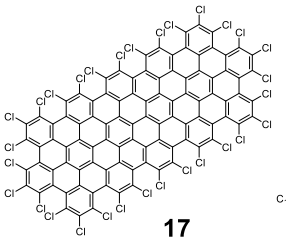

17

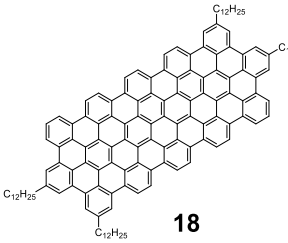

18

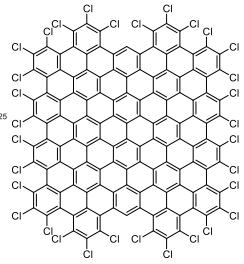

19

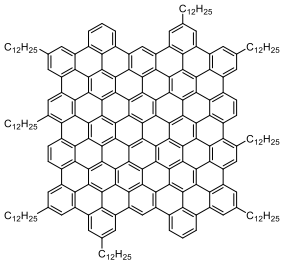

20

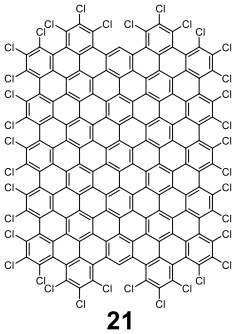

21

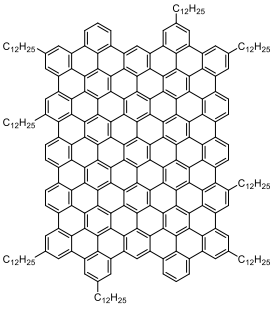

22

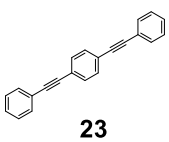

23

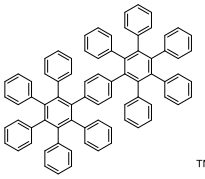

24

25

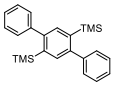

26

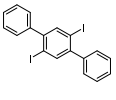

27

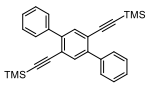

28

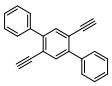

29

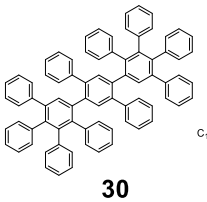

30

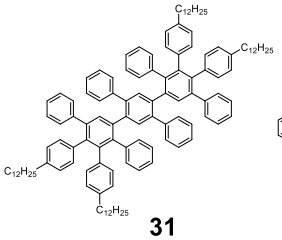

31

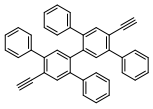

32

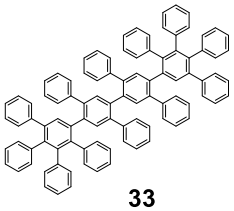

33

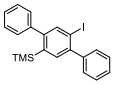

34

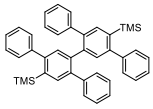

35

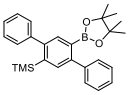

36

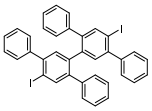

37

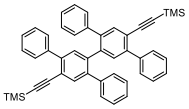

38

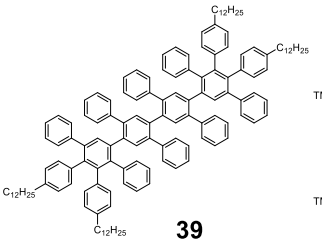

39

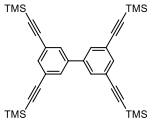

40

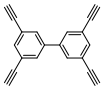

41

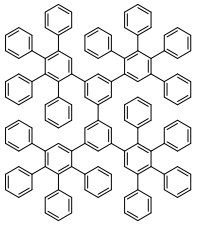

42

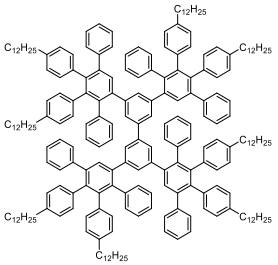

43

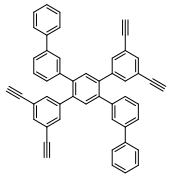

44

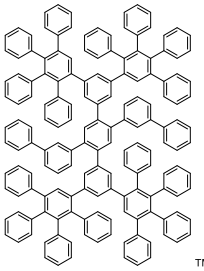

45

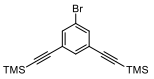

46

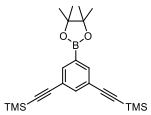

47

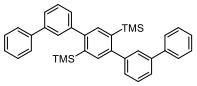

48

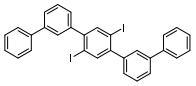

49

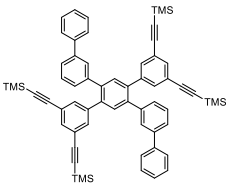

50

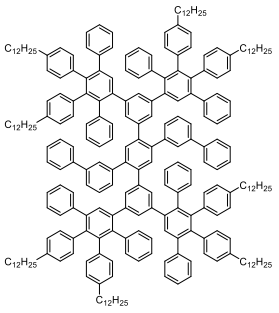

51

52

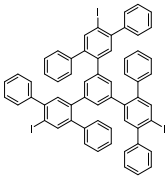

53

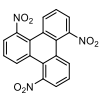

54

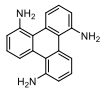

55

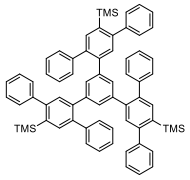

56

université PARIS-SACLAY | ÉCOLE DOCTORALE Sciences chimiques : molécules, matériaux, instrumentation et biosystèmes

Titre : Synthèse et proprietés des boites quantiques et nanomeshes de graphene.

Mots clés : Nanoparticules de graphène, Synthèse organique, Photoluminescence

Résumé : La modification des propriétés du graphène, notamment l'ouverture d'une bande interdite par la nanostructuration, est un véritable enjeu pour la physique et pour les applications du graphène. La nanostructuration peut se faire suivant l'approche « top-down » ou « bottom-up ». Au cours de cette thèse nous nous sommes intéressés à la seconde approche. L'approche « bottom-up » permet de contrôler à l'atome près la structure des matériaux. L'objectif de cette thèse est de fabriquer par synthèse chimique des boites quantiques de graphène et des motifs graphéniques contenant un réseau périodique de trous (nanomesh) et d'en étudier les propriétés physiques. Dans une première partie, une « famille » de nanoparticules de graphène a été préparée par synthèse organique *via* des réactions de Diels-Alder et de Scholl et les propriétés optiques ont été étudiées sur des solutions et à l'échelle de la molécule unique. Dans une deuxième partie, un nouveau type de structures graphéniques intermédiaires entre les boites quantiques et les nanorubans, des nano-bâtonnet de graphène (nanorods) ont été synthétisés. Enfin, plusieurs précurseurs ont été synthétisés pour la réalisation de nanomeshs de graphène. Ces précurseurs permettront d'obtenir, en utilisant le dépôt chimique en phase vapeur dans la chambre d'un microscope à effet tunnel, des nanomesh de graphène présentant des structures différentes.

Title : Synthesis and properties of graphene quantum dots and nanomeshes

Keywords : Graphene nanoparticles, organic synthesis, photoluminescence

Abstract : The manipulation of the electronic properties of graphene, and in particular the bandgap opening by nano-patterning, is a crucial issue for both physics and applications. The nanostructuration can be done either through the top-down approach or the bottom-up approach. This bottom-up approach allows controlling at the atomic level the structure of the materials. The aim of this thesis is to prepare graphene quantum dots and graphene nanomeshes (regular arrays of holes in a graphene sheet) by chemical synthesis, and to study their physical properties. In the first part, a "family" of graphene quantum dots was prepared with organic chemistry via Diels-Alder and Scholl reactions and the optical properties were studied both in solution and at the single molecule scale.
In the second part, a new type of graphenic structures intermediate between quantum dots and nanoribbons were synthesized and we named them "graphene nanorods". These objects are one dimensional but have a controlled length compared to nanoribbons prepared via polymerization. Finally, various precursors were synthesized to create graphene nanomeshes. These precursors will allow the formation, using chemical vapor deposition in a scanning tunneling microscope chamber, of nanomeshes exhibiting different structures and morphology.

Université Paris-Saclay
Espace Technologique / Immeuble Discovery
Route de l'Orme aux Merisiers RD 128 / 91190 Saint-Aubin, France